

https://dspace.org/

A functionalised carbon nanotube system for targeting of inflammatory biomakers in ischemic stroke

Komane, Phogothi Patrick

2019

https://hdl.handle.net/10539/29776

Komane, Phogothi Patrick, A functionalised carbon nanotube system for targeting of inflammatory biomakers in Ischemic stroke, University of the Witwatersrand, Johannesburg, <http://hdl.handle.net/10539/29776>

Downloaded from a DSpace repository. https://dspace.org/

A FUNCTIONALISED CARBON NANOTUBE SYSTEM FOR TARGETING OF INFLAMMATORY BIOMARKERS IN ISCHEMIC STROKE

PHOGOTHI PATRICK KOMANE

A Thesis submitted to the Faculty of Health Sciences, University of the Witwatersrand, in fulfilment of the requirements for the degree of Doctor of Philosophy



Supervisor:

Professor Viness Pillay

Department of Pharmacy and Pharmacology, Faculty of Health Sciences,

University of the Witwatersrand, South Africa

Co-Supervisors:

Professor Yahya Essop Choonara

Department of Pharmacy and Pharmacology, Faculty of Health Sciences,

University of the Witwatersrand, South Africa

Johannesburg, 2019

DECLARATION

I, Phogothi Patrick Komane, declare that this thesis is my own work. It is being submitted for the degree of Doctor of Philosophy of Pharmacy in the Faculty of Health Sciences at the University of the Witwatersrand, Parktown, Johannesburg, South Africa. It has not been submitted before for any other degree or examination at this or any other university.

……

Signed this …….. day of June 2019

RESEARCH OUTPUTS

PUBLICATIONS

1. Patrick Komane, Yahya E. Choonara, Lisa du Toit, Pradeep Kumar, Pierre Kondiah, Girish Modi, and Viness Pillay (2016). *"Diagnosis and Treatment of Neurological and Ischemic Disorders Employing Carbon Nanotube Technology."* Journal of Nanomaterials, Volume 2016 (2016), Article ID 9417874, 19 pages. (ISI, Impact Factor: 2,207) (Review Article) (Appendix A1).

2. Komane, Patrick P., Kumar, P., Marimuthu, T., Du Toit, L.C., Kondiah, P.P.D., and Choonara, Y.E., P. V. Dexamethasone-Loaded, PEGylated, Vertically Aligned, Multiwalled Carbon Nanotubes for Potential Ischemic Stroke Intervention. *Molecules* 2018, *23* (1406), 1–16. (ISI, Impact Factor: 3,098) (Original Research Article) (Appendix A2).

CONFERENCE PROCEEDINGS

1. Patrick P Komane, Yahya E Choonara, Pradeep Kumar, and Viness Pillay. Super-aligned Dexamethasone Loaded Multiwalled Carbon Nanotubes: A Potential for Ischemic Stroke Intervention. CRS, Annual Meeting and Exposition 2017,16-19 July, Hynes Convention Center, Boston, USA, 2017. (**Poster**). (Appendix B1).

2. P.P. Komane, Y.E. Choonara and V. Pillay. A Carbon Nanotube-Based Immunosensor for Detection of Atrial Natriuretic Peptide in Ischemic Stroke. AAPS, Annual Meeting and Exposition, 2016, 13-17 November, Colorado Convention Centre, Denver, USA, 2016. (**Poster**). (Appendix B2).

3. Patrick P. Komane, Sabelo D Mhlanga and Girish Modi. Vertically Aligned Multiwalled Carbon-nanotubes for use in Detection and treatment of Ischemic Stroke. 6th International Conference on Nanoscience and Nanotechnology in Africa, NanoAfrica 2016, 3-6 April, UNISA, Florida, Johannesburg, 2016. (**Podium**). (Appendix B3).

GRANTS

National Research Foundation (NRF)

Department of Higher Education and Training (DHET)

PATENTS

Komane PP, Kumar P, Marimuthu, T, du Toit LC, Choonara YE, Pillay V. Pillay. Dexamethasone loaded PEGylated Vertically Aligned Multiwalled Carbon Nanotubes for treatment of Ischemic Stroke (to be filed).

ACKNOWLEDGEMENT STATEMENT

I would like to express my sincerest gratitude to all the individuals who have played a crucial role in making me to reach this destiny of my research journey.

I express my thanksgiving to my wife, Morura Eniccah for her undying support, love, patience, perseverance and kindness throughout my research life. When I was about to terminate this journey prematurely, you gave me courage. Indeed, perseverance is the mother of success. Thank you also for having a trust in me as I was spending some nights out of our lovely house for the sake of completing my studies. A big thank you too, to my daughter, Shammah Shalom and to my two sons, Gad Phethego and Tumišang Praising for their support and understanding as they were being deprived of the parental love that they deserved most at their young age. Parental bond was temporarily broken by the lack of quality family time as I was always glued to my research work.

I would like to express my gratitude to Prof Viness Pillay, Prof. Yahya Choonara, Dr. Pradeep Kumar, Prof. Lisa du Toit, Dr. Thashree Marimuthu and Dr. Pierre Kondiah for their guidance, encouragement and useful critique to this research work. I would also like to thank Prof. Alexander Ziegler and his dedicated team at Microscopy and Microanalysis Unit (MMU), University of the Witwatersrand for their technical support towards electron microscopy analysis.

Let me take this opportunity to thank the Central Animal Service (CAS) staff, Sr. Amelia Rammekwa, Ms Lorraine Setimo, Ms Thembeka Khoza, Mr Nico Douths, Mr. Patrick Selahle and Sr. Mary-Ann Costello for their valuable assistance and expertise throughout the tenure of my *in vivo* studies. Also like to thank all the CAS staff members

who contributed to the success of this project. A special thank you goes to Prof. Elias Ndobe for his invaluable time, professional skills, efforts, advice and assistance with the surgical procedures. Prof. Elias Ndobe has got a very tight schedule but he ensured that he assisted me despite his busy schedule.

To National Foundation of Research of SA and Department of Higher Education and Training for their financial support. Money talks and if it was not the grants from NRF and DHET, this project would have been a total failure. Your financial support has been immensely appreciated. To the WADDP, University of the Witwatersrand and Department of Chemical Sciences, University of Johannesburg for availing their resources to make this project go smoothly. A special thank you goes to Prof Penny Govender for all the troubles she encountered to make this study possible for me as we all know that the technical staff is given limited privileges especially in the field of personnel development as opposed to the academic staff. She organized study leaves and finances to cater for a replacement person. In fact, she did a lot for me and I really don't know how to express my gratitude to her. Prof Penny Govender, thank you a lot for your patience, advice, understanding and kindness. You really played a crucial role in unlocking the locked door for me to complete this project successfully.

Above all, let me take this opportunity to thank my Creator, the Alpha and Omega, the Beginning and the End, the Rose of Sharon, the Lily of the Valley, the Almighty God for His mighty hand upon me, my family, my supporters and guides. He gave me strength, courage and protection from all the hazards along my journey. Without Him, I am nothing. He has been always watching my footsteps 365/6 days to ensure that I do not lose hope and energy. I am really running out of words to put together to create

thanksgiving words, sentences and paragraphs. In the Name of my Lord and Saviour, Jesus Christ, Amen.

ABSTRACT

Stroke is the fourth leading cause of death in the United States after cardiac disease and cancer, the third major cause of death in the developed countries, the second most common cause of dementia and death and the leading cause of disability worldwide. Prevalence of stroke is expected to increase significantly around the world in the years ahead as the global population older than 65 years of age continues to increase by approximately 9 million people per year. The global economic impact of stroke may be dire if effective preventive measures are not implemented to help decrease the burden of this disease. The use of the current diagnostic tools such as Computed Tomography (CT) and Magnetic Resonance Imaging (MRI) is limited by availability, cost and radiation exposure. The current treatment of stroke with thrombolytic agents such as recombinant Tissue Plasminogen Activator (rTPA) and anti-inflammatory agents such as glucocorticoids namely methylprednisolone and dexamethasone have some drawbacks which need to be dealt with in order to use these glucocorticoids for the intended purpose. The therapeutic potential of these corticosteroids is negatively affected by their short circulatory half-lives and poor pharmacokinetics requiring administration of higher doses which could lead to serious systemic side-effects. Nevertheless, nanotechnology has demonstrated promising results in resolving the shortcomings of the present diagnosis and therapy of ischemic stroke. Nanomedicine is an emerging field of medicine where engineered nanomaterials are utilized for the detection, treatment and prevention of certain diseases including neurological disorders. Carbon nanotubes (CNTs) are a new group of nanomaterials that has demonstrated promising outcomes for the advancement in technology in the field of medicine. They have a variety of unique properties making them useful tools in neurobiological applications. Based on their outstanding physico-chemical properties,

carbon nanotubes have the potential to be employed as theranostic tools for ischemic stroke diagnosis and treatment. In this study, vertically aligned multiwalled carbon nanotubes were synthesized, purified, functionalized, PEGylated and dexamethasone loaded for delivery to the ischemic brain tissue site. In addition, atrial natriuretic peptide (ANP) antibody and FITC, a fluorescent tag were attached to this complex for targeting of the ischemic site and tracking of the bionanomaterial. The conditions for optimal synthesis of carbon nanotubes were optimized using Box-Behnken Design of Experiments in order to produce multiwalled carbon nanotubes with vertical alignment, high yield, length and internal and external diameters suitable for application in diagnosis and treatment of neurological disorders. Pyrolysis conditions of chemical vapour deposition of MWCNTs were as follow; carrier gas = 95 % argon balanced with 5 % H_2, catalyst = 2,5 % ferrocene, substrate = silicon wafer, gas flow rate = 400 $mL.min^{-1}$, synthesis temperature = 775 °C and synthesis duration = 45 min. Vertically aligned MWCNTs with average length of 127 μm, average internal diameter of 11 nm and average external diameter of 73 nm were obtained under these conditions. Morphological changes were confirmed by SEM and TEM. Addition of functional groups to MWCNTs was demonstrated by FTIR and Raman Spectroscopy. Thermal stability of functionalized MWCNTs was determined by TGA. A drastic increase in weight loss was observed at 150 °C and 700 °C up to 775 °C and 825 °C in functionalised and pristine MWCNTs respectively. The surface area increased from 47,156 cm^2 (pristine CNTs) to 144,096 cm^2 (functionalized CNTs) as shown by BET. The presence of carbon at 2Θ of 25 ° and iron at 2Θ of 45 ° in MWCNTs was illustrated by XRD. They were found to be strongly electrically conductive by PPMS at temperatures from 36.85 °C - 76.85 °C when temperatures from -73.15 °C to 76.85 °C were used. The CNT yield was also found to be improved by a mixture of Fe/Co and 599.40 mg of CNTs were produced compared to 331.2 mg produced when Fe/Ni was

used. Honeycomb like structures were formed on the surface of the CNTs when treated with 5 M HCl. Polydispersive index and zeta potential were found to be 0.261 and -15.0 mV, respectively. Dexamethasone release increased by 55 %, 65 % and 95 % in pH of 7.4, 6.5 and 5.5 respectively as evaluated by UV-VIS. The functionalized VA-MWCNTs were demonstrated to be less toxic in PC-12 cells in the concentration range from 20 – 2000 µg.mL^{-1}. The functionalized MWCNTs were intravenously injected in stroke induced Sprague Dawley rats to assess their effect in the treatment of stroke. Stroke induced rats, when treated with the functionalized MWCNTs, a great improvement in their health was observed as demonstrated by reduction of eye sunkenness, fading of the redness of the eye and rat circling in all directions. The levels of ANP were higher in the stroke induced and dropped after treatment with the functionalised MWCNTs. MWCNTs were also distributed to various organs as confirmed by biodistribution studies using Fluorescence microplate reader. These findings have demonstrated the potential of VA-MWCNTs in the enhancement of fast and prolonged release of dexamethasone which could lead to the effective treatment of ischemic stroke as confirmed by reduction in the sunkenness of the left eye, fading away of redness of the eye and circling of the rat in all directions when suspended by the tail in the MWCNTs-treated CCAO rats.

DEDICATION

This thesis is dedicated to my wife, Morura Eniccah Komane and my children, Gad Phethego, Shammah Shalom and Tumišang Praising Komane for their love, patience, respect and support.

ANIMAL ETHICS DECLARATION

I hereby confirm that the following study entitled “A functionalised carbon nanotube system for targeting of inflammatory biomarkers in ischemic stroke” has received approval from the Animal Research Ethics Committee (AREC) of the University of the Witwatersrand with ethics clearance number 2017/03/17/D (Appendix C1).

TABLE OF CONTENTS

DECLARATION i

RESEARCH OUTPUTS ii

GRANTS iv

PATENTS v

ACKNOWLEDGEMENT STATEMENT vi

ABSTRACT ix

DEDICATION xii

ANIMAL ETHICS DECLARATION xiii

LIST OF ABBREVIATIONS xxiii

LIST OF FIGURES xxviii

LIST OF TABLES xlii

CHAPTER 1 1

INTRODUCTION AND RATIONALE FOR THIS RESEARCH 1

1.1. Background of stroke 1

1.2. Pathophysiological mechanisms of stroke 3

1.3. Mechanism of ischemia 4

1.4. Problem statement 6

1.5. Rationale and motivation 8

1.6. Aims and objectives 13

1.7. Novelty of the study 14

1.8. Overview of the thesis 15

1.9. Concluding remarks 17

1.10. References 18

CHAPTER 2 22

LITERATURE REVIEW ON DIAGNOSIS AND TREATMENT OF NEUROLOGICAL AND ISCHEMIC DISORDERS EMPLOYING CARBON NANOTUBE TECHNOLOGY 22

2.1. Introduction 23

2.2. Current diagnosis and treatment of ischemic stroke 26

2.3. Carbon nanotubes in the diagnosis and treatment of central nervous system disorders 27

2.4. Carbon nanotubes potential toxicity in living cells including neural tissue 29

2.5. Chemically functionalized carbon nanotubes for biomedical applications 33

2.6. Carbon nanotubes as electrochemical biosensors in neuroscience 38

2.7. Carbon nanotubes as imaging tools in CNS for localization and detection of ischemic stroke 41

2.8. Carbon nanotubes as CNS drug delivery vehicles for the treatment of ischemic stroke 43

2.9. Carbon nanotubes in neuroengineering in ischemic stroke and other CNS disorders 45

2.10. Recent advances in ischemic stroke treatment 49

2.11. Carbon nanotubes in stimuli-responsiveness in biomedical applications 51

2.12. Carbon nanotubes currently on the market and limitations to clinical application and commercialization 52

2.13. Future potential applications of CNTS 53

2.14. Conclusion remarks 54

2.15. References 56

CHAPTER 3 67

VERTICALLY ALIGNED MULTIWALLED CARBON NANOTUBES FOR USE IN DETECTION AND TREATMENT OF ISCHEMIC STROKE 67

Abstract 67

3.1. Introduction 68

3.2. Materials and Methods 71

3.2.1. Materials 71

3.2.2. Preparation of silicon wafer and catalyst 71

3.2.3. CVD synthesis of VA-MWCNTs 72

3.2.4. Box-Behnken Design of experiments (BBDOE) 73

3.2.5. Characterisation of MWCNTs by SEM and TEM 74

3.2.6. Measurement of resistivity of VA-MWCNTs 75

3.2.7. Determination of functional groups on VA-MWCNTs with Fourier Transform Infrared (FTIR) 75

3.2.8. Purification of VA-MWCNTs by thermal and acid oxidation 76

3.2.9. Determination of surface area, pore size and pore volume of VA-MWCNTs 76

3.2.10. Measurement of wettability of CNTs 76

3.2.11. Determination of particle size distribution and zeta potential of CNTs 77

3.2.12. Measurement of crystallinity and elemental composition of CNTs 78

3.2.13. Determination of the purity of CNTs using TGA 78

3.3. Results and discussion 78

3.3.1. Synthesis Parameters of VA-MWCNTS 78

3.3.2. Effect of location of substrate in the furnace on VA-MWCNT growth 78

3.3.3. Effect of reaction temperature on VA-MWCNT growth 82

3.3.4. Determination of crystallinity and elemental composition of VA-MWCNT 83

3.3.5. Elemental composition of VA-MWCNTs by SEM-EDX 84

3.3.6. Effect of reaction time on the yield and length of VA-MWCNTs 86

3.3.7. Effect of catalyst concentration on the yield and length of VA-MWCNTs 87

3.3.8. Effect of gas flow rates on the yield and length of VA-MWCNTs 88
3.3.9. Effect of synthesis time on diameters of VA-MWCNTs 89
3.3.10. Effect of carrier gas flow rate on diameters of VA-MWCNTs 91
3.3.11. Box-Behnken Design of experiments (BBDOE) 92
3.3.12. Effect of a mixture of Fe//Ni, Fe/Co and Fe/Ni/Co on MWCNT growth 93
3.3.13. Effect of different acids on VA-MWCNT purification 95
3.3.14. Electrical conductivity of VA-MWCNTs 96
3.3.15. Surface area, pore size and pore volume of VA-MWCNTs 98
3.3.16. Wettability of VA-MWCNTs 99
3.3.17. Particle size distribution and zeta potential VA-MWCNTs 101
3.3.18. Functional groups on VA-MWCNTs 103
3.3.19. Purity determination of VA-MWCNTs using TGA 104
3.4. Conclusion remarks 105
3.5. References 107

CHAPTER 4 110

PRE-FORMULATION OF ALIGNED MULTIWALLED CARBON NANOTUBES FOR POTENTIAL APPLICATION IN DIAGNOSIS AND TREATMENT OF ISCHEMIC STROKE 110

Abstract 110
4.1. Introduction 111
4.2. Materials and Methods 112
4.2.1. Materials 112
4.2.2. Preparation of silicon wafer and catalyst 113
4.2.3. CVD synthesis of VA-MWCNTs 113
4.2.4. Carboxylation and acylation of MWCNTs for drug delivery 113
4.2.5. Purification of VA-MWCNTs by thermal and acid oxidation for electrode development 114

4.2.6. Synthesis of DSPE-PEG5000-4-arm-(PEG-Amine) and CNT PEGylation..114
4.2.7. Morphological evaluation of the CNTs using electron microscopy.....115
4.2.8. Thermal analysis and electrical resistivity of VA-MWCNTs 115
4.2.9. Measurement of wettability, surface area and porosity of CNTs.....116
4.2.10. Measurement of crystallinity, elemental composition and functional groups of MWCNTs 116
4.2.11. Particle size, zeta potential and Uv-Vis analysis of MWCNTs 116
4.2.12. Preparation of carbon-based electrode.....117
4.2.13. Cyclic voltammetry and electrochemical impedance spectroscopy 118
4.3. Results and discussion 119
4.3.1. Synthesis of vertically aligned MWCNTs on different substrates.....119
4.3.2. Carboxylation and acylation of MWCNTs 121
4.3.3. Thermal and acid oxidation of VA-MWCNTs 123
4.3.4. Thermal analysis and electrical resistivity.....124
4.3.5. Contact angle, surface area and porosity measurements.....126
4.3.6. Measurement of crystallinity and functional groups of MWCNTs.....128
4.3.7. Dispersibility of MWCNTs in various solvents.....130
4.3.8. Particle size distribution and zeta potential measurements 131
4.3.9. UV-VIS analysis.....136
4.3.10. Development of a nano-electrode.....138
4.3.11. Microscopical morphological assessment of a nano-electrode.....143
4.3.12. Cyclic voltammetry and electrochemical impedance spectroscopy of a nano-electrode.....144
4.4. Concluding remarks.....146
4.5. References 147

CHAPTER 5 150

DEXAMETHASONE-LOADED, PEGYLATED, VERTICALLY ALIGNED, MULTIWALLED CARBON NANOTUBES FOR POTENTIAL ISCHEMIC STROKE INTERVENTION 150

Abstract 150

5.1. Introduction 151

5.2. Materials and Methods 152

5.2.1. Synthesis of MWCNTs using Chemical Vapor Deposition 152

5.2.2. Design and Optimization of formulations using a Design Strategy 153

5.2.3. Functionalization of MWCNTs 153

5.2.4. Morphological and Molecular Spectroscopic Evaluation of the MWCNTs 155

5.2.5. Thermogravimetric and Porositometric analyses of MWCNTs 155

5.2.6. Particle size, zeta potential, crystallinity and elemental composition MWCNTs 156

5.2.7. Dex and Dex-PEG-MWCNTs preparations and drug release Studies 156

5.2.8. Functionalization of MWCNTsCytotoxicity evaluation of VA-MWCNTs 157

5.3. Results and Discussion 157

5.3.1. Location of the Substrate, Catalyst Concentration and Acid Purification of MWCNTs 157

5.3.2. Determination of Crystallinity, Thermal properties and Raman Spectroscopy of MWCNTs 160

5.3.3. Effect of Synthesis Times and Gas Flow Rates on the Length Diameter of MWCNTs 161

5.3.4. Mixture of Ferrocene/Nickelocene/Cobaltocene on MWCNT Growth 163

5.3.5. Porositometric and Particle Size Distribution Properties of MWCNTs 164

5.3.6. FTIR Spectroscopy and H^1 NMR Analyses of PEGylated MWCNTs 166

5.3.7. Dexamethasone Loading to and Release from MWCNTs 168

5.3.8. Cytotoxicity Evaluation of the Functionalized Carbon Nanotubes 170

5.4. Conclusion remarks 172
5.5. References 173

CHAPTER 6 176

ATRIAL NATRIURETIC PEPTIDE CONJUGATION TO FITC LABELLED DEXAMETHASONE LOADED PEGYLATED ALIGNED MULTIWALLED CARBON NANOTUBES FOR TARGETING BRAIN ISCHEMIC SITE 176

ABSTRACT 176

6.1. Introduction 177
6.2. Materials and methods 181
6.2.1. Synthesis of Aligned MWCNTs and morphological evaluation 181
6.2.2. Purification, acid functionalization and acylation of Aligned MWCNTs 182
6.2.3. Dexamethasone loading to PEG- MWCNTs, FITC labelling and ANP conjugation to FITC labelled PEG-MWCNTs 183
6.2.4. Raman Spectra of the functionalised MWCNTs 184
6.2.5. Determination of Molecular and Vibrational Transitions of FITC labelled DEX-PEG-MWCNTs 185
6.2.6. Uv-Vis and fluorescence evaluation in the functionalised MWCNTs 185
6.3. Results and discussion 185
6.3.1. Surface morphological evaluation of MWCNTs 185
6.3.2. FTIR assessment of the functionalised MWCNTs 186
6.3.3. Raman evaluation of the functionalised MWCNTs 189
6.3.4. Uv-Vis scanning and FEEM evaluation of the FITC Dex PEG ANP CNTs 192
6.3.5. Fluorescence evaluation of FITC DEX PEG ANP CNT 196
6.4. Conclusion remarks 197
6.5. References 198

CHAPTER 7 200

ANP LEVELS AND BIODISTRIBUTION OF INTRAVENOUSLY ADMINISTERED PEGYLATED ALIGNED MULTIWALLED CARBON NANOTUBES DECORATED WITH DEXAMETHASONE IN ISCHEMIC STROKE SPRAGUE DAWLEY RATS. 200

Abstract 200

7.1. Introduction 201

7.2. Materials and methods 202

7.2.1. Materials 202

7.2.2. Aligned Multiwalled Carbon Nanotubes for *in vitro* and *in vivo studies* 203

7.2.3. Dexamethasone release studies 203

7.2.4. Evaluation of MWCNT cytotoxicity 204

7.2.5. Animal administration 208

7.2.6. Preparation of the intraluminal monofilament sutures for MCA occlusion 211

7.2.7. Middle cerebral artery occlusion (MCAO) 212

7.2.8. Unilateral common carotid artery occlusion (CCAO) and neurobehavioural assessment 214

7.2.9. Optimization of the formulation dose 216

7.2.10. Humane endpoints and tissue sampling 217

7.2.11. Tissue sample preparation 218

7.2.12. Determination of Fluorescence intensity in the rat tissues 218

7.2.13. Histological evaluation of the rat brain tissue 218

7.2.14. Determination of plasma ANP levels in the rat venous blood 219

7.2.15. Biodistribution of dpcaf using Raman Microscopy 221

7.3. Results and discussion 221

7.3.1. Vertically aligned MWCNTs synthesis and purification 221

7.3.2. Cytotoxicity of MWCNTs 224

7.3.3. Animal surgery and neurobehavioural assessment 227

7.3.4. Humane endpoints and sampling 235

7.3.5. Brain and total body weights following CCAO and treatment with the formulations 237
7.3.6. Optimization of the formulation dose and Fluorescence measurements 239
7.3.7. Biodistribution of dpcaf using Raman Microscopy 240
7.3.8. Biodistribution of dpcaf using Absorption Spectroscopy 241
7.3.9. Biodistribution of dpcaf using Fluorescence Spectroscopy 243
7.3.10. Determination of plasma ANP levels in the rat venous blood 247
7.3.11. Histological evaluation of dpcaf delivery into the brain by Fluorescence microscopy 253
7.3.12. Histological evaluation of dpcaf delivery into the brain by H & E staining technique 254
7.4. Concluding remarks 257
7.5. References 258

CHAPTER 8 260

CONCLUDING REMARKS, RECOMMENDATIONS AND FUTURE PERSPECTIVES 260

8.1. Concluding remarks 260
8.2. Recommendations 262
8.3. Future Perspectives 262
8.4. References 264

LIST OF ABBREVIATIONS

AD	**:** Alzheimer's Disease
ANP	**:** Atrial Natriuretic Peptide
AREC	**:** Animal Research Ethics Committee
BBB	**:** Blood Brain Barrier
BBDOE	**:** Box-Behnken Design of Experiments
BCSFB	**:** Blood Cerebrospinal Fluid Barrier
BET	**:** Brunauer–Emmett–Teller
BNP	**:** Brain Natriuretic Peptide
CBF	**:** Cerebral Blood Flow
CCAO	**:** Common Carotid Artery Occlusion
CNP	**:** C-type Natriuretic Peptide
CNS	**:** Central Nervous System
CNT-Dox	**:** Doxorubicin functionalized CNTs
CNT-FET	**:** CNT Field Effect Transistors
CNT-FITC	**:** Fluorescein functionalized CNTs
CNT-ox	**:** oxidized Carbon nanotubes
CNTs	**:** Carbon nanotubes

CNTYMEs	**:** CNT Yarn Microelectrodes
CT	**:** Computed Tomography
CV	**:** Cyclic Voltammetry
CVD	**:** Chemical Vapour Deposition
DA	**:** Dopamine
DCC	**:** Dicyclohexylcarbodiimide
DCM	**:** Dichloromethane
DDS	**:** Drug Delivery System
Dex	**:** Dexamethasone
DEX-PEG-CNTs	**:** Dexamethasone loaded PEG-CNTs
DLS	**:** Dynamic Light Scattering
DMF	**:** N, N'dimethylformamide
DOPC	**:** 1,2-dioleoyl-sn-glycero-3-phosphocholine
dpcaf	**:** dexamethasone decorated PEGylated aligned MWCNTs
DSPE-PEG5000-4-arm (PEG-amine)	**:** distearoylphosphatidylethanolamine-poly(ethylene glycol0 MW5000 4-arm (polyethylene gglycol amine)
ECA	**:** External carotid artery
EDC-NHSS	**:**1-ethyl-3-(3-dimethylaminopropyl) carbodiimide and N-hydroxysulfosuccinimide
EDS	**:** Energy Dispersive X-ray Spectroscopy

EIS	**:** Electrochemical Impedance Spectroscopy
ELISA	**:** Enzyme Linked Immunosorbent Assay
EPR	**:** Enhanced Permeability and Retention
FBS	**:** Fetal Bovine Serum
f-CNTs	**:** functionalized CNTs
FEEM	**:** Fluorescence Excitation Emission Matrix
FITC	**:** Fluorescent Isothiocyanate
FITC-DEX-PEG-CNT	**:** FITC labelled DEX-PEG-CNT
FITC-DEX-PEG-CNT-ANP	**:**FITC labelled DEX-PEG CNT Atrial Natriuretic Peptide
H & E	**:** Haematoxylin & eosin
H_2O_2	**:** Hydrogen Peroxide
H_2SO_4	**:** Sulfuric acid
HCl-CNTs	**:** HCl purified MWCNTs
hMSC	**:** human Mesenchymal Stem Cell
HNO_3	**:** Nitric acid
HOBt	**:** Hydroxybenzotriazole
HRP	**:** Horse radish peroxidase
HS	**:** Horse Serum
ICA	**:** Internal Carotid Artery
ICH	**:** Intracranial Haemorrhage

LOD	**:** Limit of Detection
MCA	**:** Middle Cerebral Artery Occlusion
MCAO	**:** Middle Cerebral Artery Occlusion
MEAs	**:** Microelectrode Arrays
MMP-9	**:** Matrix Metallopeptidase
MTT	**:** 3-[4,5-dimethylthiazol-2-yl]-2,5-diphenyl tetrazolium bromide
MWCNT	**:** Multiwalled Carbon Nanotube
NF-kB	**:** Nuclear Factor kappa B
NR2 peptide	**:**N-methyl-D-aspartate Receptor Degradation Product
PC-12 cells	**:** Pheochromocytoma derived from the rat adrenal medulla
PD	**:** Parkinson's disease
PDI	**:** Polydispersive index
PEG	**:** Polyethylene Glycol
PEG-CNTs	**:** PEGylated CNTs
PEI	**:** Polyethylenediamine
PET	**:** Positron Emission Tomography
PPF	**:** PEG and poly (propylene fumarate)
PPMS	**:** Physical Property Management System
PPy	**: P**olypyrrole
premed	**:** premedication

PSD	**:** Particle Size Distribution
RES	**:** Reticuloendothelial System
ROS	**:** Reactive Oxygen Species
RPMI1640	**:** Roswell Park Memorial Institute
rt-PA	**:** recombinant tissue Plasminogen Activator
S.D.	**:** Sprague Dawley
SAH	**:** Sub-arachnoid haemorrhage
SEM-EDS	**:** Scanning Electron Microscopy EDS
siRNA	**:** short interference RNA/small interfering RNA
$SOCl_2$	**:** Thionyl chloride
COCl-CNTs	**:** Acylated CNTs
SPECT	**:** Single Photon Emission Computed Tomography
TGA	**:** Thermogravimetric analysis
THF	**:** Tetrahydrofuran
TLR	**:** Toll like receptor family members
VA-MWCNT	**:** Vertically Aligned Multiwalled Carbon
XRD	**:** X-ray Diffraction

LIST OF FIGURES

Figure 1.1: Two types of stroke. Image adapted from Green, Odergren, & Ashwood, 2003 with permission from Elsevier. 2

Figure 1.2: Three regions in the infarcted brain due to acute ischemic stroke (Benign oligemia, penumbra and ischemic core). Image adapted from Belayev with permission from Elsevier (Belayev, Lu and Bazan, 2012). 4

Figure 1.3: Mechanism of ischemia in acute ischemic stroke. Image reproduced from 5

Culmsee & Krieglstein, 2005 with permission from Elsevier.....5

Figure 1.4. Devices approved by the FDA for acute stroke clot removal: (A) MERCI.6

retriever, (B) Solitaire stent retriever, (C) Penumbra aspiration system, and (D).....6

TREVO2 stent retriever. Images reproduced from Lin & Sanossian, 2015a 6

with permission from Elsevier. 6

Figure 1.5: Penumbra system for thromboaspiration. Image reproduced from.....7

Alexandrov et. al., 2010 with permission from Elsevier. 7

Figure 1.6: Schematic conceptualization of carbon nanotube forests synthesis for..11

detection of ANP antigens in the blood. 11

Figure 1.7: Multiwalled Carbon nanotube (MWCNT) armed with monoclonal antibodies.....12

against inflammatory biomarker (ANP) in ischemic stroke and with anti-.....12

inflammatory drug (dexamethasone) for ischemic stroke treatment. 12

Figure 2.1. Schematic representation of a Chemical Vapour Deposition tube furnace with a nebulizer. A catalyst reacts with a precursor in the atomization chamber and the reactants are then carried into the high temperature furnace by argon gas. Nucleation sites are formed by the nanoparticles from the catalyst for the growth of

carbon nanotubes from the carbon source acetylene. The evolved gases from the reaction are wiped out of the furnace by argon gas via the outlet. Adapted from Nunes and co-workers (Nunes, Al-Jamal and Kostarelos, 2012) with a permission from Elsevier. 25

Figure 2.2. Oxidation and functionalization of CNTs. Pristine CNT has sidewalls and two.....34

tips (a). During oxidation, carboxyl groups are attached to the sidewalls and 34

tips (b). Oxidized CNTs are further functionalized by acylation, amidation and.....34

addition reactions (c & d). Drug and fluorescent tags may be inserted inside 34

the CNTs as the central cavity can be accessed following removal by oxidation (e). Reproduced with permission from Prato and colleagues (Prato, Kostarelos and Bianco, 2008). Copyright (2016) American Chemical Society. 34

Figure 2.3. CNT equipped with a targeting ligand, drug and fluorescent tag. Reprinted.....42

with permission from Prato and colleagues (Prato, Kostarelos and Bianco, ...42

2008). Copyright (2016) American Chemical Society. 42

Figure 2.4. Drug delivery system (DDS). An anti-tumour drug and tumour- targeting 43

ligands are coupled to carbon nanotubes (CNTs). Tumour-targeting ligands 43

bind to the receptors on the cell membrane and the DDS is transported into 43

the cell. Drug is released from the CNTs into the cell as a result of an acidic 43

milieu. Adapted from Ji and colleagues (Ji et al., 2010). 43

Figure 3.1: A CVD setup for the synthesis of VA-MWCNTs. Nebuliser coupled to the furnace and mass flow control. 72

Figure 3.2. Optical contact angle meter equipped with a dosing unit, illumination unit, ...77

sample platform and camera. 77

Figure 3.3. SEM and TEM micrographs of VA-MWCNTs collected from zone C. (a) 79

MWCNTs from silicon wafer at low magnification (b), MWCNTs at high 79

magnification, (c) MWCNTs from quartz tube and (d) MWCNTs TEM 79

micrograph. 79

Figure 3.4. Growth mechanism of carbon nanotubes. Tip-growth model (A) and

Base- 81

growth model (B). Adapted from Azam and colleagues (Azam et al., 2013). 81

Figure 3.5. MWCNTs at different temperatures. (a) 775 °C, (b) 850 °C and (c) 900

°C. 82

Figure 3.6. XRD pattern of MWCNTs with two peaks (carbon and iron peaks). 84

Figure 3.7. Elemental composition of MWCNTs. (a) Fe-Co, (b) Fe-Ni and (c) Fe-Co-

Ni. 85

Figure 3.8. The effect of synthesis time on the yield and length of VA-MWCNTs. (a)

..... 86

Synthesis time on the CNTs yield on silicon wafer, (b) synthesis time on the 86

thickness of CNT on silicon wafer, (c) synthesis time on the CNT yield on 86

quartz tube walls and (d) synthesis time on the thickness of CNTs on quartz 86

tube. 86

Figure 3.9. VA MWCNTs at various catalyst concentrations. (a) 10 % ferrocene (b) 5

% 87

ferrocene and 2.5 % ferrocene. 87

Figure 3.11. Effect of synthesis time on diameters of MWCNTs. (a) Internal diameter

and 90

(b) External diameter. 90

Figure 3.12. The effect of gas flow rate on diameters of CNTs. (a) Internal diameter and 91
(b) External diameter. 91
Figure 3.13. MWCNTs treated with different acids (a) Concentrated H_2SO_4:HNO_3 (3:1), ...95
(b) 5 M HCl and (c) Concentrated HCl. 95
Figure 3.14. Electrical resistivity of VA-MWNTs from 200 to 350K. 97
Figure 3.15. Measurement of contact angle. Θ < 90 ° (A), Θ = 90 ° (B) and Θ > 90 ° (C). 99
Figure 3.16. The 5 M HCl treated MWCNTs (a) Particle size distribution (b) Zeta potential. 102
Figure 3.17. FTIR spectra of pristine MWCNTs and 5M HCl treated MWCNTs. 103
Figure 3.18. TGA weight loss curves of pristine MWCNTs and 5 M HCl treated MWCNTs. 104
Figure 4.1. Set-up of the cyclic voltammetry system. 118
Figure 4.2. MWCNTs grown on Si wafer using CVD technique. CNTS deposited on Si 119
wafer (A). SEM micrograph of CNTs at 844 x magnification(B). SEM 119
micrograph of CNTs at 8 430 x magnification (C). SEM micrograph of CNTs at 119
70 399 x magnification (D). TEM micrograph of CNTs with insert at very high 119
magnification (E). 119
Figure 4.3.CVD synthesised MWCNTs grown on quartz tube wall. CNTS collected from 120
quartz tube wall (A). SEM micrograph of CNTs at 1 005 x magnification (B). 120
SEM micrograph of CNTs at 3 697 x magnification (C). SEM micrograph of 120
CNTs at 64 991 x magnification (D). TEM micrograph of CNTs with insert at 120

very high magnification (E). 120

Figure 4.4. MWCNTs treated with different acids. Conc H_2SO_4:HNO_3 (3:1) (A). 5 M HCl 123

(B). Conc HCl (C). 123

Figure 4.5. Thermograms of (a) Pristine MWCNTs, (b) HCl-MWCNTs, (c) COCl-MWCNTs..... 124

and (d) COOH-MWCNTs..... 124

Figure 4.6. Electrical resistivity of VA-MWNTs from 229 to 300K. 126

Figure 4.7. Contact angles of non-functionalised and functionalised MWCNTs 127

Figure 4.8. XRD spectrum of VA-MWCNTs grown on Si wafer. 128

Figure 4.9. FTIR spectra of MWCNTs. MWCNT scans collected from KBr pellets (A). 129

MWCNT scans collected from UATR crystal (B). 129

Figure 4.10. Dispersibility of pristine and functionalised MWCNTs in water and 131

dichloromethane (DCM). COCl-CNTs in DCM (a), COCl-CNTs in water (b), ... 131

Pristine CNTs in DCM (c), Pristine CNTs in water (d) HCl-CNTs in DCM (e),..... 131

HCl-CNTs in water (f), H_2SO_4-CNTs in DCM (g) and H_2SO_4-CNT in water (h). 131

Figure 4.11. Particle size of the functionalised MWCNTs. CNTs dispersed in water (A). 132

CNTs dispersed in DCM (B). 132

Figure 4.12. Polydispersive index of MWCNTs. CNTs dispersed in water (A). CNTs 133

dispersed in DCM (B). 133

Figure 4.13. Zeta potential of functionalised MWCNTs. CNTs dispersed in water (A). 134

CNTs dispersed in dichloromethane (B). 134

Figure 4.14. Uv-Vis spectra of the functionalized MWCNTs. The functionalised CNTs have 137
different λmax.....137
Figure 4.15. Synthesis of Epoxy Resin (Epikote 862). Bisphenol F reacts with epichlohydrin to produce diglycidyl ether of bisphenol F 139
Figure 4.16. Chemical structure of amine (A) and diethyltoluene diamine (B).....139
Figure 4.17. Incorporation of VA-MWCNTs in epoxy resin. Silicone rubber moulds for 141
casting epoxy resin (A). Four sanded and polished nano-electrodes (B). 141
Figure 4.18. Incorporation of VA-MWCNTs in epoxy resin. Silicone rubber moulds for 142
casting epoxy resin (A). Four sanded and polished nano-electrodes (B). 142
Figure 4.19. Magnetic properties of MWCNTs. Magnetic stirring bar (A). MWCNTs (B). 142
Magnetic stirring bar attracting MWCNTs (C).....142
Figure 4.20. Epoxy resin with incorporated MWCNTs. Infiltrating epoxy resin into the carbon nanotubes was observed.....143
Figure 4.21. Cyclic voltammographs of nano-electrodes. Different shapes of the plots have been observed with different electrodes. 145
Figure 4.22. Nyquist impedance plots of nano-electrodes. The diameter of each electrode semi - circle increased with an increase in the resistivity.....145
Scheme 5.1. Schematic illustration showing the preparation of PEG-MWCNTs.....154
Figure 5.1 Vertically aligned MWCNTs collected from silicon wafer 14 cm from the 158
furnace inlet at 850 °C (A). Carbon nanospheres produced at 900 °C (B). 158
Carbon flakes from the furnace centre at 900°C (C). MWCNTs from quartz.....158

tube walls at 850 °C (D). TEM micrograph of aligned MWCNTs (E) with 158
magnified MWCNT insert. MWCNTs grown at 775 °C (F). 158
Figure 5.2 MWCNTs at various catalyst concentrations and purified with different
acids. 159
MWCNTs synthesised in 100 mg.mL^{-1} ferrocene (A). MWCNTs prepared in 159
50 mg.mL^{-1} ferrocene (B). MWCNTs when 25 mg.mL^{-1} ferrocene was used (C). ... 159
MWCNTs treated with different acids namely concentrated H_2SO_4:HNO_3 (3:1) 159
(D), 5 M HCl (E) and concentrated HCl (F) 159
Figure 5.3. XRD diffraction pattern, TGA and Raman spectra of MWCNTs. Diffraction
..... 160
pattern of pristine MWCNTs (A), TGA of both pristine and HCl treated 160
MWCNTs (B). Raman spectrum of pristine MWCNTs (C) and Dex and PEG- 160
CNTs (D). 160
Figure 5.4. Synthesis parameters of MWCNTs. Synthesis time on the length or
thickness 162
of MWCNTs on both the silicon wafer (black column) and the reactor tube 162
walls (red column) (A). Synthesis time on both the MWCNTs internal (red 162
column) and external (green column) diameters (B). Carrier gas flow rate on 162
both the MWCNTs internal (red column) and external (green column) 162
diameters (C). Carrier gas flow rate on MWCNTs length on both silicon wafer 162
(red column) and reactor wall (green column) (D). 162
Figure 5.5. Porositometric and particle size properties of MWCNTs. BET isotherms
for 165
both the pristine (black curve for N2 adsorption and red curve for desorption) 165
and HCl treated (green curve for N2 adsorption and blue curve for 165

desorption) MWCNTs (A). An increase in particle size distribution was observed in acid treated CNTs as the CNTs are oxidized to produce different sizes (B).....165
Figure 5.6. Molecular spectral properties of pristine and functionalized MWCNTs. FTIR 167
spectra of pristine (red spectrum) and HCl functionalised (black spectrum).....167
MWCNTs (A). ^{1}H -NMR spectra of PEG-CNTs, Dexamethasone, and.....167
Dex-PEG-CNTs (B). 167
Figure 5.7. Dexamethasone release curves. Dex – MWCNTs in PBS buffer with pH 7.4 170
and pH 5.5 (A). Dex-PEG-MWCNTs in PBS buffer with pH 7.4, pH 6.5 and.....170
pH 5.5 (B). 170
Figure 5.8 Cell viability following incubation with various concentrations of functionalized 171
carbon nanotubes. H_2SO_4-MWCNTs were used as they are highly dispersible 171
and hydrophilic. Blue column = free dexamethasone, brown column =.....171
equivalent dexamethasone concentration coupled to PEGylated MWCNTs and 171
grey column for sulfonitric acid functionalized MWCNTs without 171
dexamethasone. Concentrations of each formulation expressed as µg/mL from 171
0 – 20 000. 171
Figure 6.1. Structure of atrial natriuretic peptide (ChemicalBook). 178
Figure 6.2. Action and mechanism of natriuretic peptides in cardioprotection (Nishikimi,.....179
Maeda and Matsuoka, 2006).....179
Figure 6.3. Plasma membrane receptors of natriuretic peptide (Nishikimi, Maeda and 180
Matsuoka, 2006).....180

Figure 6.5. FITC labelling of PEG-MWCNTs. 184

Figure 6.6. Aligned multiwalled carbon nanotubes. MWCNTs harvested from quartz tube 186

wall (A), TEM micrograph of MWCNTs with Fe nanoparticle inside the cavity 186

(B) and SEM micrograph of aligned multiwalled carbon nanotubes (C). 186

Figure 6.7. FTIR spectra of functionalised PEGylated MWCNT in deionised water. 187

Figure 6.8. FTIR spectra of functionalised MWCNTs (KBr pellets). A circle and arrow 188

indicating an additional peak in $SOCl_2$ functionalised MWCNTs. 188

Figure 6.9. Raman spectra of the functionalised multiwalled carbon nanotubes. ...189

Figure 6.10. Raman spectra of the functionalised PEGylated MWCNTs. Pristine ..190

MWCNTs (A). Functionalised MWCNTs (B). 190

Figure 6.11. Dispersibility of the functionalised CNTs in water. Pristine CNTs (A). HCl 192

treated CNTs (B). H_2SO_4.HNO_3 treated CNTs (C) and $SOCl_2$ treated CNTs (D). ...192

Figure 6.12. Uv-Vis spectra of PEG-CNTs and Dex-PEG-CNTs. 193

Figure 6.13. FEEM spectra of the functionalised PEGylated MWCNTs. FITC (A), DEX-.....194

PEG-CNT (B), FITC-DEX-PEG-CNT (C) and FITC-DEX-PEG-CNT-ANP (D).....194

Figure 6.14. Contour maps showing the fluorescence intensities of FITC only and the 195

functionalised MWCNTs. FITC (A). Dex-PEG-CNT (B). FITC-Dex-PEG-CNT 195

(C). FITC-ANP-Dex-PEG-CNT. 195

FITC-DEX PEG-CNT (B). FITC-DEX-PEG-CNT-ANP (C). 197

Figure 7.1. Dexamethasone drug release. Dialysis tubing and incubation in orbital shaker 204
incubator.....204
Figure 7.2. Cytotoxicity formulations. Formulation grouping (A). Layout of incubation of 206
cells with the formulations. 206
Figure 7.3. Cleavage of the tetrazolium salt MTT to formazan by the succinate-tetrazolium.....207
reductase system in the presence of an electron-coupling reagent.....207
(Predoi *et al.*, 2007).....207
Figure 7.4. Sprague Dawley rats in cages. Environmental enrichment (B). Rats in pairs in.....209
enriched environment (B). Weighing of rat (unstable) (C). Weighing of rat 209
(stable) (D). 209
Figure 7.5. Handling of Sprague Dawley rats. Rats transferred to bigger cages and pre-.....210
surgery preparation (A). Experimental design for pilot study and main study.....210
(B). 210
Figure 7.6. Preparation of intraluminal monofilament sutures. Nylon 4-0/3-0 cut to 5cm 211
pieces and blunted at one tip (A). Measurement of the tip dimensions under 211
light microscope (B). Coating of the sutures with 0.1% poly-lysine. 211
Figure 7.7. Preparation of the rat for surgery. Inhalation anesthesia (A). Anesthetic 212
instrument (B). Venous blood collection from the tail (C). Shaving of the neck 212
area (D). Dissection of the neck area (E). 212

Figure 7.8. Dissection of the neck to isolate CCA and its bifurcation. Dissection of the 213
glandular tissue (A). Measurement of spO2 and heart rate under anaesthesia 213
(B). Isolation of CCA (C). Insertion of nylon suture into the MCA (D). 213
Figure 7.9. Bifurcation of the common carotid artery into ICA and ECA and further 214
bifurcation of ICA and ECA.....214
Figure 7.10. Unilateral common carotid artery occlusion. Blood withdrawal from...215
saphenous vein (A). Injection of local anaesthetic (lignocaine) on the neck.....215
(B). Occlusion of CCA by clamping (C). 30-minute occlusion (D). Blood 215
withdrawal from the tail vein (E). Recovering from anesthesia (F). 215
Figure 7.11. Humane endpoints. Cardiac acupuncture (A). PBS perfusion (B). Perfused.....217
organs isolated from the rat (C-H). 217
Figure 7.12. Competition ELISA (Bio-Rad, 2017). 219
Figure 7.13. Serial dilutions of ANP. Stock solution of ANP at 1000 pg.mL^{-1} was diluted 2-.....220
fold up until 15,63 pg.mL^{-1}. 220
Figure 7.14. Vertically aligned multiwalled carbon nanotubes (VA-MWCNTs) morphology.....222
Carbon nanotubes with nanoparticle layer on top (A). VA-MWCNTs at 2145 x.....222
magnification (B). VA-MWCNTs under 120 000 x magnification (C). VA- 222
MWCNT TEM microgram (D). 222
Figure 7.15. Purification of MWCNTs. Pristine VA-MWCNTs prior to purification (A). 223
Pristine MWCNT TEM microgram (B). Top view of MWCNTs following.....223

purification with 5 N HCl (C). HCl purified MWCNT TEM microgram. 223

Figure 7.16. Purification of VA-MWCNTs. MWCNTs in conc H_2SO_4 (A). MWCNTs in 2 M 223

H_2SO_4 (B). MWCNTs in 5 N HCl (C). MWCNTs TEM microgram (D).....223

Figure 7.17. PC-12 cells under light microscope and cell viability using Trypan blue 225

exclusion technique. PC-12 cells grown in tissue culture flasks (A). Viewing.....225

of cells with inverted light microscope (D-I). 225

Figure 7.18. Cell viability versus concentration of the formulations. Functionalised MWCNTs at various concentrations were incubated with PC-12 cells at 37 °C for 24 hours. (A-C).....226

Figure 7. 19. Intraluminal monofilament suture with magnified blunt tip. The tip is clearly blunt to avoid damage to the tissues of the blood vessels. 227

Figure 7.20. Neurobehaviour of Premedication rats. Perfect healthy rat with intact eyes.....230

(A). Left hand side circling (B). Right hand side circling (C). 230

Figure 7.21. Neurobehaviour of CCAO group. Left eye sunken and dark red (A). Right.....230

hand side circling (B). Right hand side circling (C). 230

Figure 7.22. Neurobehaviour of dpcaf treated group. Improved eye condition, not sunken.....231

and slightly red (A-B). Right hand side circling (C). Left hand side circling 231

(D). 231

Figure 7.23. Healthy non-ischemic and untreated rats. Perfect healthy rat with intact eyes.....232

(A-B). Left hand side circling (C). Right hand side circling (D).....232

Figure 7.24. PEG-CNT treated rats. Perfect healthy rat with intact eyes (A-B). Right hand 233
side circling (B). Left hand side circling (C). 233
Figure 7.25. Sham group. Perfect healthy rat with intact eyes (A). Right hand side circling 234
(B). leftt hand side circling (C). 234
Figure 7.26. CCAO rat (Ischemic) treated with Dex. Right eye sunken and dark red (A). 234
Left hand side circling (B). left hand side circling (C).....234
Figure 7.27. Blood collected from the tail vein (A) and heart (B) centrifugated to separate 235
plasma.....235
Figure 7.28. Brain preparation for histological evaluation. Left and right hemispheres were 236
separated and stored in formalin. 236
Figure 7.29. Organs harvesting and preservation during perfusion. 237
Figure 7.30. Brain hemisphere weights before and after treatment of the rat with the 238
formulations.....238
Figure 7.31. Total body weight loss during CCAO and following treatment. 239
Figure 7.32. Dose response curve of dpcaf in CCAO rats. 240
Figure 7.33. Loading of formulations and samples into the microcapillary tubes for Raman.....241
analysis. Sealing by flame (A). Sealed microcapillary tube with the 241
formulation/sample inside (B). 241
Figure 7.34. Calibration curve of dpcaf. 242

prepared and fluorescence intensities were determined to construct.....244
this calibration curve.....244
Figure 7.36. Average fluorescence intensities in various organs in CCAO (no treatment).....246
and CCAO-dpcaf treated rats.....246
Figure 7.37. ANP and BNP involvement in natriuresis and diuresis**.**.....247
Figure 7.38. Competitive ELISA of ANP. Substrate addition to the plate wells (A). Stop.....248
reagent addition to the plate wells (B).....248
Figure 7.39. A four-parameter logistic curve was plotted and ANP concentrations of the.....249
unknowns were determined by extrapolation from this curve.....249
Figure 7.40. Rat Plasma ANP levels from first, second and third blood withdrawal before.....252
and after surgery including 24-reperfusion.....252
Figure 7.41. ANP levels in different tissues of the treated and untreated rats.....253
Figure 7.42. H & E micrograph of the sham rat. Right hemisphere (A). Left hemisphere.....255
(B).....255
Figure 7.43. H & E micrograph of the CCAO rat. Right hemisphere (A). Left hemisphere.....256
(B).....256
Figure 7.44. H & E micrograph of the dpcaf rat. Right hemisphere (A). Left hemisphere.....256
(B).....256

LIST OF TABLES

Table 2.1: Cardiovascular effects following exposure to carbon nanotubes. Toxicity of the CNTs depends on various factors such as dose, animal type, CNT size, functionalization, exposure duration and exposure route. 32
Table 2.2: Functionalized carbon nanotubes and reduced cytotoxic effects. 36
Different functional groups on MWCNTs and SWCNTs have different.....36
toxic effects on different cell types and animal types. 36
Table 3.1. BBDOE to determine optimal pyrolysis conditions of VA-MWCNTs.....74
Table 3.2. BBDOE (A) Silicon Wafer and (B) Quartz Tube walls 93
Table 3.3. VA MWNT production using a combination of various catalysts. 94
Table 3.4: Surface area of pristine and 5M HCl treated MWCNTs.....98
Table 3.5: Wettability of MWCNTs on silicon wafer and quartz tube walls following treatment with 5M HCl 100
Table 4.1: Thickness, internal and external diameters of the VA-MWCNTs. 122
Table 5.1. MWNT production using a combination of various catalysts. 164
Table 5.2. Surface area of pristine and 5M HCl functionalized MWCNTs. 165
Table 6.1. Band shifts and intensities with the degrees of functionalisation. 191
Table 7.2. Concentrations of the standards of dpcaf. 242
Table 7.3. Concentrations determined from extrapolation of the standard curve. ...243
Table 7.4. Dpcaf calibrators for construction of 4PL standard curve. A set of six standards were prepared and scanned using Victor 3X microplate reader. 244
Table 7.5. Sample concentrations of dpcaf treated CCAO rats. The concentrations were extrapolated from the standard curve. 245
Table 7.6. ANP calibrators for construction of 4PL standard curve. A set of six standards were prepared and scanned using Victor 3X microplate reader. 249

Table 7.7. Sample concentrations of plasma ANP. The concentrations were extrapolated from the standard curve. 249
Table 7.8. Histological evaluation of the rat brain tissue following treatment with dpcaf..... 254

CHAPTER 1
INTRODUCTION AND RATIONALE FOR THIS RESEARCH

1.1. Background of stroke

Stroke is defined as a swift persistent neurological defect caused by a burst or occlusion of the blood vessels supplying the brain. Stroke can either be haemorrhagic or ischemic in nature depending on the root cause. Haemorrhagic stroke is caused by a damage of a blood vessel wall and this injury leads to the internal brain bleeding. Haemorrhagic stroke is sub-categorised into intracranial haemorrhage (ICH) and sub-arachnoid haemorrhage (SAH). ICH which is composed of 10 % refers to the direct brain bleeding. SAH is composed of 3 % and refers to the bleeding within the cranial space but outside the brain. Ischemic strokes occur when there is a major cerebral artery occlusion by thrombus or embolism as depicted in **Fig.1.1**. The blood flow to the brain is reduced leading to a major decrease in oxygen, glucose and nutrients supply to the diseased area (Mokin et al., 2014; Tjoumakaris, Pascal M. Jabbour, & Rosenwasser, 2012; Bretón, César, & Rodríguez, 2012). Ischemic stroke is the dominant type of stroke and contributes 85 - 87 % of all the strokes (Ciccone, Cappella and Borgna-Pignatti, 2011; Mokin *et al.*, 2014). If effective treatment is delayed or not given at all, about 714 km fibres, 813 billion synapses and 120 million neurons die every hour as a result of ischemic stroke (Ciccone, Cappella and Borgna-Pignatti, 2011).

Stroke is preceded by risk factors which co-exist and have an elevated inflammatory profile that contributes 60 - 80 % of stroke. The other 20-40 % is mediated by genetic and environmental factors. Stroke has co-morbidities such as diabetes mellitus, hypertension, obesity, atherosclerosis and infection (Murray et al., 2013). These co-morbidities are linked to dysfunctional systemic inflammatory processes characterised by inflammation. One of the earliest inflammatory responses to stroke is an increased levels of peripheral leukocytes. Cytokines such as TNFα and IL-6 and proteases such as matrix metallopeptidase (MMP-9) are elevated due to stroke (Denes et al., 2010). Systemic inflammation is therefore strongly linked to stroke. The non-modifiable risk factors are of a genetic nature and they include genetic inheritance of the disease. Gender, ethnicity and age are classified as non-modifiable risk factors. The modifiable

risk factors include arterial hypertension, smoking, diabetes, hyperlipidemia, atrial fibrillation, sickle cell disease, obesity, physical inactivity, alcohol abuse, hyper-homocysteinemia, hypercoagulability and oral contraceptive use (Renjen PN, Beg MA, 2015).

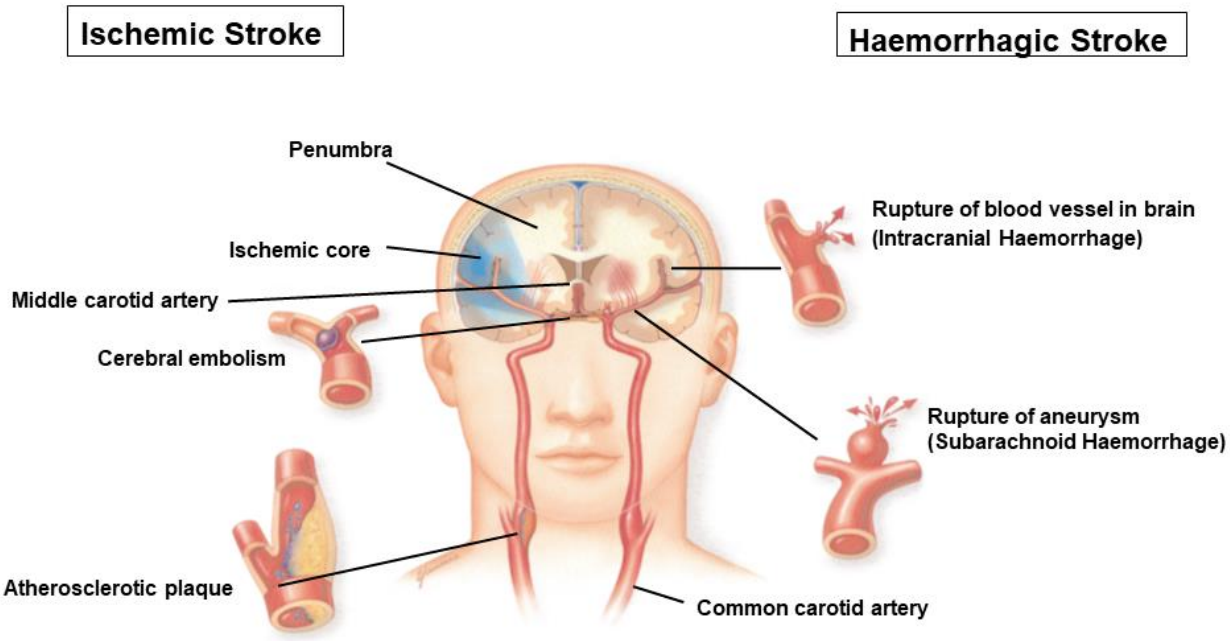


Figure 1.1: Two types of stroke. Image adapted from Green, Odergren, & Ashwood, 2003 with permission from Elsevier.

Age is the most vital non-modifiable risk factor in both males and females. Individuals of any age can suffer from stroke but it is more prevalent in the older age (Chen *et al.*, 2010). Paediatric strokes are very rare with an estimated incidence of 13/100 000. Whilst more than 80 % of strokes in adults are ischemic in children 45 % of strokes are haemorrhagic. Common risk factors in children are congenital cardiac disease, sickle cell disease, infections and a variety of prothrombotic conditions (Ciccone, Cappella and Borgna-Pignatti, 2011).

Stroke was ranked as the second most popular root cause of death in the developed countries preceded by cardiac infarction (Chen *et al.*, 2010). It became the third cause of death succeeding the heart and oncologic disorders (Shahpouri *et al.*, 2012; Tjoumakaris, Pascal M. Jabbour and Rosenwasser, 2012; Jivan, Ranchod and Modi, 2013; Modi, 2013; Hlavica *et al.*, 2015) and the second most common cause of dementia (Glickman *et al.*, 2011). As a result of improvement in the lifestyle of people, it is currently the fourth root cause of death after cardiac, oncologic and pulmonary

diseases (Towfighi and Saver, 2011; Maldonado, Kazmi and Suarez, 2014; Michelle P. Lin and Sanossian, 2015) and the primary cause of permanent disability globally (Deb, Sharma and Hassan, 2010).

It accounts for 9.7 % of global death rate of 56 x 10^6 people annually (Mukherjee and Patil, 2011). Around 15 x 10^6 people have a stroke globally every year (Macrez et al., 2011). Prevalence of stroke is expected to rise significantly around the globe in the years that lie ahead as the world population above 65 years increases by 9 million people annually.

The symptoms of stroke may involve sudden unilateral numbness of the limbs or face. In addition to these symptoms, stroke patients may have some or all of the following symptoms; amnesia, impaired speech (dysphasia), sudden loss of vision, sudden walking trouble, terrible headache, loss of coordination, reduced sensation, aphasia, ataxia, confusion, hearing difficulty, inability to move the head to one direction and loss of consciousness (Leach, 2010; Moskowitz, Lo and Iadecola, 2010). These symptoms could be averted if proper diagnosis and treatment are provided to the patient.

1.2. Pathophysiological mechanisms of stroke

Cerebral ischemia activates a cascade of events of biochemical, physiological, genetic and molecular mechanisms that have a negative impact on the functions of the neurologic set-up (Bretón, César and Rodríguez, 2012). There are three regions (**Figure 1.2**) that are formed in the infarcted brain because of the insufficient blood flow to the cerebrum (CBF) namely i) benign oligemia (reduced CBF but normal neuronal function, ii) penumbra ischemia - ischemia with neuronal function loss that is reversible with reperfusion and iii) core ischemia- tissue injury that is not reversible despite the reperfusion (Suwanwela and Koroshetz, 2007). These important three regions are depicted in **Figure 1.2**.

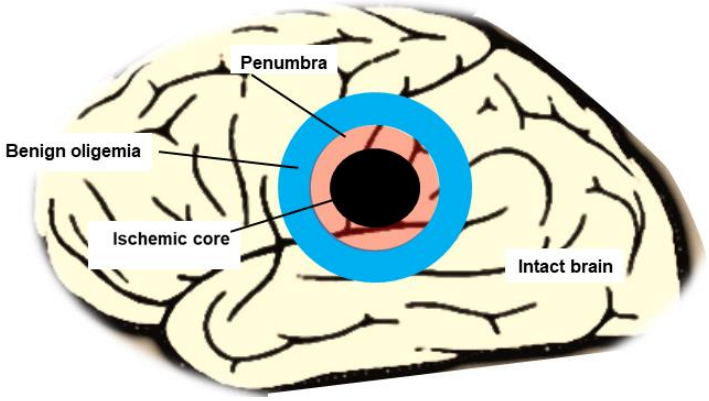


Figure 1.2: Three regions in the infarcted brain due to acute ischemic stroke (Benign oligemia, penumbra and ischemic core). Image adapted from Belayev with permission from Elsevier (Belayev, Lu and Bazan, 2012).

The intact region of the brain is fully functional as the neurons have not been affected. The ischemic core region is irreparable as the neuronal cells are dead in this region. Benign oligemia and penumbra areas can be repaired as some of the cells are still viable in these regions.

1.3. Mechanism of ischemia

Ischemia triggers brain damage by activating the ischemic cascade of events. During this process, ATP is depleted as a result of lack of oxygen and glucose that are required to phosphorylate ADP to ATP (**Fig. 1.3**). ATP in the brain is used to maintain the intracellular homeostasis and transmembrane gradients of ions namely Na^+, K^+ and Ca^{2+} (Thompson and Ronaldson, 2014). The depletion of energy in the neurons causes ion gradient disturbance via a halt of ATP-dependent Na^+/K^+-ATPase and Ca^{2+} -ATPase activity. The neuronal cells release glutamate and the extracellular levels increase which lead to activation of glutamate –mediated channels. K^+ is lost in exchange of Na^+ and Ca^{2+} and the Na^+ uptake is accompanied by influx of Cl^- (Deb, Sharma and Hassan, 2010; Ramos-Cabrer *et al.*, 2011).

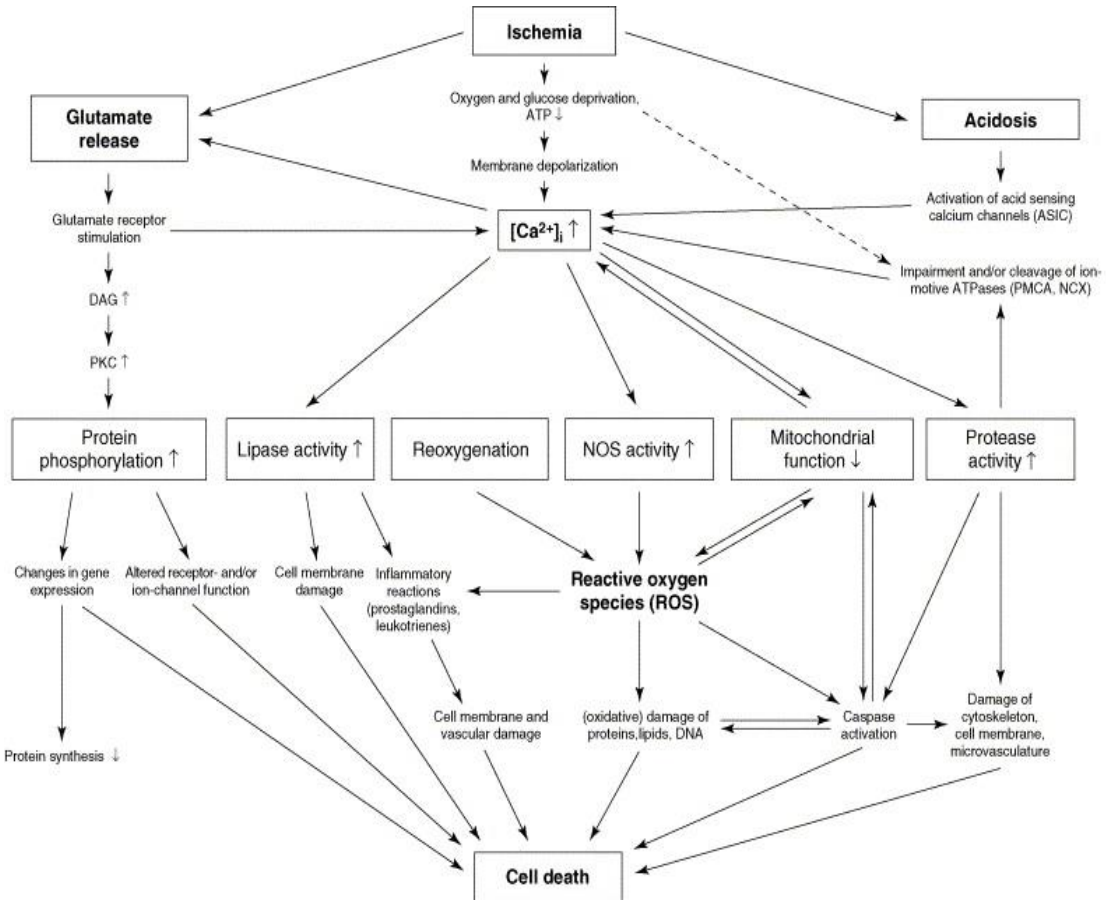


Figure 1.3: Mechanism of ischemia in acute ischemic stroke. Image reproduced from Culmsee & Krieglstein, 2005 with permission from Elsevier.

Extracellular fluid follows the direction of movement of Na^+ and Cl^- into the cell resulting in cytotoxic oedema. Ca^{2+} influx activates nitric oxide synthase leading to the generation of nitric oxide and highly toxic peroxynitrite radicals. The neuronal cells die as a result of excitotoxicity from the free radicals generated (Ramos-Cabrer *et al.*, 2011; Thompson and Ronaldson, 2014).

Understanding the mechanisms that underline neuronal death due to stroke is of the utmost importance in the design of the effective treatment agents for stroke. There is a need for proper diagnosis and therapy of stroke to curb the health problems that are associated with stroke. The impact of stroke on the world economy may be atrocious if effective and efficient therapeutic and preventive plan of action is not executed to help curb the burden of this disease.

1.4. Problem statement

Magnetic Resonance Imaging (MRI) and Computed Tomography (CT) are the imaging techniques that are currently used for diagnosing stroke but their use is limited by availability, cost and radiation exposure. The basic principles of treatment of ischemic stroke are acute supportive care, acute therapy, prevention and rehabilitation (Vangilder *et al.*, 2011; Tjoumakaris, Pascal M. Jabbour and Rosenwasser, 2012; Sander, 2013). Intra-arterial mechanical thrombolysis using FDA approved mechanical devices such as stent retrievers is also used for arterial recanalization (**Figure 1.4**).

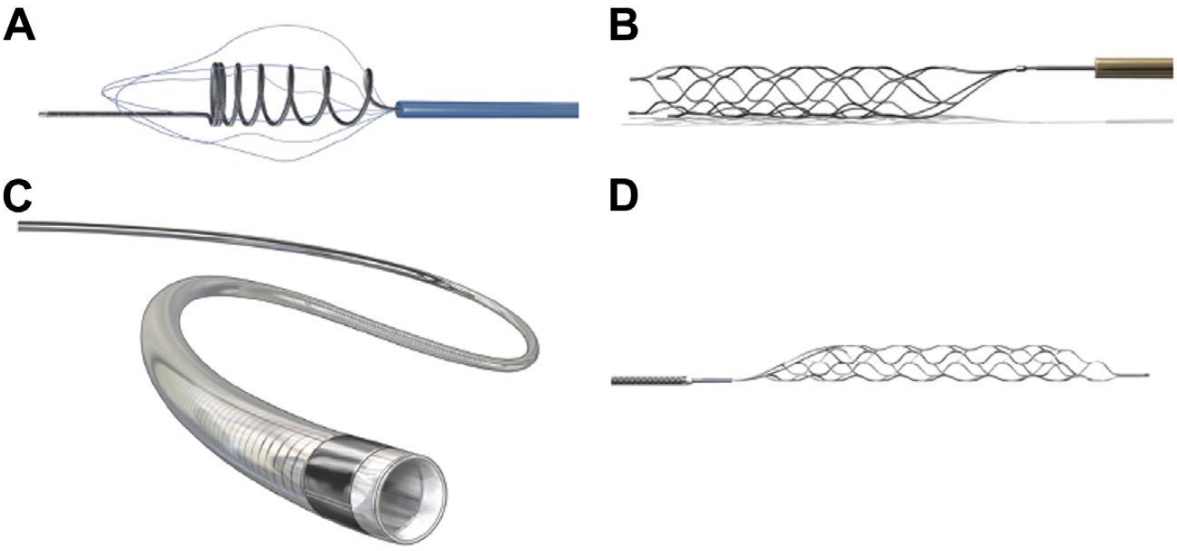


Figure 1.4. Devices approved by the FDA for acute stroke clot removal: (A) MERCI retriever, (B) Solitaire stent retriever, (C) Penumbra aspiration system, and (D) TREVO2 stent retriever. Images reproduced from Lin & Sanossian, 2015a with permission from Elsevier.

Penumbra system is a mechanical aspiration device for fragmenting and aspirating the clot distally in the blood vessel to revascularize the blood vessel in stroke patients (**Figure 1.5**). But there are risks involved in mechanical thrombolysis such as endothelial damage, permanent vascular injury, vessel rupture and the dislodged clot becoming an embolic source to the already compromised distal circulation.

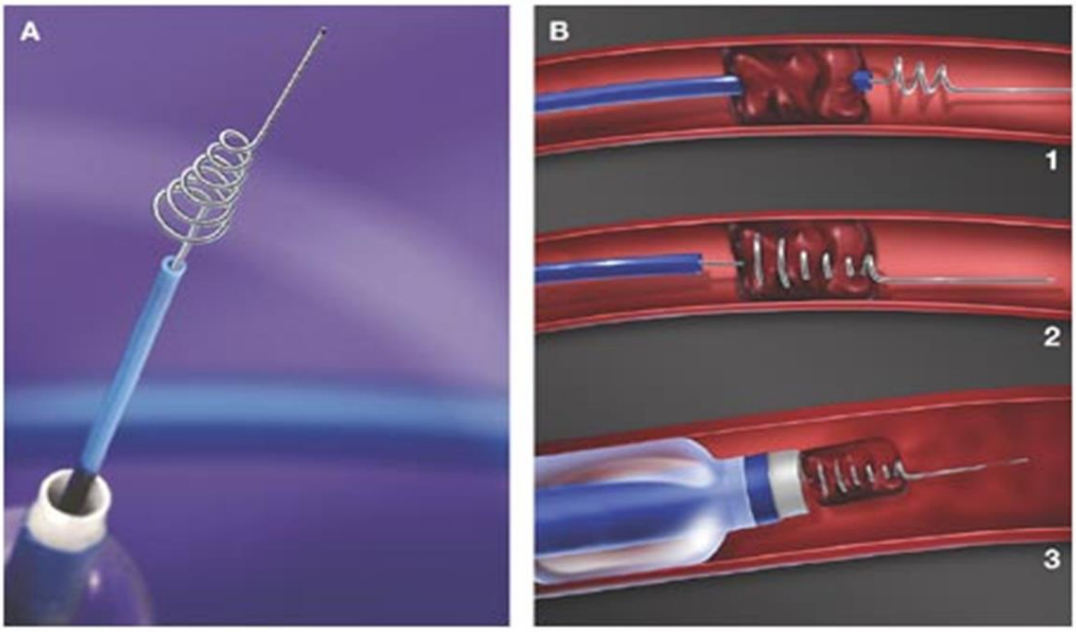


Figure 1.5: Penumbra system for thromboaspiration. Image reproduced from Alexandrov et. al., 2010 with permission from Elsevier.

Recombinant tissue plasminogen activator (rt-PA) is currently the only therapeutic drug that has been approved by FDA in 1996 for the treatment of stroke. It operates effectively by busting the intravenous clot hence recanalizing the blood vessel (Gorelick and Ruland, 2010; Jivan, Ranchod and Modi, 2013). The rt-PA plays a vital role in restoring the blood flow and oxygen supply to the ischemic site. The shortfalls of rt-PA include narrow therapeutic window (3 hours), haemorrhage within the cerebrum and other unfavourable effects (Jivan, Ranchod and Modi, 2013). Current stroke guidelines have extended therapeutic rt-PA administration window from 3hrs to 4.5hrs (Chen *et al.*, 2010; Gorelick and Ruland, 2010).

Glucocorticoids such as methylprednisolone and dexamethasone are used for the acute treatment of ischemic stroke which involves the dissolution of blood clots (Murray et al., 2013). These glucocorticosteroids have outstanding anti-inflammatory properties making them potentially effective for the ischemic stroke therapy. Glucocorticoids have been proven to be of great benefit in the treatment of cerebral oedema and cerebrovascular disease inflammation. These glucocorticoids have the ability to penetrate the blood brain barrier (BBB) to access the brain (Tuor, 1997). However, their short circulatory half-lives, poor pharmacokinetics, higher dose administration lead to adverse systemic side-effects hence affecting their therapeutic potential negatively (Tuor, 1997; Psarros et al., 2012).

The most important aim of the drug therapy for acute ischemic stroke is to rescue the penumbra as much and as early as possible (*i.e. time is brain*) to avoid the continuous enlargement of the ischemic core and aggravation of neurological outcomes (Thompson and Ronaldson, 2014). The challenge in drug delivery for treatment of ischemic stroke is a drop in the flow of blood to the penumbra. A decrease in drug central nervous system (CNS) availability reduces the drug ability to attain efficacious levels at its target site. Blood brain barrier (BBB) permeability is increased during ischemic stroke and this makes it possible for drugs and other fluid to move easily from blood to the brain (Thompson and Ronaldson, 2014).

Since our main focus is on inflammatory biomarkers in ischemic stroke, therefore dexamethasone is highly relevant in our research. The current challenges with glucocorticoid therapy may be overcome by utilization of a targeted drug delivery system to inflammatory biomarkers present in ischemic stroke such as NR2 peptide, ANP and BNP. Carbon nanotubes (CNTs) may be used as vehicles for ferrying target ligands and drugs to the diseased site. Carbon nanotubes are inert and insoluble in aqueous environment but can be modified by functionalization. Functionalization of the CNTs increases permeability of drug into tissues, coupling of the drug to CNTs, and biocompatibility. Cytotoxicity of the carbon nanotubes might as well be reduced by functionalization (Zhang, Zhang and Zhang, 2011).

In this study, dexamethasone will be used as the model anti-inflammatory drug to be targeted to the ischemic site. Dexamethasone will be tested for its efficacy for the targeted treatment of ischemic stroke. Functionalized carbon nanotubes will be used as the delivery vehicles for this anti-inflammatory drug as they are non-immunogenic, non-toxic, cell membrane penetrable, size alterable and have a high drug-loading efficiency (Ji et al., 2010).

1.5. Rationale and motivation

The diagnosis of stroke is a major challenge as the current diagnostic tools have the drawbacks such as availability due to their skyrocketing cost of the instrument (MRI and CT) and sample analysis. In addition, some of these instruments rely on the use of radioisotopes which are carcinogenetic. Based on these challenges, there is a need for an ultrasensitive diagnostic tool which is most affordable and cost effective for early

detection of stroke at its embryonic stage. There is also a need for the most efficient and effective therapeutic system for the stroke treatment.

This study involves a two-fold approach namely, a diagnostic and a therapeutic approach but the main focus will be on the ischemic stroke treatment. For diagnosis of ischemic stroke, functionalized CNTs will be designed for detection of inflammatory biomarkers of ischemic stroke using CNT forests (vertically aligned carbon nanotubes) as shown in **Figure 1.6**. CNT forests may be superior to ELISA and multiplex assays since they are rapid, cost-effective and can be synthesized easily in the laboratory. Their sensitivity can be monitored as desired. In addition, they are user-friendly and may be tailored for point of care use in the clinical setting. The main features of carbon nanotubes which make them the most important tool over other nano-carriers are cell membrane penetrability, super stability, non-immunogenicity, easy size modification, improved efficiency of drug-loading and biocompatibility when they are functionalized (Vardharajula et al. 2012).

For ischemic stroke therapy, a second injectable carbon nanotube system will be designed for drug targeting of inflammatory biomarker (ANP) that is up-regulated at the site of a stroke event. It has been demonstrated that BBB is disrupted in the acute phase following an ischemic trigger. Disruption causes a rise in the permeability of the vascular escalating to the leakage of low and high molecular weight circulating molecules into the parenchyma of the brain during cerebral ischemia (Ishii et al., 2013).

Biomarkers for ischemic stroke such as Brain Natriuretic Peptide (BNP), N-methyl-D-aspartate Receptor Degradation Product (NR2) and Atrial Natriuretic Peptide are up-regulated in ischemic stroke (Brambilla, Couch and Lambertsen, 2013). The circulating biomarkers are distributed all over the body but the highest concentration is located at the site of ischemic stroke and hence the antibody-drug complex will predominantly accumulate at the ischemic stroke site as a result of the highest concentration of these biomarkers (Aguilar, 2013).

Giuffrida and his colleagues (Giuffrida et al., 1992) demonstrated that ANP and other vasoactive peptides were significantly increased in the infarcted forebrain of the Mongolian Gerbil. A statistically significant increase in ANP-immunoreactive glial cells

in the cerebral white matter surrounding the ischemic core compared with the intact area was observed by Noqami and his co-workers (Nogami et al., 2001).

It was demonstrated by Kim and his co-workers (Kim, Moon and Bang, 2013) that cerebral infarction volume and plasma BNP in patients with cerebral infarction were positively correlated and the correlation could suggest the potential origin of plasma BNP is the damaged brain. Brosnan and his colleagues (Brosnan et al., 1999) have shown a significant increase in ANP and BNP in both the brain and plasma in stroke-prone hypertensive rats following Middle Cerebral Artery Occlusion. Nakagawaka and his co-workers (Nakagawaka et al., 2005) demonstrated a significant increase in plasma BNP in cerebral infarction patients with atrial fibrillation than in patients without atrial fibrillation and controls.

Gappoeva and co-workers (Gappoeva et al., 2003) have shown that NR2A and NR2B receptors were significantly expressed in the cortices of cerebral ischemic rat models following Middle Cerebral Artery Occlusion. A drastic increase in the NR2A/B expresssion in the cornu ammonis 1 (CA1) region of the hippocampus in rats was observed by Won and colleagues (Won et al., 2001) following induction of forebrain ischemia.

Based on the above findings, monoclonal antibodies against Atrial Natriuretic Peptide (ANP), N-methyl-D-aspartate Receptor Degradation Product (NR2 peptide) and Brain Natriuretic Peptide (BNP) are injected intravenously and have to be transported across the Blood Brain Barrier (BBB) to reach the ischemic site. But in ischemia, since the BBB is disrupted, so it will be easy for the antibody-drug complex to gain access to the ischemic core and penumbra. Also, biomarkers are highest in ischemic area, so the monoclonal antibodies should bind preferentially to the biomarkers at the ischemic site in the brain and less so peripherally outside the brain or in the blood. Since BBB is leaking, therefore the biomarkers will leak into the blood. Antibodies can reach biomarkers in the blood but predominantly in the ischemic site because of the higher levels. The antibodies against these biomarkers can then be detected in the blood using the carbon forest system (**Figure 1.6**).

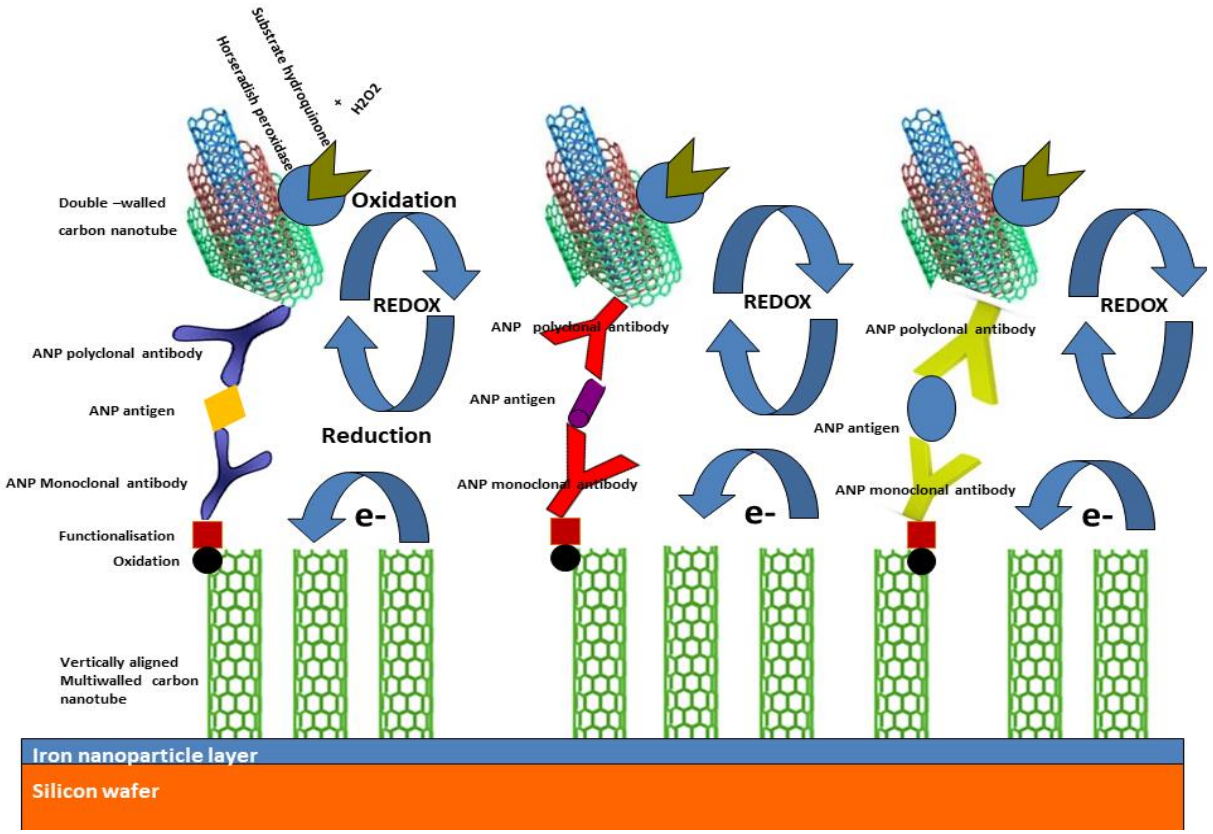


Figure 1.6: Schematic conceptualization of carbon nanotube forests synthesis for detection of ANP antigens in the blood.

Forest carbon nanotubes will be immobilised on a silicon wafer. Carbon nanotubes will be oxidized with a mixture of HNO_3 and H_2SO_4 (3:1). Capture antibody will be attached to a CNT forest through conjugation of 1-ethyl-3-(3-dimethyllaminopropyl) carbodiimide (DCC) and N-hydroxysulfosuccinimide (EDC-NHSS) to develop an immunosensor. The ANP antigen in the sample will then be detected with the secondary Ab coupled to CNT with HRP. The immunosensor will be immersed in a buffer containing hydroquinone and hydrogen peroxide for oxidation to occur. Amperometric response will be recorded following voltage application.

Capture antibody will be linked to a carbon nanotube forest through coupling by 1-ethyl-3-(3-dimethyllaminopropyl) carbodiimide and N-hydroxysulfosuccinimide (EDC-NHSS) to create an immunosensor. The sample containing the biomarker (ANP) will then be incubated with the immunosensor and bound antigen detected with a second antibody attached to carbon nanotube conjugated with horseradish peroxidase. The immunosensor will be immersed in a buffer containing hydroquinone and hydrogen

peroxide where hydroquinone oxidation occurs. Upon application of voltage, an amperometric response will be recorded.

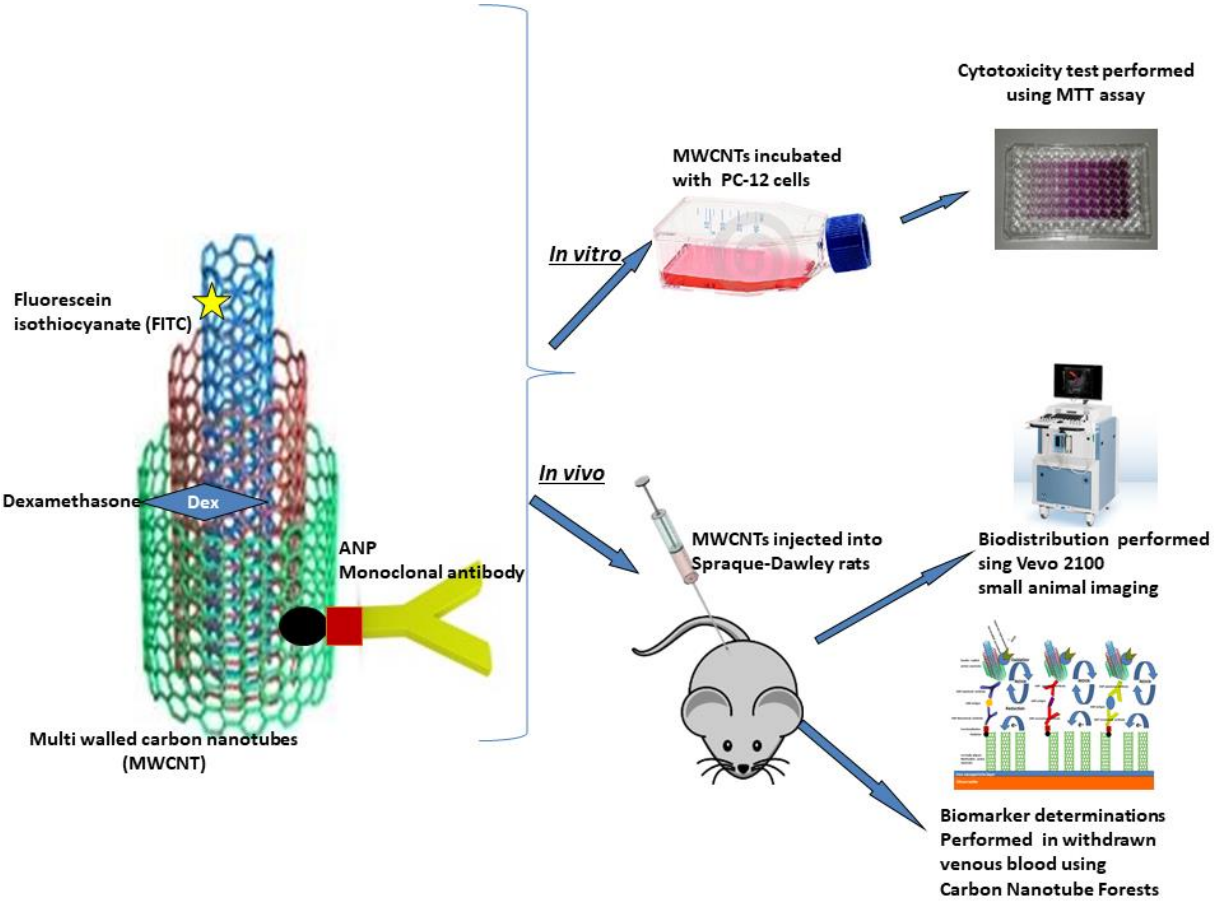


Figure 1.7: Multiwalled Carbon nanotube (MWCNT) armed with monoclonal antibodies against inflammatory biomarker (ANP) in ischemic stroke and with anti-inflammatory drug (dexamethasone) for ischemic stroke treatment.

The recommended intravenous injection of dexamethasone is 6 $mg.kg^{-1}$ body weight and for methylprednisolone is 30 $mg.kg^{-1}$ body weight. Doses above these are considered to be toxic. The MWCNTs will be oxidized and functionalized and the antibodies will then be coupled to them. A fluorescent tag (fluorescent isothiocyanate, FITC) will also be coupled to the MWCNT for intracellular distribution. The cytotoxicity of the MWCNT system will be determined by incubating the treated MWCNT with the PC-12 cells and MTT assays performed thereafter. If the treated MWCNTs are found to be non-toxic, then the treated MWCNTs will be injected into the Sprague Dawley rat via tail vein.

The CNT will be functionalized with polyethylene glycol (PEG) to increase dispersibility in the aqueous environment and to reduce toxicity, increase biocompatibility and blood

circulation times. Functionalization of the CNTs with PEG suppresses macrophage recognition by decreasing adsorption of proteins and surface opsonization leading to the prolongation of circulation which allows controllable drug release into the blood (Aguilar, 2013). The intravenously injected CNT-Drug complex gets directly into blood circulation and distributes in various internal organs and tissues (Zhang, Zhang and Zhang, 2011). CNTs equipped with drugs can be concentrated preferentially at the sites of inflammation because of the enhanced permeability and retention effect of the blood vessels (Aguilar, 2013). Carbon nanotubes can act as a localised drug warehouse following accumulation at the target site (Singh and Lillard, 2009).

PEGylated CNT-drug complex Drug carries the drug into the reticuloendothelial system (RES) organs. The *in vivo* ester bond is cleaved from the framework and is released to the site of interest. The drug clearance is done via the biliary pathway, and the drug ends up in the faeces once it has accomplished its work (Liu et al., 2008). The framework or free CNTs will also be cleared from the body once they have served their purpose. Since the corticosteroids accumulate preferentially at the ischemic stroke site, their side-effect profile will be diminished due to altered pharmacokinetics and will allow more effective concentrated low doses of drug to be administered (Ning et al., 2012). The MWCNTs will be cleared from the blood and excreted through the kidneys (Zhang, Zhang and Zhang, 2011).

The distribution of the drug in various organs will also be traced using a microplate reader equipped with fluorescence filter since the fluorescent dye will be attached to the CNT together with the drug. The organs will also be harvested, and fluorescence intensity determined using a microplate reader. This proposed system may lead to the superior treatment of ischemic stroke of which in turn may result in mortality rate reduction, a decrease in morbidity and disability rate from stroke.

1.6. Aims and objectives

The aim of this research is to design a functionalized carbon nanotube system that can be used for drug-targeting of inflammatory biomarkers that are up-regulated at the site of an ischemic stroke. In addition, a second carbon nanotube system will be designed for potential superior diagnosis of ischemic stroke. The following objectives will be fulfilled in order to achieve this aim.

- To synthesise carbon nanotube (CNT) forests (vertically aligned CNTs) for the detection of the inflammatory biomarkers (ANP) from the blood of the Sprague Dawley (S.D) Rat Stroke model.
- To characterise the synthesized CNT forests using surface characterisation techniques such as Surface Area and Pore Analyser, Raman Spectroscopy, Zetasizer, Cyclic Voltammetry, Thermogravimetry, Infra-Red Spectroscopy, and Electron Microscopy.
- To induce ischemic stroke in S.D rats using the Common Carotid Artery Occlusion (CCAO) to stimulate production of the inflammatory biomarkers
- To detect inflammatory biomarkers in the ischemic stroke model S.D. rats using CNT forests and ANP ELISA
- To load biomarker antibodies, fluorescent tag and anti-inflammatory drugs on CNTs
- To evaluate the drug-loaded CNT system for cytotoxicity using MTT assays in PC12 cell lines
- To trace the distribution of CNTs in different organs in the S.D. Rat Stroke Model using Fluorescence microplate reader

1.7. Novelty of the study

The novelty of the study lies in the coupling of dexamethasone, ANP antibody, FITC to a PEGylated vertically aligned multiwalled carbon nanotube (VA-MWCNT). Dexamethasone, an inflammatory drug will be delivered in a minute dose to an ischemic site. ANP antibody attached to VA-MWCNTs will be used for targeting purpose. In this study, MWCNTs are synthesised and used as they have many cavities for effective encapsulation and they are also vertically aligned to improve their electrical properties to enhance an interaction with drugs and other molecules. MWCNTs are also PEGylated with a multi-chain polymer DSPE-PEG5000-4-arm (PEG-amine) to further improve their interaction with drugs, antibody, FITC and biomolecules.

In addition, PEGylation improves MWCNTs delivery in circulation as PEG suppresses macrophage recognition by inhibiting protein adsorption and surface opsonization leading to the prolongation of circulation which allows controlled release of the drugs in the blood. A carbon nanotube system will be designed for drug targeting and treatment of ischemic stroke. In addition, the system will also be modified to be utilised

as a superior diagnostic device for ANP detection. The antibodies against the inflammatory biomarker namely, ANP in ischemic stroke will be coupled to the vertically aligned carbon nanotube forests. Antibodies against biomarkers of ischemic stroke, fluorescent isothiocyanate (FITC) and anti-inflammatory drug namely, dexamethasone will be attached to the carbon nanotubes for targeting and treatment of ischemic stroke. The formulations will be evaluated for cytotoxicity and followed by application in diagnosis and treatment of ischemic stroke. This hypothesis provides the first account of functionalized vertically aligned multi-walled carbon nanotubes in targeting and transporting dexamethasone in ischemic stroke intervention.

1.8. Overview of the thesis

The thesis was anatomised as follows;

Chapter 1 of this thesis is a springboard for outlining a concise background, the rationale and motivation of this study, current drawbacks in diagnosis and treatment of ischemic stroke as well as the aim and objectives of this research.

Chapter 2 of this thesis provides a comprehensive literature review on the detection and therapy of neurological disorders including ischemic stroke using carbon nanotube technology. It gives the background of carbon nanotubes, their cytotoxicity and functionalisation of the carbon nanotubes for biomedical application. This chapter carries on by outlining the use of the CNTs in CNS imaging, drug delivery and neuroengineering. It also incorporates recent advances in stroke treatment, CNTs in the market and lastly their future potential applications.

Chapter 3 of this thesis describes the step by step synthesis of multiwalled carbon nanotubes for potential application in diagnosis and treatment of ischemic stroke. Optimal pyrolysis conditions were determined to produce super-aligned multiwalled carbon nanotubes. MWCNTs were characterised using various methods such as FTIR, contact angle, XRD, SEM and TEM. Furthermore, MWCNTs were purified and functionalised using a variety of acids at different concentrations.

Chapter 4 of this thesis provides pre-formulation of the carbon nanotube system for potential use in detection and treatment of ischemic stroke. A carbon nanotube based nano-electrode was manufactured on silicon wafer and assessed for its application in

the design of an immunosensor for ANP detection. The electrode was purified using thermal oxidation and HCl treatment. It was characterised by SEM, cyclic voltammetry and electrochemical impedance spectroscopy. MWCNTs harvested from the walls of quartz tube were purified, carboxylated, and PEGylated to prepare them for implementation in stroke therapy.

Chapter 5 of this thesis describes the synthesis and characterisation of MWCNTs, loading and release of dexamethasone from carbon nanotubes. Furthermore, cytotoxicity of the dexamethasone loaded MWCNTs was evaluated in PC-12 cells. The non-cytotoxic concentration range of MWCNTs was determined using MTT assay.

Chapter 6 of this thesis details the coupling of ANP antibody to MWCNTs decorated with dexamethasone and FITC. Morphological changes were confirmed with SEM and TEM. The nano-complex was characterised with Uv-Vis, FTIR, FEEM, Fluorescence spectroscopy and Raman. In this chapter, the dexamethasone loaded PEGylated MWCNTs labelled with FITC and coupled to ANP antibody was thoroughly prepared and characterised for potential application in the treatment of stroke.

Chapter 7 of this thesis provides the application of the synthesised carbon nanotube system in the SD rats induced with stroke. In this chapter, SD rats were induced with ischemic stroke and MWCNTs were intravenously administered to assess the potential use of these carbon nanotubes in the treatment of stroke. ANP levels were measured before and after stroke induction. Fluorescence intensities were also measured after harvesting various organs from the untreated and treated groups. Neurobehavioural and histopathological studies were utilised to assess the efficacy of the carbon nanotube system in the treatment of ischemic stroke.

Chapter 8 of this thesis presents the concluding remarks of this study. In addition, this chapter includes the beneficial impact of this study and future recommendations for improvement of the system.

1.9. Concluding remarks

This chapter highlighted the challenges associated with the current diagnosis and treatment of ischemic stroke. It outlines the mitigation strategies in resolving the challenges to improve diagnosis and treatment. It further highlighted the ability of vertically aligned multiwalled carbon nanotubes to ferry dexamethasone to ischemic site. Furthermore, this chapter presented the rationale and motivation, aims and objectives, novelty and the potential therapeutic benefits of this research.

1.10. References

Aguilar, Z. P. (2013) 'Targeted Drug Delivery', in Aguilar, Z. P. (ed.) *Nanomaterials for Medical Applications*. 1st edn. Elsevier Inc, pp. 181–234.

Belayev, L., Lu, Y. and Bazan, N. G. (2012) 'Brain Ischemia and Reperfusion', *Basic Neurochemistry*, pp. 621–642.

Brambilla, R., Couch, Y. and Lambertsen, K. L. (2013) 'The effect of stroke on immune function.', *Molecular and cellular neurosciences*, 53, pp. 26–33.

Bretón, R. R., César, J. and Rodríguez, G. (2012) 'Excitotoxicity and Oxidative Stress in Acute Ischemic Stroke', in Prof. Rodriguez (ed.) *Acute Ischemic Stroke*, pp. 29–58.

Brosnan, M. J. *et al.* (1999) 'Genes Encoding Atrial and Brain Natriuretic Peptides as Candidates for Sensitivity to Brain Ischemia in Stroke-Prone Hypertensive Rats', *Hypertension*, 33(1), pp. 290–297.

Chen, R.-L. *et al.* (2010) 'Ischemic stroke in the elderly: an overview of evidence.', *Nature reviews. Neurology*, 6(5), pp. 256–265.

Ciccone, S., Cappella, M. and Borgna-Pignatti, C. (2011) 'Ischemic stroke in infants and children: practical management in emergency.', *Stroke research and treatment*, 2011, pp. 1–9.

Culmsee, C. and Krieglstein, J. (2005) 'Nervous system Mechanisms of neuronal degeneration after ischemic stroke – Emerging targets for novel therapeutic strategies', 2(4), pp. 463–470.

Deb, P., Sharma, S. and Hassan, K. M. (2010) 'Pathophysiologic mechanisms of acute ischemic stroke: An overview with emphasis on therapeutic significance beyond thrombolysis.', *Pathophysiology*. Elsevier Ireland Ltd, 17, pp. 197–218.

Denes, A. *et al.* (2010) 'Inflammation and brain injury : Acute cerebral ischaemia , peripheral and central inflammation', *Brain Behavior and Immunity*, 24(5), pp. 708–723.

Gappoeva, M. U. *et al.* (2003) 'Expression of NMDA Neuroreceptors in Experimental Ischemia', *Biochemistry (Moscow)*, 68(6), pp. 696–703.

Giuffrida, R. *et al.* (1992) 'Ischemia-induced changes in the immunoreactivity for endothelin and other vasoactive peptides in the brain of the Mongolian gerbil.', *Journal of cardiovascular pharmacology*, 20 Suppl 1, pp. S41–S44.

Glickman, S. W. *et al.* (2011) 'Discriminative capacity of biomarkers for acute stroke in the emergency department.', *The Journal of emergency medicine*, 41(3), pp. 333–9.

Gorelick, P. B. and Ruland, S. (2010) 'Diagnosis and management of acute ischemic stroke', in *Disease-a-Month*, pp. 72–100.

Green, A. R., Odergren, T. and Ashwood, T. (2003) 'Animal models of stroke: Do they have value for discovering neuroprotective agents?', *Trends in Pharmacological Sciences*, 24(8), pp. 402–408.

Hlavica, M. *et al.* (2015) ‘Pharmacological recanalization therapy in acute ischemic stroke – Evolution, current state and perspectives of intravenous and intra-arterial thrombolysis’, *Journal of Neuroradiology*, 42(1), pp. 30–46.

Ishii, T. *et al.* (2013) ‘Nanoparticles accumulate in ischemic core and penumbra region even when cerebral perfusion is reduced.’, *Biochemical and biophysical research communications*, 430(4), pp. 1201–5.

Ji, S. *et al.* (2010) ‘Carbon nanotubes in cancer diagnosis and therapy.’, *Biochimica et biophysica acta*, 1806(1), pp. 29–35.

Jivan, K., Ranchod, K. and Modi, G. (2013) ‘Management of ischaemic stroke in the acute setting: review of the current status.’, *Cardiovascular journal of Africa*, 24(3), pp. 86–92.

Kim, S. J., Moon, G. J. and Bang, O. Y. (2013) ‘Biomarkers for stroke.’, *Journal of stroke*, 15(1), pp. 27–37.

Leach, R. a (2010) ‘Patients with symptoms and signs of stroke presenting to a rural chiropractic practice.’, *Journal of manipulative and physiological therapeutics*, 33(1), pp. 62–9.

Lin, M. P. and Sanossian, N. (2015) ‘Reperfusion Therapy in the Acute Management of Ischemic Stroke’, *Cardiology Clinics*, 33(1), pp. 99–109.

Lin, M. P. and Sanossian, N. (2015) ‘Reperfusion Therapy in the Acute Management of Ischemic Stroke’, *Cardiology Clinics*, 33, pp. 99–109.

Liu, Z. *et al.* (2008) ‘Drug Delivery with Carbon Nanotubes for In vivo Cancer Treatment’, *Cancer research*, 68(16), pp. 6652–6660.

Macrez, R. *et al.* (2011) ‘Stroke and the immune system: from pathophysiology to new therapeutic strategies.’, *The Lancet. Neurology*, 10(5), pp. 471–80.

Maldonado, N. J., Kazmi, S. O. and Suarez, J. I. (2014) ‘Update in the Management of Acute Ischemic Stroke’, *Critical Care Clinics*, 30(4), pp. 673–697.

Modi, G. (2013) ‘Editorial Acute ischaemic stroke : highlighting the need for early intervention’, *Cardiovascular journal of Africa*, 24(3), p. 51.

Mokin, M. *et al.* (2014) ‘Endovascular management and treatment of acute ischemic stroke’, *Neurosurgery Clinics of North America*, 25, pp. 583–592.

Moskowitz, M. A., Lo, E. H. and Iadecola, C. (2010) ‘The science of stroke: mechanisms in search of treatments.’, *Neuron*, 67(2), pp. 181–98.

Mukherjee, D. and Patil, C. G. (2011) ‘Epidemiology and the global burden of stroke.’, *World neurosurgery*, 76(6 Suppl), pp. S85-90.

Murray, K. N. *et al.* (2013) ‘Systemic immune activation shapes stroke outcome.’, *Molecular and cellular neurosciences*, 53, pp. 14–25.

Nakagawaka, K. *et al.* (2005) 'Plasma Concentrations of Brain Natriuretic Peptide in Patients with Acute Ischemic Stroke', *Cerebrovascular Diseases*.

Ning, R. *et al.* (2012) 'Tissue plasminogen activator treatment of stroke in type-1 diabetes rats.', *Neuroscience*, 222, pp. 326–32.

Nogami, M. *et al.* (2001) 'Immunohistochemistry of atrial natriuretic peptide in brain infarction', *Histochemistry Journal*, 33(2), pp. 87–90.

Psarros, C. *et al.* (2012) 'Nanomedicine for the prevention, treatment and imaging of atherosclerosis.', *Nanomedicine : nanotechnology, biology, and medicine*, 8 Suppl 1, pp. S59-68.

Ramos-Cabrer, P. *et al.* (2011) 'Targeting the ischemic penumbra', *Stroke*, 42(SUPPL. 1).

Renjen PN, Beg MA, A. K. (2015) 'Epidemiological study of incidence and risk factors of Ischemic stroke subtypes according to Trial of ORG 10172 in acute stroke treatment criteria : A 3 years , hospital-based study', *Int J Med Public Health*, 5(1), pp. 50–55.

Sander, R. (2013) 'Prevention and treatment of acute ischaemic stroke', *Nursing Older People*, 25(8), pp. 34–38.

Shahpouri, M. M. *et al.* (2012) 'Anticoagulant therapy for ischemic stroke: A review of literature.', *Journal of research in medical sciences*, 17(4), pp. 396–401.

Singh, R. and Lillard, J. W. (2009) 'Nanoparticle-based targeted drug delivery.', *Experimental and molecular pathology*, 86(3), pp. 215–23.

Suwanwela, N. and Koroshetz, W. J. (2007) 'Acute ischemic stroke: overview of recent therapeutic developments.', *Annual review of medicine*, 58, pp. 89–106.

Taylor, A. *et al.* (2011) 'The Potential use of Carbon Nanotubes for Cancer Treatment', pp. 1–16.

Thompson, B. J. and Ronaldson, P. T. (2014) *Drug delivery to the ischemic brain.*, *Advances in pharmacology (San Diego, Calif.)*.

Tjoumakaris, S. I., Pascal M. Jabbour, A. S. D. and Rosenwasser, L. F. G. and R. H. (2012) 'Endovascular Management of Acute Ischemic Stroke', in Rodriguez, P. J. C. G. (ed.) *Acute Ischemic Stroke*, pp. 121–144.

Towfighi, A. and Saver, J. L. (2011) 'Stroke declines from third to fourth leading cause of death in the United States: Historical perspective and challenges ahead', *Stroke*, 42(8), pp. 2351–2355.

Tuor, U. I. (1997) 'Glucocorticoids and the Prevention of Hypoxic-Ischemic Brain Damage', *Neuroscience & Biobehavioral Reviews*, 21(2), pp. 175–179.

Vangilder, R. L. *et al.* (2011) 'Targeting the neurovascular unit for treatment of neurological disorders.', *Pharmacology & therapeutics*, 130(3), pp. 239–47.

Vardharajula, S. *et al.* (2012) ‘Functionalized carbon nanotubes : biomedical applications’, *International Journal of Nanomedicine*, 7, pp. 5361–5374.

Won, M. H. *et al.* (2001) ‘The alterations of N-Methyl-D-aspartate receptor expressions and oxidative DNA damage in the CA1 area at the early time after ischemia-reperfusion insult’, *Neuroscience Letters*, 301(2), pp. 139–142.

Zhang, W., Zhang, Z. and Zhang, Y. (2011) ‘The application of carbon nanotubes in target drug delivery systems for cancer therapies.’, *Nanoscale research letters*, 6(1), p. 555.

CHAPTER 2
LITERATURE REVIEW ON DIAGNOSIS AND TREATMENT OF NEUROLOGICAL AND ISCHEMIC DISORDERS EMPLOYING CARBON NANOTUBE TECHNOLOGY

Published in Journal of Nanomaterials: Patrick Komane, Yahya E. Choonara, Lisa du Toit, Pradeep Kumar, Pierre Kondiah, Girish Modi and Viness Pillay (2016). "Diagnosis and Treatment of Neurological and Ischemic Disorders Employing Carbon Nanotube Technology." Journal of Nanomaterials, Volume 2016 (2016), Article ID 9417874, 19 pages.

Abstract

Extensive research on carbon nanotubes has been conducted due to their excellent physico-chemical properties. Based on their outstanding physico-chemical properties, carbon nanotubes have the potential to be employed as theranostic tools for neurological pathologies such as Alzheimer's disease and Parkinson's disease including ischemic stroke diagnosis and treatment. Stroke is currently regarded as the third root cause of death and the leading source of immobility around the globe. The development and improvement of efficient and effective procedures for central nervous system disease diagnosis and treatment is necessitated. The main aim of this review is to discuss the application of nanotechnology, specifically carbon nanotubes, to the diagnosis and treatment of neurological disorders with an emphasis on ischemic stroke. Areas covered include the conventional current diagnosis and treatment of neurological disorders, as well as a critical review of the application of carbon nanotubes in the diagnosis and treatment of ischemic stroke, covering areas such as functionalization of carbon nanotubes and carbon nanotube-based biosensors. A broad perspective on carbon nanotube stimuli-responsiveness, carbon nanotube toxicity and commercially available carbon nanotubes is provided. Potential future studies employing carbon nanotubes have been discussed, evaluating their extent of advancement in the diagnosis and treatment of neurological and ischemic disorders.

2.1. Introduction

Neurological and ischemic disorders incorporate a variety of sporadic and hereditary conditions. They are characterized by the progressive loss of structure and function of neurons often associated with neuronal death. The causes of neurological and ischemic diseases are very complex and are linked to a variety of factors such as aging, lifestyle, environmental factors and heredity (Gilmore et al., 2008; Modi, Pillay and Choonara, 2010; Re, Gregori and Masserini, 2012).

Alzheimer's disease (AD) and Parkinson's disease (PD) are the most common neurodegenerative diseases. An estimated 24 million people around the globe suffer from dementia and AD comprises 60 % of this number. AD is characterized pathologically by cerebral atrophy and clinically by memory and learning impairment (Modi, Pillay and Choonara, 2010). According to the Alzheimer's Association, 13% of people over 65 suffer from AD in developed countries. It is the fifth leading cause of death in patients at this age (Folch, J., Petrov, D., Ettcheto, M., Abad, S., Sanchez-Lopez, E., Garcia, M.L., Olloquequi, J., Beas-Zarate, C., Auladell, C., Antoni, 2015). The cause of AD is unknown and current treatment are symptomatic. Current treatments for cognitive impairment in AD are based on neurotransmitter or enzyme replacement. These provide a wide spectrum of symptomatic benefits and include acetylcholinesterase inhibitors, antioxidants, amyloid-targeted drugs and nerve growth factors. It seems that none of the available therapies are able to cure AD or to attenuate its progression. Nanotechnology may provide a possible solution to overcoming many obstacles for the treatment of AD by affording targeted drug delivery and enhancing the bioavailability and efficacy of various drugs and other bioactive agents (Modi et al., 2009).

Parkinson's disease (PD) is a central nervous system disease with difficulties in body movements. Typical symptoms include tremor, rigidity and bradykinesia, unstable posture, difficulty in walking (Singh, Pillay and Choonara, 2007). PD is the second most common neurodegenerative disorder after Alzheimer's disease. It affects more than 5 million people globally and approximately a million people in the USA. The hallmark features of PD pathology include progressive loss of dopaminergic neurons leading to significant loss of the dopaminergic levels. Dopamine (DA) is the neurotransmitter responsible for transmitting the electrical signals required for normal physical motion. This deficit is treated by restoration of dopaminergic activity by levodopa (precursor of

dopamine) and dopamine receptor antagonist. Currently, frontline therapy for PD is the oral administration of dopamine agonists such as levodopa. Patients become less responsive to levodopa as the disease progresses and begin to develop motor side-effects. Adverse effects include constipation, urinary retention, glaucoma and cognitive impairment (Kakkar and Dahiya, 2015). PD remains incurable to date. The current pharmacological and non-pharmacological treatments are able to offer only symptomatic relief for the patients. Available therapies aim to improve the functional capacity of the patient for as long as possible; however they do not modify the progression of the neurodegenerative disorder (Singh, Pillay and Choonara, 2007). The advent of nanotechnology may provide a solution to overcome the diagnostic and neurotherapeutic challenges of this disease.

Ischemic disorders include ischemic stroke which can be defined as a rapid onset of a persistent neurologic deficit. It is a cerebrovascular disorder whereby the brain is deprived of oxygen, nutrients and glucose as a result of an obstruction of the vessels supplying the brain (Nair, Dileep and Rajanikant, 2012; Kyle and Saha, 2014) Symptoms are usually sudden, within seconds to hours, and can include unilateral weakness or numbness of the face, arms or legs, aphasia, visual impairment, dysarthria, confusion, loss of balance and coordination, difficulty with walking and in severe cases, even death. Stroke is considered as the fourth highest cause of death in the United States. It is the third major cause of death in developed countries, and the second root cause of death around the world (Grossman and Broderick, 2013).

Of all stroke cases, ischemic stroke contributes 80 - 87 % of all the stroke cases, with the remainder being haemorrhagic stroke. Current treatment of ischemic stroke with tissue plasminogen activator (tPA) have various drawbacks such as short window period, non-specificity, cell death, cerebral oedema and damage to blood brain barrier (BBB) (Turner and Vink, 2012). Nanotechnology has been widely considered as a promising tool for theranosis of neurodegenerative diseases including ischemic disorders (Grossman and Broderick, 2013).

The main challenge of the successful diagnosis and treatment of the neurological and ischemic disorders is the central nervous system (CNS) access. The delivery of drugs and imaging agents to the nervous system is mainly limited by the presence of two anatomical and biochemical dynamic barriers: the blood–brain barrier (BBB) and blood cerebrospinal fluid barrier (BCSFB). These barriers tightly seal the central nervous

system (CNS) from the changeable milieu of blood. There is a need to design novel therapeutic systems to target the CNS in an effective and efficient manner for successful diagnosis and treatment of neurological and ischemic disorders.

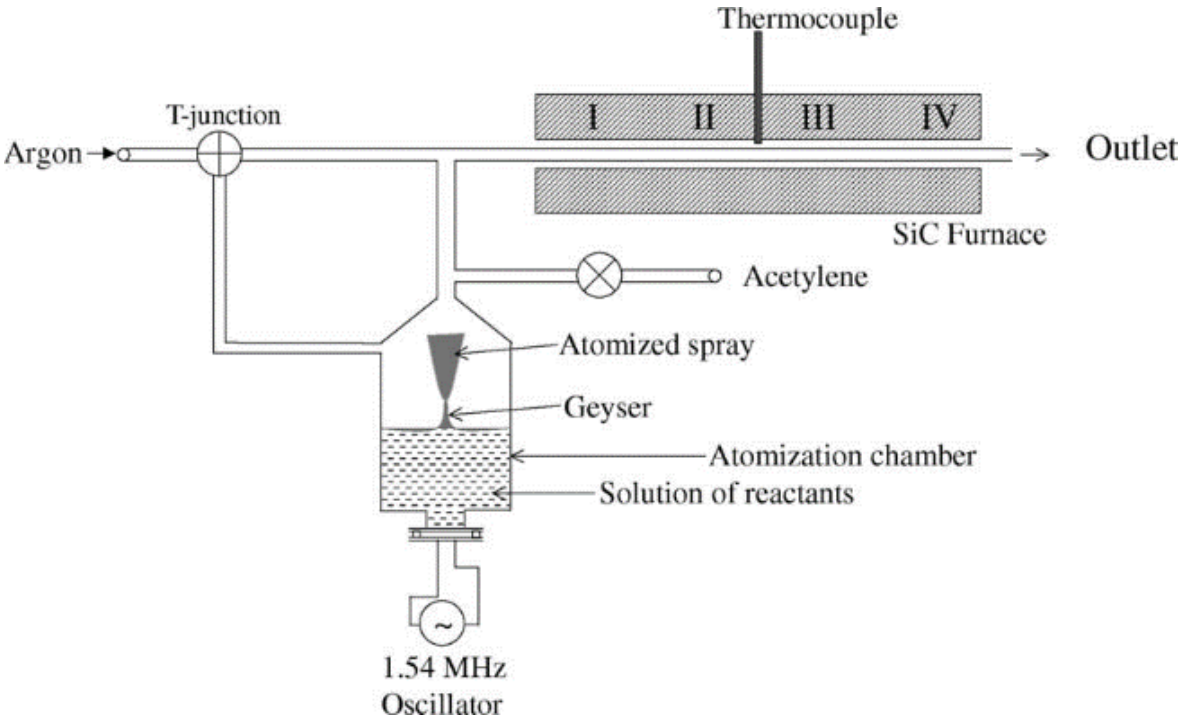


Figure 2.1. Schematic representation of a Chemical Vapour Deposition tube furnace with a nebulizer. A catalyst reacts with a precursor in the atomization chamber and the reactants are then carried into the high temperature furnace by argon gas. Nucleation sites are formed by the nanoparticles from the catalyst for the growth of carbon nanotubes from the carbon source acetylene. The evolved gases from the reaction are wiped out of the furnace by argon gas via the outlet. Adapted from Nunes and co-workers (Nunes, Al-Jamal and Kostarelos, 2012) with a permission from Elsevier.

Advances in nanomedicine are expected to have a major impact in neurological research. These will significantly contribute to our further understanding of the CNS and the development of novel therapeutic approaches for neurological intervention (Gilmore et al., 2008; Modi et al., 2009). The use of carbon nanotubes (CNTs) is one of the most attractive strategies for neurological applications. They are synthesized by using the most common technique namely chemical vapour deposition (CVD) as illustrated in **Fig. 2.1**. CNTs can be synthesized and functionalized for the intended purpose. They have shown evidence of their electrical conductive capacity, strong mechanical properties and morphological similarity to neurites (Zhang and Webster, 2009). Therefore, the emergence of nanotechnology provides hope that it will revolutionize diagnosis and treatment of CNS disorders.

This paper discusses the application of carbon nanotubes in neurological and ischemic disorders. In this paper, the use of carbon nanotubes in diagnosis and treatment of neurological pathologies and ischemic disorders are discussed in detail with more emphasis on ischemic stroke. Areas covered include the conventional current diagnosis and treatment of neurological disorders, as well as a critical review of the application of carbon nanotubes in the diagnosis and treatment of ischemic stroke, covering areas such as functionalization of carbon nanotubes and carbon nanotube-based biosensors. A broad perspective on carbon nanotube stimuli-responsiveness, carbon nanotube toxicity and commercially available carbon nanotubes is provided. Potential future studies employing carbon nanotubes have been discussed, evaluating their extent of advancement in the diagnosis and treatment of neurological and ischemic disorders.

2.2. Current diagnosis and treatment of ischemic stroke

Radiation and chemotherapy are the current therapies for stroke, however they produce notable adverse effects. They are painful and inefficient and cause death to healthy cells and tissues in addition to the diseased. The most commonly used tools for diagnosis of stroke are computed tomography and magnetic resonance imaging. Their use is very limited as a result of cost, unavailability and radiation exposure from these instruments. Acute therapy, which involves the dissolution of blood clots, is currently preferred over radiation and chemotherapy for ischemic stroke treatment (Ciccone, Cappella and Borgna-Pignatti, 2011).

Glucocorticoids such as methylprednisolone and dexamethasone are utilized in ischemic stroke therapy. Glucocorticosteroids possess anti-inflammatory properties rendering them potentially effective in the treatment of ischemic stroke. Glucocorticoids have been proven effective in the treatment of cerebral oedema and cerebrovascular disease inflammation since they are able to cross blood brain barrier (BBB) (Chen et al., 2010). However, the therapeutic potential of glucocorticoids is negatively affected by the short circulatory half-lives and poor pharmacokinetics. Administration of extremely high concentrations of glucocorticoids is required in order for the glucocorticoids to be effective and this could result in serious systemic side-effects (Beg, Ahmad and Renjen, 2015).

In addition, stenting is also used for treatment of ischemic stroke but it has many disadvantages such as lysis of the thrombus which circulates to adjacent arteries, invasiveness as it requires surgery of the vessels, and possible damage to vessels during surgery and the need of antiplatelet therapy during this procedure (Ansari et al., 2011).

Based on the current challenges, there is an urgent need for proper diagnosis and effective and efficient treatment of neurological diseases including ischemic stroke.

2.3. Carbon nanotubes in the diagnosis and treatment of central nervous system disorders

Nanomedicine is emerging field where engineered nanomaterials are utilized for the detection, treatment and prevention of certain diseases including neurological disorders. Despite impressive research that is adding value to the body of knowledge in the field of nanomedicine at an alarming rate, this field is currently at its embryonic stage (Gilmore et al., 2008; Modi, Pillay and Choonara, 2010).

Carbon nanotubes (CNTs) are a new group of nanomaterials that has demonstrated promising outcomes for the advancement in technology in the field of medicine (Singh, Pillay and Choonara, 2007; Modi et al., 2009; Folch, J., Petrov, D., Ettcheto, M., Abad, S., Sanchez-Lopez, E., Garcia, M.L., Olloquequi, J., Beas-Zarate, C., Auladell, C., Antoni, 2015). They have a variety of properties making them useful tools in neurobiological applications. Iijima discovered CNTs in 1991 (Iijima, 1991). CNTs are electrically and thermally conductive and have ultralight weight. They are highly flexible, very strong and inert but can undergo chemical modification with various functional groups depending on their intended use (Nair, Dileep and Rajanikant, 2012; Grossman and Broderick, 2013; Kyle and Saha, 2014). CNTs structural backbone consists of carbon atoms which exhibit thermal and electronic conductivity including great strength.

CNTs are synthesized by various methods; the widely used approaches are chemical vapour deposition (CVD), laser ablation and arc discharge (Zhang and Webster, 2009; Turner and Vink, 2012). CVD is the most suitable and preferred method of CNT synthesis as illustrated in **Fig. 2.1** for mass production due to low deposition, low cost and scalability (Ravindra and Bhat, 2011). CNTs in their native state do not dissolve in

most aqueous solvents, with this property rendering their application in nanomedicine extremely difficult. CNTs need to be functionalized to enhance their distribution in aqueous solvents and to improve their biocompatibility for application in physiological conditions including the central nervous system (CNS) (Chen et al., 2010; Grossman and Broderick, 2013; Beg, Ahmad and Renjen, 2015).

The delivery of drugs to the nervous system is mainly limited by the presence of two anatomical and biochemical dynamic barriers: the blood–brain barrier (BBB) and blood– cerebrospinal fluid barrier (BCSFB) separating the blood from the cerebral parenchyma (Re, Gregori and Masserini, 2012). These barriers tightly seal the central nervous system (CNS) from the changeable milieu of blood. The presence of these barriers restrict drug delivery to the CNS leading to inefficient and ineffective diagnosis and therapy of neurological disorders (Lacerda et al., 2006; Marchesan et al., 2015).There is a promise that nanotechnology will revolutionize neurological disease diagnosis and treatment (Gilmore et al., 2008).

Richard Feynman recognized the potential of engineering atoms and molecules at the nanometer range in 1959. He suggested that materials at this nanometer level are in possession of distinctive physical properties which could be of great benefit to humankind (Feynman, 1960). Nanotechnology involves the development and application of materials at nanometer level with very distinctive functional properties lacking in huge materials. Nanomaterials can interact with physiological systems at the molecular and supra-molecular level. They can be redesigned to respond to particular cell milieu and trigger desired biological activities in cells and tissues while reducing adverse effects (Gilmore et al., 2008).

Notwithstanding the promising research outcomes, *in vivo* implementation of nanotechnological procedures and CNT platforms particularly for neuroregeneration is only at an early stage with only a limited number of pilot studies performed to date. CNTs have been utilized *in vivo* with great success in bone implants and as drug delivery vehicles for the treatment of rheumatoid arthritis and osteoporosis in bone diseases and cancer in various body organs (Ando et al., 2004; Malarkey and Parpura, 2007; Santiago-Rodríguez, Sánchez-Pomales and Cabrera, 2010; Ravindra and Bhat, 2011; Fabbro et al., 2012; Gottipati, Verkhratsky and Parpura, 2014; Kyle and Saha, 2014). Very few preclinical studies for the successful *in vivo* usage of CNTs in

neuroregeneration and neuroprotection have been performed (Fabbro, Prato and Ballerini, 2013).

CNTs have shown evidence of their electrical conductive capacity, strong mechanical properties and morphological similarity to neurites (Zhang and Webster, 2009). Based on their unique properties, CNTs seem to be promising in diagnosis and treatment of neurological and ischemic diseases.

2.4. Carbon nanotubes potential toxicity in living cells including neural tissue

Clinical trials of CNTs for diagnostic and therapeutic applications can only be initiated when a clear picture about their toxicity in the biological environment has been obtained (Lee and Geckeler, 2010). CNT toxicity in living cells is currently a controversial issue. CNTs have different effects in different cells, tissues and organs, being biologically benign in some cells and hazardous in other cell types (Ryman-Rasmussen et al., 2009). Efficacy and side effects of CNTs are highly dependent on a variety of parameters including dose and route of administration of CNTs, type of exposure, length and diameter of CNTs, and other factors as illustrated in **Table 2.1**.

There is a need for research for determination of the penetration mechanism of CNTs into cells, tracking of location of CNTs once internalized, and identification of relevant cytotoxic mechanisms. Furthermore, research needs to be executed to relook the nanotoxicity effect as a result of physico-chemical parameters, which include impurities, length and diameter, surface functionalization and wettability of CNTs. CNTs use three common routes to gain access into the body, namely ingestion, absorption through the skin and inhalation (Buzea, Pacheco and Robbie, 2007). Other routes of administration include intratracheal administration, abdominal implantation and intravenous injection with subsequent investigation of their nanotoxicity (Mutlu et al., 2010).

Functionalized CNTs are internalized into the cells via two most widely accepted mechanisms, namely active endocytosis and passive nanopenetration. Cells undergo oxidative stress following CNT internalization as a result of induction of oxidants and toxic enzymes. Oxidative stress generates free radicals and reactive oxygen species (ROS). Excessive free radicals stimulate lipid peroxidation, protein degradation and

oxidative damage to DNA. ROS may lead to harmful effects in cells such as apoptosis, DNA damage, amino acid oxidation and inhibition of enzymes (Valko et al., 2007).

Proinflammatory cytokines and apoptosis are regulated by protein kinase and nuclear factor kappa B (NF-kB) signalling pathways in response to oxidative stress (Jain, Singh and Pillai, 2012). Wizmann and Monteiro-Riviere demonstrated that MWCNTs could initiate inflammatory responses. Incubation of human keratinocytes with MWCNTs reduced cell viability and a rise in proinflammatory cytokines was also noted (Witzmann and Monteiro-Riviere, 2006).

Successful CNT application in the CNS depends on their biocompatibility with the CNS cells. There is much concern about their cytotoxicity as a result of their resemblance in structure with asbestos. Moreover, the biological application of CNTs requires their complete purification following their synthesis to eradicate both metal and carbonaceous particles that might be toxic to the cells and tissue (Flavin et al., 2011). It was demonstrated for the first time by Ni and colleagues (Ni et al., 2005) that the viability of the neurons from hippocampus incubated with co-polymer-SWCNTs was not affected although there were changes in their morphology.

Gaillard and colleagues demonstrated the biocompatibility of functionalized MWCNTs with neuronal cells (Gaillard et al., 2009). It was found that there was no effect of functionalized MWCNTs on the cell viability and neuronal architecture and normal function of primary neurons remained intact. In another study, neurotoxicity as a result of the presence of impurities from the metals during CNT synthesis was evaluated. The findings demonstrated that the impurities from iron in MWCNTs had a negative impact on cell viability and cytoskeleton. The ability of the neurons to produce mature neurites was reduced (Meng et al., 2013).

Cell viability in PC-12 neuronal cells was impaired and damage on the cell membrane was observed during incubation of these cells with SWCNTs. Furthermore, there was a reduction in the potential of the mitochondrial membrane. SWCNTs triggered the formation of ROS and enhanced lipid peroxidation. Reduction in superoxide dismutase, glutathione peroxidase, catalase and GSH was observed (Buzea, Pacheco and Robbie, 2007; Mutlu et al., 2010).

Exposure of PC-12 cells to SWCNTs was also demonstrated to lead to condensation of chromatin, fragmentation of nuclei and blockage of cell cycle in G2/M phase (Wang et al., 2011). These negative impacts were prevented by pre-incubation of the cells with vitamin E (Wang et al., 2012). Toxicity to cells can be reduced by coating CNTs with surfactants or polymers like polypyrrole (PPy) to reduce direct contact between CNT and cells or tissues (Hernández-Ferrer et al., 2014).

Qi and colleagues demonstrated for the first time the curing effect of 1,2-dioleoyl-sn-glycero-3-phosphocholine (DOPC) /or simvastatin (TD) on the MWCNT toxicity in mice. Oxidized MWCNTs (o-MWCNTs) were intravenously injected into mice. DOPC and TD were then intravenously injected into the mice to observe the effect on the o-MWCNT toxicity. CT imaging and isotope tracing indicated that the low doses of DOPC and TD did not have any effect on the distribution of o-MWCNTs. The distribution and metabolism of these two drugs were affected by o-MWCNT (Qi *et al.*, 2017).

In another study, Perepelytsina and colleagues embarked on an *in vitro* and *in vivo* studies on the toxicity of oxidized carbon nanotubes (CNT-ox), doxorubicin functionalized CNTs (CNT-Dox) and fluorescein functionalized CNTs (CNT-FITC). In cytotoxicity studies, HT29 tumour cells were incubated with CNTs and MTT assay was used to determine the extent of toxicity. In animal studies, CNTs were administered parenterally and doxorubicin intraperitoneally. Low doses had a moderate cytotoxic effect on the cells and medium to high doses yielded a dose-dependent decrease in cell viability. Systemic introduction of CNT-ox had no effect on enzyme and protein profile. CNT-dox and dox administration had a toxic effect and induced hepatic damage in mice (Perepelytsina *et al.*, 2018). Further research on toxicity of carbon nanotubes has been summarised in **Table 2.1**.

Table 2.1: Cardiovascular effects following exposure to carbon nanotubes. Toxicity of the CNTs depends on various factors such as dose, animal type, CNT size, functionalization, exposure duration and exposure route.

Absolute dose	Dose (mg/kg)	Animal	Number	Diameter	Length	Characteristics	Exposure form	Exposure time	Effects	Type
-	0,064	Rat	8-10	0,9-1,7 nm	<1µm	-	Tube feed	1 dose, 24 hrs	Modified nucleotides in the DNA of the lung and liver	SWCNT
10 µg	0,3	Mouse	-	-	-	Unfunctionalized	Intratracheal	1 dose	No significant effects	SWCNT
10 µg	0,4	Mouse	-	0,7-1,5 nm	1 µm	-	Pharyngeal instillation	1 dose, 60 days	Damage to mitochondrial DNA in the aorta	SWCNT
-	0,64	Rat	8-10	0,9-1,7 nm	<1µm	-	Tube feed	1 dose, 24hrs	Modified nucleotides in the DNA of the lung and liver	SWCNT
-	1	Rat	8	1,2-1,6 nm	2-5 nm	-	Intratracheal	2 does over 4 weeks	Modified baroreflex, the influence of autonomic cardiovascular control	SWCNT
40 µg	1,3	Mouse	-	-	-	Unfunctionalized	Intratracheal	1 dose	Increase of creatine kinase, cardiac fibre degeneration	SWCNT
40 µg	1,3	Mouse	-	-	-	Acid-functionalized	Intratracheal	1 dose	Significant increase in size of infarction, creatine kinase, cardiac fibre degeneration	SWCNT
10 µg	1,3	Mouse	-	-	-	Acid-functionalized	Intratracheal	1 dose	No significant effects	SWCNT
40 µg	1,4	Mouse	-	0,7-1,5 nm	1 µm	-	Pharyngeal instillation	1 dose, 60 days	Damage to mitochondrial DNA	SWCNT
40 µg	1,5	Mouse	-	0,8-1,2 nm	0,1-1 µm	8,8 wt% Iron	Pharyngeal aspiration	4 h	Local and systemic effect on inflammatory parameters	SWCNT
40 µg	1,5	Mouse	-	80 nm	10-20 µm	0,2% wt% Iron	Pharyngeal aspiration	4 h	Local and systemic effect on inflammatory parameters	MWCNT
20 µg x 4	2,8	Mouse	-	0,7-1,5 nm	1 µm	-	Pharyngeal instillation	4 does over 8 weeks	Atherosclerosis was increased in ApoE-/- transgenic mice. Plaque formation in aorta, mtDNA damage	SWCNT

The table has been adapted from Gustavsson and colleagues (Gustavsson, Hedmer and

Based on the findings above, it is therefore impossible to decisively classify CNTs as toxic or nontoxic *in vivo* based on the fact that their impacts on cells rely on their application. It is indeed very difficult to draw clear conclusions about the toxicity of

carbon nanotubes at the present moment. Nevertheless, they should be treated as toxic until further research confirm their classification.

2.5. Chemically functionalized carbon nanotubes for biomedical applications

Carbon-based nanomaterials have limited dispersion in organic matrices as a result of their tendency to agglomerate due to their chemical inertness and van der Waals forces on their surfaces. Functionalization methods have been developed in order to eradicate this obstacle to augment biocompatibility (Monaco and Giugliano, 2014). Non-covalent and covalent functionalization are two procedures that are utilized to functionalize CNTs in order to enable their applications in a physiological environment (Chen et al., 2010; Gustavsson, Hedmer and Rissler, 2011). These methods reduce agglomeration of native CNTs hence debundling and enabling easy handling of the CNTs (**Fig.2.2**).

In non-covalent functionalization, CNTs are coated with hydrophilic macromolecules with their hydrophobic groups attached to CNTs to create repulsive forces (Ni et al., 2005; Witzmann and Monteiro-Riviere, 2006; Gaillard et al., 2009). This is achieved by coating the CNTs with surfactants (Moore, Strano and Haroz, 2003), polymers (Shvartzman-Cohen et al., 2004), peptides (Dieckmann et al., 2003), and ssDNA (Zheng et al., 2003). The drawback of this method is the easy dissociation of the coating molecules from the CNTs.

In covalent functionalization, the charged group is coupled to the CNT backbone by organic reactions to create repulsive forces between individual nanotubes (Gustavsson, Hedmer and Rissler, 2011; Wang et al., 2012; Hernández-Ferrer et al., 2014; Beg, Ahmad and Renjen, 2015). Covalent functionalization is achieved by covalent coupling of functional groups on the sidewall and tip of the CNT. Functionalization on the sidewall involves chemical reactions by 1,3-dipolar cycloaddition. A highly soluble material was produced by attaching amino functional groups to the CNT sidewalls and tips (Chen et al., 2010; Beg, Ahmad and Renjen, 2015) This functionalization method is robust and does not have the dissociation challenge.

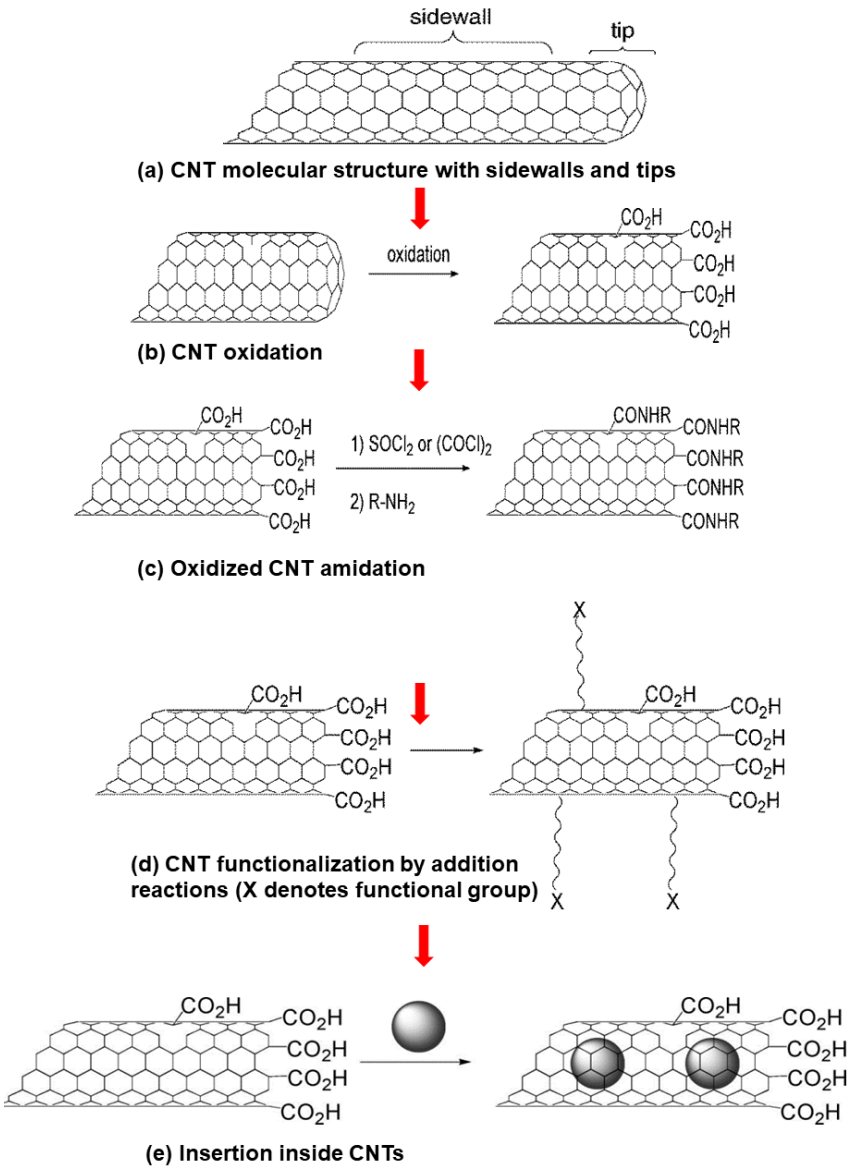


Figure 2.2. Oxidation and functionalization of CNTs. Pristine CNT has sidewalls and two tips (a). During oxidation, carboxyl groups are attached to the sidewalls and tips (b). Oxidized CNTs are further functionalized by acylation, amidation and addition reactions (c & d). Drug and fluorescent tags may be inserted inside the CNTs as the central cavity can be accessed following removal by oxidation (e). Reproduced with permission from Prato and colleagues (Prato, Kostarelos and Bianco, 2008). Copyright (2016) American Chemical Society.

Functionalization is a pivotal procedure in achieving homogenous aqueous dispersion to tailor CNTs for biomedical applications (Singh, Pillay and Choonara, 2007; Monaco and Giugliano, 2014). This procedure modifies the physico-chemical properties of the CNTs, their pharmacokinetic profiles and biodegradability (Tasis et al., 2006; Prato, Kostarelos and Bianco, 2008). It was found earlier that pristine CNTs could not be metabolized and their persistence *in vivo* resulted in chronic inflammation. However, recent findings demonstrated the phenomenon of oxidized SWCNT biodegradation in

neutrophils and macrophages, with no inflammatory response following aspiration of CNTs into the lungs of mice (Kagan et al., 2010).

The biodegradation process of chemically functionalized CNTs has been shown to be mediated by an oxidative milieu in phagocytic cells and this has been demonstrated in *in vivo* and *ex vivo* studies (Zheng et al., 2003; Singh, Pillay and Choonara, 2007). Functionalized CNTs should therefore not be regarded as toxic based on these findings. Pristine CNTs have been found to have a tendency of agglomeration and accumulation in reticuloendothelial system (RES) while functionalized CNTs were better tolerated (Moore, Strano and Haroz, 2003; Prato, Kostarelos and Bianco, 2008). Pristine and functionalized MWCNTs accumulated in RES following 30 min intravenous injection whereas only pristine CNTs were retained for months in the liver and lungs. Functionalized CNTs (f-CNTs) were easily cleared from the body via excretion in the urine and further investigations confirmed these findings (Dieckmann et al., 2003; Shvartzman-Cohen et al., 2004).

Various types of chemical groups, for example hydrophobic, hydrophilic, neutral, charged, etc., have an impact on the dispersibility of the functionalized CNTs (f-CNTs) as illustrated in **Table 2.2**. The debundled f-CNTs do not trigger inflammatory responses as observed in the bundled pristine and f-CNTs (Ali-Boucetta et al., 2013). Functionalization degree has an effect on cytotoxicity of CNTs and this was demonstrated by Ji and colleagues (Ji et al., 2009) and Jain and colleagues (Jain et al., 2011).

Single-dose injections of pristine MWCNTs and low level functionalized CNTs induced liver damage in mice which became apparent 7 days post-treatment. Mice with single dose injections of CNTs with a high level of functionalized groups did not display any toxicity in the work undertaken by Jain and colleagues (Jain et al., 2011). Metal impurities associated with CNTs during synthesis also contribute to cytotoxicity and this could be mitigated by an acid-oxidation of CNTs to remove the metals (Jain et al., 2011).

Table 2.2: Functionalized carbon nanotubes and reduced cytotoxic effects. Different functional groups on MWCNTs and SWCNTs have different toxic effects on different cell types and animal types.

Functional group or structure	Toxicological studies	Application	Target site	Reference
Acid-oxidized SWCNTs	Apoptosis studies showed no apparent cell toxicity	Intracellular protein transporters	Mammalian cells	Kagan et al., 2010
Acid-treated, water-soluble SWCNTs	No changes in cell viability or structure in lysosomes and cytoplasm		Human monocyte–derived macrophage cells	Keefer et al., 2008
Purified COOH–SWCNTs	No cytotoxicity	Pharmacological applications	Cultured mammalian cells	Al-Jamal et al., 2012
Oxidized ultrashort SWCNTs	Showed no cytotoxic effects	Intracellular delivery of oligonucleotide molecules	Human macrophages	Cellot et al., 2009
Amine-terminated CNTs	Cross cellular membrane without cytotoxicity	Delivery of amino acids, peptides, nucleic acids or drugs		Webster, Sundaram and Byrne, 2013; Shein et al., 2009; He et al., 2004
SWCNT–PL–PEG	Gene silencing with no apparent cytotoxic effects	SH–small interfering RNA delivery	Human T cells	Modi, Pillay and Choonara, 2010
SWCNT–PEG–drug	Decreased reactive oxygen species–mediated toxicological response and exhibited less cytotoxicity	Drug delivery	Neuronal PC-12 cells	Grossman and Broderick, 2013
SWCNT–PEG–cisplatin/doxorubicin	Remarkable reduction of cytotoxicity	Drug-delivery and imaging tool	Human cancer cells/mice	Sharma, Muresanu and Sharma, 2013; Ansari et al., 2011
SWCNT–PEG–mAb (αvβ3)	Without harming adjacent normal cells	Cancer-cell targeting	αvβ3-positive U87MG cells	Tan et al., 2012
SWCNT–PEG	Revealed no evidence of toxicity over 4 months	Mice		Kotchey et al., 2013
MWNT–CS–(PC)	Chitosan and PC reduced the cytotoxic effects on normal cells with specific photo-induced toxicity towards malignant cells	Photothermal therapy	MCF-7, HepG2 and L-O2 cell lines	John et al., 2015
Polyoxylethylene sorbitan monooleate (PS80) CNTs	Suppressed cytotoxicity		Human lung mesothelium cells (MSTO-211-H)	Zheng et al., 2003
HMDA–SWCNTs; PDDA chloride–SWCNTs	Negligible cytotoxic effects	Intracellular delivery of negatively charged biomolecules	Rat heart cells	Pardridge, 2012
SWCNTs with human serum proteins	Blood proteins altered SWCNT cellular interaction pathways and reduced cytotoxicity	Biological applications	Human acute monocytic leukemia cell lines and human umbilical vein endothelial cells	Ciccone, Cappella and Borgna-Pignatti, 2011
BSA-dispersed SWCNTs	No acute deleterious cellular effects		Human mesenchymal stem cells and HeLa cells	Ben-Jacob and Hanein, 2008
Albumin–SWCNTs	Induced cyclooxygenase-2 and modulating toxicity effects of SWCNTs		RAW264.7 macrophage cell lines	Malarkey et al., 2009
DNA-encased MWCNTs	Does not exert cytotoxic effect on lymphocytes	Selective thermal ablation of malignant tissue *in vivo*	*In vivo*	Vidu et al., 2014
Lectin-functionalized CNTs	Increase in cell viability without signs of apoptosis	Nanovaccine fabrication	J774A macrophage (MOs) cell line	Kesharwani, Gajbhiye and Jain, 2012
Fluorescent–CNT-FITC/biotin conjugates	Reduced cytotoxicity	Delivery systems	HL60 cells	Nho et al., 2010
Cationic f-CNTs	Lowers cytotoxicity *in vitro*	Delivery of drugs and biomolecules	CHO, 3T3 fibroblast, Jurkat, HL60 cell lines	Kim et al., 2012

The Table has been adapted from Vardharajula and colleagues (Vardharajula et al., 2012).

It is thus imperative to modify CNTs chemically by oxidation and amidation to couple functional groups to CNTs in order to overcome their toxic effects. Non-homogeneity of the coupled functional groups on the surface of the f-CNT may cause this approach to be sub-optimal for biomedical applications (Tagmatarchis and Prato, 2004; Bianco, Kostarelos and Prato, 2011). Polyethylene glycol (PEG) is most commonly utilized to

augment CNT blood circulation to achieve stable and well dispersed drug delivery systems (Bottini, Rosato and Bottini, 2011).

The PEGylation mechanism of action with regard to CNTs is not clear at the current stage but PEG plays a pivotal role in reducing opsonin binding to CNTs and hence causes a reduction in an early CNT removal from the blood circulation (Andersen, Wibroe and Moghimi, 2012). Polymers such as PEG tend to adopt different confirmations when they are attached to CNTs. A brush-like conformation when PEG is coupled to SWCNTs reduces CNT blood circulation, and increases renal clearance and relative spleen versus liver uptake as opposed to PEG with a mushroom conformation (Sacchetti et al., 2013).

Furthermore, the functionalization process, which includes the level of functionalization, surface density and homogeneity of the functional group, contributes significantly to the success of CNT application in the biomedical field (Bottini, Rosato and Bottini, 2011). Cirillo and colleagues performed CNT covalent functionalization with a molecule of biomedical interest namely gallic acid, for the first time (Cirillo et al., 2011). Gallic acid is a natural antioxidant found in various vegetables and possesses anti-allergic, anti-mutagenic, anti-inflammatory, anti-carcinogenic and radical scavenging activities. Gallic acid-functionalized CNTs were found to be effective in reducing oxidative stress in biological environment (Jain et al., 2011; Al-Jamal et al., 2012; Kotchey et al., 2013).

Transport of fluorescein isothiocyanate (FITC)-MWCNTs across immortalized murine microvascular cEND cells using Transwell device was investigated by Shityakov and colleagues. It was found that the FITC-MWCNT aggregates were non-fluorescent and localized on the surface of the cell whereas the dispersed FITC-MWCNTs were fluorescent and localized intracellularly as well as on the cell membrane (Shityakov et al., 2015).

Oxidation of CNTs can also be undertaken which yields pure and shorter CNTs using a strong oxidizing agent such as nitric acid. The carboxylic acid groups might be coupled to the carbon nanotubes and be further functionalized by coupling with ester and amide groups. The enhanced attainment of CNT dispersibility has widened the extent of their application in physiological systems from diagnostics and therapeutics

in oncology (Bonifazi et al., 2006; Ji et al., 2009; Vardharajula et al., 2012) to neuroprosthetic devices (Bottini, Rosato and Bottini, 2011; Cirillo et al., 2011; Andersen, Wibroe and Moghimi, 2012; Sacchetti et al., 2013).

Functionalization can therefore be applied in carbon nanotubes to convert their hydrophobic nature to hydrophilic nature. In addition, their toxicity has been found to be reduced or eliminated following functionalization as demonstrated from the findings summarized in **Table 2.2**.

2.6. Carbon nanotubes as electrochemical biosensors in neuroscience

There are two types of biosensors namely CNT field effect transistors (CNT-FET) and CNT-electrochemical sensors. In CNT-FET, the conductive channel can be SWCNTs and this system has been proven to have superior performance by Fam and colleagues (Fam et al., 2009). The CNT-FET biosensors have high sensitivity hence they are suitable for detection of very low concentrations of analytes in the sample.

The detection of chemical redox interactions has been performed by CNT-based electrochemical biosensors. The CNT unique properties, such as electrical conduction and small size in particular, are preferred since they enable them to act as electrodes with direct contact to the physiological environment. CNT electrochemical biosensors have been utilized successfully for detection of enzymes, H_2O_2, DNA, RNA, proteins, glucose and many other biomolecules. CNT functionalization plays a vital role in augmenting the specificity of the electrochemical biosensors (Lin et al., 1998; Kesharwani, Gajbhiye and Jain, 2012).

Carbon-based electrochemical sensors have been used widely for neurotransmitter analysis due to surface oxides, facilitating electron transfer and readily adsorbing neurotransmitters due to electrostatic interactions. Functionalized CNT electrodes have been used for neurotransmitter detection with high sensitivity and selectivity. Vertically aligned CNTs can lead to more reproducible surfaces with CNT ends exposed to enhance sensitivity (Yang et al., 2015). CNT yarns are made of multiple CNT fibres twisted together and these have been utilized by Yang and team for production of CNT yarn microelectrodes (CNTYMEs). The CNTYMEs are used for speedy measurements of dopamine (Jacobs et al., 2014).

CNTs can be used to determine the level of disease severity and other pathological conditions. CNTs are utilized as artificial smart intelligent tools such as nanosensors which are designed in such a way as to easily implant them in the body. These devices are capable of detecting a slight change in a physiological condition and may be used for qualitative and quantitative work. CNTs are used to design pressure nanosensors due to their physical properties (Beg et al., 2011).

Biosensors, nanosized materialistic devices applied in the detection of biological disorders of human bodies, are manufactured from CNTs. Sotiropoulou and Chaniotakis have demonstrated that MWCNTs with vertical alignment can be used as substrates to develop an amperometric biosensor (Sotiropoulou and Chaniotakis, 2003). The use of CNT-based nanobiosensors enables the detection of DNA sequences in the body and this may play a crucial role in the cancer treatment and other diseases (Gabay et al., 2005; Keefer et al., 2008; Bhirde et al., 2009). Bionanosensors are also applied in determination of blood glucose levels, monitoring of blood pressure, detection of potassium and sodium, and measurement of blood pH. Furthermore, CNTs can be used in measurement of respiratory gases.

Ghosh and colleagues demonstrated that SWCNTs can be used to design heart pacemakers with energy saving mechanism (Ghosh, 2003). CNTs presented themselves as excellent candidates for the development of electrodes, namely microelectrode arrays (MEAs), based on their large surface area and outstanding electrical conductivity (Cellot et al., 2009; Fam et al., 2009; Bottini, Rosato and Bottini, 2011; Andersen, Wibroe and Moghimi, 2012; Nair, Dileep and Rajanikant, 2012). MEAs consist of metallic microelectrodes inserted in a substrate which is well aligned and connected to an electrical circuit. Neural electrical activity can be stimulated in a non-invasive manner using individual microelectrodes. MEAs are biocompatible and have a large signal to noise ratio (Monaco and Giugliano, 2014). CNTs synthesised on silicon dioxide substrates enhanced the electrical properties of CNT-MEAs (Gabay et al., 2007).

Shein and colleagues confirmed that the MEAs tool was capable of measuring the spontaneous activity in the rat cortical neuron (Shein et al., 2009). Neurons were cultured on MEAs in which CNTs were deposited. Lin and colleagues were the pioneers in the synthesis of CNT electrode arrays on silicon substrates. The success in this work inspired Lin and colleagues to modify it for easy use. The system was

applied in recording the action potentials of nerves from crayfish (Lin et al., 2009). There is a limited understanding of the interaction of CNTs and the CNS and their potential application requires further investigation as a result (Bardi et al., 2013).

SWCNTs are fluorescent in the spectral region of 700-1100 nm with minimal interference from biological media. They have been functionalized for biocompatibility, stability and selective molecular recognition by Iverson and team for use as *in vivo* biosensors (Iverson et al., 2013). The functionalized SWCNTs were injected via the tail vein of the mouse and circulation time and biodistribution studies were performed. Nitric oxide produced during inflammation *in vivo* was detected and the sensor was found to be stable for years. These findings have demonstrated the potential of these SWCNTs to be utilized as *in vivo* biosensors for biomarkers of various inflammatory diseases including ischemic stroke.

MWCNTs functionalized with diethylene triaminepenta-acetic acid and labelled with indium were delivered into the brain by intravenous injection via mouse tail vein for biodistribution studies (Kafa et al., 2015). DTPA-^{111}In MWCNTs were retained in the brain parenchyma for 24 hours following intravenous injection while the levels in the blood capillaries diminished considerably. These findings have demonstrated that functionalized MWCNTs could be delivered to the brain parenchyma via intravenous injection. Based on these findings, CNTs have the potential to be used as vehicles to transport molecules and therapeutics to the brain for targeting and neurological disease treatment including ischemic stroke.

The findings demonstrate the potential of carbon nanotubes for use in the fabrication of carbon-based sensors for the detection of biomarkers of various diseases including neurological and ischemic disorders.

2.7. Carbon nanotubes as imaging tools in CNS for localization and detection of ischemic stroke

CNTs are very useful in imaging of the tissues for location of the diseased site and delivery of drug to the site of action (He et al., 2004; Kostarelos, Bianco and Prato, 2009). Imaging is a pivotal tool in the study of physiological and biochemical activities in the CNS, for the brain and spinal cord, in particular. Technological advancements in this area improved understanding of the effect of cellular damage on the CNS. The precision of neurological interventions and reduced invasiveness to the CNS have been enhanced to a greater extent (Nunes et al., 2012). The current technologies in CNS imaging include electroencephalography and magnetoencephalography. In these techniques, electrodes are placed on the skull to measure electrical signals coming from the brain. The skull is surgically opened to gain access to the brain to insert electrodes for the measurement of the signals directly from the brain. This technique is very invasive, and it requires an alternative non-invasive approach.

Methotrexate has been demonstrated in cancer imaging to improve visibility in the body when coupled with fluorescein probe-functionalized CNTs (**Fig. 2.3**). This system could be tailored for use as an imaging tool for localization of ischemic site and treatment of ischemic stroke.

A drug of interest is coupled to carbon nanotube. A targeting ligand such as monoclonal antibody is attached to the carbon nanotube for targeting the site of interest. Fluorescent tag is also coupled to carbon nanotube either externally or internally for localization of the targeting ligand-drug complex.

A longer excitation time is achieved at higher laser intensity when SWCNTs are utilized as a result of their high photostability as opposed to quantum dots and fluorophores (Vidu et al., 2014). Fluorescence, absorption, and scattering characteristics of a biological material enables the visibility of the opaque tissue in the range of 700 – 1400 nm. CNTs enhance the visibility since they allow imaging of the entire thick tissue (Heller et al., 2006). CNTs have a large resonance and enhanced Raman scattering properties hence they can be easily detected (Heller et al., 2005).

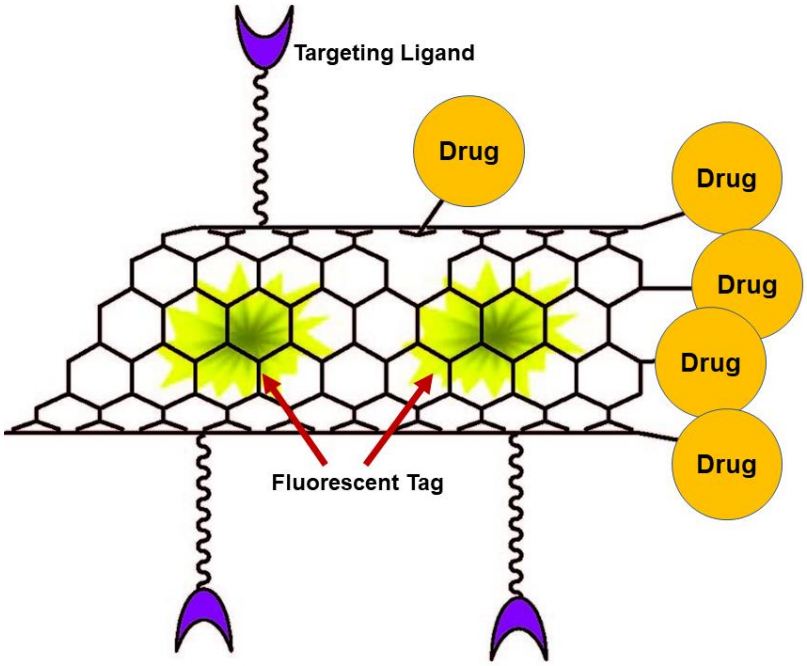


Figure 2.3. CNT equipped with a targeting ligand, drug and fluorescent tag. Reprinted with permission from Prato and colleagues (Prato, Kostarelos and Bianco, 2008). Copyright (2016) American Chemical Society.

The imaging techniques, namely magnetic resonance imaging, positron emission tomography and computer tomography, have led to a better understanding of neuronal circuit functioning. Despite their benefits, they do have drawbacks which include lack of sensitivity, inability to permeate the BBB and reduction of half-life following intravenous administration (Nunes, Al-Jamal and Kostarelos, 2012). Miniaturized video devices can be encapsulated into CNTs and be administered orally to assist in imaging the diseased site within a tissue (Beg et al., 2011).

Bio-medical imaging has a vital role to play in testing both the efficacy of new therapies and investigating their biodistribution. Attaching radionuclide labels onto CNTs allows three dimensional (3D) whole body, *in vivo* molecular imaging such as positron emission tomography (PET) and single photon emission computed tomography (SPECT). These techniques have high sensitivity, moderate resolution and have the advantage of being well established medical techniques.

Hong and colleagues reported the first non-invasive brain imaging in a narrow 1.3 - 1.4 μm region (named as the NIR-IIa region). This procedure allows penetration through intact scalp and skull and resolves cerebral vasculatures with a previously unattainable spatial resolution of sub-10μm at a depth of >2mm underneath the surface

of the scalp skin in an epifluorescence imaging mode. Furthermore, dynamic NIR-IIa cerebrovascular imaging with high temporal resolution (< 200 ms/frame) was used to reveal drastically reduced blood flow due to arterial occlusion in an acute stroke model on mice (Hong et al., 2014).

The findings confirm that carbon nanotubes have a potential to be used as non-invasive imaging tools in the brain disorders.

2.8. Carbon nanotubes as CNS drug delivery vehicles for the treatment of ischemic stroke

Stereotactic surgery is an invasive procedure which is clinically used for delivering drugs and other biologically important molecules into the brain. This procedure paves a way to direct access to the specific site of interest within the brain (Ben-Jacob and Hanein, 2008; Jacobs et al., 2014). Application of nanodrug delivery could be of great benefit in the future for neuroprotection success in chronic neurological diseases including ischemic stroke (**Fig. 2.4**).

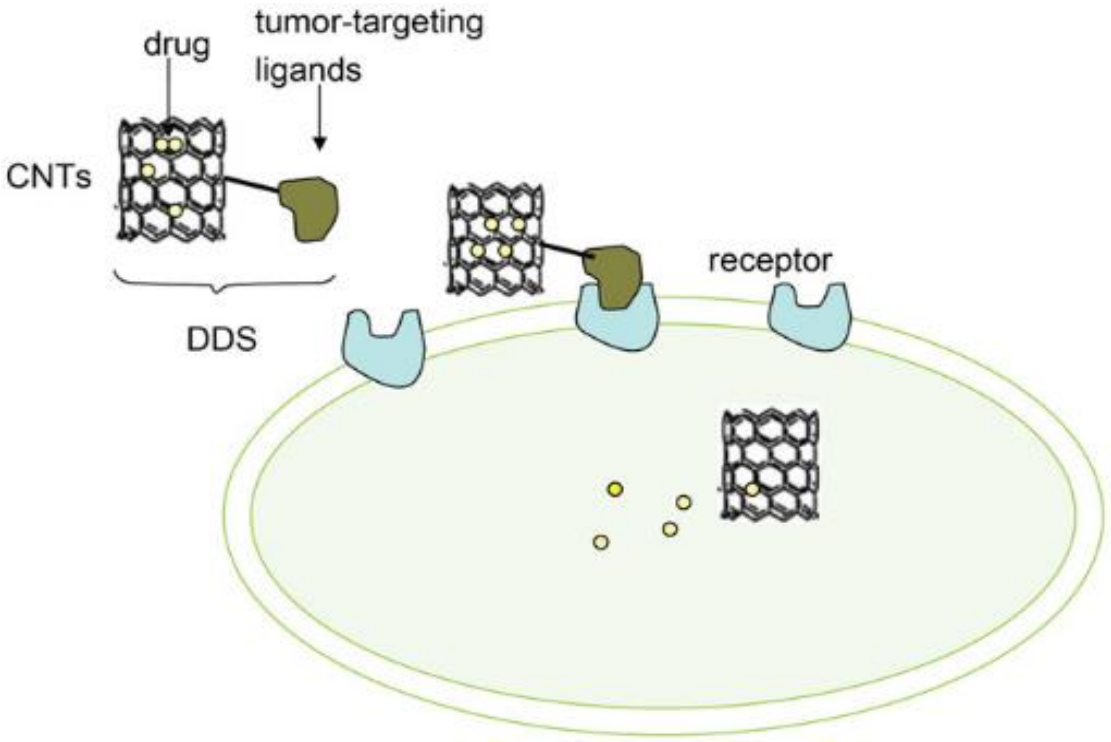


Figure 2.4. Drug delivery system (DDS). An anti-tumour drug and tumour- targeting ligands are coupled to carbon nanotubes (CNTs). Tumour-targeting ligands bind to the receptors on the cell membrane and the DDS is transported into the cell. Drug is released from the CNTs into the cell as a result of an acidic milieu. Adapted from Ji and colleagues (Ji et al., 2010).

Delivery of drugs through the BBB could be attained by application of nanotechnology (Sharma, Muresanu and Sharma, 2013). Nanotechnological advances for neurotrophin delivery systems are promising regarding their ability to activate neurotrophin signalling for neuroprotection and neuroregeneration (Tan et al., 2012). Neutrophins are indispensable for the development and functions of neurons and can be delivered to their site of action by CNTs (Lin et al., 2009; Bardi et al., 2013).

Use of CNTs as delivery vehicle for CNS disease treatment is dependent on their physico-chemical properties, mainly their improved solubility in physiological solvents due to their functionalization, large surface area, ability to be easily modified with drug molecules and biocompatibility with the neural system (John et al., 2015). Anti-tumour drug molecules have very low permeability across the BBB and this poses a negative impact on brain tumour treatment.

Iverson et al. (Iverson et al., 2013) used CNT drug delivery system to enhance CpG oligodeoxynucleotide immunotherapy in the treatment of glioma. SWCNTs were functionalized with PEG followed by conjugation with CpG oligonucleotide. Toll like receptor family members (TLR) are located intracellularly and recognize lipids, carbohydrates, nucleic acid structures and peptides expressed by microorganisms. When CpG was conjugated to SWCNTs, there was an enhancement of the uptake of CpG both *in vivo* and intracranial gliomas. CpG stimulated TLR in the glial cells to inhibit tumour growth in glioma models (Zhao et al., 2011). Yang and colleagues had also shown that CNTs are able to cross BBB for acetylcholine delivery into neurons of mice for Alzheimer's disease treatment (Yang et al., 2010).

Neurotherapy with the use of CNTs would be extremely useful in the treatment of various neurological pathologies including ischemic stroke. SWCNT functionalized with amine groups via amidation reaction enhances the tolerance of neurons to ischemic injury. Neurons are protected from injury and their functions are also regained with amine-modified SWCNTs without therapeutic intervention (Lee et al., 2011). Al-jamal and colleagues demonstrated the effectiveness of amine-MWCNTs in delivery of small interfering RNA (siRNA) decreased apoptosis at the injury site and promoted recovery of functional motor neurons in a mouse model of endothelin-1 stroke (Al-jamal et al., 2011).

The presence of the BBB poses a major problem in transporting drugs to the brain for tumour treatment and other neurological disorders including stroke. The BBB is rigorously selective and permits a very small amount of substances in the blood circulation to gain access to the CNS (Heller et al., 2005). It prevents therapeutic molecule delivery into the CNS resulting in delivery of less than 1 % of the administered drug through intravenous injection to the CNS (Bjartmarz and Rehncrona, 2007; Hong et al., 2014). This intensive selection of substances into the brain plays a crucial role in the regulation of homeostasis of the CNS. Moreover, it protects the CNS from invasion by foreign material such as toxins, viruses, bacteria and other unwanted substances (Ji et al., 2010; Tan et al., 2012; Sharma, Muresanu and Sharma, 2013; Hong et al., 2014).

Neuroprotection could be achieved in the future by use of nanodrug delivery in chronic neurological disorders. Neurotrophins are proteins involved in neuroprotection. Neurotrophins are essential for the development and function of neurons in both the CNS and PNS. They can be delivered into the brain using CNTs. The use of CNTs as a delivery mechanism for the treatment of CNS pathology is based on their structural features, especially their improved solubility in physiological solvents due to their functionalization, large surface area, ability to be easily modified with drug molecules, and biocompatibility with neural systems (John et al., 2015).

Carbon nanotubes, therefore have demonstrated their potential to be used as delivery vehicles of drugs to the diseased site in the brain.

2.9. Carbon nanotubes in neuroengineering in ischemic stroke and other CNS disorders

CNT use in neuroengineering scaffolds is an emerging technology. Neural tissue engineering contributes significantly in developing and improving biological scaffolds to promote neural tissue functioning (Nunes et al., 2012). Neural tissue engineering is a promising approach in recovery from neurodegenerative disorders including stroke. Research in this field is extensive to create an effective scaffold for the development of neural networks.

There are two types of scaffold: CNT-scaffolds and CNT-composite scaffolds. A major challenge in the development of scaffolds are the limited methods for the production of

scaffolds with the structure of interest. The advantage of the scaffolds is that they provide undiluted CNT physico-chemical properties. Promising results recommend CNTs to be the most relevant substrate for neural tissue growth, aiding in repair and regeneration of damaged neurons, although research work in this area is currently in the early stages. Incorporation of CNTs into scaffolds facilitates interfacing of neurons with CNTs hence stimulating neurons electrically to re-establish neural interconnections (Skaper, 2008).

Kuzmenko and colleagues developed an effective method of scaffold fabrication for neuronal engineering (Kuzmenko et al., 2016). This method utilizes a renewable resource as a precursor and exploits the advantages of an electrospun architecture together with conductive functionalization. All the scaffolds provided attachment and growth of neural cells. CNTs can act as substrates for the successful repair of damaged neurons since they can integrate with neurons to promote their functions due to their biocompatibility and electro-mechanical properties (Gilmore et al., 2008; Zhao et al., 2011).

Development of an effective scaffold depends entirely on its biocompatibility with the cells of interest and the surrounding cells. Several *in vitro* biocompatibility studies of CNTs were conducted by optimizing the conditions with the main focus on CNT concentrations, purity status, functionalization type, and CNT composites. Biocompatibility studies involve loose CNTs in suspension and physically contained within a structure (Edwards and Ramshaw, 2009).

CNTs may be functionalized with carboxyl groups, polymers and sugars to facilitate growth and adhesion properties of cells. It was demonstrated that acid-functionalized MWCNTs enhanced neuronal neurite outgrowth in neurons and rat pheochromocytoma cell line in culture media supplemented with nerve growth factor (Nair, Dileep and Rajanikant, 2012). Cellular interactions with a scaffold could be affected by the size and structure of the scaffold generated from CNTs (Fisher et al., 2012).

The human mesenchymal stem cell (hMSC) growth can be directed by various patterns of CNTs. Fibrinectin-CNTs promoted hMSC growth and differentiation whereas carboxylated CNTs had negative impact on the stem cells growth and differentiation

(Fisher et al., 2012). Heterostructures can be produced by addition of CNTs to polymer compounds for scaffolding. CNTs are dispersed with PEG and poly (propylene fumarate) (PPF) to produce porous polymer composites. Porous polymers become electrically conductive following dispersion of CNTs and this may result in stimulation of cell growth (Fisher et al., 2012). These composites have been used to enhance bone regeneration and also neural regeneration (Al-jamal et al., 2011; Lee et al., 2011).

The CNS of mammals has very little auto-repair capability and as a result, there is a need for neural stem cells and human mesenchymal stem cells transplantation for recovery of functioning of neurons following neurodegenerative diseases and CNS injuries including stroke (Bokara et al., 2013). Mesenchymal and neural stem cells interacted well with vertically aligned CNTs and growth on arrays was successful (Nho et al., 2010). The hMSC differentiation was enhanced in the presence of MWCNT sheets when these cells were grown on CNT sheets (Kim et al., 2012).

CNTs can be utilized in stem cell transportation to CNS for treatment of damaged neuronal tissue in stroke victims since they have been proven to have the capacity to enhance differentiation of neural stem cells. CNTs contribute significantly to the advances in tissue engineering for repair of damaged tissues as a result of their mechanical strength and electrical conductivity and resemblance to neurites (Bokara et al., 2013).

Neural stem cells were used to assess their preferred growth environment and it was found that they had enhanced growth in CNT environment than in a polyurethane surrounding (Nho et al., 2010). CNTs are not degraded in a biological environment, thus CNTs can be utilized as implants for long term intervention following injury in the brain and spinal cord. PC-12 cells and hippocampal neurons were cultured on carbon threads from SWCNTs and the growth was successful, further confirming biocompatibility. Nanothreads can be used for development of electrodes or nanowires which can be used in implantable devices due to their biocompatibility characteristics.

Biomaterials science and stem cell biology integration in the brain of the ischemic mouse was performed by Stockwell and colleagues (Pathan et al., 2009; Stockwell et al., 2014). The use of polyglycolic acid in scaffolding provides a platform for integration of multipotent stem cells and contributes to damaged neural tissue restoration. CNTs

that were impregnated with neural progenitor cells enhanced differentiation of those cells. The cells migrate to the injured tissue to restore the damaged tissue around the ischemic core region (Moon et al., 2012).

Nanofibers and stem cell combination improved efficacy for neuronal function restoration in stroke models. Impregnation of carbon nanofibers promoted differentiation of neural stem cells after being injected into brains of the rats induced with stroke and this procedure had also resulted in glial tissue formation (Edwards and Ramshaw, 2009; Wang, 2015) The ability of CNTs to trigger differentiation of neural stem cells to neurons implies that CNTs have a potential to be utilized as a vehicle to transport stem cells to the damaged neural tissues for treatment of stroke. Roman and colleagues demonstrated that CNTs play a pivotal role in the treatment of brain and spinal cord injuries (Roman et al., 2011). Direct injection of PEG-SWCNTs was demonstrated to enhance restoration of damaged axons in rat spinal cords with lesion at T9.

The two main approaches to promoting auto-repair of damaged connections in axons are axonal regrowth and neuronal circuitry reorganization. The requirements for successful regenerative engineering are neurorestoration, neurogenesis, reconnection of neuronal circuits and neuroplasticity (Lin et al., 2009; Tran, Zhang and Webster, 2009). It has been demonstrated for the first time by Mattson and colleagues that neurons of rat hippocampus could be grown on MWCNT layer functionalized with 4-hydroxynonenal (Mattson, Haddon and Rao, 2000). Furthermore, functionalization of the surface of CNTs has been demonstrated to have an impact on the growth patterns of the neurites, lengthening, branching, and the number of growth cones.

It has been shown by Hu and colleagues that functionalization of positively charged MWCNTs with polyethylendiamine led to a rise in the number of growth cones and neurite branches in neurons (Hu et al., 2004). SWCNTs that have been chemically modified with the cationic polymer, polyethylenediamine (PEI), were found to enhance growth of neurites and the number of branches as opposed to PEI alone (Hu et al., 2004). Matsumoto and colleagues functionalized MWCNTs with brain derived neutrophic factor to promote growth and differentiation of neurons (Matsumoto et al., 2007). The mechanism of action by which neurons reconstruct and rebuild active synapses in the presence of CNTs is not known (Giugliano, Prato and Ballerini, 2008).

Since CNTs have the capability to stimulate growth and differention of neurons, *in vitro* studies have triggered the interest of translating this work into *in vivo* outcomes in order to enhance motor functional recovery from ischemic stroke in rats or mice. Implantation of CNTs coupled to neural progenitor cells at the diseased sites in the brain of stroke-induced rat led to reduction of the infarct cyst volume and a rise in neuronal markers when compared to untreated neuronal progenitor cells (Moon et al., 2012).

The CNT potential in neurodegeneration application has been envisaged. However, CNT based neuroregenerative approaches are still far from clinical application as a result of major concerns linked to their toxicity, degradation and safe use. There is an evidence that an appropriate functionalization and administration route can make CNTs biocompatible and biodegradable thus shortening the way to clinical trials (Fabbro, Prato and Ballerini, 2013).

2.10. Recent advances in ischemic stroke treatment

Short interference RNA (siRNA) have the ability to disperse CNTs by a wrapping mechanism. The siRNAs are composed of hydrophobic bases and alternative hydrophilic phosphates and riboses. Such structure facilitates CNT dispersion by the bases wrapping to CNTs and the hydrophilic sugar-phosphate groups extending to the water phase (Shao et al., 2013). Dispersibility promotes the interaction of siRNA with the living cells and tissues.

The siRNA knocks out apoptotic genes resulting in silencing and inhibition of these genes, hence an effective stroke treatment (Mattson, Haddon and Rao, 2000; Bhatia, 2010). Direct siRNA delivery to the CNS enhanced the efficacy of siRNA in treating neurological disorders in animal models (Hu et al., 2004; Matsumoto et al., 2007). Sufficient siRNA delivery is needed direct to the diseased tissues and cells to maintain effective silencing of gene. This is regarded as a major obstacle because high siRNA doses are required to be administered into the CNS by continuous pump infusion. Neuronal tissue damage and apoptosis may be induced by electroporation techniques and lipid transfection reagents (Giugliano, Prato and Ballerini, 2008; Shao et al., 2013). Al-Jamal and colleagues used functionalized CNTs to deliver caspase-3 siRNA into the brain of the rat via stereotactic injection. Neurodegeneration was reduced and functional preservation was enhanced in the pre- and post-ischemic damaged motor cortex of the mouse (Al-jamal et al., 2011). This work proves that CNTs have a potential

to deliver siRNA into the brain leading to stroke prevention and treatment in stroke victims.

The neuroprotective agents are active in preventing the oxidative stress due to blood flow restoration or reperfusion surgery (Elger et al., 2006). This mechanism aids in the treatment of stroke. Stem cells that contain scaffolds can be transplanted into the diseased sites of the CNS and this procedure is considered as one of the strategies for treatment of stroke (Park, Teng and Snyder, 2002). Positive results have been obtained when CNTs were used as scaffolds in neuronal cells and tissues (Chen et al., 2009; Bottini, Rosato and Bottini, 2011; Cirillo et al., 2011).

Stroke causes a disruption of the structure of the brain. However, neurons are protected from injury in the presence of amine-modified SWCNTs (Pramanik et al., 2009). Neurons were protected from injury and functional motor recovery was enhanced in stroke-induced rats following pre-treatment with amine-functionalised SWCNTs. Sprague Dawley rats were pre-treated with amine SWCNTs and phosphate buffered saline (PBS) in the right lateral ventricles of the brain one week prior to induction of ischemic brain injury. Damage in the brain tissue of stroke-induced rats was assessed and it was found that damage in the rats treated with amine-functionalized SWCNTs was much less as opposed to untreated rats. Hemispheric lesion area of 95% in PBS treated stroke induced rats was decreased to 15% in amine SWCNT-treated stroke induced rats after 90 days of middle cerebral artery occlusion (MCAO) (Lee et al., 2011).

In order to evaluate their motor functions, rats were placed on the rotating rod and the time taken to fall ascertained, with those administered the SWCNTs maintaining their balance for longer. These findings suggest the beneficial role of functionalized SWCNTs in improving functioning of neurons following stroke. It was demonstrated in another study that CNTs enhanced recovery of motor functions in stroke when they were impregnated with neural progenitor cells and implanted in the brain. The use of CNTs for the improvement of stem cell differentiation for the treatment of stroke was first demonstrated by Moon and colleagues (Moon et al., 2012).

The findings demonstrate the instrumental role of the siRNA functionalized CNTs in the improvement of neuronal functions after stroke.

2.11. Carbon nanotubes in stimuli-responsiveness in biomedical applications

As highlighted, CNTs have the potential to be applied in biosciences as nanodevices (e.g. bioprobes or biosensors). CNTs assist in enabling nanodevices to respond to stimuli such as enzymes, glutathione, proteins, ions, pH and temperature. However, they do not have capabilities to innately respond to stimuli. In order for the CNTs to be applied in nanodevices, they need to be first functionalized using various organic and organometallic structures, linear and hyperbranched polymers and biological and bioactive species such as proteins. Functionalization of CNTs increases their solubility in aqueous media, biocompatibilities and sensitivities to surrounding conditions which include temperature, ionic strength, pH and biomolecules (Hong and Pan, 2008). The functionalized CNTs have the ability to respond to environmental stimuli and as a result they have potential to be applied in the diagnosis and treatment of stroke.

Wang and Chen suspended SWCNTs in poly(N-isopropylacrylamide) and poly-L-lysine solutions for temperature- and pH-responsiveness, respectively (Wang and Chen, 2007). The suspensions were sonicated, centrifuged and the supernatants were finally dialyzed and assessed for their stimuli-responsiveness. For temperature-responsiveness, when poly(N-isopropylacrylamide)-CNTs were heated at 40°C, the solution became turbid and subsequently clear again when it was cooled down. For pH-responsiveness, the poly-L-lysine-CNT solution was exposed to various pH ranges (acidic, neutral and alkaline). The solution became turbid at high pH (9.7) and turbidity decreased with a drop in pH. The solution became clear at neutral and low pH values (Wang and Chen, 2007).

In summary, the change in temperature and pH enables reversibility of dispersion and aggregation states of SWCNTs in poly(N-isopropylacrylamide) and poly-L-lysine solutions. Polymer-SWCNTs responsive to environmental stimuli have the capacity to be utilized in biosensing, and drug and gene delivery, and these may revolutionize diagnosis and treatment of ischemic stroke. Töröcsik and colleagues (Torocsik, Angelastro and Greene, 2002) developed a controlled release system containing CNTs responsive to environmental stimuli. Fluorescein was encapsulated into MWCNTs by opening the CNTs at the tips through oxidation and filling their cavities with fluorescein. The CNTs were then sealed with silica nanospheres. The release of fluorescein from the CNTs was done in a controlled fashion by cleaving the chemical bond between

CNTs and silica nanospheres by various external stimuli (e.g. addition of disulphide reducing agents or thermal treatment) (Chen et al., 2011).

This system has a potential application in the diagnosis including treatment of ischemic stroke and other neurological pathologies.

2.12. Carbon nanotubes currently on the market and limitations to clinical application and commercialization

There is a broad spectrum of applications of CNTs in electronics, energy storage, materials science and engineering, diagnostics and biomedicine. The controversy of CNTs with regard to their toxicity has slowed down the efforts for further innovation in their implementation especially in the clinical setting and hinders the CNT progress from the lab to clinical trials (Jain, Singh and Pillai, 2012). There is a lack of long-term toxicity research on CNTs as a higher proportion of toxicity studies conducted were for a short duration. As highlighted, toxicity also depends on CNT functionalization and physico-chemical properties of CNTs.

As highlighted, CNT nanoscaffolds contribute significantly to stem cell therapy as they have the ability to regulate stem cell growth and differentiation in a controlled manner. CNTs do have their drawbacks despite their fascinating benefits. They are hydrophobic and heterogeneous in size leading to non-reproducible results. Based on this, there is a need for the design of a system for producing CNTs of homogenous size for future applications of therapeutics consisting of CNTs in clinical trials (Shao et al., 2013). The inability of CNTs to attain adequate and controllable drug release has also contributed to the slow pace of CNT use in clinical trials (Wong et al., 2013). CNT–drug complexes are less active as compared to free drugs as a result of a generally uncontrollable and low rate of drug release from the complexes.

It is also a major challenge to ensure the uniformity and consistency of CNT–drug complexes due to heterogeneity of CNTs. There are also several challenges in drug release which include development costs. Very expensive equipment and materials for achieving controlled drug release may be needed (Nokhodchi et al., 2012). The release of the drug might be changed by food ingestion and gastric transit time. Orally administered systems should not be chewed as this may affect controlled release leading to loss of slow release (Nokhodchi et al., 2012).

Thus, despite innumerable promising results of CNTs in biomedicine, there are challenges which need to be dealt with prior to CNT integration into biomedical devices and technology. The advances that are required to witness CNT application in the clinical setting and commercialization include:

i. Improvement of the sensitivity of the CNT based biosensors
ii. Efficient loading and unloading of drugs to and from the CNTs
iii. Reduction in nonspecific bonding of CNT to the site of interest
iv. Further investigation of long term nanotoxicity of CNTs employing a variety of animal models and various doses
v. Identification of non-invasive methods for direct injection of CNT-Drug complexes at diseased site
vi. Prevention of leakage of encapsulated drugs from the CNTs
vii. Production of homogenous CNTs to improve *in vivo* pharmacokinetics of CNTs
viii. Higher doses to facilitate bioavailability of siRNA for effective gene silencing
ix. Development of effective scaffolds from CNT hybrid to promote cell adhesion, growth, differentiation and proliferation (Wang and Chen, 2007; Kesharwani, Gajbhiye and Jain, 2012).

Ensysce Bioscience developed SWCNTs conjugated siRNA for treatment of cancer. They received regulatory approval to conduct clinical trials on siRNA delivery into tumour cells. Use of CNTs for improving the imaging of colorectal cancer was approved by the U.S. Food and Drug Administration (Kirkpatrick et al., 2012).

There is a very slow rate of CNT clinical trials as a result of their toxicity controversy. Further work is required to ascertain the toxicity of the CNTs prior to implementation in clinical trials.

2.13. Future potential applications of CNTS

Intensive research on CNTs is being undertaken in the areas of targeted drug delivery, nanoscaffolds for tissue engineering, biomedical imaging and detection for treatment of diseases and health monitoring. CNTs have potential in the design of theranostic systems for simultaneous targeted drug delivery and detection of disease due to their physico-chemical properties (Kushwaha et al., 2012). In future, CNTs could be used

as theranostic tools for simultaneous detection and treatment of ischemic stroke for a potential reduction in adverse side effects compared to conventional stroke treatments as demonstrated from previous studies (Shao et al., 2013).

Ultrasensitive markers could be coupled to CNTs to enhance their targeting properties. This approach could be implemented in future to differentiate between the diseased and healthy tissues (He et al., 2013). MWCNTs have a potential for use as nano-devices to enhance therapeutic protocols for transplantation and homing of stem cells for *in vivo* treatment of neurological disorders (Vittorio et al., 2009).

Since CNTs can act as vectors for siRNA *in vivo*, they have the future potential for use in silencing the genes of the Caspase-3 enzyme resulting in a reduction in neuronal damage and promotion of neuroprotection (Bates and Kostarelos, 2013). In future, robust and reproducible biosensors employing CNTs that can be used at the point of care could be fabricated and these biosensors would be of low cost and could be disposed of after use or be recycled. They could be user-friendly for use by even the layman for detection of biomarkers in neurological diseases including stroke (Yang et al., 2015).

The small size, high surface area, specificity and multifunctionality of CNTs are expected to play a pivotal role in the revolutionary development of brain-specific diagnostic, imaging and drug delivery tools. These nanoengineered systems have the potential to contribute significantly to novel approaches for better understanding of the diagnosis and treatment of acute and chronic neurological CNS disorders (Nair, Dileep and Rajanikant, 2012). The use of CNTs in drug delivery, detection and tissue engineering has shown the potential to revolutionize medicine (Ellis-Behnke, 2007; Kirkpatrick et al., 2012).

2.14. Conclusion remarks

In this review we discussed the promising future of CNT incorporation into neuromedicine with a special focus on their roles in imaging, drug delivery, biosensing and neuroengineering with a specific focus on ischemic stroke. A broad perspective on CNT toxicity, functionalization, and stimuli-responsiveness, and CNTs in neural tissue repair was provided. Future applications of CNTs have been discussed, evaluating their extent of advancement in the detection and treatment of neurological

and ischemic disorders. There are certain challenges ahead such as toxicity, heterogeneity and dispersibility that must be dealt with prior to successful integration of CNTs into biomedical devices and technology. Functionalization was found to play a paramount role in enhancing the potential of CNTs for application in clinical settings. Indeed, application of CNT technology may revolutionize the diagnosis and treatment of ischemic stroke and other neurological disorders.

2.15. References

Al-jamal, K. T. *et al.* (2011) 'Functional motor recovery from brain ischemic insult by carbon nanotube-mediated siRNA silencing', *Proceedings of the National Academy of Sciences, U.S.A.*, 108(27), pp. 10952–10957.

Al-Jamal, K. T. *et al.* (2012) 'Degree of chemical functionalization of carbon nanotubes determines tissue distribution and excretion profile.', *Angewandte Chemie (International ed. in English)*, 51(26), pp. 6389–93.

Ali-Boucetta, H. *et al.* (2013) 'Asbestos-like Pathogenicity of Long Carbon Nanotubes Alleviated by Chemical Functionalization', *Angewandte Chemie*, 52(8), pp. 2274–2278.

Andersen, A. J., Wibroe, P. P. and Moghimi, S. M. (2012) 'Perspectives on carbon nanotube-mediated adverse immune effects', *Advanced Drug Delivery Reviews*, 64(15), pp. 1700–1705.

Ando, Y. *et al.* (2004) 'Growing carbon nanotubes', *Materials Today*. Elsevier Ltd, 7(10), pp. 22–29.

Ansari, S. *et al.* (2011) 'Peer-Review Reports Intracranial Stents for Treatment of Acute Ischemic Stroke : Evolution and Current Status', *WNEU*, 76(6), pp. S24–S34.

Bardi, G. *et al.* (2013) 'Functionalized carbon nanotubes in the brain: cellular internalization and neuroinflammatory responses.', *PloS one*, 8(11), p. e80964 (10pp).

Bates, K. and Kostarelos, K. (2013) 'Carbon nanotubes as vectors for gene therapy: Past achievements, present challenges and future goals', *Advanced Drug Delivery Reviews*, 65(15), pp. 2023–2033.

Beg, M., Ahmad, K. and Renjen, P. (2015) 'Epidemiological study of incidence and risk factors of Ischemic stroke subtypes according to Trial of ORG 10172 in acute stroke treatment criteria: A 3 years, hospital-based study', *International Journal of Medicine and Public Health*, 5(1), pp. 50–54.

Beg, S. *et al.* (2011) 'Advancement in carbon nanotubes: Basics, biomedical applications and toxicity', *Journal of Pharmacy and Pharmacology*, 63(2), pp. 141–163.

Ben-Jacob, E. and Hanein, Y. (2008) 'Carbon nanotube micro-electrodes for neuronal interfacing', *Journal of Materials Chemistry*, 18(43), pp. 5181–5186.

Bhatia, S. K. (2010) 'Biomaterials for clinical applications', in Bhatia, S. K. (ed.) *Biomaterials for Clinical Applications*. New York, USA: Springer, pp. 1–283. doi:

10.1007/978-1-4419-6920-0.

Bhirde, A. A. *et al.* (2009) ‘Targeted killing of cancer cells in vivo and in vitro with EGF-directed carbon nanotube-based drug delivery.’, *ACS nano*, 3(2), pp. 307–16.

Bianco, A., Kostarelos, K. and Prato, M. (2011) ‘Making carbon nanotubes biocompatible and biodegradable’, *Chemical Communications*, 47(37), pp. 10182–8.

Bjartmarz, H. and Rehncrona, S. (2007) ‘Comparison of accuracy and precision between frame-based and frameless stereotactic navigation for deep brain stimulation electrode implantation’, *Stereotactic and Functional Neurosurgery*, 85(5), pp. 235–242.

Bokara, K. K. *et al.* (2013) ‘Biocompatability of carbon nanotubes with stem cells to treat CNS injuries.’, *Anatomy & cell biology*, 46(2), pp. 85–92.

Bonifazi, D. *et al.* (2006) ‘Microscopic and spectroscopic characterization of paintbrush-like single-walled carbon nanotubes’, *Nano Letters*, 6(7), pp. 1408–1414.

Bottini, M., Rosato, N. and Bottini, N. (2011) ‘PEG-modified carbon nanotubes in biomedicine: Current status and challenges ahead’, *Biomacromolecules*, 12(10), pp. 3381–3393.

Buzea, C., Pacheco, I. I. and Robbie, K. (2007) ‘Nanomaterials and nanoparticles: sources and toxicity.’, *Biointerphases*, 2(4), pp. MR17-MR71.

Cellot, G. *et al.* (2009) ‘Carbon nanotubes might improve neuronal performance by favouring electrical shortcuts’, *Nature Nanotechnology*, 4(February), pp. 126–133.

Chen, C. *et al.* (2009) ‘Early inhibition of HIF-1 α with small interfering RNA reduces ischemic – reperfused brain injury in rats’, *Neurobiology of Disease*, 33(3), pp. 509–517.

Chen, R.-L. *et al.* (2010) ‘Ischemic stroke in the elderly: an overview of evidence.’, *Nature reviews. Neurology*, 6(5), pp. 256–265.

Chen, X. *et al.* (2011) ‘Carbon-Nanotube-Based Stimuli-Responsive Controlled-Release System’, *Chemistry European Journal*, 17, pp. 4454–4459.

Ciccone, S., Cappella, M. and Borgna-Pignatti, C. (2011) ‘Ischemic stroke in infants and children: practical management in emergency.’, *Stroke research and treatment*, 2011, pp. 1–9.

Cirillo, G. *et al.* (2011) ‘Antioxidant multi-walled carbon nanotubes by free radical

grafting of gallic acid: new materials for biomedical applications.', *The Journal of pharmacy and pharmacology*, 63(2), pp. 179–88.

Dieckmann, G. R. *et al.* (2003) 'Controlled Assembly of Carbon Nanotubes by Designed Amphiphilic Peptide Helices', *J. Am. Chem. Soc.*, 125(7), pp. 1770–1777.

Edwards, S. L. and Ramshaw, J. A. M. (2009) 'Carbon nanotubes in scaffolds for tissue engineering', *Expert reviews of medical devices*, 6(5), pp. 499–505.

Elger, B. *et al.* (2006) 'Extended therapeutic time window after focal cerebral ischemia by non-competitive inhibition of AMPA receptors.', *Brain research*, 1085(1), pp. 189–94.

Ellis-Behnke, R. (2007) 'Nano neurology and the four P's of central nervous system regeneration: preserve, permit, promote, plasticity.', *The Medical clinics of North America*, 91(5), pp. 937–62.

Fabbro, A. *et al.* (2012) 'Carbon Nanotubes: Artificial Nanomaterials to Engineer Single Neurons and Neuronal Networks', *ACS Chemical Neuroscience*, 3, pp. 611–618.

Fabbro, A., Prato, M. and Ballerini, L. (2013) 'Carbon nanotubes in neuroregeneration and repair.', *Advanced drug delivery reviews*, 65(15), pp. 2034–2044.

Fam, D. W. H. *et al.* (2009) 'Selective sensing of hydrogen sulphide using silver nanoparticle decorated carbon nanotubes', *Sensors and Actuators, B: Chemical*, 138, pp. 189–192.

Feynman, R. P. (1960) 'There's plenty of room at the bottom.', *Engineering and science*, 23(5), pp. 22–36.

Fisher, C. *et al.* (2012) 'Applications and Nanotoxicity of Carbon Nanotubes and Graphene in Biomedicine', *Journal of Nanomaterials*, 2012, pp. 1–19.

Flavin, K. *et al.* (2011) 'Controlled carboxylic acid introduction: a route to highly purified oxidised single-walled carbon nanotubes', *Journal of Materials Chemistry*, 21(44), pp. 17881–17887.

Folch, J., Petrov, D., Ettcheto, M., Abad, S., Sanchez-Lopez, E., Garcia, M.L., Olloquequi, J., Beas-Zarate, C., Auladell, C., Antoni, C. (2015) 'Current Research Therapeutic Strategies for Alzheimer's Disease Treatment', *Neural Plasticity*, 2016, p. 15.

Gabay, T. *et al.* (2005) 'Engineered self-organization of neural networks using carbon nanotube clusters', *Physica A: Statistical Mechanics and its Applications*, 350(2–4),

pp. 611–621.

Gabay, T. *et al.* (2007) ‘Electro-chemical and biological properties of carbon nanotube based multi-electrode arrays’, *Nanotechnology*, 18(3), p. 035201 (6pp).

Gaillard, C. *et al.* (2009) ‘Carbon Nanotubes Carrying Cell-Adhesion Peptides do not Interfere with Neuronal Functionality’, *Advanced Materials*, 21(28), pp. 2903–2908.

Ghosh, S. (2003) ‘Carbon Nanotube Flow Sensors’, *Science*, 299(5609), pp. 1042–1044.

Gilmore, J. L. *et al.* (2008) ‘Novel Nanomaterials for Clinical Neuroscience’, *Journal of neuroimmune pharmacology : the official journal of the Society on NeuroImmune Pharmacology*, 3(2), pp. 83–94.

Giugliano, M., Prato, M. and Ballerini, L. (2008) ‘Nanomaterial/neuronal hybrid system for functional recovery of the CNS’, *Drug Discovery Today: Disease Models*, 5(1), pp. 37–43.

Gottipati, M. K., Verkhratsky, A. and Parpura, V. (2014) ‘Probing astroglia with carbon nanotubes: modulation of form and function.’, *Philosophical transactions of the Royal Society of London. Series B, Biological sciences*, 369(1654), pp. 20130598–20130604.

Grossman, A. W. and Broderick, J. P. (2013) ‘Advances and Challenges in Treatment and Prevention of Ischemic Stroke’, *Annals of Neurology*, 74(3), pp. 363–372.

Gustavsson, P., Hedmer, M. and Rissler, J. (2011) ‘Carbon Nanotubes’, in *Carbon Nanotubes- Exposure, toxicology and protective measures in the work environment*, pp. 1–72.

He, H. *et al.* (2013) ‘Carbon Nanotubes : Applications in Pharmacy and Medicine’, *Biomed Research International*, 2013, p. 13pp.

He, P. *et al.* (2004) ‘Aligned carbon nanotube – DNA electrochemical sensors’, *Chemical Communications*, pp. 348–349.

Heller, D. A. *et al.* (2005) ‘Single-walled carbon nanotube spectroscopy in live cells: Towards long-term labels and optical sensors’, *Advanced Materials*, 17(23), pp. 2793–2799.

Heller, D. A. *et al.* (2006) ‘Optical Detection of DNA Conformational Polymorphism on Single-Walled Carbon Nanotubes’, *Science*, 311(5760), pp. 508–511.

Hernández-Ferrer, J. *et al.* (2014) 'Study of neuron survival on polypyrrole-embedded single-walled carbon nanotube substrates for long-term growth conditions.', *Journal of biomedical materials research. Part A*, 102(12), pp. 4443–54.

Hong, C. and Pan, C. (2008) 'Functionalized carbon nanotubes responsive to environmental stimuli', *Journal of Materials Chemistry*, 18, pp. 1831–1836.

Hong, G. *et al.* (2014) 'Through-skull fluorescence imaging of the brain in a new near-infrared window', *Nature Photonics*, 8(9), pp. 723–730.

Hu, H. *et al.* (2004) 'Chemically Functionalized Carbon Nanotubes as Substrates for Neuronal Growth.', *Nano letters*, 4(3), pp. 507–511.

Iijima, S. (1991) 'Helical microtubules of graphitic carbon', *Nature*, 354(6348), pp. 56–58.

Iverson, N. M. *et al.* (2013) '[Supplementary] In vivo biosensing via tissue-localizable near-infrared-fluorescent single-walled carbon nanotubes.', *Nature nanotechnology*, 8(11), pp. 873–80.

Jacobs, C. B. *et al.* (2014) 'High temporal resolution measurements of dopamine with carbon nanotube yarn microelectrodes', *Analytical Chemistry*, 86(12), pp. 5721–5727.

Jain, S. *et al.* (2011) 'Toxicity of multiwalled carbon nanotubes with end defects critically depends on their functionalization density', *Chemical Research in Toxicology*, 24(11), pp. 2028–2039.

Jain, S., Singh, S. R. and Pillai, S. (2012) 'Toxicity Issues Related to Biomedical Applications of Carbon Nanotubes', *Journal of nanomedical nanotechnology*, 3(5), pp. 1–15.

Ji, S. *et al.* (2010) 'Carbon nanotubes in cancer diagnosis and therapy.', *Biochimica et biophysica acta*, 1806(1), pp. 29–35.

Ji, Z. *et al.* (2009) 'The hepatotoxicity of multi-walled carbon nanotubes in mice.', *Nanotechnology*, 20(44), p. 445101 (9pp).

John, A. A. *et al.* (2015) 'Carbon nanotubes and graphene as emerging candidates in neuroregeneration and neurodrug delivery', *International Journal of Nanomedicine*, Volume 10, pp. 4267–4277.

Kafa, H. *et al.* (2015) 'The interaction of carbon nanotubes with an in vitro blood-brain barrier model and mouse brain in vivo', *Biomaterials*, 53, pp. 437–452.

Kagan, V. E. *et al.* (2010) 'Carbon nanotubes degraded by neutrophil myeloperoxidase induce less pulmonary inflammation.', *Nature nanotechnology*, 5(5), pp. 354–359.

Kakkar, A. K. and Dahiya, N. (2015) 'Management of Parkinson's disease: Current and future pharmacotherapy', *European Journal of Pharmacology*, 750, pp. 74–81.

Keefer, E. W. *et al.* (2008) 'Carbon nanotube coating improves neuronal recordings', *Nature Nanotechnology*, 3(7), pp. 434–439.

Kesharwani, P., Gajbhiye, V. and Jain, N. K. (2012) 'A review of nanocarriers for the delivery of small interfering RNA', *Biomaterials*, 33(29), pp. 7138–7150.

Kim, J. A. *et al.* (2012) 'Regulation of morphogenesis and neural differentiation of human mesenchymal stem cells using carbon nanotube sheets', *Integrative Biology*, 4(6), p. 587.

Kirkpatrick, D. L. *et al.* (2012) 'Carbon Nanotubes: Solution for the Therapeutic Delivery of siRNA?', *Materials*, 5(12), pp. 278–301.

Kostarelos, K., Bianco, A. and Prato, M. (2009) 'Promises, facts and challenges for carbon nanotubes in imaging and therapeutics.', *Nature nanotechnology*, 4(10), pp. 627–633.

Kotchey, G. P. *et al.* (2013) 'Peroxidase-mediated biodegradation of carbon nanotubes in vitro and in vivo', *Advanced Drug Delivery Reviews*, 65(15), pp. 1921–1932.

Kushwaha, S. *et al.* (2012) 'Novel Drug Delivery System for Anticancer Drug: A Review', *Sphinxsai.Com*, 4(2), pp. 542–553.

Kuzmenko, V. *et al.* (2016) 'Enhanced growth of neural networks on conductive cellulose-derived nano fibrous scaffolds', *Materials Science & Engineering C*. Elsevier B.V., 58, pp. 14–23.

Kyle, S. and Saha, S. (2014) 'Nanotechnology for the detection and therapy of stroke', *Advanced Healthcare Materials*, (August), pp. 1703–1720.

Lacerda, L. *et al.* (2006) 'Carbon nanotubes as nanomedicines: From toxicology to pharmacology', *Advanced Drug Delivery Reviews*, 58(14), pp. 1460–1470.

Lee, H. J. *et al.* (2011) 'Amine-modified single-walled carbon nanotubes protect neurons from injury in a rat stroke model', *Nature Nanotechnology*, 6(2), pp. 121–125.

Lee, Y. and Geckeler, K. E. (2010) 'Carbon nanotubes in the biological interphase: The

relevance of noncovalence', *Advanced Materials*, 22(36), pp. 4076–4083.

Lin, C. M. *et al.* (2009) 'Flexible carbon nanotubes electrode for neural recording', *Biosensors and Bioelectronics*, pp. 2791–7.

Lin, J.-K. *et al.* (1998) 'Survey of Catechins, Gallic Acid, and Methylxanthines in Green, Oolong, Pu-erh, and Black Teas', *Journal of Agricultural and Food Chemistry*, 46(9), pp. 3635–3642.

Malarkey, E. B. and Parpura, V. (2007) 'Applications of carbon nanotubes in neurobiology.', *Neuro-degenerative diseases*, 4(4), pp. 292–9.

Marchesan, S. *et al.* (2015) 'The winding road for carbon nanotubes in nanomedicine', *Materials Today*. Elsevier Ltd., 18(1), pp. 12–19.

Matsumoto, K. *et al.* (2007) 'Neurite outgrowths of neurons with neurotrophin-coated carbon nanotubes', *Journal of bioscience and bioengineering*, 103(3), pp. 216–20.

Mattson, M. P., Haddon, R. C. and Rao, a M. (2000) 'Molecular functionalization of carbon nanotubes and use as substrates for neuronal growth.', *Journal of molecular neuroscience : MN*, 14, pp. 175–182.

Meng, L. *et al.* (2013) 'Inhibitory effects of multiwall carbon nanotubes with high iron impurity on viability and neuronal differentiation in cultured PC12 cells', *Toxicology*, 313(1), pp. 49–58.

Modi, G. *et al.* (2009) 'Nanotechnological applications for the treatment of neurodegenerative disorders', *Progress in Neurobiology*, 88(4), pp. 272–285.

Modi, G., Pillay, V. and Choonara, Y. (2010) 'Advances in the Treatment of Neurodegenerative Disorders Employing Nanoparticles', *Annals of the New York Academy of Sciences*, 1184, pp. 154–172.

Monaco, A. M. and Giugliano, M. (2014) 'Carbon-based smart nanomaterials in biomedicine and neuroengineering.', *Beilstein journal of nanotechnology*, 5(1), pp. 1849–63.

Moon, S. U. *et al.* (2012) 'Carbon nanotubes impregnated with subventricular zone neural progenitor cells promotes recovery from stroke', *International Journal of Nanomedicine*, 7, pp. 2751–2765.

Moore, V., Strano, M. and Haroz, E. (2003) 'Individually suspended single-walled carbon nanotubes in various surfactants', *Nano Letters*, 3(10), pp. 1379–1382.

Mutlu, G. M. *et al.* (2010) 'Biocompatible nanoscale dispersion of single-walled carbon nanotubes minimizes in vivo pulmonary toxicity.', *Nano letters*, 10(5), pp. 1664–70.

Nair, S. B., Dileep, A. and Rajanikant, G. K. (2012) 'Nanotechnology Based Diagnostic and Therapeutic Strategies for Neuroscience with Special Emphasis on Ischemic Stroke', *Current Medicinal Chemistry*, 19, pp. 1–13.

Nho, Y. *et al.* (2010) 'Adsorption of mesenchymal stem cells and cortical neural stem cells on carbon nanotube/polycarbonate urethane', *Nanomedicine : nanotechnology, biology, and medicine*, 5(3), pp. 409–417.

Ni, Y. *et al.* (2005) 'Chemically functionalized water soluble single-walled carbon nanotubes modulate neurite outgrowth.', *Journal of Nanoscience and Nanotechnology*, 5(10), pp. 1707–1712.

Nokhodchi, A. *et al.* (2012) 'The role of oral controlled release matrix tablets in drug delivery systems', *BioImpacts*, 2(4), pp. 175–187.

Nunes, A. *et al.* (2012) 'Application of carbon nanotubes in neurology : clinical perspectives and toxicological risks', *Arch Toxicol*, 86(7), pp. 1009–1020.

Nunes, A., Al-Jamal, K. T. and Kostarelos, K. (2012) 'Therapeutics, imaging and toxicity of nanomaterials in the central nervous system.', *Journal of controlled release : official journal of the Controlled Release Society*, 161(2), pp. 290–306.

Park, K. I., Teng, Y. D. and Snyder, E. Y. (2002) 'The injured brain interacts reciprocally with neural stem cells supported by scaffolds to reconstitute lost tissue', *nature biotechnology*, 20(November), pp. 1111–1118.

Pathan, S. *et al.* (2009) 'CNS drug delivery systems: novel approaches.', *Recent patents on drug delivery & formulation*, 3, pp. 71–89.

Perepelytsina, O. M. *et al.* (2018) 'Influence of Carbon Nanotubes and Its Derivatives on Tumor Cells In Vitro and Biochemical Parameters , Cellular Blood Composition In Vivo', *Nanoscale Research Letters*, 13, p. 286.

Pramanik, M. *et al.* (2009) 'Single-walled carbon nanotubes as a multimodal-thermoacoustic and photoacoustic-contrast agent', *Journal of Biomedical Optics*, 14(3), p. 034018 (8pp).

Prato, M., Kostarelos, K. and Bianco, A. (2008) 'Functionalized Carbon Nanotubes in Drug', *Accounts of Chemical Research*, 41(September 2007), pp. 60–68.

Qi, W. *et al.* (2017) *Curing the toxicity of multi-walled carbon nanotubes through native small-molecule drugs*, *Scientific Reports*.

Ravindra, R. and Bhat, B. (2011) 'Synthesis of Aligned Carbon Nanotubes by Floating Catalyst Method Using Ferrocene', *Journal of Metals, Materials and Minerals*, 21(2), pp. 95–99.

Re, F., Gregori, M. and Masserini, M. (2012) 'Nanotechnology for neurodegenerative disorders', *Nanomedicine: Nanotechnology, Biology, and Medicine*, 8, pp. S51–S58.

Roman, J. A. *et al.* (2011) 'Single-walled carbon nanotubes chemically functionalized with polyethylene glycol promote tissue repair in a rat model of spinal cord injury.', *Journal of neurotrauma*, 28(11), pp. 2349–62.

Ryman-Rasmussen, J. P. *et al.* (2009) 'Inhaled carbon nanotubes reach the subpleural tissue in mice.', *Nature nanotechnology*, 4(11), pp. 747–51.

Sacchetti, C. *et al.* (2013) 'Surface polyethylene glycol conformation influences the protein corona of polyethylene glycol-modified single-walled carbon nanotubes: Potential implications on biological performance', *ACS Nano*, 7(3), pp. 1974–1989.

Santiago-Rodríguez, L., Sánchez-Pomales, G. and Cabrera, C. R. (2010) 'DNA-Functionalized Carbon Nanotubes: Synthesis, Self-Assembly, and Applications', *Israel Journal of Chemistry*, 50(3), pp. 277–290.

Shao, W. *et al.* (2013) 'Carbon Nanotubes for Use in Medicine : Potentials and Limitations, Syntheses and Applications of Carbon Nanotubes and Their Composites', in Suzuki, S. (ed.) *Nanotechnology and Nanomaterials*. In Tech, pp. 285–311. doi: 10.5772/51785.

Sharma, H. S., Muresanu, D. F. and Sharma, A. (2013) 'Novel therapeutic strategies using nanodrug delivery, stem cells and combination therapy for CNS trauma and neurodegenerative disorders.', *Expert review of neurotherapeutics*, 13(10), pp. 1085–8.

Shein, M. *et al.* (2009) 'Engineered neuronal circuits shaped and interfaced with carbon nanotube microelectrode arrays', *Biomedical Microdevices*, 11(2), pp. 495–501.

Shityakov, S. *et al.* (2015) 'Blood-brain barrier transport studies, aggregation, and molecular dynamics simulation of multiwalled carbon nanotube functionalized with fluorescein isothiocyanate.', *International journal of nanomedicine*, 10, pp. 1703–1713.

Shvartzman-Cohen, R. *et al.* (2004) 'Generic approach for dispersing single-walled carbon nanotubes: the strength of a weak interaction.', *Langmuir : the ACS journal of surfaces and colloids*, 20(18), pp. 6085–6088.

Singh, N., Pillay, V. and Choonara, Y. E. (2007) ‘Advances in the treatment of Parkinson’s disease’, *Progress in Neurobiology*, 81(1), pp. 29–44.

Skaper, S. D. (2008) ‘The biology of neurotrophins, signalling pathways, and functional peptide mimetics of neurotrophins and their receptors.’, *CNS & neurological disorders drug targets*, 7(1), pp. 46–62.

Sotiropoulou, S. and Chaniotakis, N. a. (2003) ‘Carbon nanotube array-based biosensor’, *Analytical and Bioanalytical Chemistry*, 375(1), pp. 103–105.

Stockwell, J. *et al.* (2014) ‘Novel Central Nervous System Drug Delivery Systems’, *Chemical Biology & Drug Design*, 83(5), pp. 507–520.

Tagmatarchis, N. and Prato, M. (2004) ‘Functionalization of carbon nanotubes via 1 , 3-dipolar cycloadditions’, *Journal of Materials Chemistry*, 14, pp. 437–439.

Tan, J. *et al.* (2012) ‘Nanoporous peptide particles for encapsulating and releasing neurotrophic factors in an animal model of neurodegeneration’, *Advanced Materials*, 24(25), pp. 3362–3366.

Tasis, dimitrios *et al.* (2006) ‘Chemistry of Carbon Nanotubes’, *Chemistry Reviews*, 106(3), pp. 1105–1136.

Torocsik, B., Angelastro, J. M. and Greene, L. A. (2002) ‘The Basic Region and Leucine Zipper Transcription Factor MafK Is a New Nerve Growth Factor-Responsive Immediate Early Gene That Regulates Neurite Outgrowth’, *Journal of Neuroscience*, 22(20), pp. 8971–8980.

Tran, P. A., Zhang, L. and Webster, T. J. (2009) ‘Carbon nanofibers and carbon nanotubes in regenerative medicine’, *Advanced Drug Delivery Reviews*, 61(12), pp. 1097–1114.

Turner, R. J. and Vink, R. (2012) ‘Combined tissue plasminogen activator and an NK1 tachykinin receptor antagonist: an effective treatment for reperfusion injury following acute ischemic stroke in rats.’, *Neuroscience*, 220, pp. 1–10.

Valko, M. *et al.* (2007) ‘Free radicals and antioxidants in normal physiological functions and human disease’, *The international journal of biochemistry & cell biology*, 39(1), pp. 44–84.

Vardharajula, S. *et al.* (2012) ‘Functionalized carbon nanotubes : biomedical applications’, *International Journal of Nanomedicine*, 7, pp. 5361–5374.

Vidu, R. *et al.* (2014) ‘Nanostructures: a platform for brain repair and augmentation’,

Frontiers in systems neuroscience, 8(June), p. 24 pp.

Vittorio, O. *et al.* (2009) 'Imaging and Biomedical Application of Magnetic Carbon Nanotubes'.

Wang, D. and Chen, L. (2007) 'Temperature and pH-Responsive Single-Walled Carbon Nanotube Dispersions', *Nano Letters*, 7(6), pp. 1480–1884.

Wang, J. *et al.* (2011) 'Cytotoxicity of single-walled carbon nanotubes on PC12 cells', *Toxicology in Vitro*. Elsevier Ltd, 25(1), pp. 242–250.

Wang, J. *et al.* (2012) 'Vitamin E renders protection to PC12 cells against oxidative damage and apoptosis induced by single-walled carbon nanotubes.', *Toxicology in vitro : an international journal published in association with BIBRA*, 26(1), pp. 32–41.

Wang, J. T. (2015) 'Functionalized carbon nanotubes : revolution in brain delivery', *Nanomedicine (London, England)*, 10(17), pp. 2639–2642.

Witzmann, F. and Monteiro-Riviere, N. (2006) 'Multi-walled carbon nanotube exposure alters protein expression in human keratinocytes', *Nanomedicine: Nanotechnology, Biology, and Medicine*, 2(3), pp. 158–168.

Wong, B. S. *et al.* (2013) 'Carbon nanotubes for delivery of small molecule drugs', *Advanced Drug Delivery Reviews*, 65(15), pp. 1964–2015.

Yang, C. *et al.* (2015) 'Analytica Chimica Acta Recent trends in carbon nanomaterial-based electrochemical sensors for biomolecules : A review', *Analytica Chimica Acta*, 887, pp. 17–37.

Yang, Z. *et al.* (2010) 'Pharmacological and toxicological target organelles and safe use of single-walled carbon nanotubes as drug carriers in treating Alzheimer disease.', *Nanomedicine : nanotechnology, biology, and medicine*, 6(3), pp. 427–41.

Zhang, L. and Webster, T. J. (2009) 'Nanotechnology and nanomaterials: Promises for improved tissue regeneration', *Nano Today*, 4(1), pp. 66–80.

Zhao, D. *et al.* (2011) 'Carbon Nanotubes Enhance CpG Uptake and Potentiate Antiglioma Immunity', *Clinical Cancer Research*, 17(4), pp. 771–782.

Zheng, M. *et al.* (2003) 'DNA-assisted dispersion and separation of carbon nanotubes', *Nature Materials*, 2(5), pp. 338–342.

CHAPTER 3

VERTICALLY ALIGNED MULTIWALLED CARBON NANOTUBES FOR USE IN DETECTION AND TREATMENT OF ISCHEMIC STROKE

Abstract

Carbon nanotubes have been extensively studied due to their excellent physico-chemical properties. They have a potential to be employed as theranostic tools in the detection and treatment of ischemic stroke. Stroke is currently the fourth root cause of death and the leading cause of disability in the world. The effective strategies need to be developed for the prevention, diagnosis and treatment of central nervous system disorders. The development of these strategies requires better understanding of neurological diseases. In this study, aligned multiwalled carbon nanotubes (VA-MWCNTs) were synthesized on a substrate and quartz tube walls using chemical vapour deposition (CVD). Parameters such as synthesis temperature, catalyst concentration, synthesis duration, gas flow rate, and location of the substrate in the furnace were varied to obtain optimal pyrolysis conditions for well aligned MWCNT production. Well aligned MWCNTs were deposited on silicon wafer at 125 mm between the centre and entrance of the furnace at 775 °C with ferrocene concentration of 2.5 % in toluene with a gas flow rate of 400 $mL.min^{-1}$ and synthesis duration of 45 min. VA - MWCNTs with average length of 127 µm, average internal diameter of 11 nm and average external diameter of 73 nm were obtained under these pyrolysis conditions. Electrical resistivity of CNTs was measured and CNTs were found to be strongly electrically conductive at temperatures ranging from 26.85 - 76.85 °C. Functional groups of CNTs were also determined by FTIR. CNT yield was also found to be improved by a mixture of Fe/Co and 599.40 mg of CNTs were produced compared with 331.2 mg produced when Fe/Ni was used. Honeycomb like structures were formed on the surface of the VA-MWCNTs when treated with 5 M HCl during purification process. Treatment of the CNTs with 5 M HCl improved the purity of the CNTs. These findings suggest that well aligned quality MWCNTs can be produced with CVD technique and be treated with 5 M HCl to increase their porositometric features such as pore volume, pore size and surface area to improve loading capacity of target ligand and drug for the diagnosis and treatment of ischemic stroke.

3.1. Introduction

Carbon nanotube synthesis and their application in various fields have been growing at an alarming rate. CNTs are a new emerging group of nanomaterials that have illustrated promising data in different fields of nanomedicine for the advancement of technology in medicine (Bianco *et al.*, 2005; Lacerda *et al.*, 2006; Marchesan *et al.*, 2015). They have been considered as the most promising nanoscale building blocks for future applications in technology due to their very special architecture and outstanding physico-chemical properties (Dai, 2002; Cao *et al.*, 2008). Since a report by Iijima in 1991, carbon nanotubes have been the centre of attraction based on their unique properties, (Iijima, 1991). They are composed of a single a rolled graphene sheet with diameters of nanometer size and length up to several µm to cm.

There are three classes of CNTs namely single walled, double walled and multiwalled CNTs. CNTs are electrically and thermally conductive and have ultralight weight. They are highly flexible, very strong and inert but can be chemically modified with various functional groups depending on their intended use (Malarkey and Parpura, 2007; Fabbro *et al.*, 2012; Gottipati, Verkhratsky and Parpura, 2014). They are potential candidates for various applications such as field emission devices, biosensors, chemical sensors, hydrogen storage, nanoelectronics, catalyst support, nanocomposites in mechanical reinforcing agents, targeting and drug delivery systems (Ravindra and Bhat, 2011). Carbon nanotubes are semiconducting metallic nanomaterials depending on their diameter and chirality (Saito *et al.*, 1992; Mahanandia and Nanda, 2008). Without these materials, the success of many technologies could have been hindered.

The nature and quality of carbon nanotubes rely on the method of synthesis. The synthesis method monitors the extent of graphitization, diameter and helicity. A spectrum of procedures for the production of carbon nanotubes have been presented and the most widely used techniques are laser ablation, arc discharge, and chemical vapour deposition (Ando *et al.*, 2004; Santiago-Rodríguez, Sánchez-Pomales and Cabrera, 2010). Out of the three methods, the most common and preferred method for the synthesis of carbon nanotubes is the catalytic chemical vapour deposition (CCVD). This technique has many advantages including mass production, affordability, less running cost and high quality CNTs production (Ravindra and Bhat, 2011).

Nebulised spray pyrolysis is an upgraded format Chemical Vapour Deposition. The method utilises ultra-high RF to nebulise the standard or sample solution to generate an aerosol. The nebulised solution is ferried into a high temperature furnace by an inert carrier gas such as argon or nitrogen (Cele and Coville, 2009). A reaction mixture is then placed in a reservoir coupled to a piezo electric transducer and frequency generator. The CCVD is divided into a floating catalyst and fixed catalyst methods where the catalyst is in a gaseous phase in floating catalyst method and and in a solid phase in fixed catalyst method.

In a floating method, catalyst preparation is not required as the catalyst particles are constantly formed in the reactor tube. Toluene is utilised as a solvent to dissolve the precursor, ferrocene. Furthermore, toluene serves as a source of carbon. Ferrocene is a responsible for production of Fe nanoparticles for nucleation. This method is characterised by a simple experimental set-up, easily available reagents and continuous controllable synthesis. This technique is based on the hydrocarbon decomposition on the catalysts such as Co, Mo, iron and nickel (Sengupta and Jacob, 2010; Journet, Picher and Jourdain, 2012). The catalyst particle size is a very important factor in CNT synthesis. With this method, quality well aligned CNTs can be produced (Ravindra and Bhat, 2011).

Organic solvents such as alkenes, aromatics, alkanes and alcohols are used as carbon sources for the production of carbonaceous materials in the CVD technique, (Zhang *et al.*, 2007). A catalyst is also required for the CNT synthesis and transition metals such as Fe, Co and Ni are the most widely used metals for this purpose. The hydrocarbon solution is wiped into a furnace at a very high temperature using argon or nitrogen. In this technique, ultra-fine solution droplets are produced to provide catalyst particles to form a platform for the CNTs growth.

The procedure has been used with great success to manufacture both SWCNTs and MWCNTs using a variety of catalysts, solvents, and synthesis conditions. Drawbacks include the poor solubility of some catalyst precursors in some solvents. The quality and purity of the CNTs is dependent on many factors such as temperature, gas flow rate, synthesis time, substrate location within reactor tube, solvent and catalyst.

.

In this study, we have investigated the effect of a variety of parameters on the quality and yield of VA-MWCNTs. These factors include the reaction temperature, gas flow rate, synthesis duration and silicon wafer location in the furnace. Organometallic materials such as ferrocene were used as precursors and toluene as organic solvent for carbon source. We also investigated the effect of a combination of transition metals in a catalyst on the yield of VA-MWCNTs.

Moreover, we also investigated the effect of various acids and their concentrations on VA-MWCNTs during purification process. VA-MWCNTs were successfully synthesised and their yield was improved by an introduction of a mixture of ferrocene and cobaltocene in the catalyst solution. The CNTs were purified by treatment with H_2SO_4:HNO_3 (3:1) which resulted in the damage of the VA-MWCNT array and HCl which resulted in the formation of honey comb structures on the surface of CNTs. The generation of honey comb structures resulted in a rise in pore volume, pore size and surface area. These parameters play a pivotal role in enhancing the loading capacity of the CNTs for target ligands and drugs for detection, imaging and delivery of drugs to the diseased site in the stroke patient brain.

Electrical resistivity of CNTs was also determined and the CNTs were found to be electrically conductive. This property is useful in the design of a biosensor for the biomarkers in ischemic stroke and other biomolecules. The wettability of the CNTs was also determined using contact angle technique and the HCl treated CNTs were found to be hydrophilic. This property will be extremely useful for delivering drugs to the diseased site via blood circulation. These findings suggest that the quality vertically aligned multiwalled carbon nanotubes could be synthesised under specific pyrolysis conditions and be functionalised for potential application in diagnosis and drug delivery for the treatment of diseases including neurological disorders.

3.2. Materials and Methods

3.2.1. Materials

The following chemicals were purchased from Sigma-Aldrich (St. Louis, MO, USA): Ferrocene, 98 %, toluene chromaSolv for HPLC, ≥ 99.9 %, hydrochloric acid ≥32 %, acetone chromaSolv for HPLC, ≥ 99.8 %, ethanol 99.8 %, bis-(cyclopentadienyl) cobalt(II) (colbaltocene) and bis-(cyclopentadienyl) nickel (II) (nickelocene). Circular silicon wafer with single side polished, N-type, without dopant, diam. × thickness 2 in. × 0.5 mm was also purchased from Sigma-Aldrich. Baseline argon (95 %) balanced with 5 % hydrogen was purchased from African Oxygen Ltd (Afrox) (Germiston, South Africa). Copper grids with holey lacey carbon, Whatman filter paper and Pasteur pipettes were purchased from SPI supplies (West Chester, PA, USA). Quartz reactor (1140 mm x 35 mm I.D.) was purchased from Wits University, Dept of Chemistry (Johannesburg, South Africa).

3.2.2. Preparation of silicon wafer and catalyst

A circular silicon wafer was cut into 1 cm x 1 cm pieces and sonicated in an ultrasonic bath (UMC-5, Integral Systems (Pty) Ltd, Randburg, South Africa) in acetone for 5min followed by a second ultrasonication in water for another 5 min. The silicon wafer pieces were allowed to dry under nitrogen and stored away from dust at ambient temperature for future use.

In catalyst preparation, toluene was used as a carbon source and ferrocene as a source of iron nanoparticles for nucleation. Various concentrations (2.5 %, 5 % and 10 %) of ferrocene were prepared in toluene for ferrocene catalyst. Ferrocene was weighed on ME 104 Mettler Toledo analytical balance (Merck (Pty) Ltd, Modderfontein, South Africa) and dissolved in toluene and sonicated in UMC- 5 ultrasonic bath for 15min to generate a homogenous mixture.

For ferrocene-nickelocene catalyst, a solution of 1,25 $mg.mL^{-1}$ of nickelocene was prepared in 2.5 % of ferrocene in toluene. The mixture was ultrasonicated for 15 min to ensure that nickelocene was completely dissolved. This bimetallic catalyst was used to evaluate the effect of ferrocene-nickelocene in CNT growth.

For ferrocene-cobaltocene catalyst, a solution of 1,25 mg.mL^{-1} of cobaltocene was prepared in 2.5 % of ferrocene in toluene. The mixture was ultrasonicated for 15 min to ensure that cobaltocene was completely dissolved. This bimetallic catalyst was used to determine the effect of cobaltocene in CNT growth. Trimetallic catalyst was also prepared by mixing ferrocene-nickelocene and ferrocene-cobaltocene together. The mixture was ultrasonicated and evaluated for the effect on the growth of MWCNTs.

3.2.3. CVD synthesis of VA-MWCNTs

The CVD setup used is depicted in **Fig.3.1**. The clean silicon wafer (1 cm x 1 cm) was weighed, placed in a quartz boat and loaded in a quartz reactor tube. The quartz tube was inserted horizontally in a horizontal high temperature tube furnace (Elite TSH 12/38/500-2216E, Leicestershire, UK). The ultrasonic nebuliser catalyst reservoir was filled up with 40mL catalyst and attached to the gas line inlet and the outlet was attached on the inlet of the quartz tube.

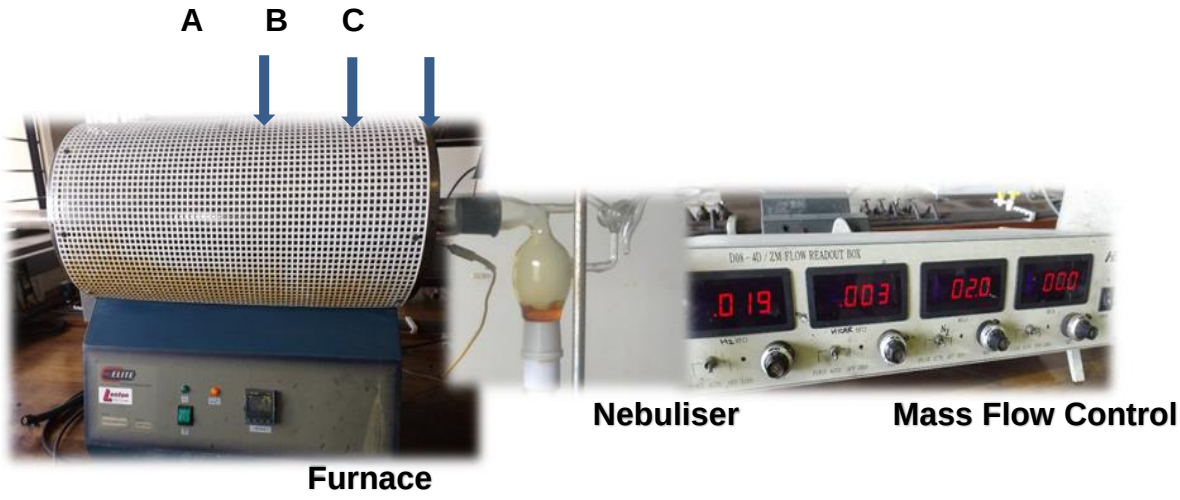


Figure 3.1: A CVD setup for the synthesis of VA-MWCNTs. Nebuliser coupled to the furnace and mass flow control.

A gas line with a mixture of 95 % baseline argon balanced with 5 % hydrogen was opened and the mass flow controller (D08-4D/ZM, Beijing Sevenstar, Huachuang Electronic Co., Ltd, China) was switched on and flow rate was set to 50 mL.min^{-1}. The nebuliser (Dr Hielscher UM20-1.6 MHz Sonic, Germany) was not switched on until the temperature reached the set point. Argon was used as a carrier gas to ferry argon into the furnace and hydrogen as a reducing gas to etch away amorphous carbon and impurities to produce clean CNTs (**Fig. 3.1**).

The outlet of the quartz tube was connected to the exhaust pipe. The furnace was switched on and temperature adjusted to 775 °C or 850 °C at a ramp of 10 °C.min^{-1} depending on the experimental set-up. Flow rate was increased to 400 mL.min^{-1} once the temperature reached its set-point. The nebuliser was switched on for 45 min to generate an aerosol of catalyst. The aerosol that was generated was ferried into the high temperature furnace by argon gas (**Fig. 3.1**). All experiments were carried at atmospheric pressure. The furnace was switched off and flow rate reduced to 50 mL.min^{-1} following a 45 min synthesis to cool the furnace down to ambient temperature. Mass flow controller and gas line were switched off and silicon wafer containing synthesised CNTs was collected from the furnace.

The silicon wafer with CNTs was weighed to obtain the mass of CNTs deposited on the wafer. Some CNTs were also collected from the quartz furnace tube by scrapping and weighed to determine the amount of CNTs synthesised in the quartz tube. Precautionary measures were taken to collect only the CNTs half way tube zone facing the nebuliser since the centred samples were full of flakes and nanospheres. The collected samples were characterised as-synthesised using various techniques.

3.2.4. Box-Behnken Design of experiments (BBDOE)

BBDOE was performed to obtain the most favourable conditions for successful MWCNT synthesis with a specific diameter and length on both the reactor and substrate with a greater focus on the three variables namely gas flow rate, reaction time, and reaction temperature according to **Table 3.1**.

A three-factor Box-Behnken experimental design (BBD) was generated using Minitab® V15 statistical software (Minitab® Inc., PA, USA) to determine the optimal pyrolysis conditions for the synthesis of vertically aligned MWCNTs. High, low and optimal factors were generated and yielded a desirability value of 1 to produce optimal factor levels for most desirable response behaviour.

The variables that were used in the experimental set-up were gas flow rate, reaction temperature, and synthesis time. The lower and upper limits for the reaction time were 30 min and 60 min. The reaction temperature limits were 650 °C and 950 °C and that of gas flow rates were 100 and 600 mL.min^{-1}. The variables of the formulations were

assessed for their effect on the length, diameter and yield of MWCNTs on both the reactor and wafer.

Table 3.1. BBDOE to determine optimal pyrolysis conditions of VA-MWCNTs

Formulation	Synthesis time (min)	Synthesis temperature (°C)	Gas flow rate ($mL.min^{-1}$)
1	45	775	400
2	60	650	400
3	60	775	600
4	30	650	400
5	30	775	200
6	30	775	600
7	60	775	200
8	45	650	600
9	60	900	400
10	45	650	200
11	45	900	200
12	45	775	400
13	45	900	600
14	45	775	400
15	30	900	400

3.2.5. Characterisation of MWCNTs by SEM and TEM

As-synthesised CNTs were peeled off from the substrate and prepared for SEM and TEM analyses in order to study their morphology and size. For SEM, CNTs were placed on a carbon tape or aluminium tape on the stub and coated with Pd/Au using Emitech K550X (Emitech Ltd, Kent, England) for 4 min at 25 mA and 2 x 10^{-1} mbar.

For TEM, a small amount of CNTs was transferred into a 1.5 mL Eppendorf tube and dispersed in an absolute ethanol. The CNTs were sonicated in ultrasonic water bath and Materials, Inc., Danbury, CT, USA) for 10 - 15 min to disperse CNTs. Pasteur pippete was used to transfer dispersed CNTs onto a Cu grid that was placed on

Whatman filter paper and was dried under light. The sample loaded Cu grids were analysed immediately or stored in vials for future analysis.

Samples were loaded in FEI Nova NanoLab 600 FEG-SEM/FIB (**FEI** Company, Hillsboro, OR, USA) for the determination of morphology and length of the synthesized CNTs. Samples were also loaded in FEI Tecnai T12 TEM for the determination of external and internal diameters of CNTs. ImageJ software was used to measure the length and diameters of the CNTs.

3.2.6. Measurement of resistivity of VA-MWCNTs

Electrical resistivity of VA-MWCNTs was determined using physical property measurement system (PPMS) (PPMS, Quantum Design). The PPMS is an automated low-temperature and magnet system for the measurement of material properties like specific heat, magnetic AC and DC susceptibility and both electrical and thermal transport properties. In this study, VA-MWCNT with the dimension of 1 mm x 1mm x 6 mm was loaded on the PPMS and electrical resistivity was measured at temperatures ranging from 200K – 350 K.

3.2.7. Determination of functional groups on VA-MWCNTs with Fourier Transform Infrared (FTIR)

In order to determine the functional groups on carbon nanotubes, KBr must be mixed first with the CNTs as the CNTs alone will absorb all the light and there will be no transmission of light to the detector. KBr was ground to fine particles using mortar and pestle and mixed with CNTs in a ratio of 1:200 (sample:KBr). The mixture was further ground to finest particles and mixed thoroughly to ensure even distribution of the CNTs in KBr. The homogenous mixture was loaded on KBr die and pressed at 4-ton pressure under vacuum for 15 min to produce KBr pellet with a KBr press (ICL, International Crystal Labs, Garfield, USA). The pellet was loaded on sample holder and scanning was performed from 450 to 4 000 cm^{-1} to determine the functional groups on CNTs with FTIR (Spectrum 100, Perkin Elmer, USA).

3.2.8. Purification of VA-MWCNTs by thermal and acid oxidation

For the CNTs to be used in various experiments, they need to be purified first to remove amorphous carbon, catalyst nanoparticles and other contaminants. CNTs were subjected to a temperature of 450 °C for 1 hour at 200 mL.min^{-1} oxygen in a horizontal tube furnace. CNTs were transferred into a vial and 3 mL of HNO_3:H_2SO_4 (1:3) was added and incubated for 2 hrs at 80 °C in an oven (Binder, SA Geolab International, Singapore). CNTs were then rinsed thrice with distilled water to get rid of an excessive acid. CNTs were then dried in furnace at 450 °C for 30 min. Another experiment was done in the similar manner but using varying amount of HCl; 2.5, 5.0 and 10.0 M HCl.

3.2.9. Determination of surface area, pore size and pore volume of VA-MWCNTs

It is very important to know the surface area and pore size of the CNTs for the development of a carbon based theranostic device for both detection and treatment of neurological disorders. A porositometric analyzer (Micromeritics, ASAP 2020, Norcross, GA, USA) was employed to determine the porositometric properties of the pristine and functionalized MWCNTs. Samples with weights ranging from 0.2- 0.3 g were loaded in sample tubes, degassed and analysed by the Brunauer–Emmett–Teller (BET) N_2 gas adsorption method at 77 K. The surface area, pore size and pore volume were determined using BET method.

3.2.10. Measurement of wettability of CNTs

The optical analysis of drops that hang from a dosing needle or are placed on a solid surface facilitates the determination of different surface and interfacial parameters. The contact angle that a liquid drop establishes on a solid surface characterizes the solid's wetting properties with the liquid. The surface energy of the solid can be determined and be used to calculate the adhesiveness of liquids following the measurements of the contact angles of the liquids of interest. The reliable and experimentally robust determination of the contact angle assists in the development of composite materials, surface coatings, cleaning agents, paints and varnishes.

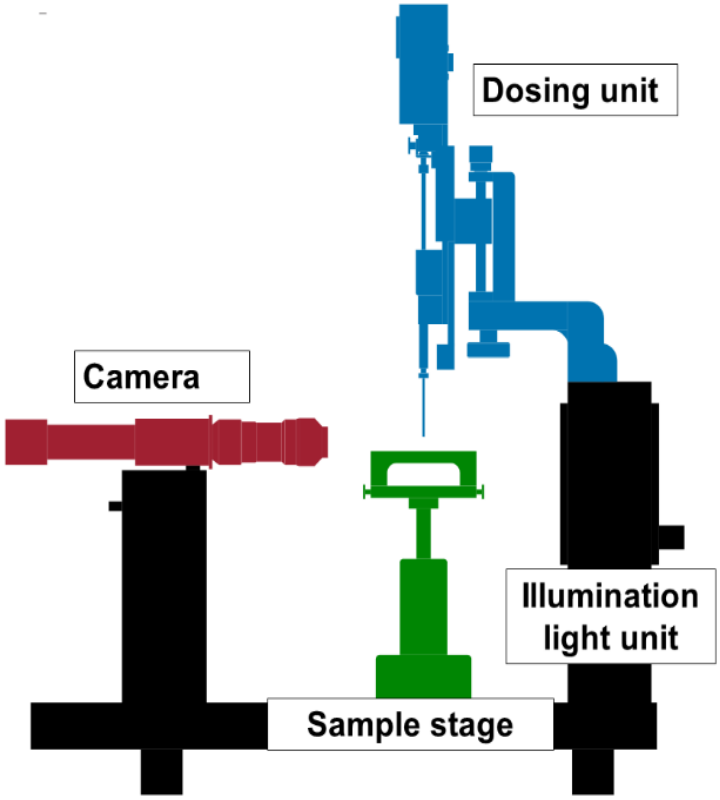


Figure 3.2. Optical contact angle meter equipped with a dosing unit, illumination unit, sample platform and camera.

CNTs were evenly spread on a thin double-sided tape on the sample platform of the goniometer (contact angle, Dataphysics) (**Fig. 3.2**). Drops of water were added at various spots on the pristine and 5 M HCl treated CNT layers. Contact angles were measured using sessile drop method and recorded. Snaps were taken for both the pristine and acid treated CNTs.

3.2.11. Determination of particle size distribution and zeta potential of CNTs

The 5 M HCl treated CNTs were suspended in deionized water at a concentration of 0.2 mg.mL^{-1}. The solution was ultrasonicated for 2hrs in an ultrasonic waterbath. Solution was allowed to settle for 30min. The supernatant was collected for the measurements of particle size distributions and zeta potential using ZetaSizer NanoZS (Malvern Instruments, UK). This instrument was equipped with a non-invasive backscatter technology technology set at a fixed angle of 173 ° and a light source with wavelength of 532 nm. Zeta potential and relative hydrodynamic diameter distribution of the MWCNTs solutions were measured and averages were determined.

3.2.12. Measurement of crystallinity and elemental composition of CNTs

As-synthesised CNT samples on the silicon wafers were loaded on the XRD sample holders. The sample holders were then loaded into the diffractometer (Phillips PANalytical X'pert Pro Xray Diffractometer, USA). Cu X-ray diffraction (XRD) patterns of the MWCNTs were examined on X-ray diffractometer at 40 kV and 40 mA with Cu Kα radiation (1.54060) equipped with K-beta filter. Each sample was scanned for 2 hrs because of high iron content in MWCNTs and the raw data processed with High Score Plus software.

3.2.13. Determination of the purity of CNTs using TGA

Thermal stability of MWCNTs were determined using a thermogravimetric analyzer (PerkinElmer TGA 4000, Llantrisant, Wales, UK). MWCNTs samples were heated from 30 ˚C to 990 ˚C under nitrogen gas purging environment at a constant flow rate of 20 $mL.min^{-1}$ and temperature ramp of 10 ˚$C.min^{-1}$. Thermograms were generated as percentage weight loss vs. temperature and processed using PyrisTM software (PerkinElmer, Llantrisant, Wales, UK).

3.3. Results and discussion

3.3.1. Synthesis Parameters of VA-MWCNTS

The location of the substrate, catalyst concentration, synthesis duration, argon flow rate and synthesis temperature were varied in order to determine the optimal pyrolysis conditions for a successful growth of quality VA-MWCNTs.

3.3.2. Effect of location of substrate in the furnace on VA-MWCNT growth

The location of the silicon wafer within the tube furnace plays a major role in the synthesis and quality of the VA-MWCNTs. The reason for this is because the zones have different temperatures as the result of the exposure of some zones to the outside environment. The temperatures vary from zone to zone within the tube. The temperatures of the inlet and outlet (exhaust) of the quartz tube are different from that of the central zone as they are exposed to the outside environmental conditions (Kapoor *et al.*, 2018).

In our study, VA-MWCNTs were deposited on the silicon wafer when it was placed 125 mm between the centre and the entrance into the furnace (zone C in **Fig.3.1**). In this zone, the iron nanoparticles and toluene reach high temperature quickly and CNTs are deposited on both the substrate and walls of quartz tube. Carbon atoms from toluene are added to the catalytic surface of a catalyst composed of ferrocene, where atoms diffuse into the catalyst. Carbon atoms then precipitate onto the catalyst surface. As the precipitation proceeds, the C atom concentration within the catalyst becomes constant. A relatively stable solution is reached when the in and out diffusion of the catalyst stabilizes. The stabilization triggers the initiation of the cap nucleation stage. In this stage, the precipitated carbon, along with new catalysed carbon, combine to initiate the formation of carbon chains and networks on top of the catalyst surface (Gomez-Ballesteros *et al.*, 2015).

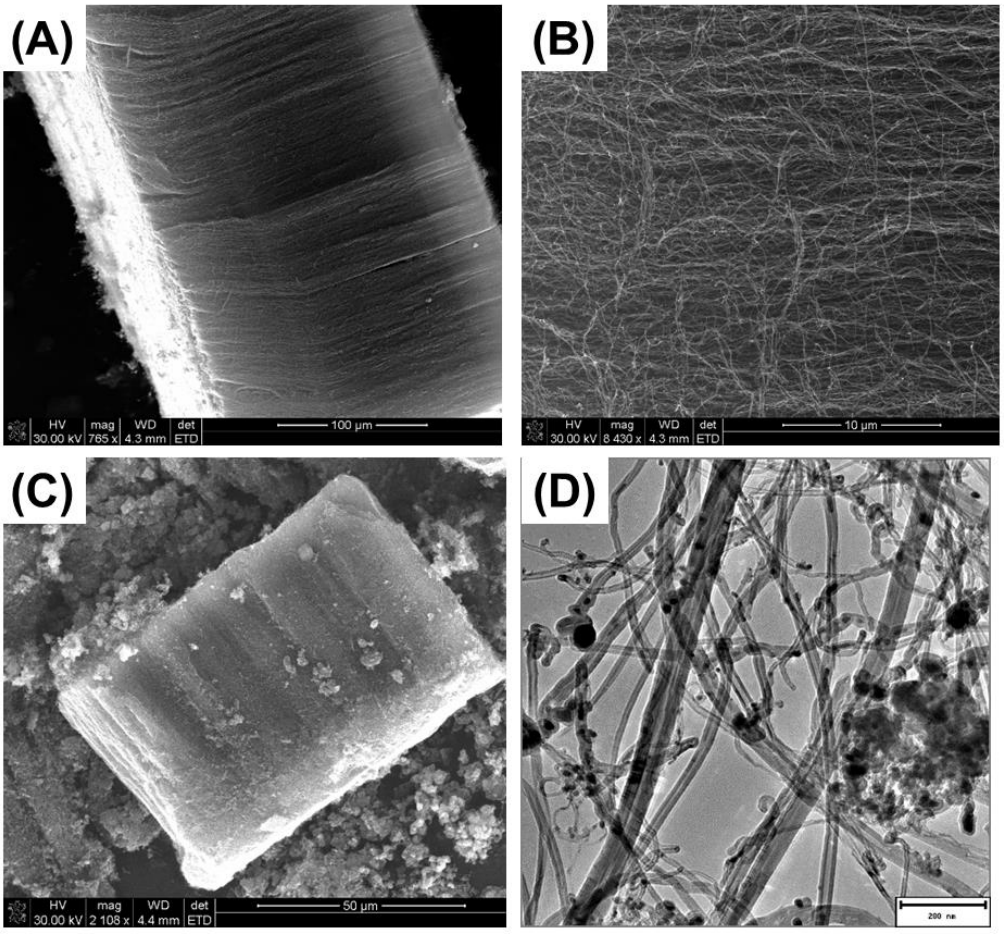


Figure 3.3. SEM and TEM micrographs of VA-MWCNTs collected from zone C. (a) MWCNTs from silicon wafer at low magnification (b), MWCNTs at high magnification, (c) MWCNTs from quartz tube and (d) MWCNTs TEM micrograph.

Changes in shape and local composition take place in the catalyst nanoparticle throughout this process as a result of the dynamics of the C atoms diffusing in and out and association of C atoms on the surface. Variations in C composition of the particle throughout the nucleation process are driven by local differences in C chemical potential: dissolved carbon, carbon precipitated to the particle surface and carbon at the edges of the islands with unsaturated bonds. Therefore, as the nanotube begins to nucleate, a decrease in the subsurface carbide species is expected due to variations in the local environment of C atoms and changes in the metal-carbon interaction. The drop in C concentration prevents the formation of new islands on the catalyst surface, and favours coalescence of the existing carbon formations on the surface (Gomez-Ballesteros *et al.*, 2015; Allaedini *et al.*, 2016).

The transition metals such as Ni, Co and Fe are used as a catalyst since they offer nucleation and growth sites for carbon nanotubes. This is because carbon has a high solubility and higher diffusion rate in these metals at high temperatures. The high melting point and low equilibrium-vapor pressure of these metals also offer wide temperature options for the CVD method for different ranges of carbon precursors. Previous studies have found that Fe, Co and Ni have stronger adhesion with CNTs when compared to the other transition metals (Allaedini *et al.*, 2016).

The catalyst–substrate interactions play a determinant role for the growth mechanism where weak interactions yield catalyst–substrate interaction is weak. Therefore, hydrocarbon decomposes on top surface of the metal, carbon diffuses down through the metal, and CNT precipitates out across the metal bottom, pushing the whole metal particle off the substrate. CNT continues to grow longer and longer as long as the metal's top is open for fresh hydrocarbon decomposition. Growth of CNT is stopped once the metal is fully covered with excess carbon and this is called, "tip-growth model" as demonstrated in **Fig.3.4A**.

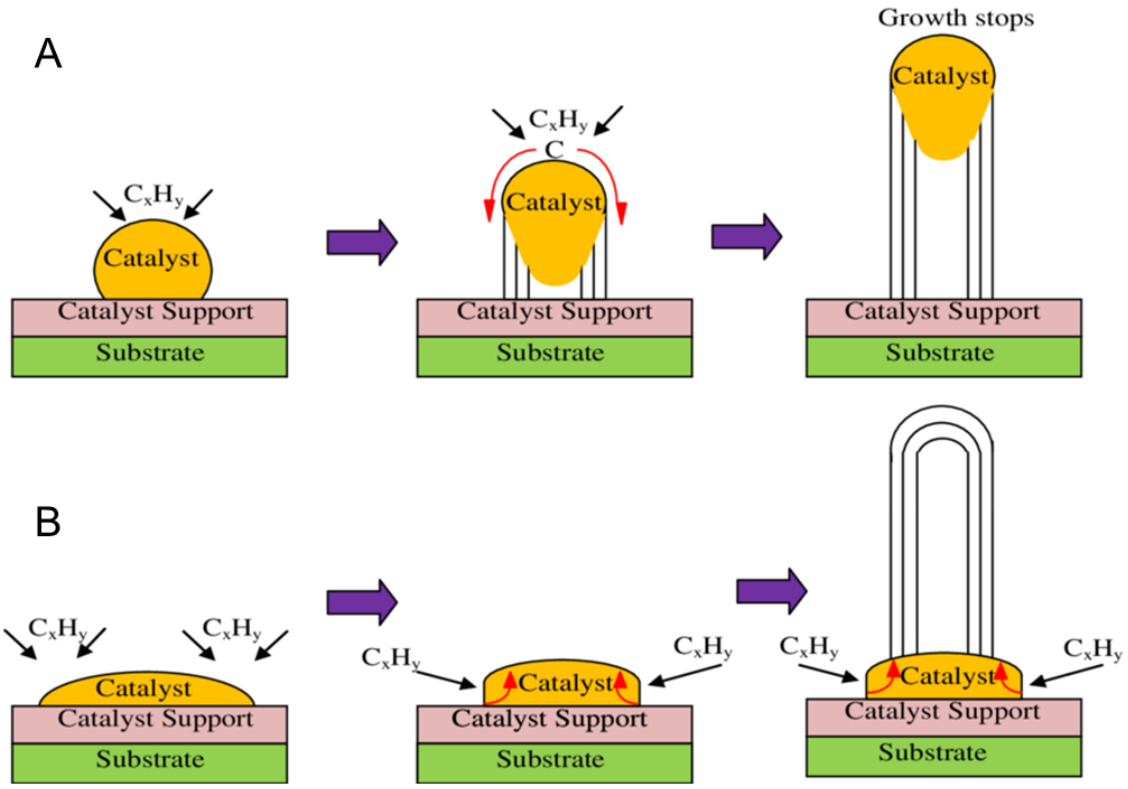


Figure 3.4. Growth mechanism of carbon nanotubes. Tip-growth model (A) and Base-growth model (B). Adapted from Azam and colleagues (Azam et al., 2013).

However, in the case when the catalyst– substrate interaction is strong, metal has an obtuse contact angle with the substrate. Initial hydrocarbon decomposition and carbon diffusion take place similar to that in the tip-growth case, but the CNT precipitation fails to push the metal particle up; so, the precipitation is compelled to emerge out from the metal and farthest from the substrate. When CNT grows up with the catalyst particle rooted on its base, this is known as “base-growth model” as shown in **Fig. 3.4B** (Azam *et al.*, 2013).

In this study, CNTs synthesized using CVD method were collected from the substrate and were found to be clean and well aligned whereas those collected from the tube were contaminated with damaged and disarrayed CNTs and amorphous carbon. CNTs were well aligned and had multiple walls as confirmed by TEM in **Fig.3.3A-D**. Iron nanoparticles could also be seen lodged inside the central cavities of the MWCNTs as revealed by TEM in **Fig. 3.3D**.

3.3.3. Effect of reaction temperature on VA-MWCNT growth

Temperature plays a major role in the synthesis of carbon nanotubes. In general, low-temperature CVD (600 – 900 °C) yields MWCNTs, whereas high-temperature (900 – 1200 °C) reaction favours SWCNT growth. This indicates that SWCNTs have a higher energy of formation. Perhaps that is why MWCNTs are easier to grow (than SWCNTs) from most of the hydrocarbons, while SWCNTs grow from selected hydrocarbons (viz. carbon monoxide, methane, etc. which have a reasonable stability in the temperature range of 900 – 1200 °C). Commonly efficient precursors of MWCNTs (viz. acetylene, benzene, toluene, etc.) are unstable at higher temperature and lead to the deposition of large amounts of carbonaceous compounds other than the nanotubes (Kumar and Ando, 2010).

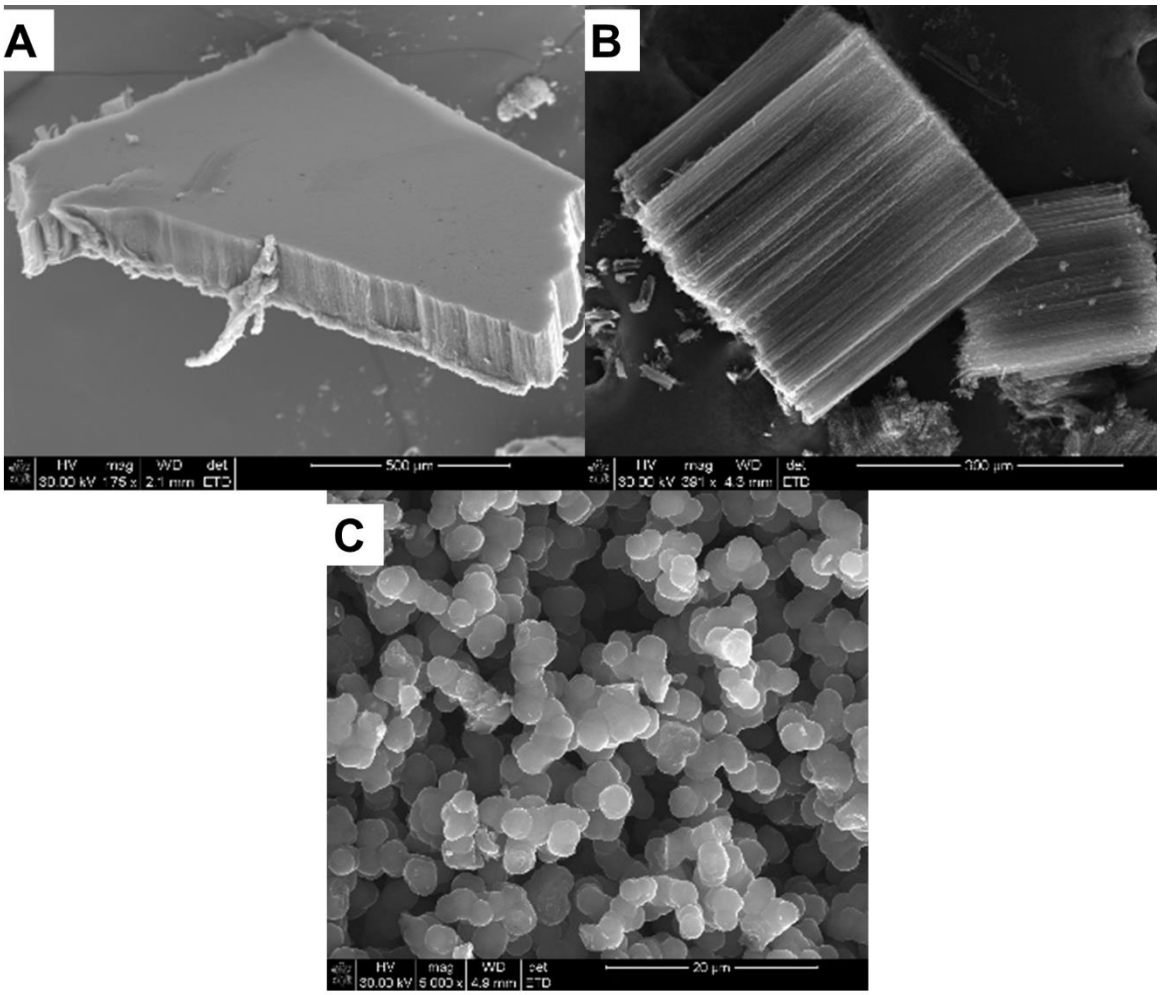


Figure 3.5. MWCNTs at different temperatures. (a) 775 °C, (b) 850 °C and (c) 900 °C.

In this study, various temperatures were used and VA-MWCNTs were observed when temperatures from 750 °C to 850 °C were used. This temperature range is higher enough to cause pyrolysis of catalyst and toluene and yield vertically aligned MWCNTs

as depicted in **Fig. 3.5A-B**. The alignment was affected by temperature at 900 °C and CNT nanospheres were also produced under these conditions as toluene is unstable at this temperature and leads to the formation of flakes and nanospheres as demonstrated in **Fig.3.5C**.

The temperature range from 775 °C to 850 °C was found to be the optimal temperature range for Fe atoms mobility to form catalytic particles and toluene decomposition to form carbon and nucleate CNT. At temperatures below 750 °C, the Fe atoms are not mobile enough to aggregate together into particles to nucleate and grow nanotubes. Catalytic decomposition of toluene to form carbon may be too slow for the formation of CNTs. At temperatures above 850 °C, Fe atoms are too mobile, and the particles grow to a size too large to nucleate and grow CNTs. The large particles formed overcoat with carbon (Bronikowski, 2006).

3.3.4. Determination of crystallinity and elemental composition of VA-MWCNT

The extent of diffracted X-rays is dependent on the arrangement of the atomic planes of the material within the crystal lattices. CNT is a non-crystalline material but possesses a periodic structure with unique X-ray diffraction pattern. XRD is a technique that has been used to study the morphological and structural characteristics of entangled and aligned carbon nanotubes. The intensities of diffraction peaks are dependent on the morphological orientation of carbon nanotubes. Peaks (002) with parallel (h k l) reflections are formed upon X-ray beam CNT bombardment. On the other hand, some additional hexagonal peak arrays (h k o) are produced when X-ray beams travel through an empty CNT central core (Das *et al.*, 2014).

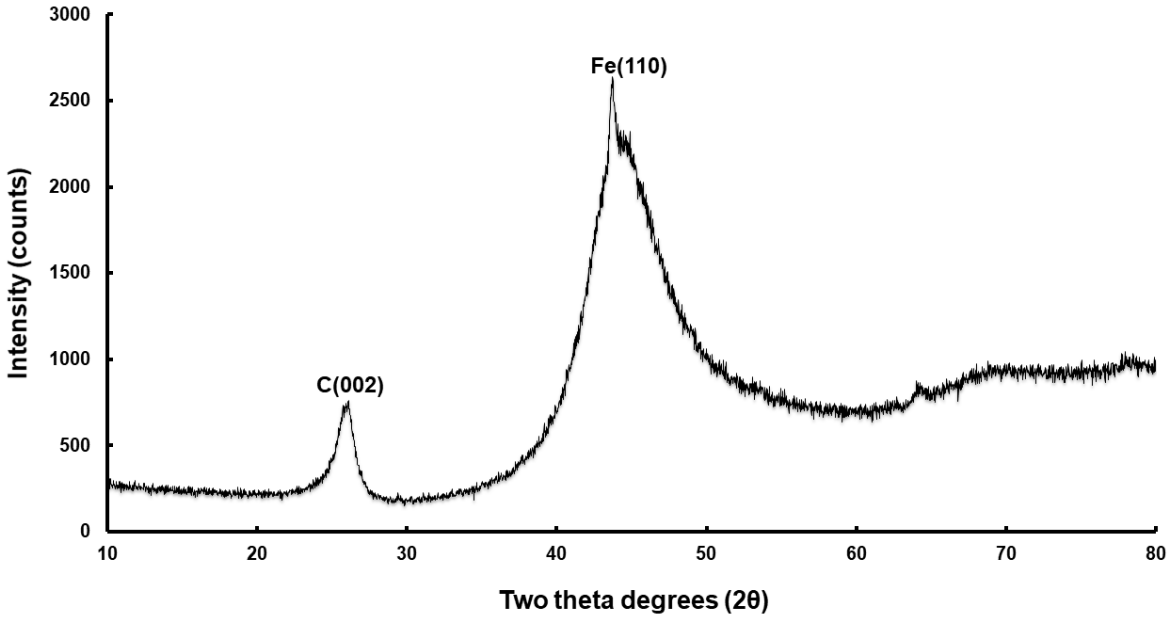


Figure 3.6. XRD pattern of MWCNTs with two peaks (carbon and iron peaks).

In our study, elemental composition and crystallinity of the CNTs were determined by an XRD method. There were two unique peaks that were noticed at the angle (2Ɵ) of 25 °and 45 °. **Figure 3.6** shows the powder XRD patterns Cu Kα radiation (1.54060) of the as-synthesized VA-MWCNTs. The peaks for the as-synthesized MWCNTs arrays indexed to (002) and (110) at 2Ɵ of 25 ° and 45 ° are indicative of the hexagonal graphite and catalytic impurities respectively.

These peaks were due to the carbon in MWCNTs from pyrolysis of toluene and iron in ferrocene from the catalyst. The peaks of carbon were sharp indicating the presence of graphitic structure of MWCNTs and high crystallinity. Iron peak had a higher intensity compared to carbon as high concentration of ferrocene (2.5 %) was used in toluene for preparation of the catalyst (**Fig.3.6).**

3.3.5. Elemental composition of VA-MWCNTs by SEM-EDX

Energy dispersive X-ray spectroscopy is a spectroscopic technique for the qualitative and quantitative analysis of the surface elements of the compound. SEM-EDS was used to determine the elemental composition of MWCNTs in this study. The results show the presence of carbon and iron since MWCNTs contains carbon from toluene and iron from ferrocene in the catalyst. Co has been detected but at a very low level which could not be quantified (**Fig. 3.7A**). The concentration of Co in the catalyst solution containing Co and ferrocene in toluene was far much lower than the limit of

detection (LOD) of the FEI Nova NanoLab 600 FEG-SEM/FIB. Ni was not detected in these CNTs as it was not included in the catalyst solution.

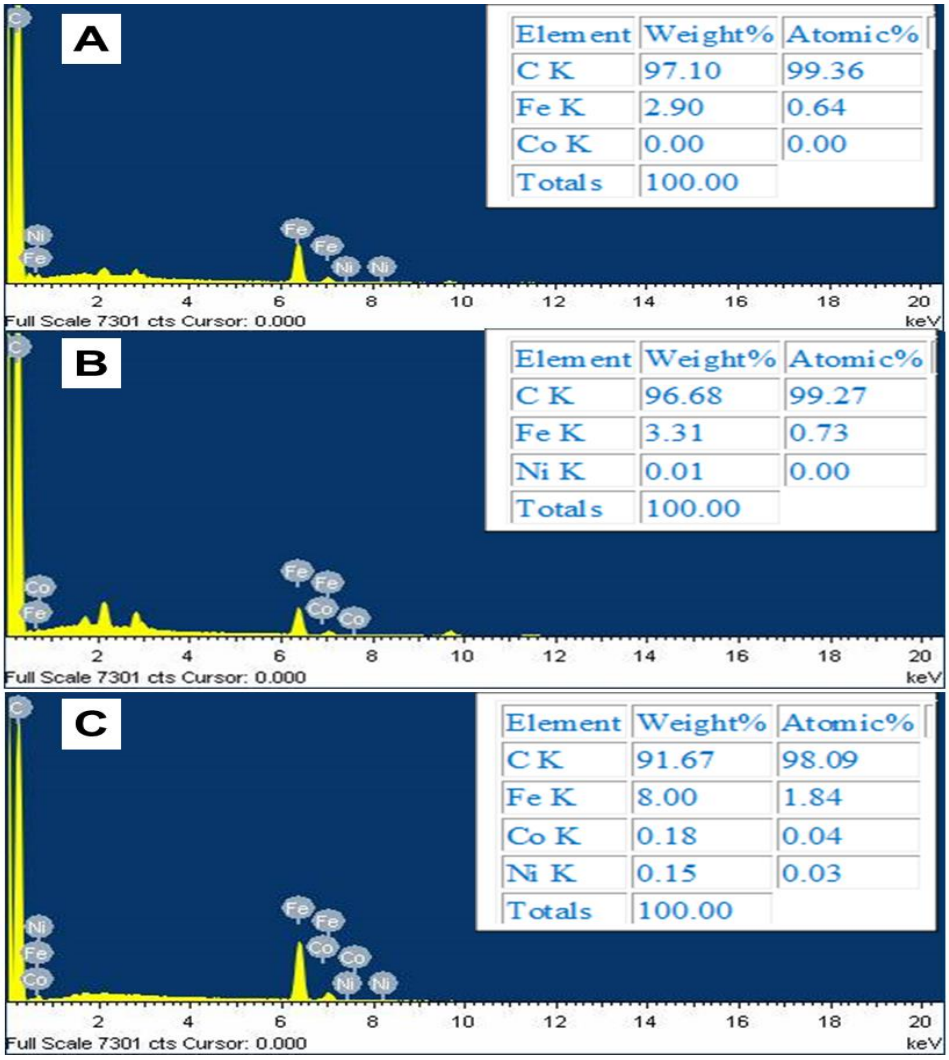


Figure 3.7. Elemental composition of MWCNTs. (a) Fe-Co, (b) Fe-Ni and (c) Fe-Co-Ni.

Nickel (Ni) was detected but at a very low level when Fe-Ni catalyst (bimetallic catalyst) was used for CNT synthesis. Co was not detected in the CNTs as it was not included in the catalyst. Fe and carbon were detected as their sources were used to prepare the catalyst (**Fig.3.7B**). Fe, Ni, Co and carbon were detected in the MWCNTs synthesised using ferrocene-nickelocene-cobaltocene catalyst (trimetallic catalyst). Ni and Co were detected in less amount as a result of overcoating by iron (**Fig. 3.7C**). These results are an indicative that the vertically aligned MWCNTs were successfully synthesised using bimetallic and trimetallic catalysts.

3.3.6. Effect of reaction time on the yield and length of VA-MWCNTs

Reaction time is one of the variables that has an effect on the growth of MWCNTs as it affects the length or thickness, the yield and diameters of the VA-MWCNTs. The van der Waals interactions between the growing individual carbon nanotubes contribute significantly on the alignment of CNT forests. CNTs grow disorderly and non-perpendicularly at the embryonic stage of growth but the orientation improves with time and growth length. The orientation of the CNTs is initiated at a certain length of the tubes resulting in “forest formation” or vertical alignment (Szabó *et al.*, 2017).

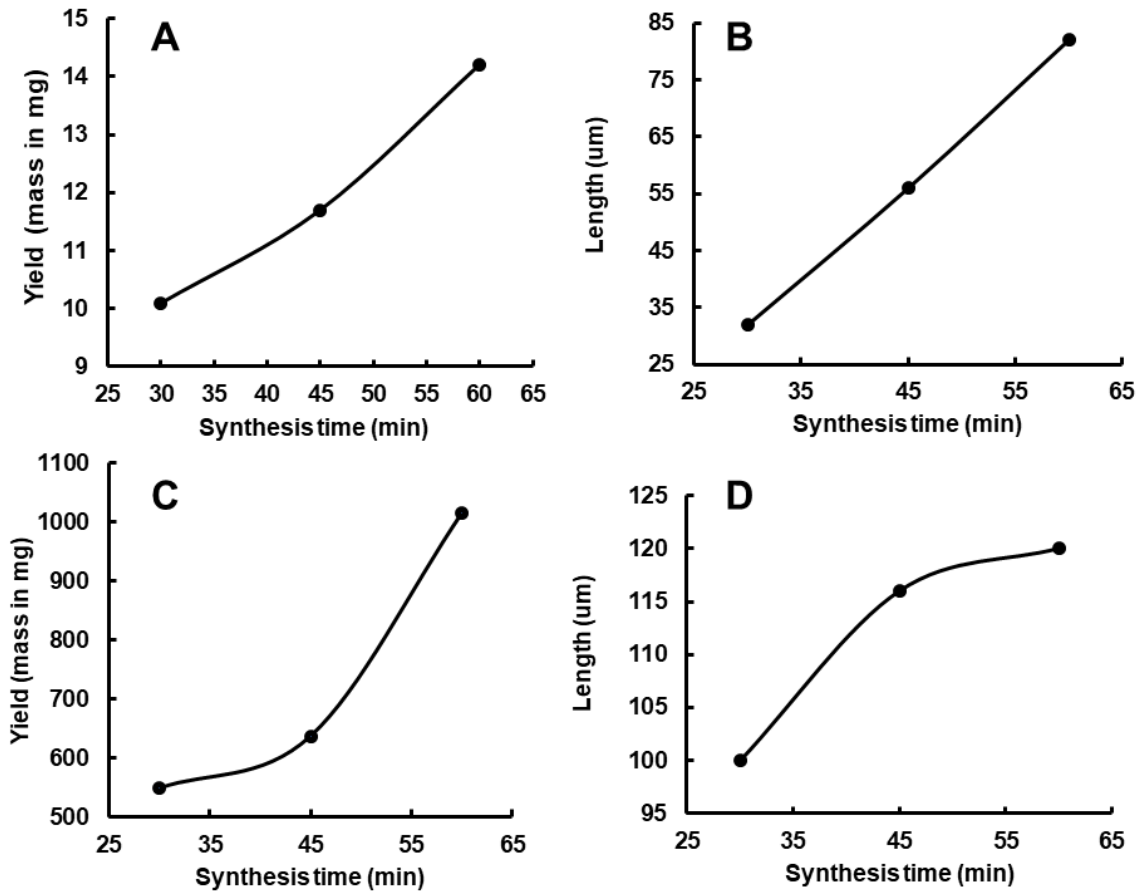


Figure 3.8. The effect of synthesis time on the yield and length of VA-MWCNTs. (a) Synthesis time on the CNTs yield on silicon wafer, (b) synthesis time on the thickness of CNT on silicon wafer, (c) synthesis time on the CNT yield on quartz tube walls and (d) synthesis time on the thickness of CNTs on quartz tube.

When different reaction times (30, 45 and 60 min) were used, the quality and vertical alignment of MWCNTs improved greatly. A direct proportional linear relationship was observed between the synthesis time, amount and thickness of CNTs synthesised on both the silicon wafer and quartz tube. The longer the time of synthesis, the thicker or

the longer the VA-MWCNTs and the higher the yield of MWCNTs as depicted in **Fig.3.8A-D**). The improvement in the length and yield is due to the fact that the reaction is given enough time for the pyrolysis of the catalyst hence an increase in the length and yield.

3.3.7. Effect of catalyst concentration on the yield and length of VA-MWCNTs

Carbon nanotube morphology and yield is dependent on the concentration of the available catalyst. At very high concentrations, catalyst aggregates may lead to the evaporation of solvent from aspirated droplets which may result in the formation of unwanted carbon structures, rather than the carbon nanotubes of interest. However, there may be no product yield, or the yield might be too low as a result of lack of catalyst site for the growth of the CNTs if catalyst concentrations are too low.

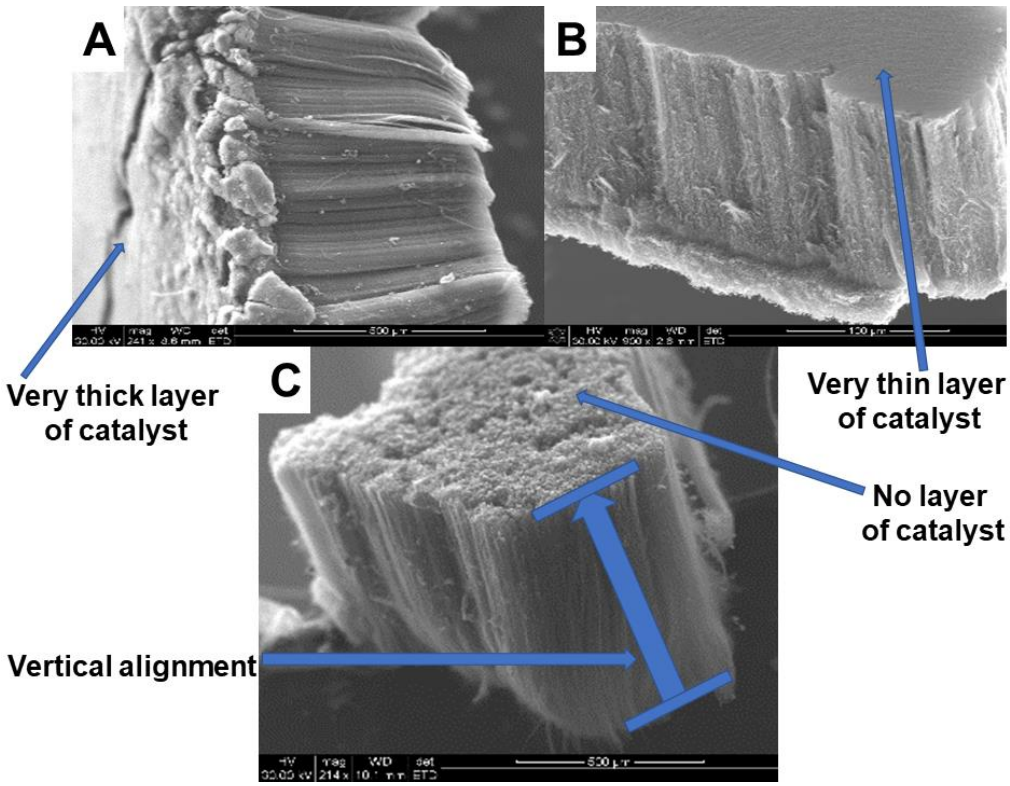


Figure 3.9. VA MWCNTs at various catalyst concentrations. (a) 10 % ferrocene (b) 5 % ferrocene and 2.5 % ferrocene.

Ferrocene was dissolved in toluene to prepare standards of different concentrations (2.50, 5.00 and 10.00 $mg.mL^{-1}$). The effect of the content of transition metal on the growth of MWCNTs was determined using these concentrations. Other parameters such as carrier gas flow rate, catalyst flow rate and reaction temperature were kept constant. In our study, the thickness or length or height of VA-MWCNTs increased with

an increase in the amount of ferrocene. Clean VA-MWCNTs were produced and there was no formation of the nanoparticle layer on the surface of the CNTs when low concentration of catalyst was used (**Fig. 3.9C**).

However, a very thick layer of iron nanoparticles was observed on the surface of CNTs following the use of high catalyst concentration (**Fig. 3.9A**). Iron nanoparticles are required for nucleation to form a platform for synthesis of CNTs from carbon derived from pyrolysed toluene. If the amount of iron nanoparticles is very high, it reaches the saturation point where it is no longer needed, and it starts accumulating on the top surface of the CNTs. The data obtained is an indicative that the MWCNTs favoured a low (2,5 %) and medium concentration (5 %) of ferrocene for a successful growth as depicted in **Fig. 3.9B-C.**

3.3.8. Effect of gas flow rates on the yield and length of VA-MWCNTs

A change in the flow rate of the carrier gas has an impact on the structure and morphology of carbon nanotubes. When a mixture of gases contacts the catalyst surface, an equilibrium is achieved between the molecules in the gaseous phase and the adsorbed species on the catalyst.

There won't be any synthesis of CNTs when there is no flow of carrier gas to deliver the catalyst into the reactor. CNT synthesis is initiated when there is a flow of carrier gas and the yield and length increase until the gaseous molecules and adsorbed species bound to the catalytic surface reach an equilibrium. The yield is negatively affected as the flow rate is too high hence the formation of amorphous carbon is observed.

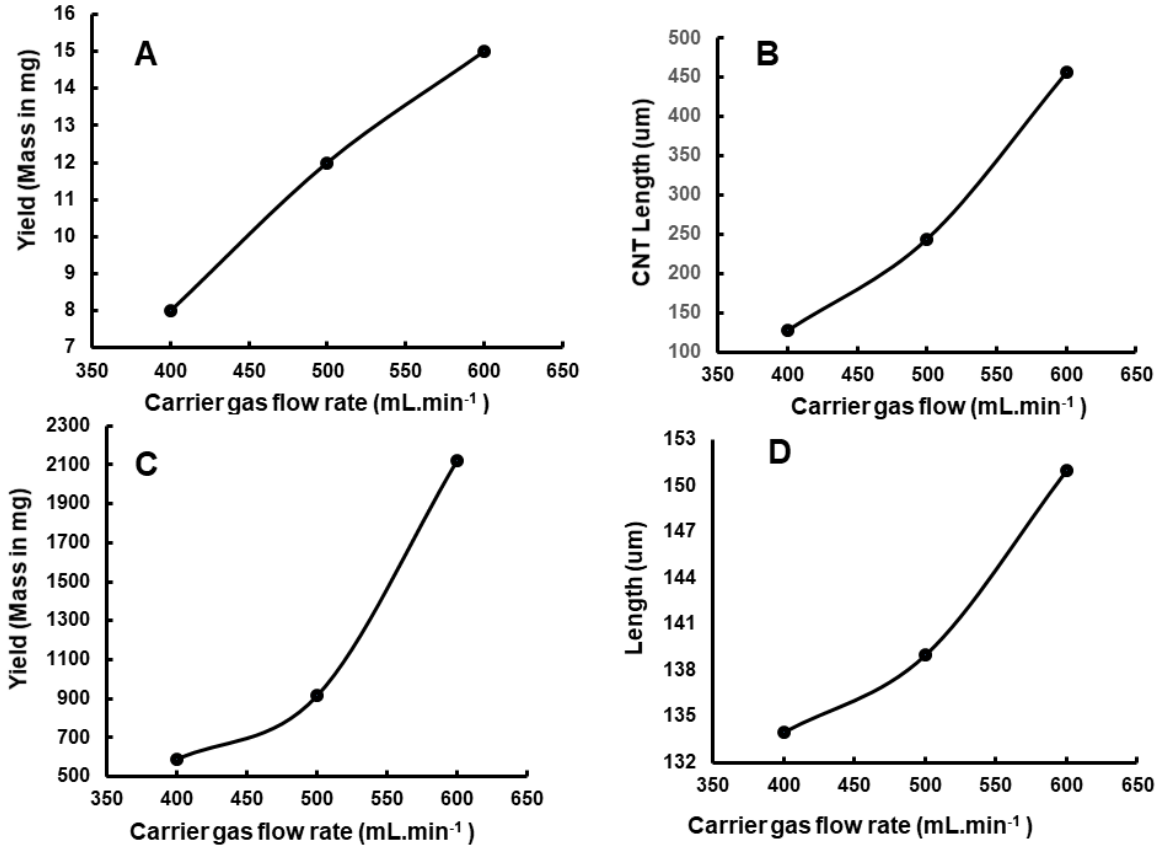


Figure 3.10. MWCNT yield at various carrier gas flow rate. (a) CNT yield on silicon wafer, (b) CNT length on silicon wafer, (c) CNT yield from quartz tube walls and (d) CNT length from quartz tube walls.

In our study, various argon flow rates from 400 to 600 mL.min^{-1} were used and a direct linear relationship was observed between the flow rate of the carrier gas and thickness and yield of carbon nanotubes. The yield and thickness of CNTs increased with a rise in the flow rate of carrier gas as depicted in **Fig. 3.10**. The flow rate of the carrier gas had an impact on the deposition of the carbonaceous products on the reactor walls and on the wafer. It can be concluded that an increase in the flow rate of the carrier gas led to the increase in the CNT yield and length.

3.3.9. Effect of synthesis time on diameters of VA-MWCNTs

The type of carbon nanotubes that are formed and their yield depend on the reaction parameters such as synthesis time, H_2 gas concentration, flow rate ratio (CH_4:H_2) and reaction. Othman and Wilkinson prolonged the reaction time above three hours and this led to an increase in both the internal and outer diameters of the entangled carbon nanotubes (Othman and Wilkinson, 2016).

In our study, we used reaction time of 30min to 60min for the VA-MWCNTs. The carrier gas flow rate, catalyst concentration and reaction temperature were kept constant. The internal and external diameters were measured following the various synthesis times for multiwalled carbon nanotube growth. The internal diameter of the CNTs was not affected as the synthesis time was increased.

The size of the internal diameter of CNTs is restricted by the size of nanoparticles used for nucleation. Iron nanoparticles of 10 nm in diameter was used hence internal diameter of MWCNTs was found to be 10 nm in both the wafer and the reactor carbon nanotubes (**Fig. 3.11A**).

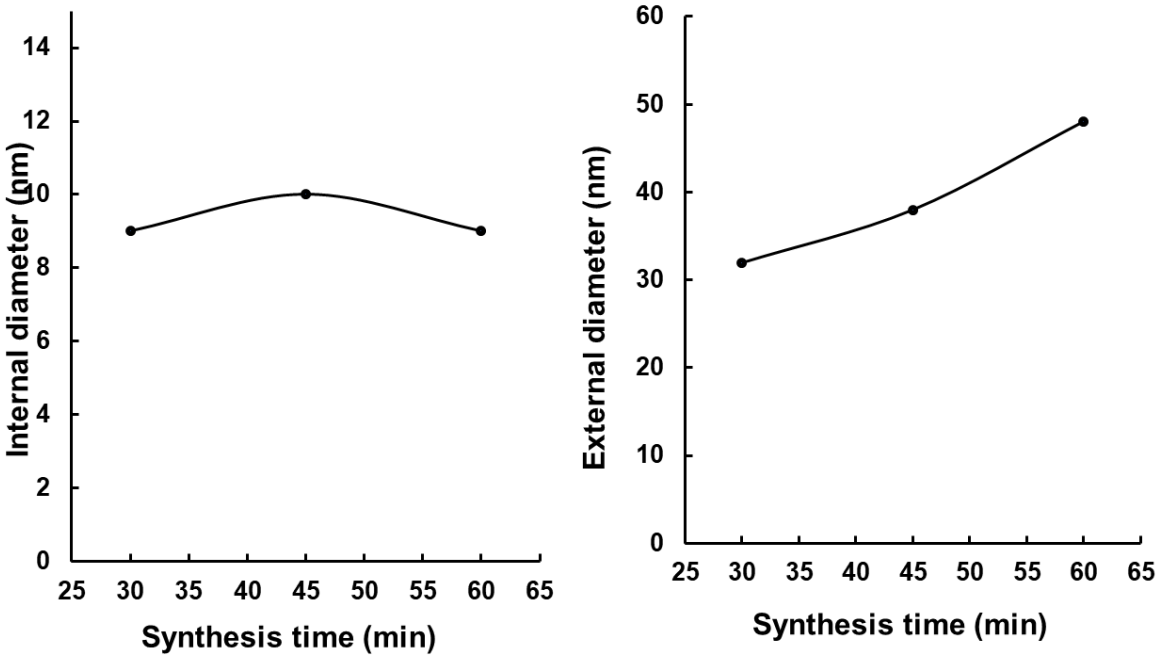


Figure 3.11. Effect of synthesis time on diameters of MWCNTs. (a) Internal diameter and (b) External diameter.

The number of walls on CNTs increased with synthesis time. As the number of walls increased, the external diameter increased too as depicted in **Fig.3.11B**. Longer time of reaction creates enough time for the carbon from pyrolysis of the hydrocarbon source to diffuse into the catalyst and this leads to a better yield and more walls added to the carbon nanotubes.

3.3.10. Effect of carrier gas flow rate on diameters of VA-MWCNTs

Carrier gas flow rate is one of the factors that plays a major role in the successful carbon nanotube growth. As the flow rates increases, vapour gas is carried out to the bubbler much faster leading to insufficient time for pyrolysis to take place hence a decrease in carbon nanotube synthesis. The external diameter of the carbon nanotubes was reduced as the synthesis of CNTs was decreased.

In our study, internal and external diameters were measured following synthesis of MWCNTs using various gas flow rates. The internal diameter of the CNTs was not affected by an increase in gas flow rate. In this experiment, iron nanoparticles used were around 10 nm, but the measured diameters were about 12 nm. However, the external diameter was reduced by an increase in gas flow rate as depicted in **Fig. 3.12B**.

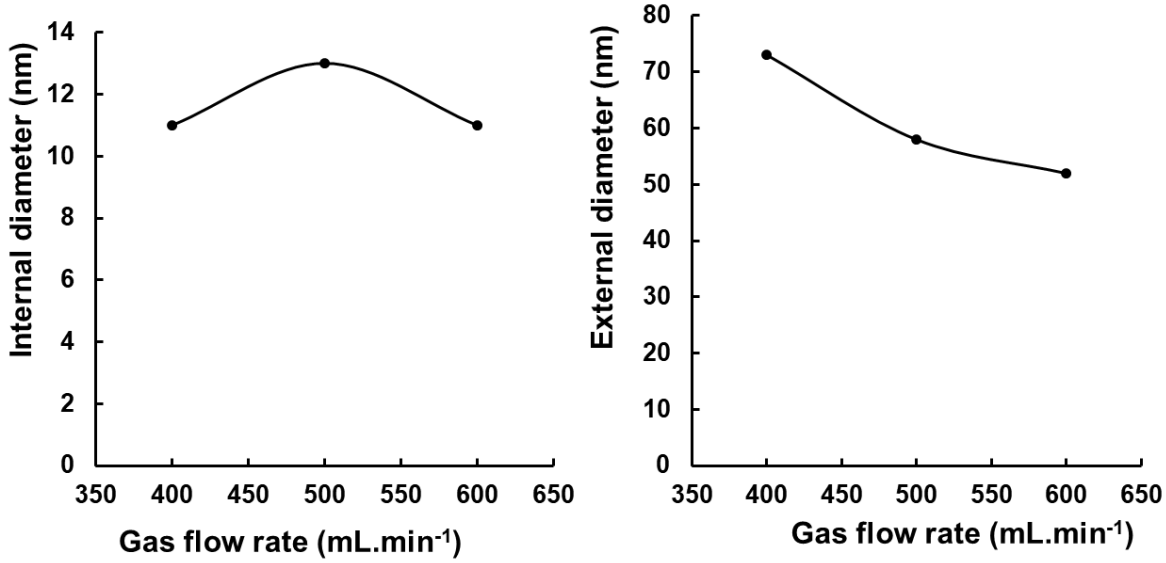


Figure 3.12. The effect of gas flow rate on diameters of CNTs. (a) Internal diameter and (b) External diameter.

A decrease in external diameter could be as the result of lack of enough time for the toluene pyrolysis for the formation of CNTs as the carrier gas wiped away toluene at a much faster rate.

3.3.11. Box-Behnken Design of experiments (BBDOE)

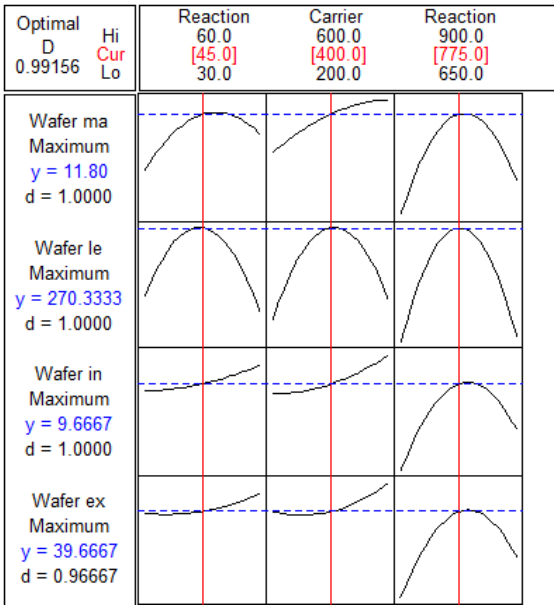
In BBDOE, a response results as a variable is introduced in an experimental set-up. The main goal of this design is for the optimization of analytical methods. The design was pioneered by George E.P. Box and Donald Behnken in 1960 (Shahmohammadi *et al.*, 2016).

Box-Behnken Design of experiments was performed to synthesise VA-MWCNTs with specific thickness, external diameter and internal diameter in both the quartz tube and on the substrate. This design was employed to obtain the optimal pyrolysis conditions for the successful VA-MWCNT growth with those features of interest with the main focus on the three variables namely synthesis temperature, gas flow rate and synthesis time according to **Table 3.1** in the Methods section.

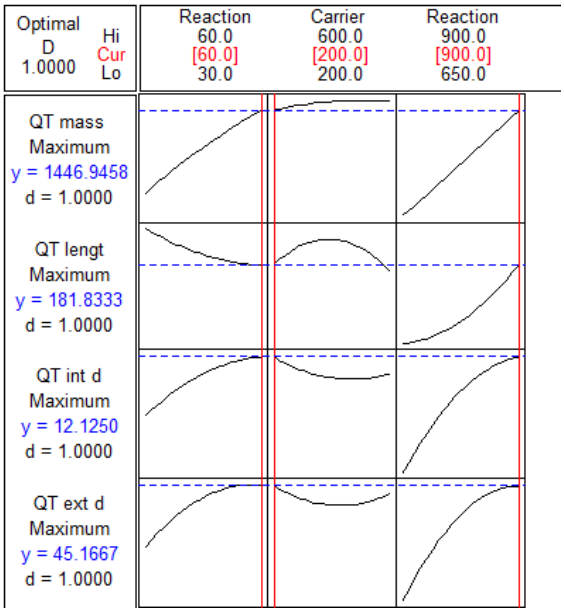
MWCNTs were produced on wafer with max mass 11.80 mg, max length 270.33 µm, max internal diameter 9.67 nm and max external diameter 39.67 nm, when the following pyrolysis conditions were applied; reaction duration = 45 min, carrier gas flow rate = 400 $mL.min^{-1}$ and reaction temperature = 775 °C (**Table 3.2**).

Table 3.2. BBDOE (A) Silicon Wafer and (B) Quartz Tube walls

A.



B.



In order to produce MWCNTs on QT walls with max mass 1446.95 mg, max length 181.83 µm, max internal diameter 12.13 nm and max external diameter 45.17 nm, the pyrolysis conditions should be as follow; reaction duration = 60 min, flow rate of gas = 200 mL.min^{-1} and reaction temperature = 900 °C as shown in **Table 3.2**.

3.3.12. Effect of a mixture of Fe//Ni, Fe/Co and Fe/Ni/Co on MWCNT growth

The substrate, catalyst type, mixture of catalysts and the catalyst concentration play a pivotal role in the catalytic activity of metal particles formed on the substrate. Furthermore, the nature of distribution of the nanoparticles on the substrate influences the catalytic activity of the transition metals. The distribution state of the of metallic catalyst particles on the support is dependent on the type of metal–substrate interaction which in turn is also dependent on the nature of the support (Shokry *et al.*, 2014).

In our study, the effects of monometallic, bimetallic and trimetallic catalysts were determined using ferrocene, ferrocene-nickelocene and ferrocene-nickelocene-cobaltocene in toluene. A higher total yield of CNTs was obtained when a mixture of ferrocene and cobaltocene was used as compared to ferrocene or cobaltocene alone and nickelocene –ferrocene mixture. A slight reduction in the yield was noticed when

a trimetallic catalyst was used but still higher than ferrocene alone. The yield of CNTs on the substrate was lower and very thin layers of CNTs were observed.

Table 3.3. VA MWNT production using a combination of various catalysts.

Catalyst	Support	Mass (g) before run	Mass (g) after run	Final mass (g)	Total mass (g)
Fe 2.5 %	Wafer	0.1114	0.1222	0.0108	0.1879
	QT	-	0.1771	0.1771	-
Fe 2.5 %+Ni 0.125 %	Wafer	0.1278	0.1282	0.0004	0.3312
	QT	-	0.3312	0.3312	-
Fe 2.5 %+Co 0.125 %	Wafer	0.0933	0.0935	0.0002	0.5994
	QT	-	0.5992	0.5992	-
Fe 2.5 %+Co 0.125 % +Ni 0.125 %	Wafer	0.0435	0.0454	0.0019	0.2733
	QT	-	0.2714	0.2714	-
Fe 5 %+Co 0.25 % + Ni 0.25 %	Wafer	0.1476	0.1481	0.0005	0.5097
	QT	-	0.5092	0.5092	-

Cobaltocene and nickelocene improved the yield of CNTs on quartz tube walls but reduced the yield on the substrate (**Table 3.3**). The results imply that the Ni and Co have a negative impact on the formation of nucleation sites for CNT growth on the substrate. This could be due to the coating effect of Fe on Ni and Co nanoparticles. Our findings are in agreement with the findings of Shokry and colleagues (Shokry *et al.*, 2014). The yield in MWCNT from bimetallic catalyst was higher than that of the monometallic catalyst.

Furthermore, the MWCNT yield doubled when the ferrocene-cobaltocene-nickelocene catalyst concentrations were doubled as more catalytic sites are created leading to improved growth of the MWCNTs (**Table 3.3**). This is an indicative that the catalyst

type, mixture and concentration are very important in the yield and quality of the carbon nanotubes.

3.3.13. Effect of different acids on VA-MWCNT purification

Impurities may be found in commercial raw and MWCNT synthesised in the laboratory. These impurities may have a negative impact on the bio-activity of these CNTs. MWCNTs must be purified prior to application in the biological milieu. HCl refluxing has been found to play a major role in purifying raw “as-received or synthesized” MWCNT by eradicating the unwanted amorphous carbon and metal impurities such as Ni, Fe, and Co from MWCNTs.

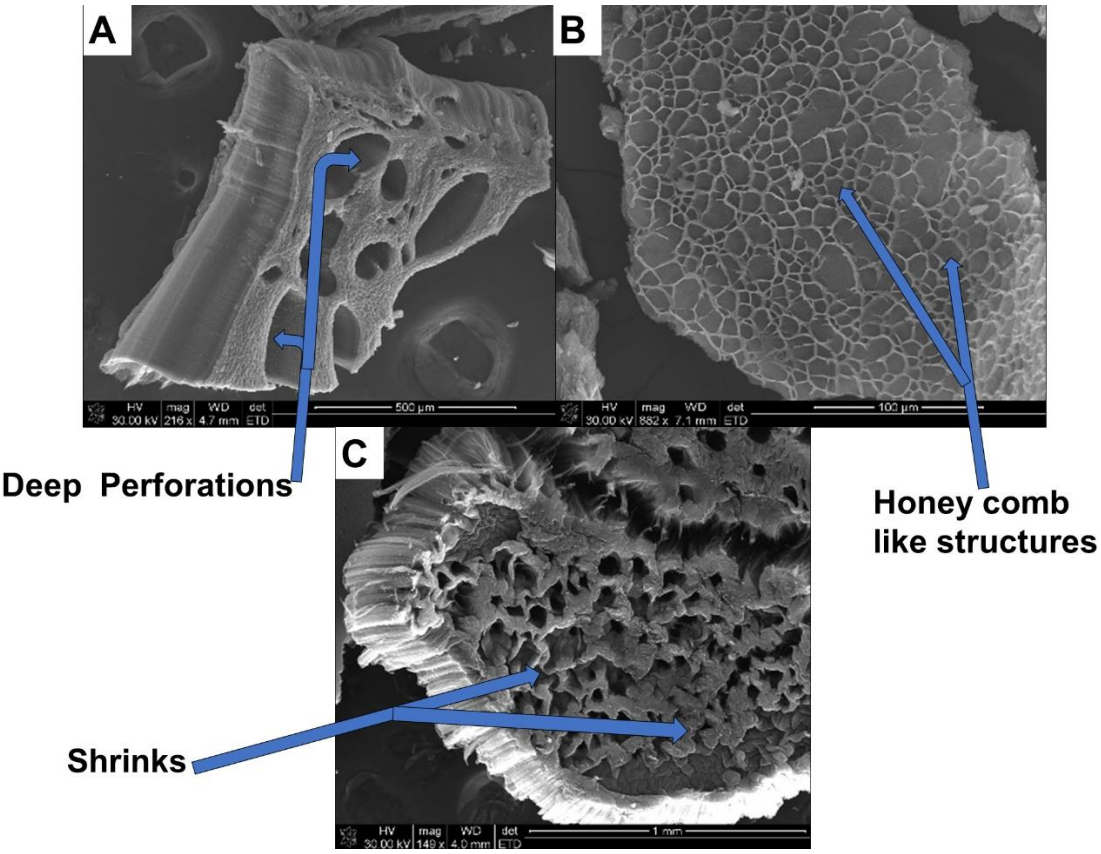


Figure 3.13. MWCNTs treated with different acids (a) Concentrated H_2SO_4:HNO_3 (3:1), (b) 5 M HCl and (c) Concentrated HCl.

Moreover, purification increases the number of reaction sites on the MWCNTs and this leads to the enhancement of sidewall functionalization by carboxylation using acids such as HNO_3, H_2SO_4 and a mixture of the two acids.

In this study, thermal and acid oxidation method was employed in purification and carboxylation of the VA-MWCNTs grown on silicon wafer. Honeycomb-like structures with mean diameter of 12.30 µm were formed on the CNTs when the CNTs were incubated with 5 M HCl. Concentrated HCl created holes with mean diameter of 85.82 µm and shrinkage on the surface of CNTs (**Fig. 3.13**). Concentrated HCl oxidized the surface of the CNTs.

Furthermore, holes with mean diameter of 104.31 µm were formed on the surface of MWCNTs following an exposure to HNO_3:H_2SO_4 (1:3), (**Fig. 3.13**). HNO_3 and H_2SO_4 combination oxidized the catalyst nanoparticle and amorphous carbon layers on the MWCNT surface. The mixture was too strong to even penetrate into the CNTs beneath these layers leading to the formation of holes on the CNTs.

3.3.14. Electrical conductivity of VA-MWCNTs

Electrical resistivity (ρ) measurements in bulk CNTs seem to be less appealing hence less attention is given to them. However, a better understanding of the transport behaviour in bulk samples can shed light on the fundamental physical properties of individual carbon nanotubes. Moreover, it can offer physical guidelines on the potential applications of CNTs as sensors in biomedical fields and industrial world (Barberio *et al.*, 2007).

In order to understand electrical conductivity, it must be born in mind that CNTs can organise themselves into aligned bundles during their synthesis as a result of the presence of van der Waals forces. The alignment maintains close contact of the individual CNTs resulting in the far much better electrical conduction between the aligned CNTs in the same bundle (Miao, 2011).

In this study, electrical resistivity was measured at various temperatures in order to shed light in the electrical conductivity of VA-MWCNTs. The large external surface area and interstitial sites are within the bundle of CNTs provide an access of the functional groups to interact with the CNTs. The adsorbed molecules, such as sulfuric acid (H_2SO_4), nitric acid (HNO_3), hydrogen peroxide (H_2O_2), and thionyl chloride ($SOCl_2$) can then increase the electrical conductivity of CNTs. Purification, carboxylation, amination, PEGylation and any other form of functionalization have a greater impact

on the electrical resistivity and conductivity of carbon nanotubes. The functionalization changes the physico-chemical architecture of the carbon nanotubes hence their electrical properties.

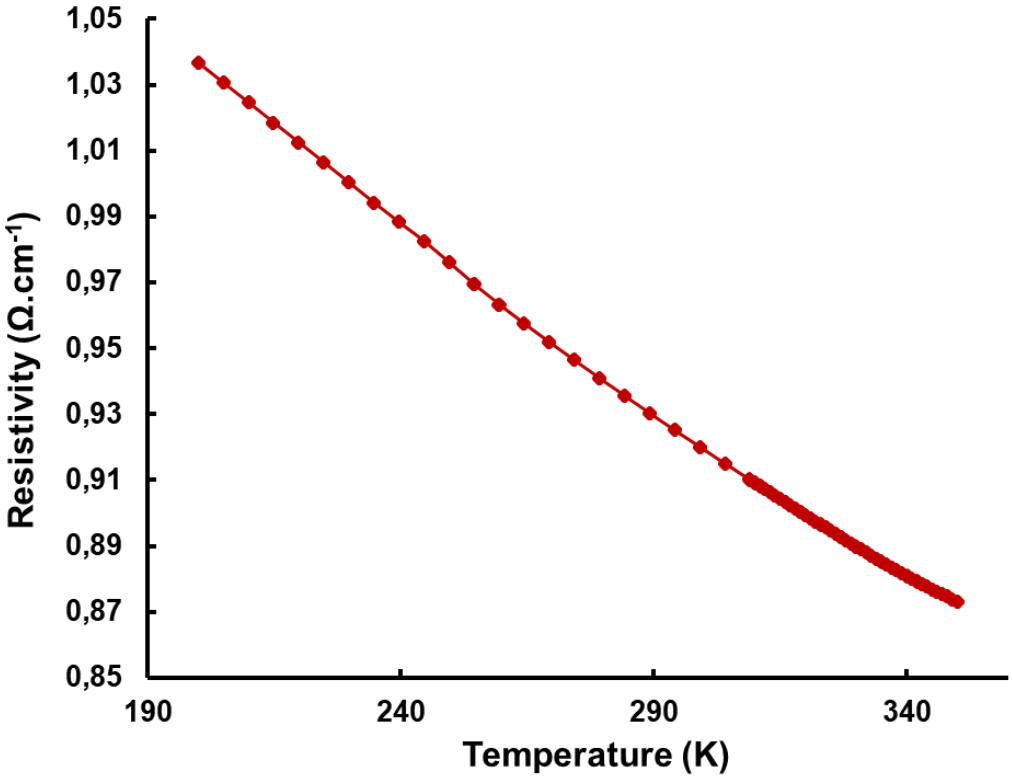


Figure 3.14. Electrical resistivity of VA-MWNTs from 200 to 350K.

The electrical resistivity of the pristine VA-MWCNTs measured at various temperatures is depicted in **Fig. 3.14**. Resistivity of VA-MWCNTs was measured by PPMS from 200-350 K. As the temperature increased from 200 to 350 K, resistivity decreased which implies that the CNTS are electrically conductive.

CNTs are highly conductivity from 310 K as depicted by the points getting closer at this point (**Fig. 3.14**). Our findings have demonstrated the high electrical conductivity of VA-MWCNTs and these CNTs have a potential to be used in designing an immunosensor for the detection of biomarkers of diseases and neurological disorders including ischemic stroke.

3.3.15. Surface area, pore size and pore volume of VA-MWCNTs

Brunauer-Emmett-Teller (BET) theory gives a better understanding of the physical adsorption of the gaseous molecules on a solid surface. It serves as the solid foundation for the porositometric measurements of the solid materials. The pioneers of this theory is Stephen **Brunauer**, Paul Hugh **Emmett**, and Edward **Teller.** They published their first article in the Journal of the American Chemical Society in 1938.

The theory is applicable to systems of multilayer adsorption. It uses inert gases to avoid chemical reaction of these gases with the material surfaces. The inert gas adsorbates on the solid material to quantify specific surface area of that material. BET uses nitrogen as the gaseous adsorbate for probing the surface. Standard BET analysis is most often performed at the boiling temperature of N_2 (77 K) (Birch *et al.*, 2015).

Table 3.4: Surface area of pristine and 5 M HCl treated MWCNTs.

Parameter	Pristine MWCNTs	5 M HCl MWCNTs
BET surface area	47.1563 $m^2.g^{-1}$	144.0962 $m^2.g^{-1}$
Pore size	13.08973 nm	18.08957 nm
Pore volume	0.154316 $m^3.g^{-1}$	0.651660 $m^3.g^{-1}$

In our study, 0.2-0.3 g MWCNTs were degassed overnight and analysed the following day. The pore size, surface area and pore volume of pristine and 5 M HCl treated MWCNTs were determined from the adsorption and desorption isotherms. The pore size, surface area, and pore volume of MWCNTs increased following the treatment of the MWCNTs with an acid as depicted in **Table 3.4**. Purification of the CNTs using HCl removed the amorphous carbon and metal impurities hence an increase in the surface area. Carboxylation using sulphonitric acid further increased the surface area of the MWCNTs.

3.3.16. Wettability of VA-MWCNTs

Contact angle denoted θ, is a quantitative measure of the wetting properties of a solid by a liquid. Goniometer or contact angle meter is the instrument that is used to measure the contact angle of the solid material. Contact angle is an angle which is formed when a liquid interacts with the solid at the three-phase boundary (liquid, vapour and solid) and the Young equation describing the balance at the three-phase intersection of solid-liquid and gas is expressed as: $\gamma_{sv} = \gamma_{sl} + \gamma_{lv} \cos \theta_Y$. **(Equation 3.1)**

The contact angle below 90 ° is an indicative of a hydrophilic material whereas the contact angle above 90 ˚ is an indicative of a hydrophobic material. The liquid wets the surface when the contact angle is less than 90 °. The complete wetting occurs when the contact angle is zero. The material is non-wetting or water-proof when the contact angle is greater than 90 °. The material is said to be semi-wetting when the contact angle is 90 ° (**Fig.3.15**).

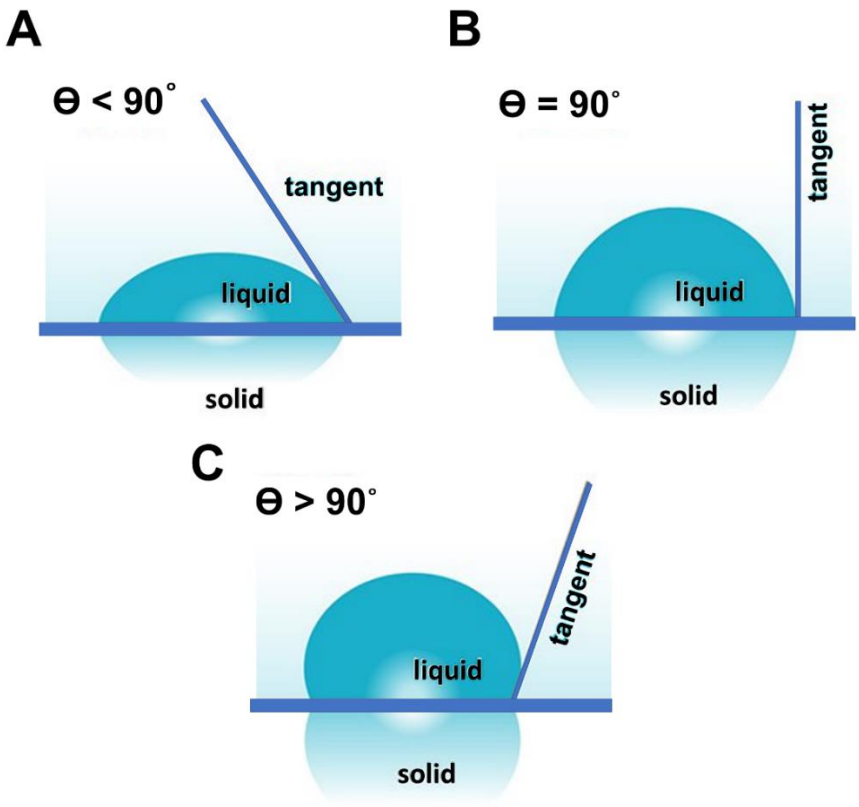
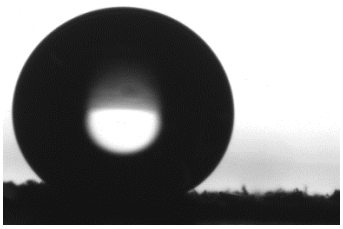
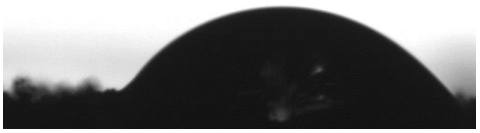
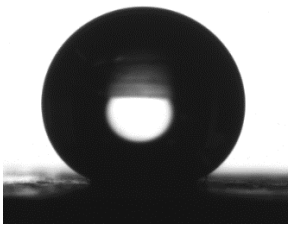
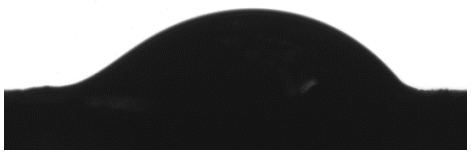


Figure 3.15. Measurement of contact angle. Θ < 90 ° (A), Θ = 90 ° (B) and Θ > 90 ° (C).

There are two types of contact angles namely static and dynamic angles. In static contact angle measurements, the angles are recorded while the liquid droplet is stationary and there is no movement of the three-phase boundary. In dynamic contact angle measurements, the angles are recorded while the three-phase boundary is in motion. The dynamic contact angles are regarded as advancing or receding angles.

Contact angle measurements can be applied in carbon nanotubes following their synthesis for specific application. The wettability of the carbon nanotube surface is a very important property which is influenced by both chemical composition and geometrical microstructure of the contact surface (Pavese *et al.*, 2008).

Table 3.5: Wettability of MWCNTs on silicon wafer and quartz tube walls following treatment with 5 M HCl

Substrate	**Pristine MWCNTs, Θ**	**5M HCl MWCNTs, Θ**
Quartz Tube	135.5 ° ± 7.9 °	55.3 ° ± 6.9 °
		
Silicon Wafer	146.4 ° ± 2.2 °	44.8 ° ± 7.7 °
		

In our work, drops of water were applied on the various spots of MWCNTs to measure their contact angles using a sessile drop technique. The average contact angle for the pristine MWCNTs was 135.5 ˚ ± 7.9 ° and for 5 M HCl treated MWCNTs was 55.3 °± 6.9 ° from quartz tube walls. The average contact angles were 146.4 ° ± 7.9 ° and 44.8 ° ± 7.7 ° for both pristine MWCNTs and 5 M HCl treated MWCNTs respectively from silicon wafer (**Table 3.5**).

These results imply that the pristine MWCNTs are hydrophobic and the HCl treated MWCNTs are hydrophilic. Acid treatment increased the wettability of the CNTs. It is very important to ensure that the carbon nanotubes should be hydrophilic as they will be used as nanocarriers in delivering dexamethasone to the ischemic site in stroke induced rats.

3.3.17. Particle size distribution and zeta potential VA-MWCNTs

Particle size distribution is an index giving a clear picture of the sizes of particles and their proportions in the sample of interest. Particles are very complex and have irregular shapes such as spheres, cubes, rectangular, long, thick and thin. Since their particle size and shape cannot be directly defined, they are therefore, defined as "sphere-equivalent diameter" to make them measurable.

There is a variety of techniques to determine the quantity vs. equivalent size distribution of particles. The techniques used in particle size distribution are as follows; dynamic light scattering (DLS), air permeability, the electrical sensing zone, X-ray sedimentation, dynamic image analysis and static light scattering (SLS).

In our study, we used DLS since it measures both the size and zeta potential of the particles. Zeta potential develops at the interaction point of the solid and liquid. This charge is measured in millivolts (mV). In this study, 5 M HCl-treated CNTs were suspended in deionized water at a concentration of 0,2 $mg.mL^{-1}$. Particle sizes and zeta potentials were measured using the nanosizer. The 5 M HCl-treated CNTs were completely dispersed in water than the untreated ones.

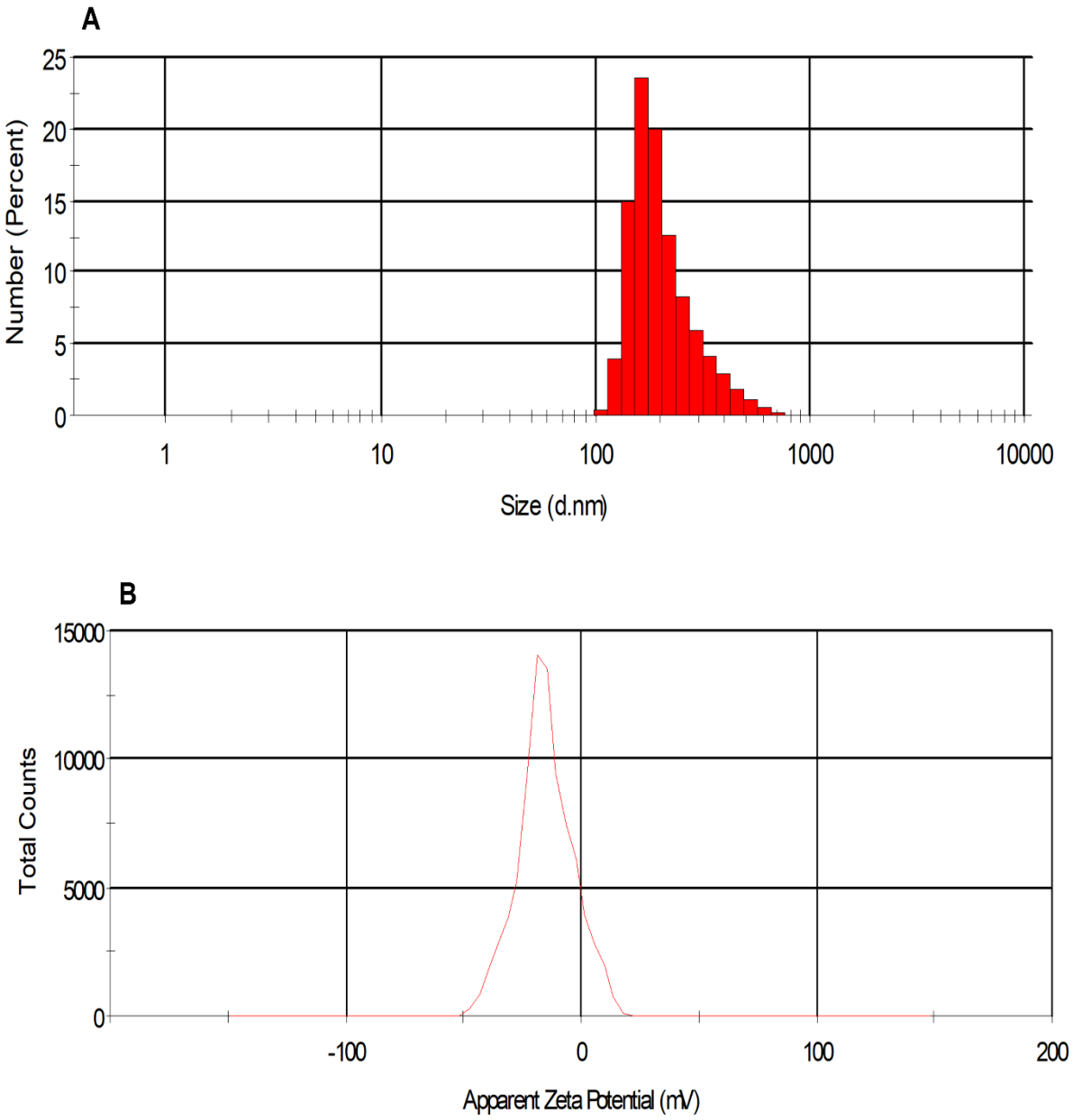


Figure 3.16. The 5 M HCl treated MWCNTs (a) Particle size distribution (b) Zeta potential.

The Z-average diameter was found to be 287.08 nm and polydispersity index (PDI) was 0.261 (**Fig. 3.16**). The Z-average diameter was quite large and this could have been attributed by the agglomeration of the carbon nanotubes. The PDI obtained is an indicative that the CNTs have a moderate size distribution. The zeta potential in these 5 M HCl treated CNTs was -15.0mV and conductivity was found to be 0.0213 $mS.cm^{-1}$. The CNTs possess negative charge on their surface and the zeta potential magnitude of 15 mV is an indicative that the MWCNTs are slightly agglomerated.

3.3.18. Functional groups on VA-MWCNTs

The functional groups of molecules can be determined using FTIR. When IR radiation passes through a sample, some radiation is absorbed by the components of the sample and some radiation is transmitted. The transmitted radiation reaches the detector and displays a signal as a spectrum representing a molecular 'fingerprint' of the sample. This technique is very important as different chemical structures of the samples produce different spectral fingerprints.

The samples can either be loaded on KBr pellet sample holder or directly to the ATR crystal (attenuated total reflectance). ATR system is used for the light samples and KBr system for the dark samples. For aqueous sample analysis, samples can be loaded on ATR with a specific accessory for the liquid samples. Aqueous samples can also be loaded on NaCl window accessory for analysis.

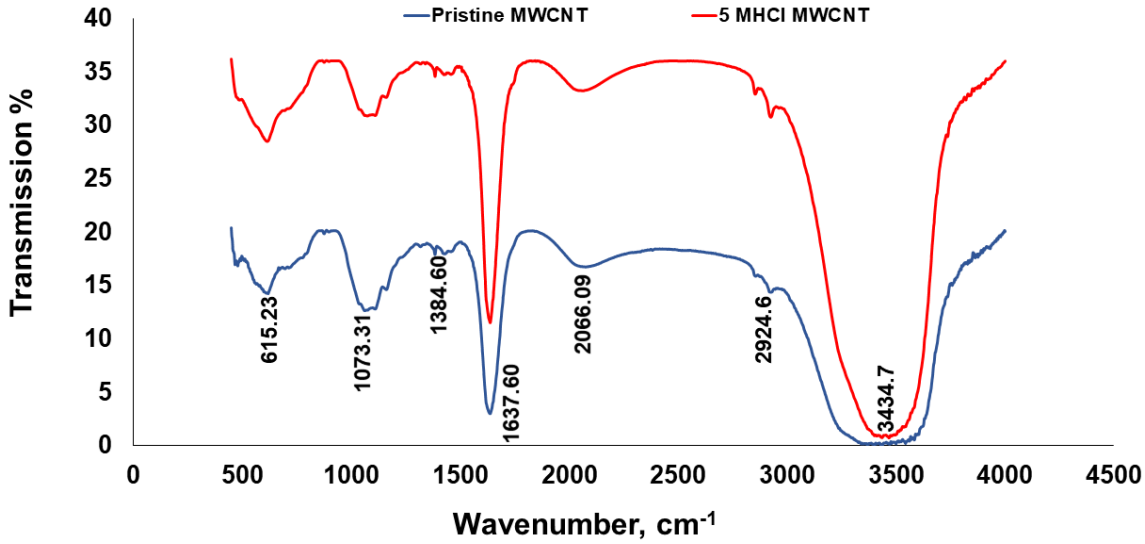


Figure 3.17. FTIR spectra of pristine MWCNTs and 5M HCl treated MWCNTs.

In our study, we used FTIR equipped with KBr accessory for the CNTs since the CNTs are dark and absorb all the light if not mixed with KBr. In both the treated and pristine MWCNTs, the spectral pattern was found to be the same as depicted in **Fig.3.17**. The difference that was observed in the pristine and acid treated MWCNT spectra was the size of the peaks. The 5 M HCl treated CNTs had bigger peaks compared to the pristine CNTs (**Fig.3.17**). HCl was used to purify the CNTs by removal of amorphous carbon and other contaminants to provide more reaction sites for functionalization.

The peaks that were observed at 615,24 cm^{-1}, 1073,31 cm^{-1}, 1637,60 cm^{-1}, 2066 cm^{-1}, 2924 cm^{-1}, and 3434 cm^{-1} were due to C-H bend, C-O stretch, C=O stretch, C≡C stretch, C-H stretch, and O-H stretch in MWCNTs respectively (**Fig.3.17**). The peak at 3434.76 cm^{-1} was due to the presence of hydroxyl group (OH) from the water in the samples. These data imply that purification was successful as confirmed by an increase in the size of the peaks following purification process.

3.3.19. Purity determination of VA-MWCNTs using TGA

Thermogravimetric analysis (TGA) is a technique used in thermal analysis to analyse the changes in physical and chemical properties of materials as the temperature is increased at a constant heating rate or as the time is increased at the constant temperature. TGA can be hyphenated to GC, MS and FTIR to measure the evolved gases.

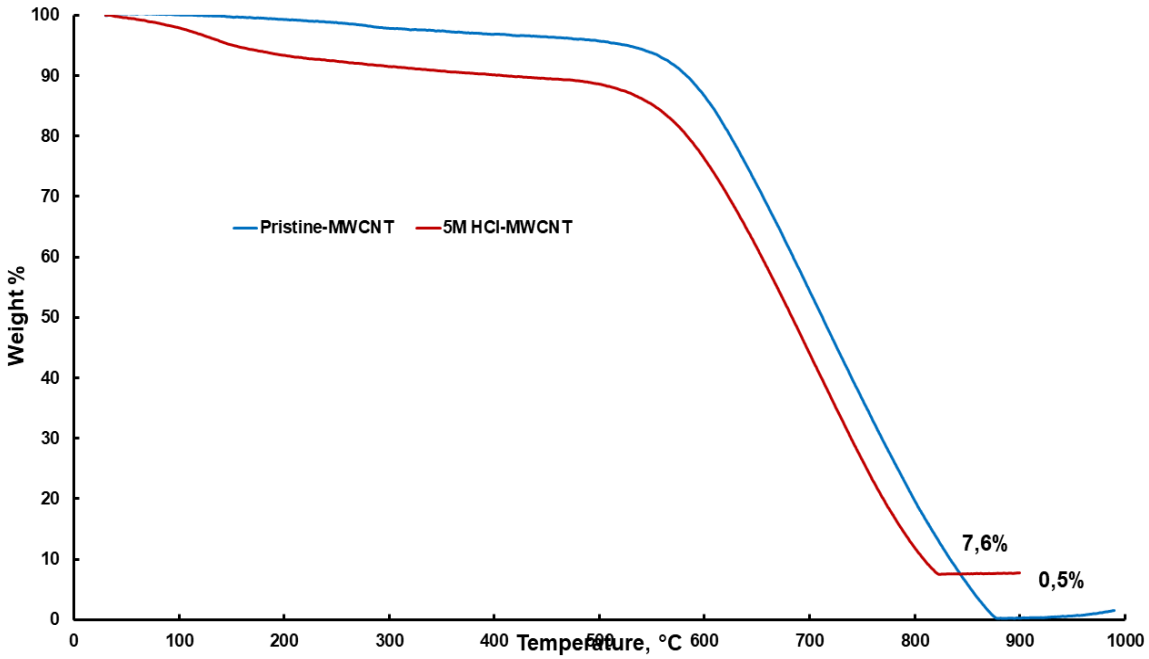


Figure 3.18. TGA weight loss curves of pristine MWCNTs and 5 M HCl treated MWCNTs.

In our work, TGA was performed for the quantitative analysis of the modification degree of MWCNTs by chemical oxidation using 5 M HCl. The temp ramp was kept constant and the temperature increased from 30 to 900 °C. A loss in weight of the pristine and 5 M HCl treated MWCNTs was observed as the temperature increased (**Fig.3.18**).

For pristine MWCNTs, thermal degradation was initiated when the temperature reached 577.47 °C and complete decomposition was found to be at 873.71 °C. For the 5 M HCl treated MWCNTs, thermal decomposition was initiated when the temperature increased to 559.18 °C and complete degradation at 816.51 °C. A slight drop in weight was observed at temperatures below 580 °C and this drop was due to the loss of moisture from the samples as the temperature was increased from 30 °C.

Complete decomposition of the CNTs was observed at 816.51 °C and 873.71 °C with 7,6 % and 0,5 % sample leftovers of pristine and 5 M HCl treated samples respectively as depicted in **Fig. 3.18**. The leftovers (ashes) of the pristine CNTs were higher than that of the HCl-treated CNTs. This could be due to the HCl inhibiting a complete decomposition of the CNTs as it reacts with the amorphous carbon and metal impurities and other contaminants. The reduction in thermal stability of CNTs could be due to the removal of impurities from the CNTs during purification with acid oxidation.

3.4. Conclusion remarks

The production of well aligned MWCNTs was found to be best at temperature of 775 $^{\circ}$C with a ferrocene concentration of 2.5 % in toluene, carrier gas flow rate of 400 mL.m^{-1} synthesis duration of 45 min with silicon wafer 125 mm between the centre and entrance point of the furnace. The total yield was greatly improved when a mixture of ferrocene and cobaltocene catalysts were used. The mixture of cobaltocene, ferrocene and nickelocene had a negative impact on the MWCNT production as the yield was reduced as a result of coating of Ni and Co by Fe.

Variation of synthesis parameters did not have any impact on the CNT internal diameter. The internal diameter is dependent on the size of iron nanoparticles. Catalyst concentration and temperature increased yield, thickness and external diameter of the CNTs. An increase in the flow rate of a carrier gas had a negative impact on the yield and external diameter of CNTs.

Thermal oxidation and 5 M HCl used during purification of the MWCNTs oxidized the surface of the CNTs. An exposure of CNTs to acid and thermal oxidation resulted in the formation of holes and honey-comb structures. Furthermore, the surface area, pore volume and size of the MWCNTs increased. Wettability of the MWCNTs was also improved by the acid treatment. MWCNTs were also found to be electrically

conductive. Chemical oxidation also improved CNT dispersion and reduced their thermal stability which implied that the impurities were removed during oxidation process.

These findings suggest that quality and well aligned MWCNTs could be synthesized, yield improved and be purified and functionalized for use in various applications such as diagnosis and treatment of ischemic stroke.

3.5. References

Allaedini, G. *et al.* (2016) 'Carbon nanotubes via different catalysts and the important factors that affect their production : A review on catalyst preferences', *Int j nano dimens*, 7(3), pp. 186–200.

Ando, Y. *et al.* (2004) 'Growing carbon nanotubes', *Materials Today*. Elsevier Ltd, 7(10), pp. 22–29.

Azam, M. A. *et al.* (2013) 'Aligned carbon nanotube from catalytic chemical vapor deposition technique for energy storage device: A review', *Ionics*, 19(11), pp. 1455–1476.

Barberio, M. *et al.* (2007) 'Electric resistivity of multi-walled carbon nanotubes at high temperatures', *Surface Science*, 601, pp. 2814–2818.

Bianco, A. *et al.* (2005) 'Biomedical applications of functionalised carbon nanotubes.', *Chemical communications (Cambridge, England)*, (5), pp. 571–577.

Birch, M. E. *et al.* (2015) 'Properties that Influence the Specific Surface Areas of Carbon Nanotubes and Nanofibers', *Ann Occup Hyg*, 57(9), pp. 1148–1166.

Bronikowski, M. J. (2006) 'CVD growth of carbon nanotube bundle arrays', *Carbon*, 44(13), pp. 2822–2832.

Cao, L.-C. *et al.* (2008) 'Wet Purification of Aligned Carbon Nanotube Arrays and Its Impact on the Morphology of the Carbon Nanotube Arrays', *acta phys. -Chim.Sin.*, 24(6), pp. 951–954.

Cele, L. M. and Coville, N. J. (2009) 'The negative effects of alcohols on carbon nanotube synthesis in a nebulised spray pyrolysis process', *Carbon*. Elsevier Ltd, 47(7), pp. 1824–1832. doi: 10.1016/j.carbon.2009.03.031.

Dai, H. (2002) 'Carbon nanotubes: Synthesis, integration, and properties', *Accounts of Chemical Research*, 35(12), pp. 1035–1044.

Das, R. *et al.* (2014) 'Carbon Nanotubes Characterization by X-ray Powder Diffraction – A Review', *Current Nanoscience*, 11(1), pp. 23–35.

Fabbro, A. *et al.* (2012) 'Carbon Nanotubes: Artificial Nanomaterials to Engineer Single Neurons and Neuronal Networks', *ACS Chemical Neuroscience*, 3, pp. 611–618.

Gomez-Ballesteros, J. L. *et al.* (2015) ‘Nanocatalyst shape and composition during nucleation of single-walled carbon nanotubes’, *RSC Advances*, 5(129), pp. 106377–106386.

Gottipati, M. K., Verkhratsky, A. and Parpura, V. (2014) ‘Probing astroglia with carbon nanotubes: modulation of form and function.’, *Philosophical transactions of the Royal Society of London. Series B, Biological sciences*, 369(1654), pp. 20130598–20130604.

Iijima, S. (1991) ‘Helical microtubules of graphitic carbon’, *Nature*, 354(6348), pp. 56–58.

Journet, C., Picher, M. and Jourdain, V. (2012) ‘Carbon nanotube synthesis: from large-scale production to atom-by-atom growth.’, *Nanotechnology*, 23(14), p. 142001.

Kapoor, A. *et al.* (2018) ‘3d transition metals and oxides within carbon nanotubes by co-pyrolysis of metallocene & camphor: High filling efficiency and self-organized structures’, *Carbon*, 132(February), pp. 733–745.

Kumar, M. and Ando, Y. (2010) ‘Chemical Vapor Deposition of Carbon Nanotubes: A Review on Growth Mechanism and Mass Production’, *Journal of Nanoscience and Nanotechnology*, 10(6), pp. 3739–3758.

Lacerda, L. *et al.* (2006) ‘Carbon nanotubes as nanomedicines: From toxicology to pharmacology’, *Advanced Drug Delivery Reviews*, 58(14), pp. 1460–1470.

Mahanandia, P. and Nanda, K. K. (2008) ‘A one-step technique to prepare aligned arrays of carbon nanotubes.’, *Nanotechnology*, 19(15), p. 155602.

Malarkey, E. B. and Parpura, V. (2007) ‘Applications of carbon nanotubes in neurobiology.’, *Neuro-degenerative diseases*, 4(4), pp. 292–9.

Marchesan, S. *et al.* (2015) ‘The winding road for carbon nanotubes in nanomedicine’, *Materials Today*. Elsevier Ltd., 18(1), pp. 12–19.

Miao, M. (2011) ‘Electrical conductivity of pure carbon nanotube yarns’, *Carbon*, 49(12), pp. 3755–3761.

Othman, R. N. and Wilkinson, A. N. (2016) ‘Assessment of the Reaction Time on the Morphology and Quality of Carbon Nanotubes – Silica Microparticles’, *Procedia Chemistry*. Elsevier Ltd., 19, pp. 571–576.

Pavese, M. *et al.* (2008) ‘An analysis of carbon nanotube structure wettability before and after oxidation treatment’, *Journal of Physics Condensed Matter*, 20(47).

Ravindra, R. and Bhat, B. (2011) ‘Synthesis of Aligned Carbon Nanotubes by Floating Catalyst Method Using Ferrocene’, *Journal of Metals, Materials and Minerals*, 21(2), pp. 95–99.

Saito, R. *et al.* (1992) ‘Electronic structure of chiral graphene tubules’, *Applied Physics Letters*, 60(18), pp. 2204–2206.

Santiago-Rodríguez, L., Sánchez-Pomales, G. and Cabrera, C. R. (2010) ‘DNA-Functionalized Carbon Nanotubes: Synthesis, Self-Assembly, and Applications’, *Israel Journal of Chemistry*, 50(3), pp. 277–290.

Sengupta, J. and Jacob, C. (2010) ‘The effect of Fe and Ni catalysts on the growth of multiwalled carbon nanotubes using chemical vapor deposition’, *Journal of Nanoparticle Research*, 12(2), pp. 457–465.

Shahmohammadi, H. R. *et al.* (2016) ‘Optimization of puffed corn-fish snack extrusion conditions using response surface methodology’, *International Food Research Journal*, 23(4), pp. 1685–1693.

Shokry, S. A. *et al.* (2014) ‘Study of the productivity of MWCNT over Fe and Fe–Co catalysts supported on SiO2, Al2O3and MgO’, *Egyptian Journal of Petroleum*, 23(2), pp. 183–189.

Szabó, A. *et al.* (2017) ‘Influence of synthesis parameters on CCVD growth of vertically aligned carbon nanotubes over aluminum substrate’, *Scientific Reports*, 7(1), pp. 1–11.

Zhang, Q. *et al.* (2007) ‘The effect of phase separation in Fe/Mg/Al/O catalysts on the synthesis of DWCNTs from methane’, *Carbon*, 45(8), pp. 1645–1650.

CHAPTER 4

PRE-FORMULATION OF ALIGNED MULTIWALLED CARBON NANOTUBES FOR POTENTIAL APPLICATION IN DIAGNOSIS AND TREATMENT OF ISCHEMIC STROKE

Abstract

Currently, there is a lack of ultrasensitive diagnostic tool to detect ischemic stroke and a lack of effective and efficient treatment for ischemic stroke at an embryonic stage. Carbon nanotubes have a potential to be employed in resolving the diagnostic and treatment challenges in stroke. Atrial Natriuretic Peptide (ANP) is one of the promising biomarkers for ischemic stroke. In this study, vertically aligned multi-walled carbon nanotubes (VA-MWCNTs) were purified with HCl, carboxylated with H_2SO_4:HNO_3 (3:1) and acylated with $SOCl_2$ for use in targeting ANP and the design of the carbon-based electrode for potential application in stroke diagnosis. VA-MWCNTS were refluxed at 80 ˚C for 24 hours. VA-MWCNTs were centrifuged and supernatants were filtered, and the precipitates washed until pH was neutral. MWCNTs were washed, extracted from the filter membranes and dried in a vacuum oven at 60 °C for 24 hours prior to functionalization and PEGylation for use in drug release studies. For designing the carbon-based electrode, MWCNTs on wafer were incorporated into epoxy resin. CNTs were characterized by TGA, SEM, TEM, OCA, DLS, UV-VIS, BET, and FTIR. The HCl treated CNT internal diameter, outer diameter and thickness were 10 nm, 46 nm and 75 µm respectively. The H_2SO_4-HNO_3 treated CNT internal diameter, outer diameter, contact angle and thickness were 8nm, 23 nm, 44,8 ° ±7,7 ° and 42 µm respectively. PEGylated CNT zeta potential, polydispersive index and particle size distribution were 6 mV, 0,33 and 98 nm respectively. VA-MWCNTs from quartz tube were successfully purified, carboxylated, acylated and PEGylated for further functionalization for use in drug release study. VA-MWCNTs on the wafer was successfully incorporated into epoxy resin for formation of an electrode for diagnostic purpose. The findings of this work suggest that VA-MWCNTs may be functionalized for potential application in both the diagnosis and treatment of ischemic stroke.

4.1. Introduction

Stroke is regarded as the 5th root cause of death and the primary cause of permanent disability. Ischemic stroke contributes 80 % and haemorrhagic stroke makes up the remaining 20 % (Joshi, 2016). There is a dire need for effective diagnosis and treatment of stroke at the present moment. Nanotechnology in medicine is an emerging field with a possible application of the engineered nanomaterials that could be implemented in the treatment of diseases, including neurological disorders. Carbon nanotubes are a new class of nanomaterials and have been demonstrated to have a potential application in different areas of nanomedicine (Nunes *et al.*, 2012).

Currently, more attention has been directed to carbon nanotubes as a result of their nanosize, electronic, optical, thermal, electrical, mechanical and chemical characteristics (Sedaghat, 2014). These unique properties of CNTs make them desirable as a material for use in neurobiological applications especially in ischemic stroke. Pristine carbon nanotubes are hydrophobic and thus insoluble in water. They have a tendency to agglomerate due to their chemical inertness and van der Waals forces on their surfaces. This property creates an obstacle in their biomedical application (Farahani, Behbahani and Javadi, 2016). As a result, a variety of functionalization methods have been developed in order to facilitate dispersion in an aqueous milieu to enable their application in a physiological environment (Flavin *et al.*, 2011).

There are two procedures that are commonly employed in functionalization of carbon nanotubes, namely non-covalent and covalent functionalization. Carbon nanotubes are coated with hydrophilic molecules in non-covalent functionalization whereas the functional groups are attached to the backbone of carbon nanotubes in covalent functionalization (Shulga *et al.*, 2011). Functionalization of carbon nanotubes has been found to reduce their cytotoxicity (Vardharajula *et al.*, 2012). Therefore, carbon nanotubes are considered to be the smart nanomaterials of the 21st century with a wide spectrum of application in diverse fields including biomedical, tissue engineering, neuroengineering biosensor technology and drug delivery (Firme and Bandaru, 2010).

In this study, well aligned MWCNTs were purified with HCl, carboxylated with H_2SO_4:HNO_3 and acylated with $SOCl_2$. Their inertness and hydrophobicity were

drastically changed following purification and functionalization. They became highly hydrophilic, electrically conductive, highly stable and reduced in size for use in biomedical application. The functionalised MWCNTs were used in the treatment of ischemic stroke in stroke induced SD rats. VA-MWCNTs grown on silicon wafer were incorporated in epoxy resin for development of a system that has a potential to be applied in the diagnosis of stroke.

Our findings have demonstrated that the vertically aligned multiwalled carbon nanotubes could be functionalised for application in targeting atrial natriuretic peptide for treatment of ischemic stroke. In addition, they have also demonstrated that they may be engineered to design a carbon-based electrode that has a potential for application in the diagnosis of stroke.

4.2. Materials and Methods

4.2.1. Materials

Hydrochloric acid ≥32 % was purchased from Associated Chemical Enterprises (Johannesburg, South Africa). Ferrocene, 98 %, toluene chromaSolv for HPLC, ≥ 99.9 %, hydrochloric acid ≥32 %, acetone chromaSolv for HPLC, ≥ 99.8 %, ethanol 99.8%. Circular silicon wafer with single side polished, N-type, without dopant, diam. × thickness 2 in. × 0.5 mm, sulphuric acid 95-98 %, succinic anhydride ≥99 %, N, N'dimethylformamide (DMF), absolute ethanol and thionyl chloride ($SOCl_2$) were purchased from Sigma-Aldrich Corp. (St. Louis, MO, USA). N,N'dicyclohexylcarbodiimide) ≥99 % was purchased from Fluka (CH-9470 Buchs, Switzerland). Tetrahydrofuran (THF), dichloromethane (DCM) and nitric acid (HNO_3) 55 %, and Millipore filter papers, 0.22 µm were purchased from Merck (Pty) Ltd (Johannesburg, SA). Copper grids with holey lacey carbon, carbon tape, Whatman filter paper and Pasteur pipettes were purchased from SPI Supplies (West Chester, USA). MWCNTs were synthesised in the laboratory at the University of Johannesburg (Johannesburg, South Africa). DSPE-PEG5000-amine and 4-Arm PEG-amine 10 K were purchased from Nanocs Inc. (Boston, USA). Baseline argon (95 %) balanced with 5 % hydrogen was purchased from African Oxygen Ltd (Germiston, South Africa). Quartz reactor (1140 mm x 35 mm) was purchased from Wits University (Johannesburg, South Africa). Epikote 862 and epikure 3402epikote 3402 were purchased from Servochem (PTY) Ltd, South Africa.

4.2.2. Preparation of silicon wafer and catalyst

Silicon wafer and catalyst were prepared as in **Chapter 3**. A circular silicon wafer was cut into 1 cm x 1 cm pieces and sonicated in an ultrasonic bath (UMC-5, Integral Systems (Pty) Ltd, Randburg, South Africa) in acetone for 5min followed by a second ultrasonication in water for another 5 min. The silicon wafer pieces were dried under nitrogen and stored away from dust at ambient temperature for future use. Toluene was used as a carbon source and ferrocene as a source of iron catalyst particles for nucleation. A catalyst comprised of 2.5 % ferrocene in toluene was prepared. Ferrocene was weighed on ME 104 Mettler Toledo analytical balance (Merck (Pty) Ltd, Modderfontein, South Africa) and dissolved in toluene and sonicated in UMC- 5 ultrasonic bath for 15 min to produce a homogenous mixture.

4.2.3. CVD synthesis of VA-MWCNTs

VA-MWCNTs were prepared as in **Chapter 3**. The CVD setup used in the synthesis of VA-MWCNTs is depicted in **Fig.3.1** in **Chapter 3**. The clean silicon wafer (1 cm x 1 cm) was weighed, placed in a quartz boat and loaded in a quartz reactor tube. The ultrasonic nebuliser catalyst reservoir was filled up with 4 0mLcatalyst and attached to the gas line inlet and the outlet was attached on the inlet of the quartz tube. Synthesis temperature was set to 775 °C, synthesis duration to 45 min and 95 % argon and 5 % hydrogen mixture was used as a carrier gas and the flow rate was set at
400 $mL.min^{-1}$.

4.2.4. Carboxylation and acylation of MWCNTs for drug delivery

MWCNTs were purified by refluxing with HCl and oxidized by refluxing with H_2SO_4:HNO_3 (3:1). An amount of 1.8 g of the HCl purified MWCNTs was refluxed for 6 hours at 70 °C in H_2SO_4:HNO_3 (3:1). MWCNTs were then washed through centrifugation until pH was neutral. They were dried under vacuum at 70 °C for 24 hours. Carboxylated MWCNTs were collected for characterisation and further functionalisation. Following carboxylation, MWCNTs were acylated with $SOCl_2$. An amount of 1 g MWCNT-COOH was added to 21 mL of $SOCl_2$: DMF (20:1) mixture. The solution was refluxed for 48 hours at 80°C under nitrogen. The product was centrifuged at 5 000 rpm for 15 min. Both the supernatant and precipitate were washed with THF using filtration via 0.22 µm filter and centrifugation respectively until the brown colour

due to $SOCl_2$ vanished. The COCl - MWCNTs were collected from the filters and centrifuge tubes and dried at 80 ˚C for 24 hours using dry a vacuum oven (Trade Raypa, Spain).

4.2.5. Purification of VA-MWCNTs by thermal and acid oxidation for electrode development

CNTs were subjected to a temperature of 450 °C for 1 hour at 200 $mL.min^{-1}$ oxygen in a horizontal tube furnace. CNTs were transferred into a vial and 3 mL of HNO_3:H_2SO_4 (1:3) was added and incubated for 2 hours at 80 °C in an oven (Binder, SA Geolab International, Singapore). CNTs were then rinsed thrice with distilled water to remove the acid. CNTs were dried in the furnace at 450 ˚C for 30 min. Another experiment was done in the similar manner but using 2.5, 5.0 and 10.0 M HCl.

4.2.6. Synthesis of DSPE-PEG5000-4-arm-(PEG-Amine) and CNT PEGylation

A one molar equivalent DSPE-PEG5000-amine was reacted with 5 molar equivalent succinic anhydride in dichloromethane for 24 hours at room temperature. The resulting product was evaporated to dryness and reconstituted in 5mL de-ionised water. The solution was transferred into a dialysis tubing with MWCO 3,5 kDa. De-ionised water with pH value of around 7 was used as a dialysis buffer. The dialysis was performed at ambient temperature for 48 hours and then the solution was lyophilized into powder using Virtis Benchtop K Series freeze drier (SP Scientific, USA.). A volume of 5 mL of dialysis buffer was collect for determination of succinic anhydride using a Shimadzu UV- 2450 spectrophotometer (Kyoto, Japan).

The resulting DSPE-PEG5000-COOH was reacted with 1.5 molar equivalent dicyclohexylcarbodiimide (DCC, Aldrich) and 2 molar equivalent hydroxybenzotriazole (HOBt, Aldrich) in DCM at room temperature for 1 hour. A 4 molar equivalent 4-Arm-(PEG-Amine) was then added to the solution and stirred for 2 days. The product was evaporated to dryness and reconstituted with 10mL de-ionised water and stirred for 1 hour. The solution was filtered through 0.22 µm Milipore filter to remove unreacted DCC and HOBt to yield DSPE-PEG5000-4-Arm-(PEG-Amine). Acylated MWCNTs (0.2 $mg.mL^{-1}$) were sonicated with 0.2 mM DSPE-PEG5000-4-arm-(PEG-Amine) at room temperature for 1 hour using an ultrasonicator (Scientech, SA). The solution was centrifuged at 24 000 x g for 6 hours using Centrofriger-BL ultracentrifuge (P-Selecta,

Spain). Supernatant which contained PEG-MWCNTs was collected for characterisation and further use.

4.2.7. Morphological evaluation of the CNTs using electron microscopy

As-synthesised CNTs were peeled off from the substrate and prepared for SEM and TEM analyses in order to study their morphology and size. For SEM, CNTs were placed on a carbon tape and aluminium tape on the stub and coated with Pd/Au using EmitechK550X (Emitech Ltd, Kent, England) for 4 min at 25 mA and 2 x 10^{-1} mbar.

For TEM, a small amount of CNTs was transferred into a 1.5 mL Eppendorf tube and dispersed in an absolute ethanol. The CNTs were sonicated in ultrasonic water bath for 10-15 min to disperse CNTs. Pasteur pippete was used to transfer dispersed CNTs onto a Cu grid that was placed on Whatman filter paper and was dried under light. The sample loaded Cu grids were analysed immediately or stored in vials for future analysis.

Samples were loaded in for the determination of morphology and length of the synthesized CNTs. Samples were also loaded in FEI Tecnai T12 TEM (Hillsboro, USA) operating at 120 kV for the determination of external and internal diameters of CNTs. ImageJ software was used to measure the length and diameters of the CNTs.

4.2.8. Thermal analysis and electrical resistivity of VA-MWCNTs

Thermogravimetric analysis was performed under air atmosphere at a temperature ramp of 20 °C.min^{-1} and purge gas flow rate of 20 mL.min^{-1} from 50 °C to 900 °C using the PerkinElmer TGA 4000 (Wales, UK). VA-MWCNTs with the dimension of 1mm x 1 mm x 6 mm were loaded on the physical property measurement system (PPMS, Quantum Design). Electrical resistivity was measured at temperatures ranging from 229-300 K.

4.2.9. Measurement of wettability, surface area and porosity of CNTs

Contact angle measurements were carried out using OCA 25 contact angle analyzer (DataPhysics Instruments, Filderstadt, Germany). As-synthesised VA-MWCNTs were loaded on the double-sided tape attached to sample platform. Measurements were carried out with water as the liquid and the volume of the sessile drop was maintained at 5 µL in all cases using a micro syringe. Drops of water were dispensed from the dosing syringe of the dispensing unit to the top of the MWCNT surface and contact angles were measured and recorded using SCA 20 software. The contact angle measurements were recorded for both the pristine and acid treated CNTs. Specific surface areas, pore sizes and pore volumes of the MWCNTs were measured using the BET method by nitrogen adsorption at 77 K. MWCNTs were weighed and 0.2 - 0.3 g was degassed and analysed using ASAP2020 Surface area and porosity analyser (Micromeritics, USA).

4.2.10. Measurement of crystallinity, elemental composition and functional groups of MWCNTs

As synthesised CNT samples on the silicon wafers were loaded on the sample holders of the XRD. The sample holders were then loaded into the diffractometer (Phillips Panalytical X-pert Pro X-ray Diffractometer, USA) and each sample was scanned for 2 hours. High Score Plus was used to process and interpret the raw data for crystallinity and elemental composition. For determination of functional groups, MWCNTs and KBr were mixed in a 1:200 ratio and ground to very fine particles using mortar and pestle. Pellets were generated using PerkinElmer KBr die and press. KBr pellets were analysed using PerkinElmer Spectrum 2000 FTIR spectrophotometer with a single-reflection diamond MIRTGS detector (PerkinElmer Spectrum 100, Llantrisant, Wales, UK). The remaining KBr sample powders were also used for FTIR analysis using UATR. MWCNTs dispersed in de-ionised water and DCM were included in the UATR analysis.

4.2.11. Particle size, zeta potential and Uv-Vis analysis of MWCNTs

A solution of 400 µg.mL^{-1} MWCNTs was prepared in de-ionised water and DCM. The samples were sonicated for one hour and centrifuged at 5 000 rpm for 10 min using Eppendorf centrifuge 5804 (Hamburg, Germany). Zetasizer Nano ZS (Malvern

Instruments Ltd., UK) equipped with backscatter with 173 ° angle was used to measure the particle size and zeta potential of the MWCNTs. For UV-VIS analysis, pristine and functionalised MWCNTs in de-ionised water and DCM were scanned at a wavelength from 500 nm to 190 nm using Shimadzu UV-2450 spectrophotometer (Kyoto, Japan). The synthesised DSPE-PEG5000-4-arm-(PEG-Amine), PEG-4-arm and dialysis buffer were also scanned.

4.2.12. Preparation of carbon-based electrode

Epikote 862 (EK862) and epicure 3402 (EC3402) were dispensed into separate vials and incubated at 80 °C for one hour. An epoxy resin mixture was prepared by mixing EK862 and EC3402 in a ratio of 100:26.6 respectively. The mixture was further incubated at 80 °C for 30 min. The Si wafers with as-synthesised CNTs (purified and oxidized with acids) were placed in the wells of the silicone rubber moulds. Conducting wires were attached to the surface of the CNTs. Epoxy resin mixture was poured on top of the conducting wires ensuring that air bubbles are not formed. The castings were incubated overnight at 80 °C to ensure that epoxy resin is cured properly. The casts were trimmed to remove excessive epoxy resin.

The embedded CNTs within the casts were exposed by fine sanding and polishing. The exposed CNTs were coated with Pd/Au using Emitech K550X (Emitech Ltd, Kent, England) for 4 min at 25 mA and 2 x 10^{-1} mbar and their morphology studied by SEM. The electrode electrical conductivity was assessed by electrical conductivity meter. The surface of the CNTs covered by epoxy resin was exposed by sanding and polishing. The surface was washed with water and dried out. Magnetic bar was placed near the as-synthesised MWCNTs and they got attracted to it. The +ve and -ve terminals of the electrical conductivity meter were attached to the conducting wire of the cast and exposed CNTs and the deflection of the needle on the meter was observed. Non - conductive and less conductive casts were further polished to expose the MWCNTs to improve their electrical contact.

4.2.13. Cyclic voltammetry and electrochemical impedance spectroscopy

MWCNTs incorporated in epoxy resin with conducting wires were used as working electrodes. Platinum wire was used as a counter electrode and Ag/AgCl (3M KCl) as a reference electrode. An electrolyte comprised of 1 mM $K_3Fe(CN)_6$ and 1 mM $K_4Fe(CN)_6$ in 0.1 M KCl as shown in **Fig.4.1**.

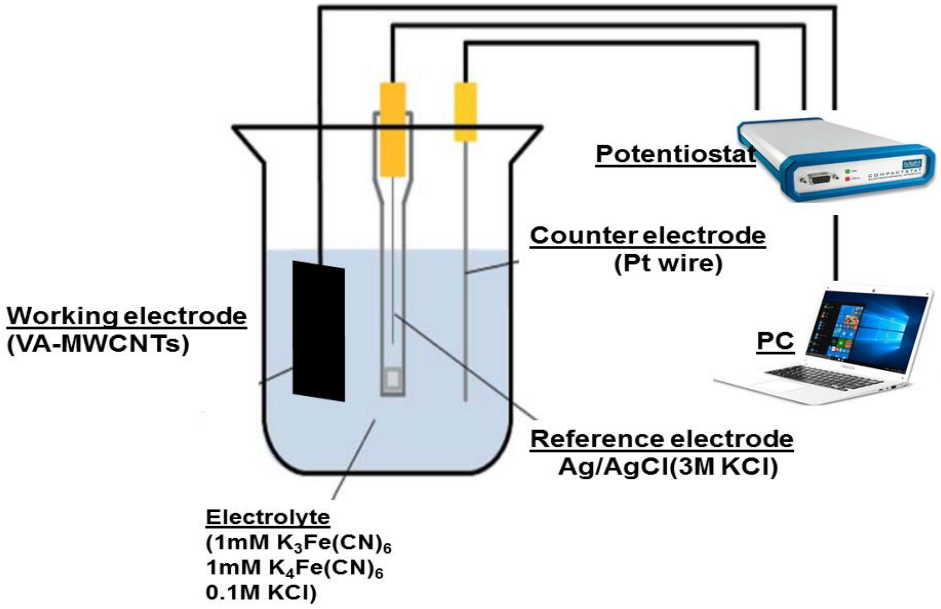


Figure 4.1. Set-up of the cyclic voltammetry system.

Cyclic voltammetry (CV) and electrochemical impedance spectroscopy (EIS) measurements were performed on the carbon-based electrodes using Ivium Compactstat Electrochemical workstation (**Fig.4.1**). CV data were recorded between -0.4 and 0.4 V with a scan rate of 50mV.S^{-1} in a solution of 1 mM $K_3Fe(CN)_6$ and 1 mM $K_4Fe(CN)_6$ in 0.1 M KCl. Spectra were taken at frequency of 100 kHz to 100 mHz with an amplitude of 0.01 V and potential of 0.220 V.

4.3. Results and discussion

4.3.1. Synthesis of vertically aligned MWCNTs on different substrates

Carbon nanotubes were grown on silicon wafer and quartz tube wall using CVD. A solution of 2,5 % ferrocene in toluene was used as a catalyst. Vertically aligned multiwalled carbon nanotubes were successfully produced at 775 °C with a gas flow rate of 400 mL.min^{-1} for 45 min on both the silicon wafer and reactor wall.

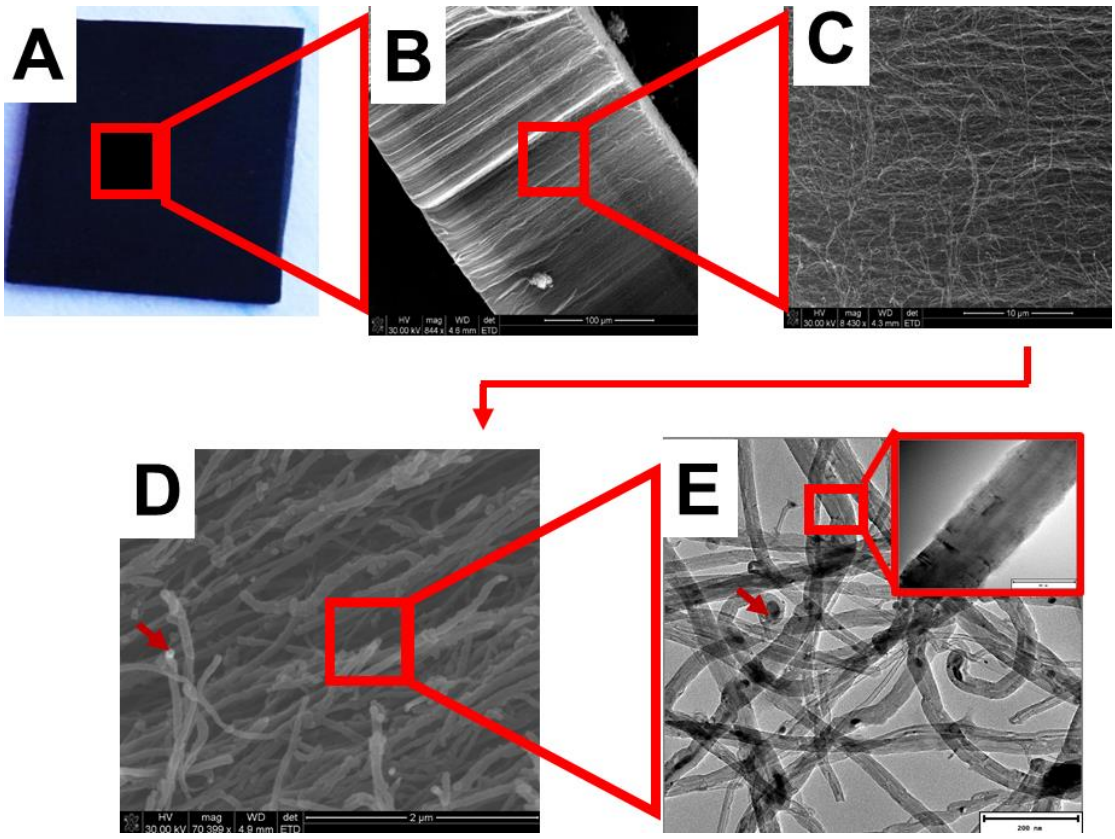


Figure 4.2. MWCNTs grown on Si wafer using CVD technique. CNTS deposited on Si wafer (A). SEM micrograph of CNTs at 844 x magnification(B). SEM micrograph of CNTs at 8 430 x magnification (C). SEM micrograph of CNTs at 70 399 x magnification (D). TEM micrograph of CNTs with insert at very high magnification (E).

The pyrolysis conditions for the CNT growth was highly suitable for the growth of super-aligned MWCNTs on Si wafer (**Fig.4.2A-B**). The super alignment was further confirmed at higher magnification as depicted in **Fig. 4.2C-D**. Fewer tips were still having Fe nanoparticles as seen in **Fig.4.2D** (*see red arrow*).

TEM scan further revealed the Fe nanoparticles embedded in the central cavity of the CNT (**Fig.4.2E**) (*see red arrow*). The CNTs had more than one wall hence a multiwalled CNT, as depicted in **Fig. 4.2E** insert. From these data it can be concluded that the

pyrolysis conditions were highly suitable for the growth of super-aligned MWCNTs with very few nanoparticles embedded in the central cavity of CNT.

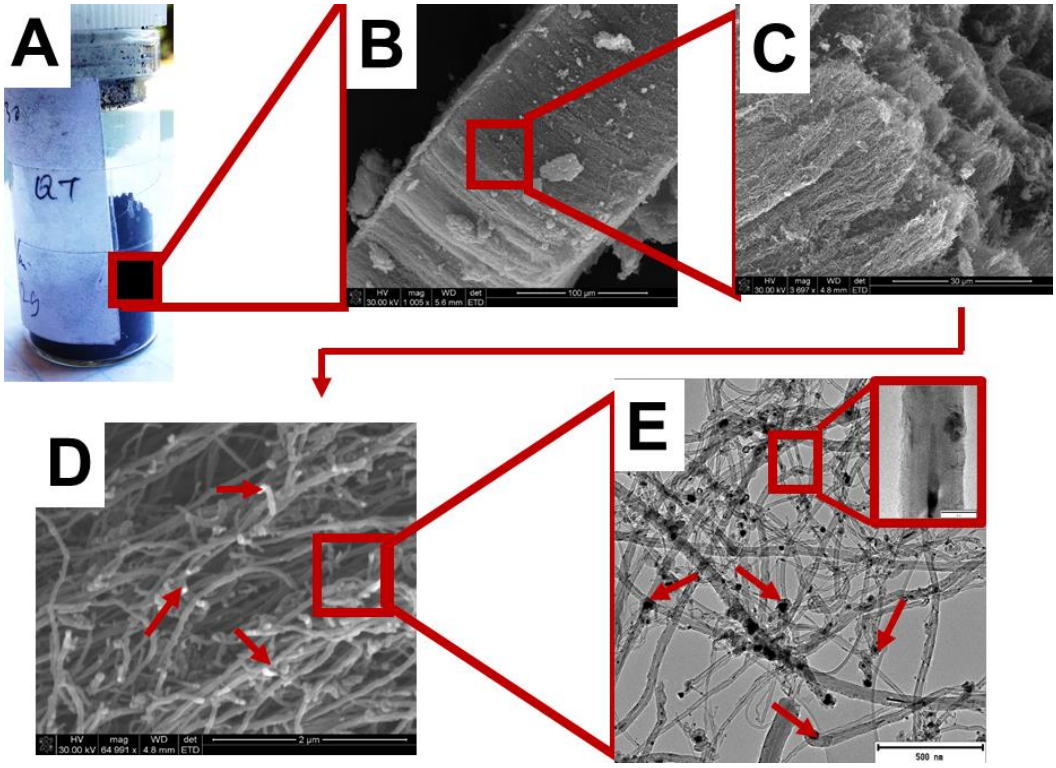


Figure 4.3.CVD synthesised MWCNTs grown on quartz tube wall. CNTS collected from quartz tube wall (A). SEM micrograph of CNTs at 1 005 x magnification (B). SEM micrograph of CNTs at 3 697 x magnification (C). SEM micrograph of CNTs at 64 991 x magnification (D). TEM micrograph of CNTs with insert at very high magnification (E).

CNTs collected from the quartz tube wall were stored in the vials for future use. They were also vertically aligned but not as perfect and clean as the Si wafer ones. The quartz tube wall CNTs were contaminated with amorphous carbon and Fe nanoparticles as seen in **Fig.4.3B-C**. Alignment and contamination was further confirmed when magnification was increased from 1 005 to 3 697x (**Fig.4.3.C**). As seen in **Fig. 4.3D**, alignment was clear, and most of the tips had Fe nanoparticles as opposed to Si wafer CNTs. TEM micrograph revealed the contamination by amorphous carbon and Fe nanoparticles (**Fig.4.3E**).

The CNTs were also having more than one wall with Fe nanoparticles embedded in the central cavity of the CNT as demonstrated in **Fig.4.3E** insert. Contamination from amorphous carbon and Fe nanoparticles was due to the variation of temperature in different zones of the quartz tube. It was also due to the variation of the gas flow rate as the gas travels in different temperature zones within the tube. Since there was a

temperature variation within the tube, this could also lead to variation in the evaporation rate of the catalyst. Our data has demonstrated that there are more contaminants in the quartz tube wall grown CNTs compared to Si wafer CNTs. Since two different substrates were used, the difference is expected as there are different degrees of interaction between the CNTs and the substrates.

4.3.2. Carboxylation and acylation of MWCNTs

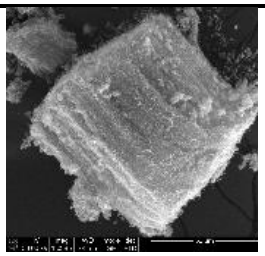
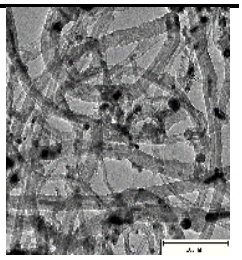
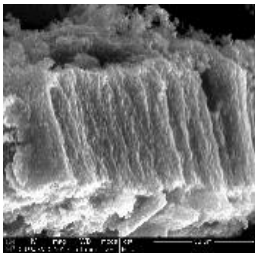
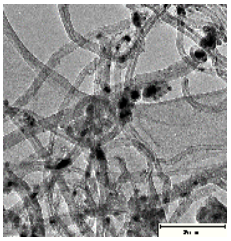
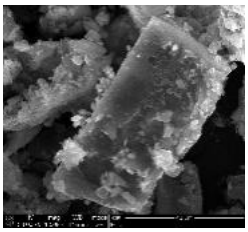
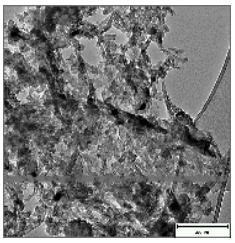
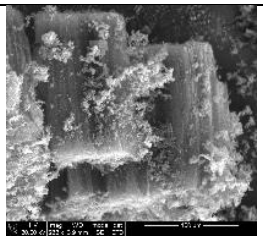
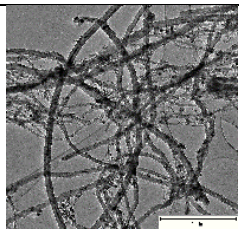
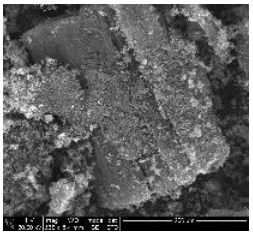
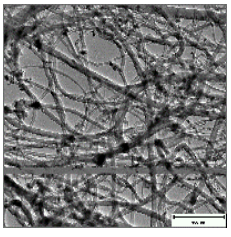
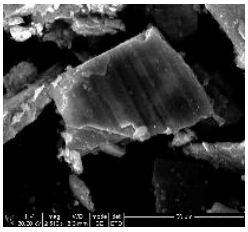
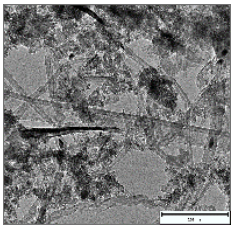
VA-MWCNTs were carboxylated and acylated to attach functional groups to improve coupling with other molecules of interest. MWCNTs were refluxed with conc HCl and HNO_3 to remove carbon and iron prior to further treatment. MWCNTs were refluxed with H_2SO_4: (3:1 ratio) to add COOH to generate MWCNT-COOH for further functionalization. MWCNTs were refluxed with $SOCl_2$ in DMF to add acyl group to generate MWCNT-COCl (more reactive) for further functionalization.

VA-MWCNTs were then coated with Pd/Au prior to scanning with SEM for morphological evaluation and size determination. For TEM scanning, CNTs were dispersed in ethanol for determination of external and internal diameters. It was found that functionalization of the MWCNTs with HCl and H_2SO_4:HNO_3 reduced the thickness or length of the MWCNTs. A greater reduction in the thickness of the CNTs was observed in the H_2SO4:HNO_3 treated CNTs than in the HCl treated CNTs (**Table 4.1**).

The external diameters of the MWCNTs were also drastically decreased in the H_2SO_4:HNO_3 treated CNTs as depicted in **Table 4.1**. This is indicative that sulphonitric acid has a very strong oxidizing strength than HCl. Cheng and colleagues also found that MWCNTs were reduced in length following an oxidation with H_2SO_4:HNO_3 (Cheng *et al.*, 2011). On average, the internal diameters remained constant around 10nm.

The internal diameter was expected to remain constant as it is dependent on the size of the Fe nanoparticles (10 nm) used for the formation of nucleation sites in the synthesis of the CNTs (Çınar, Yuca and Karatepe, 2012). The sulphonitric acid treated MWCNTs has demonstrated a deformation of the surface and individual CNTs as depicted in the TEM micrographs in **Table 4.1**. The individual CNTs were not clear as they looked like they were melted, and this made it difficult to identify them clearly.

Table 4.1: Thickness, internal and external diameters of the VA-MWCNTs.

ID	Rx	T (µm)	ID (nm)	OD (nm)	SEM	TEM
30201406	p CNTs	75	10	40		
	HCl	75	8	34		
	H_2SO_4:HNO_3	41	9	20		
04201406	p CNTs	150	10	58		
	HCl	140	11	46		
	H_2SO_4:HNO_3	42	8	23		

Legend: ID=sample ID, Rx=treatment, T=thickness, ID=internal diameter, OD=outer diameter

The pristine and HCl treated CNTs were not deformed as individual CNTs with encapsulated Fe nanoparticles were observed as demonstrated in the SEM and TEM micrographs in **Table 4.1**. The amorphous carbon and Fe nanoparticles were observed in pristine and acid treated CNTs as the purification and oxidation could not completely remove the contaminants.

4.3.3. Thermal and acid oxidation of VA-MWCNTs

An exposure of VA-MWCNTs to conc HNO_3:H_2SO_4 (1:3) caused a deformation of the CNTs. The CNTs shrunk and formed a cone like structure with two layers (**Fig. 4.4A**). A mixture of HNO_3 and H_2SO_4 oxidized the iron nanoparticle and amorphous carbon layers. But when VA-MWCNTs were exposed to 5 M HCl, honeycomb-like structures with mean diameter of 10.5 µm were formed on the surface of the CNTs (**Fig.4.4B**). Concentrated HCl resulted in the shrinkage of the CNTs (**Fig.4.4C**).

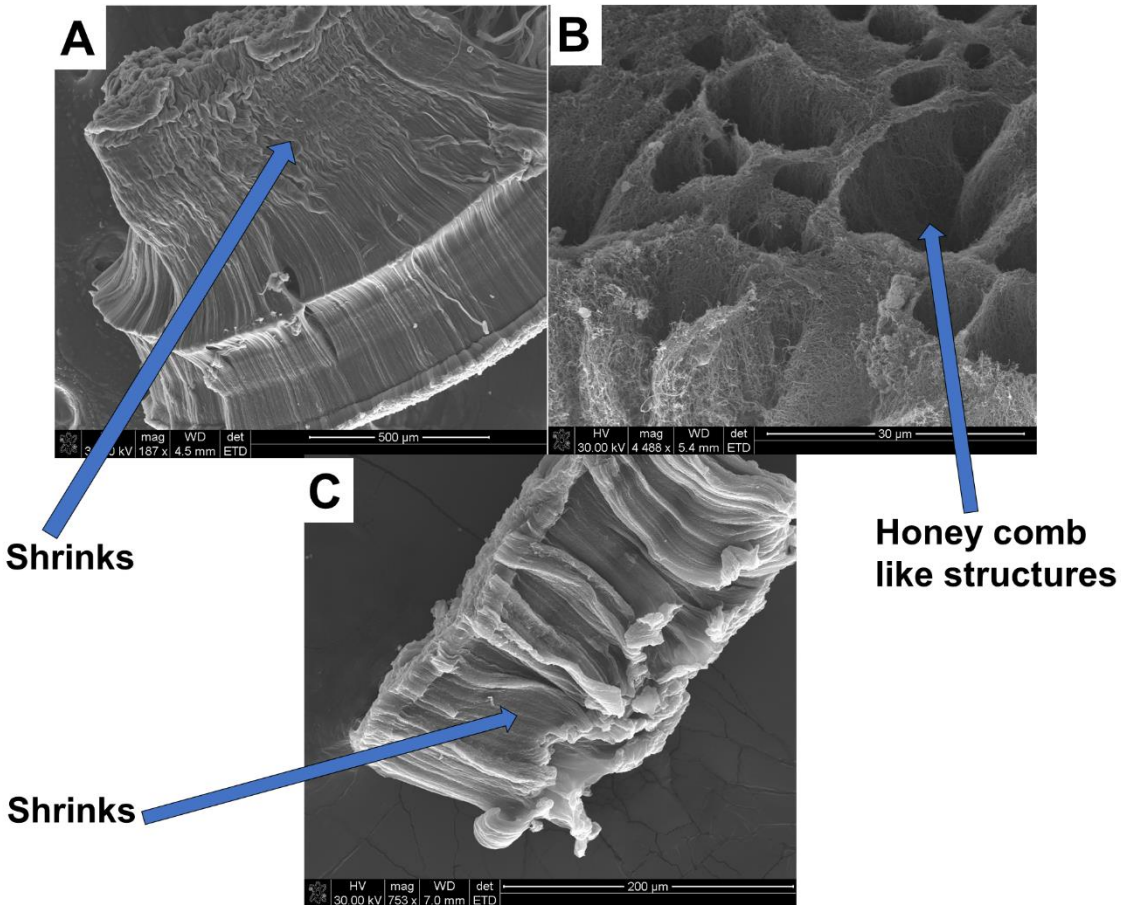


Figure 4.4. MWCNTs treated with different acids. Conc H_2SO_4:HNO_3 (3:1) (A). 5 M HCl (B). Conc HCl (C).

Li and colleagues synthesised aligned CNTs using iron phthalocyanine as a catalyst. Honeycomb-like aligned CNTs were produced and were found to be super-hydrophobic (Li *et al.*, 2002). In our study, aligned CNTs were produced when ferrocene was used as a catalyst. As-synthesised CNTs were hydrophobic and developed honeycomb-like structures when treated with HCl and a mixture of H_2SO_4:HNO_3 (3:1) which made them hydrophilic.

4.3.4. Thermal analysis and electrical resistivity

TGA was done to determine the thermal stability, the degree of functionalization and purity of the MWCNTs. The analysis of MWCNT powder was carried out under synthetic air flow which implies that a thermal oxidation is been investigated and the residual at the end of thermal degradation is iron oxide.

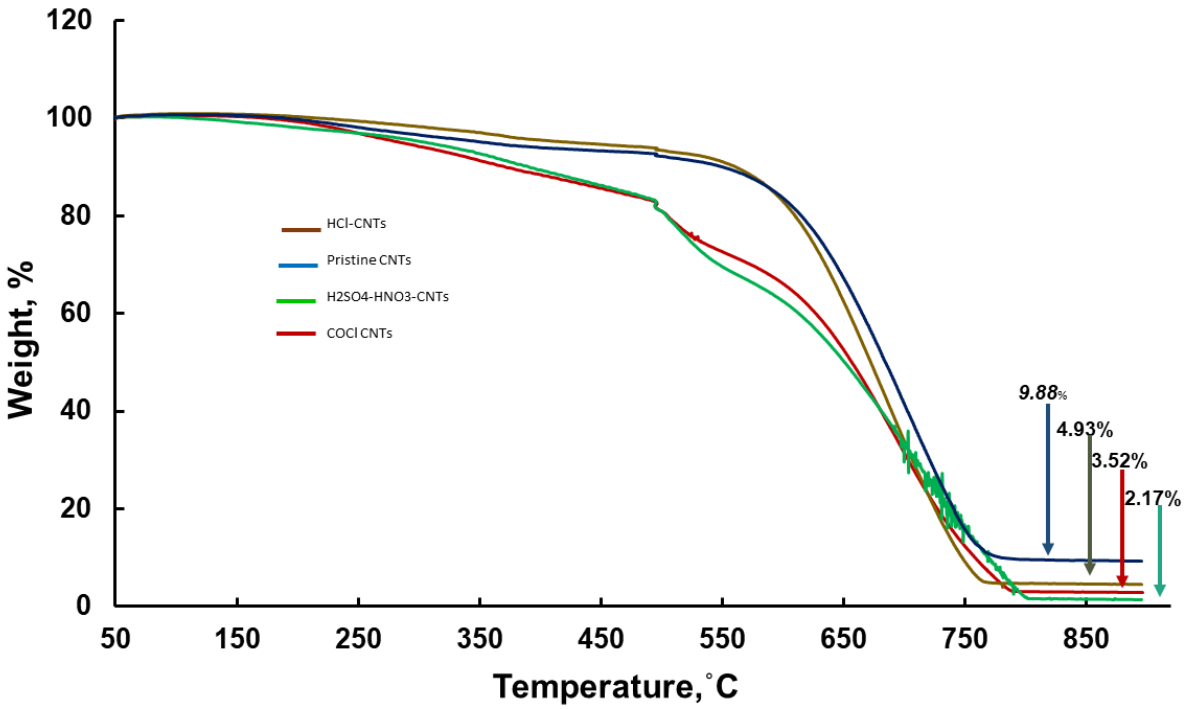


Figure 4.5. Thermograms of (a) Pristine MWCNTs, (b) HCl-MWCNTs, (c) COCl-MWCNTs and (d) COOH-MWCNTs.

A minor weight loss observed from 50 °C to 150 °C corresponds to evaporation of the physi-adsorbed water from MWCNTs. A gradual drop in weight from 150 °C to 500 °C is attributed to amorphous carbon, metal catalyst and other impurities in MWCNT samples. A drastic weight loss was observed around 550 °C in both pristine and HCl-MWCNTs. In COOH- MWCNTs and COCl-MWCNTs, a drastic weight loss occurred around 500 °C.

A complete decomposition occurred around 830 °C in the pristine and functionalised MWCNTs as confirmed by a change in colour of MWCNTs from black to orange. Functionalisation of MWCNTs with acids and $SOCl_2$ purified the MWCNTs as confirmed by less residual content in functionalised MWCNTs (2.17, 3.52 and 4.93 %) as opposed to pristine MWCNTs with a residual content of 9.88 % as depicted in **Fig. 4.5**. High percentage of the residue in pristine was due to the impurities, Fe nanoparticles and amorphous carbon.

Dependence of resistivity (ρ) of the CNTs on temperature (*T)* is an important parameter characterising the electrical transport in the CNTs. As the temperature of the CNTs increases, the scattering of the charges is increased leading to a decrease in resistivity hence an improved electrical transport as current is inversely proportional to resistance according to Ohm's law equation;

Equation 4.1: *V=IR* equation 1, where V=voltage, I=current and R=resistance

Metals in CNTs are encapsulated from the catalysts during the synthesis process hence the CNTs are electrically conductive. Semiconductor resistivity decreases as the temperature increases as a result of the increase in the number of charge carriers and their mobility. The changes in the features of the ρ – *T* curves depend on the CNT morphology. The characteristics of the structure which would be suitable for electrical wires include higher share of metallic CNTs in the assembly, improved purity, crystallinity, alignment and packing density of the CNTs as well as doping result in more metal-like features of the resistance–temperature (*R* – *T*) curves (Lekawa-Raus *et al.*, 2014). The measurement of the resistance-temperature may be used as a helpful tool for an assessment of the quality and state (doped/undoped) of the CNTs and their suitability for application in nanoelectrode development.

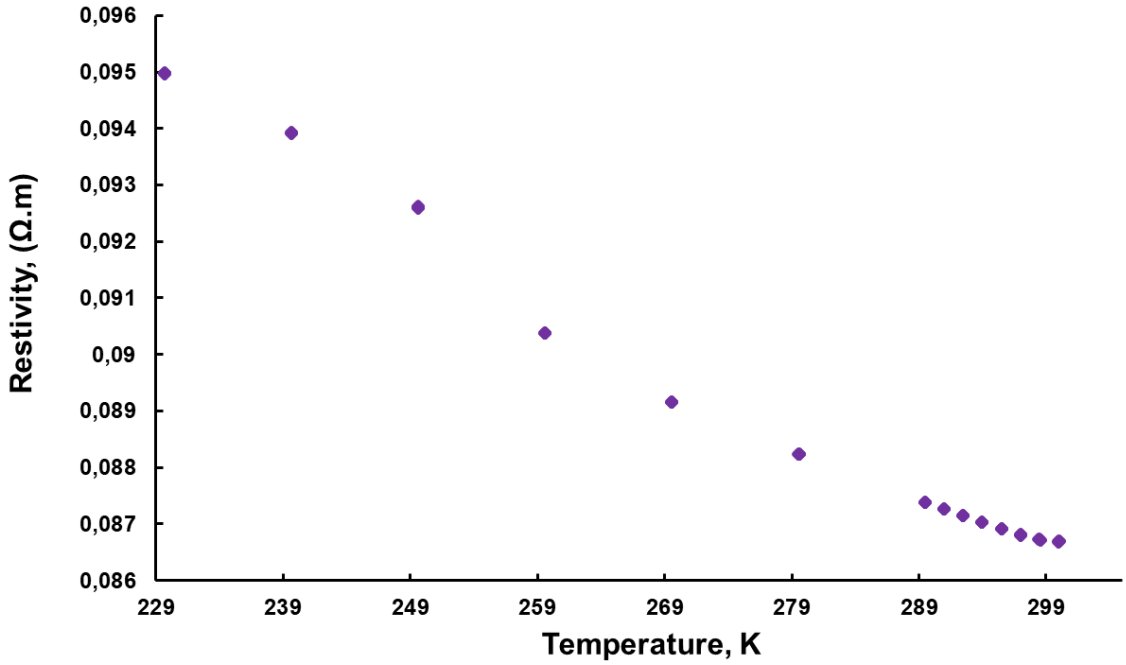


Figure 4.6. Electrical resistivity of VA-MWNTs from 229 to 300K.

In our study, resistivity of VA-MWCNTs was measured by Physical Property Management System (PPMS, Quantum Design) to assess the electrical properties of the VA-MWCNTs prior to a carbon-based electrode development. As the temperature increased from 229-300 K, resistivity decreased which implied that the CNTS were electrically conductive. CNTs were highly conductivity from 290-300 K as depicted by the points getting closer within this range (**Fig. 4.6**).

Barberio and colleagues demonstrated that the electrical resistivity of the clean multiwalled carbon nanotubes decreased monotonously when they were exposed to temperature from 300 K to 1900 K (Barberio *et al.*, 2007). They used very high temperatures with a wider range whereas very low temperatures with a low range were used in our study.

4.3.5. Contact angle, surface area and porosity measurements

Contact angles were calculated to determine the wettability of the MWCNTs. There is a direct relationship between the contact angle and hydrophobicity. When the contact angle is big, the material under test is hydrophobic which implies that there are less OH groups to bond with water molecules. The smaller the contact angle, the higher the number of OH groups on the material of interest to bind to water molecules.

Application of carbon nanotubes in the biomedical field is a major challenge as a result of their hydrophobic nature creating low dispersity (Li, Cheng and Shen, 2016). Drops of water were applied on the various spots of MWCNTs to measure their contact angles.

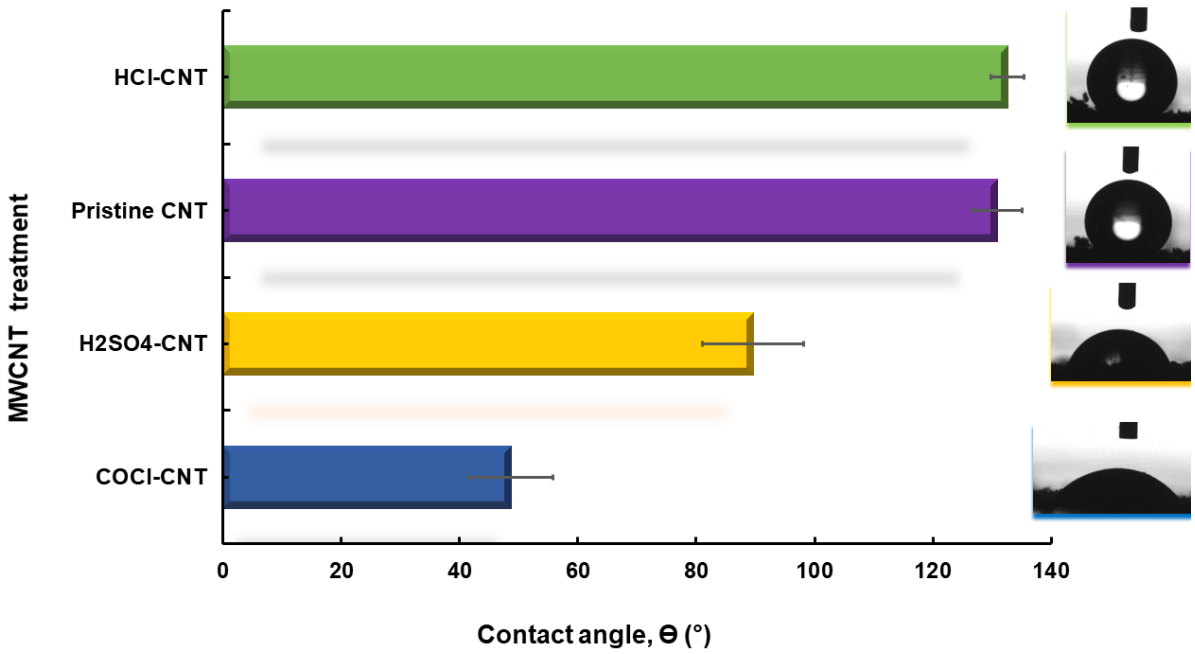


Figure 4.7. Contact angles of non-functionalised and functionalised MWCNTs

There was no difference in the contact angle of the pristine and HCl-MWCNTs. A significant drop in the contact angle was noticeable in H_2SO_4-MWCNTs and COCl-MWCNTs as depicted in **Fig.4.7**. Contact angle of pristine MWCNTs was found to be 131 ° and for HCl-MWCNTs was 133 °. Contact angle of COOH-MWCNTs was 90 ° and that of COCl-MWCNTs was 50 ° as shown in **Fig.4.7**. Acid treatment increased the wettability of the CNTs as depicted in **Fig.4.7**. These results confirm the role of carboxylation and acylation in increasing the hydrophilicity of the MWCNTs.

Turgenev and colleagues studied the effect of sulphuric acid and hydrochloric acid mixture and found that acid treatments donated carboxylic groups on the surface of carbon nanotubes. It was also found that there was less damage to carbon nanotubes under vacuum freeze drying than under vacuum heat drying (Turgunov, Oh and Yoon, 2014). In our, MWCNTs were grown on Si wafers, treated with thermal and acid oxidation. They were found to be highly hydrophilic as demonstrated in **Fig.4.7**.

Surface area measurements are very important to assess the surface of the particles. When the particle size is decreased, its surface area increases and become more available for contact with the reactants. The rate of collisions increases and hence the reaction rate increases. Pristine and functionalized MWCNTs were analysed with BET for surface, pore size and pore volume in **Chapter 3**.

4.3.6. Measurement of crystallinity and functional groups of MWCNTs

The XRD was performed as in **Chapter 3** on CNTs grown on Si wafer prior to nanoelectrode development. When XRD was performed on the CNT samples, two unique peaks were detected at the angle (2Θ) of 25 ° and 45 ° as demonstrated in **Figure 4.8**.

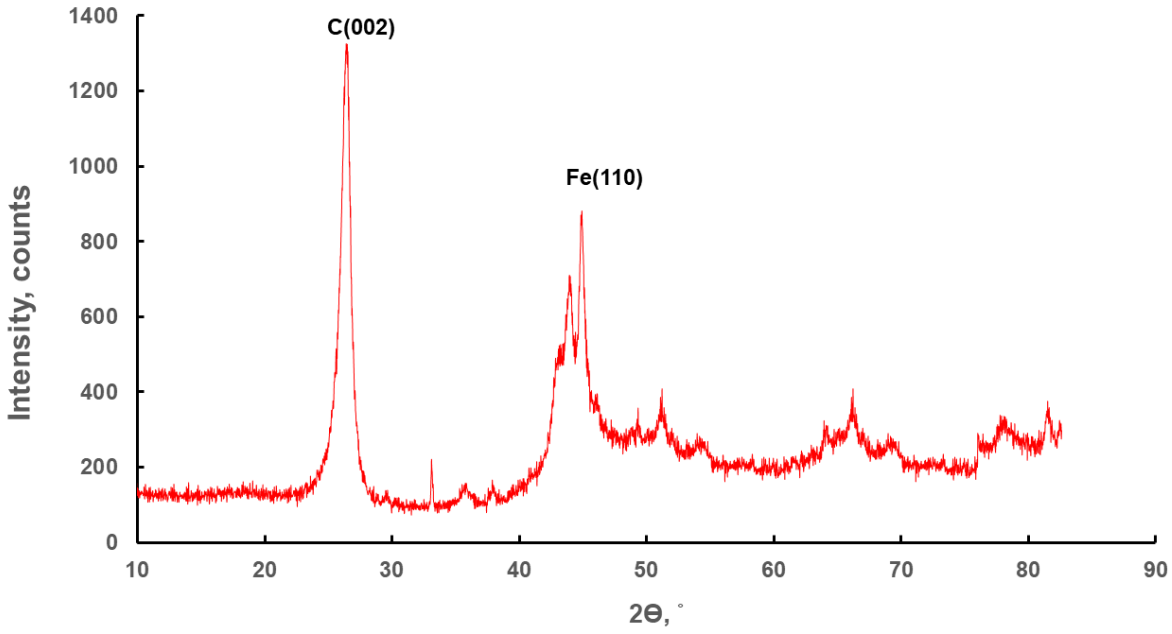


Figure 4.8. XRD spectrum of VA-MWCNTs grown on Si wafer.

The peaks for the as-synthesized MWCNTs arrays on Si wafer indexed to (002) and (110) at 2Θ of 25 ° and 45 ° are indicative of the presence of hexagonal graphite (carbon) and catalytic impurities (iron) respectively. The Fe peak has less intensity as compared to C peak and this observation could be due to the fact that the CNTs were purified and oxidized leading to a reduction in Fe content in the as-synthesised CNTs. FTIR was performed to assess the functional groups coupled to MWCNTs following functionalisation with acids and carbonyl chloride.

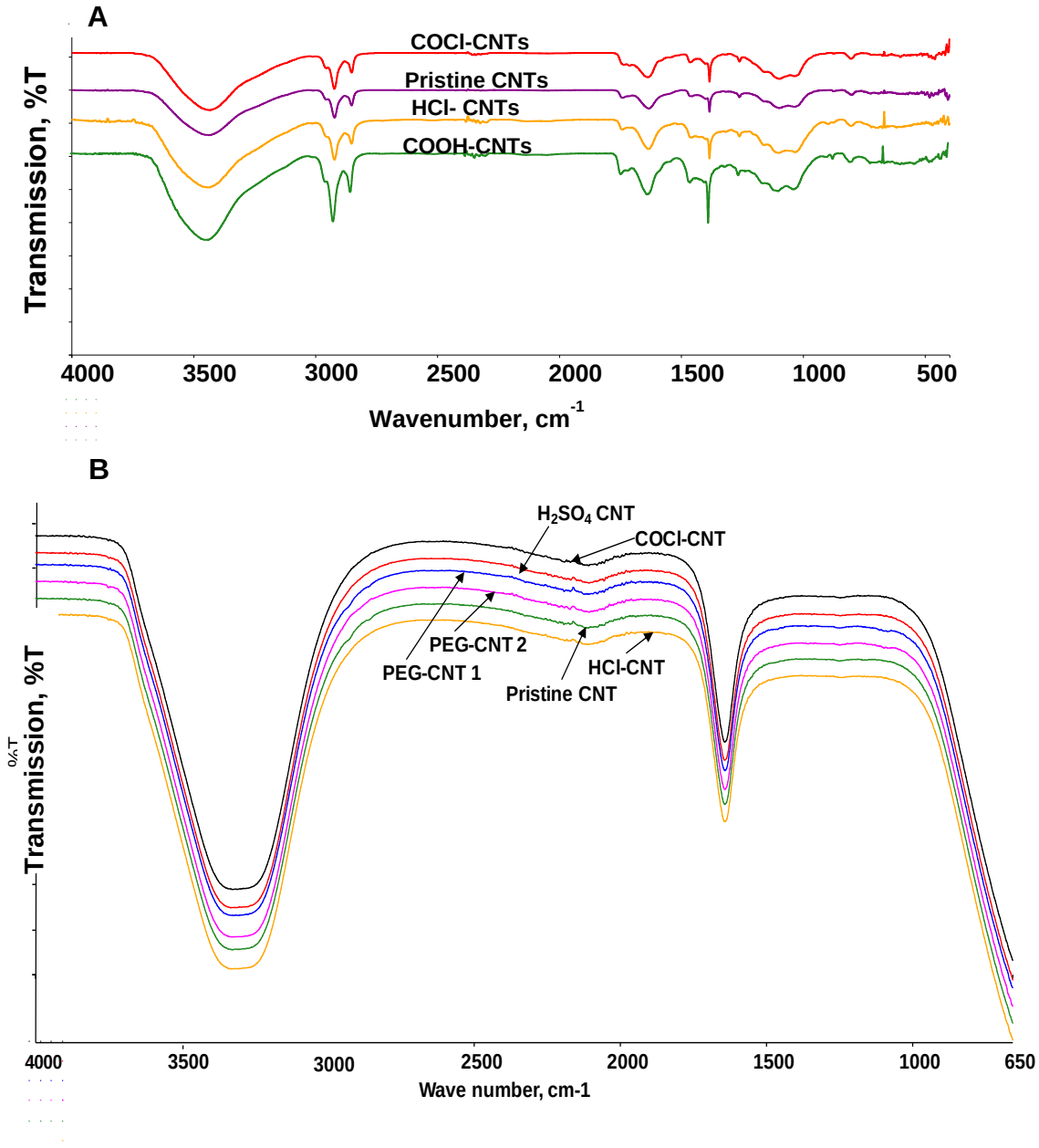


Figure 4.9. FTIR spectra of MWCNTs. MWCNT scans collected from KBr pellets (A). MWCNT scans collected from UATR crystal (B).

Pristine MWCNTs showed important absorption bands at 3444.6 cm^{-1} (O-H), 2852-2923 cm^{-1} (C-H), 1636.1 cm^{-1} (C=C) and 1097.6 cm^{-1} (C-O). These functional groups including other functional groups have been introduced during synthesis process (Avilés *et al.*, 2009). Oxidized MWCNTs have absorption peaks at 1741.1 cm^{-1} as depicted in **Fig. 4.9A**. This is due to C=O stretching vibration from the introduction of carboxylic groups from the acids (HCl, H_2SO_4 and HNO_3). This peak was also observed in pristine MWCNTs but not as intense as in acid functionalised MWCNTs and could have been introduced during the synthesis process.

A broad peak at 3441.2 – 3451.4 cm^{-1} in all the MWCNTs corresponds to O-H stretch as a result of moisture in the MWCNTs. This peak was much stronger in H_2SO_4:HNO_3 functionalised MWCNTs followed by HCl treatment and lastly the $SOCl_2$ treatment (**Fig. 3I**). A very narrow and sharp peak at 1456.6 cm^{-1} (C=C) was observed in all the MWCNTs but with a very high intensity in H_2SO_4:HNO_3 functionalised MWCNTs followed by HCl treatment and lastly the $SOCl_2$ treatment (Avilés *et al.*, 2009).

Only two peaks (3400 cm^{-1} and 1600 cm^{-1}) were observed in all the MWCNTs under different treatments (including PEGylation) dispersed in water were scanned using UATR FTIR (**Fig.4.9B**). The peaks at 3400 cm^{-1} and 1600 cm^{-1} were due to the O-H (from water) and C=O functional groups in the CNTs respectively. The disappearance of other peaks could be due to the low concentration of the treated MWCNTs in water.

MWCNTs in dichloromethane and the KBr power samples did not yield satisfactory results. These results confirm that the MWCNTs can be oxidized using acids and acylated using $SOCl_2$. They also confirm that FTIR analysis of the MWCNTs using KBr pellets is the most appropriate technique as opposed to KBr powders and an aqueous CNTs.

4.3.7. Dispersibility of MWCNTs in various solvents

CNT dispersibility differs from dispersant to dispersant as a result of their physico-chemical architecture. MWCNTs functionalized with carbonyl chloride were readily dispersed in water than in DCM as demonstrated by a dark solution in **Fig. 4.10b** and a crystal clear solution in **Fig. 4.10a**. COCl-CNTs in DCM dispersant sedimented at the bottom of the tube implying that there was no reaction of the CNTs with the DCM.

DCM is less polar than water as it has a polar index of 3.1 and water has a polar index of 10. Therefor water is the most polar solvent compared to other solvents. Pristine MWCNTs were moderately dispersed in DCM than in water due to their hydrophobic nature. There was a minor dispersion in water as demonstrated by a moderate change in colour from clear to light dark colour (**Fig.4.10c & d**).

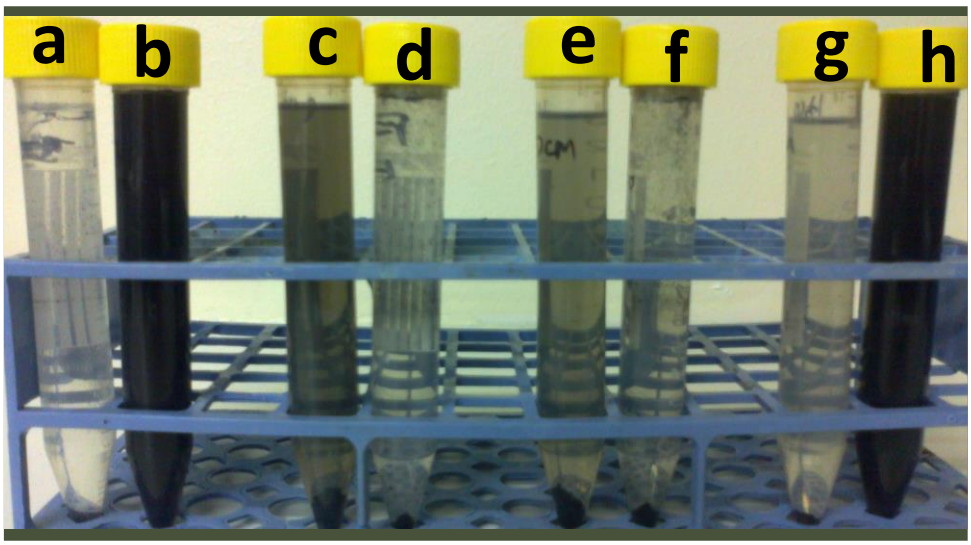


Figure 4.10. Dispersibility of pristine and functionalised MWCNTs in water and dichloromethane (DCM). COCl-CNTs in DCM (a), COCl-CNTs in water (b), Pristine CNTs in DCM (c), Pristine CNTs in water (d) HCl-CNTs in DCM (e), HCl-CNTs in water (f), H_2SO_4-CNTs in DCM (g) and H_2SO_4-CNT in water (h).

HCl-CNTs were moderately dispersed in DCM than in water but with a slight increase in intensity in water compared to pristine CNTs in water above (**Fig.4.10e & f**). In H_2SO_4-CNTs in DCM, the solution was crystal clear which implies that there was no reaction or there was a very slight unnoticeable reaction of the CNTs with DCM. H_2SO_4-CNTs dispersed readily in water dispersant as demonstrated in **Fig.4.10g & h**.

These findings have demonstrated that MWCNTs functionalised with carbonyl chloride ($SOCl_2$) and H_2SO_4 are highly dispersible in water hence highly reactive.

4.3.8. Particle size distribution and zeta potential measurements

Dynamic light scattering spectroscopy provides information on the size distribution of nanomaterials (Cheng *et al.*, 2011). This technique is most suitable for the determination of diameter of spherical particles but it is still applicable for measuring hydrodynamic diameters of nanotubes (Moon *et al.*, 2009; Smith *et al.*, 2009). Zeta potential is based on electrophoretic mobility for charge determination on the particles. Zeta nanosizer was used to measure both the zeta potential and particle size distribution (Castell *et al.*, 2013).

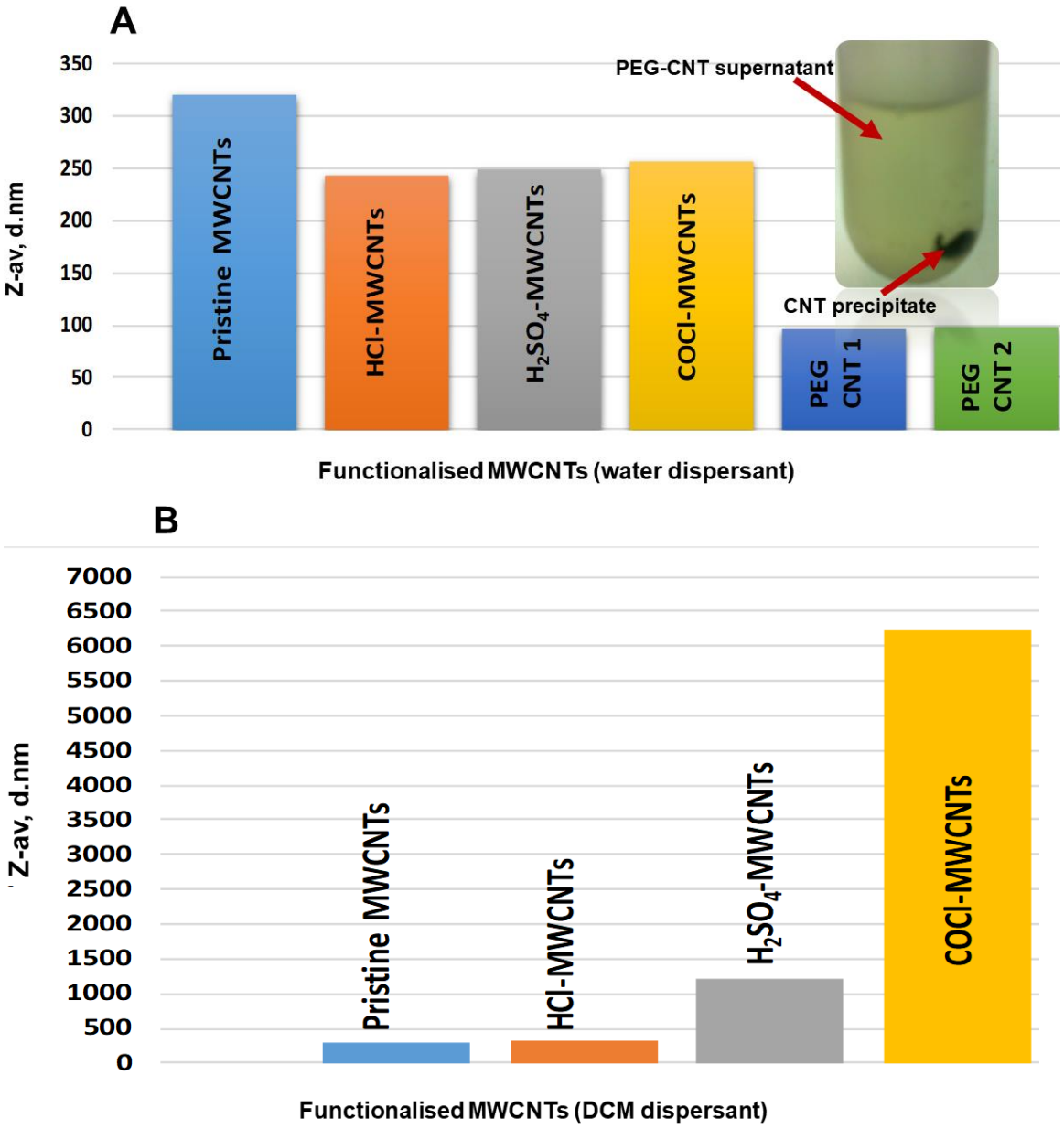


Figure 4.11. Particle size of the functionalised MWCNTs. CNTs dispersed in water (A). CNTs dispersed in DCM (B).

Pristine MWCNTs dispersed in water had a higher particle size than MWCNTs dispersed in DCM (**Fig.4.11A & B**). Individual MWCNTs in their native state have a tendency of agglomerating to each other hence agglomerates with bigger hydrodynamic diameters are formed. Pristine MWCNTs particles were readily dispersed in DCM than in water due to their hydrophobic nature as confirmed by their inability to disperse readily in water (**Fig. 4.11A)**.

Water is a polar dispersant whereas DCM is 3x less polar than water. Pristine CNTs are hydrophobic and will not disperse in a polar dispersant. DCM will disperse pristine CNTs as it is a less polar dispersant. The particle size will drop as the less polar

dispersant will disperse the hydrophobic pristine CNTs as demonstrated by a reduction in particle size (**Fig.4.11B**).

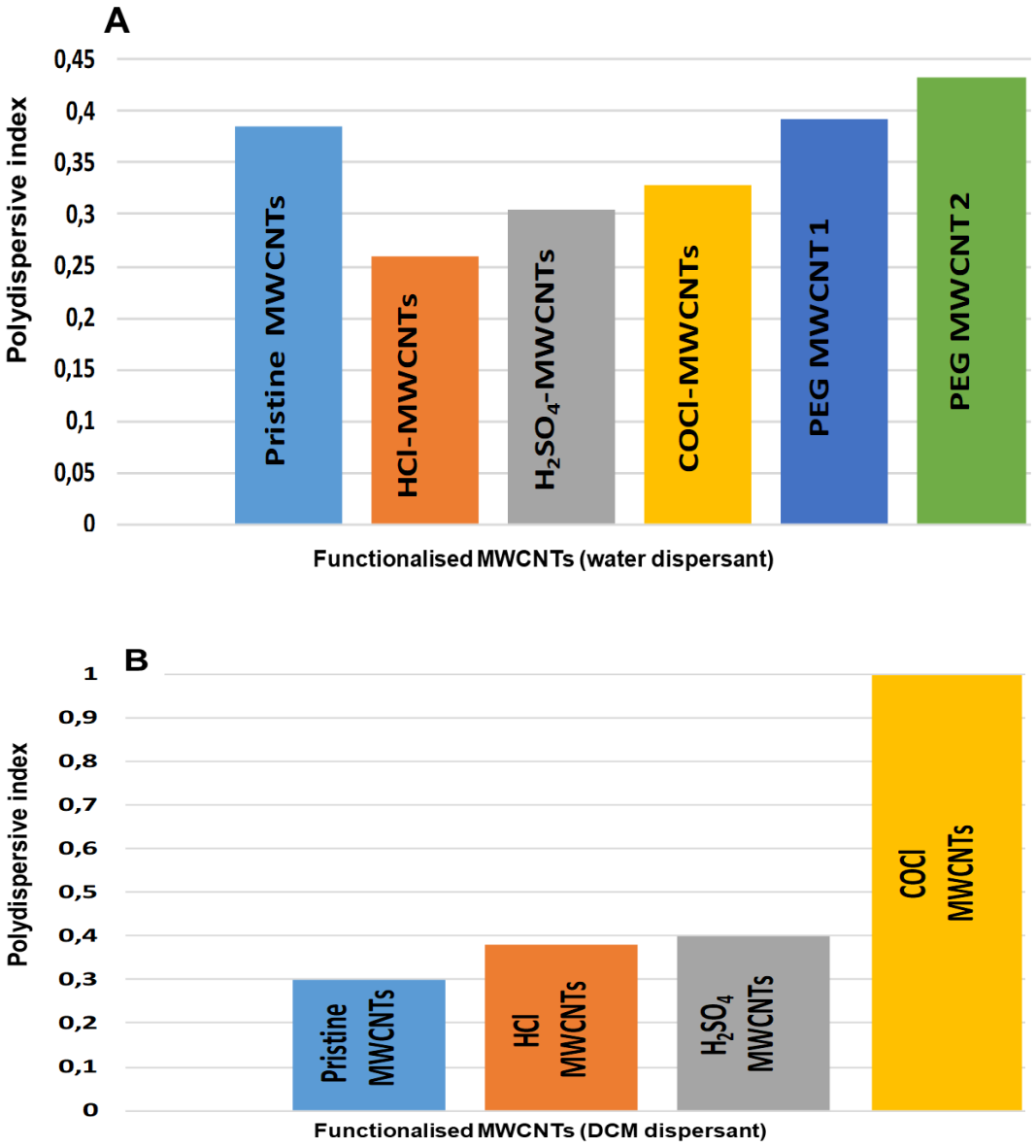


Figure 4.12. Polydispersive index of MWCNTs. CNTs dispersed in water (A). CNTs dispersed in DCM (B).

COCl-MWCNTs are hydrophilic and will not disperse in hydrophobic dispersant as shown by the increase in particle size due to the agglomeration of the particles (**Fig.4.11B**). Functionalisation of CNTs with HCl, H_2SO_4, COCl, and PEG changes the hydrophobic nature of CNTs to hydrophilic nature and this improves the dispersibility of the CNTs in water. As the dispersibility is increased, then the agglomerates are broken down and particle size of the CNTs is reduced in water (**Fig.4.11A-B**).

In PEGylated CNTs, the particle size dropped drastically as the PEGylated CNTs were readily dispersed in water. The unreacted and bigger particles of the CNTs were sedimented at the bottom of the tube and the supernatant rich in PEG-CNTs were used in this dispersibility studies (**Fig.4.11A**). The reason for this event could be due to the fact that the reduction in size of the CNTs increased the surface area and this could have led to an improvement in the reaction of CNTs with PEG. The unreacted and large particles settled at the bottom as the result of force of gravity.

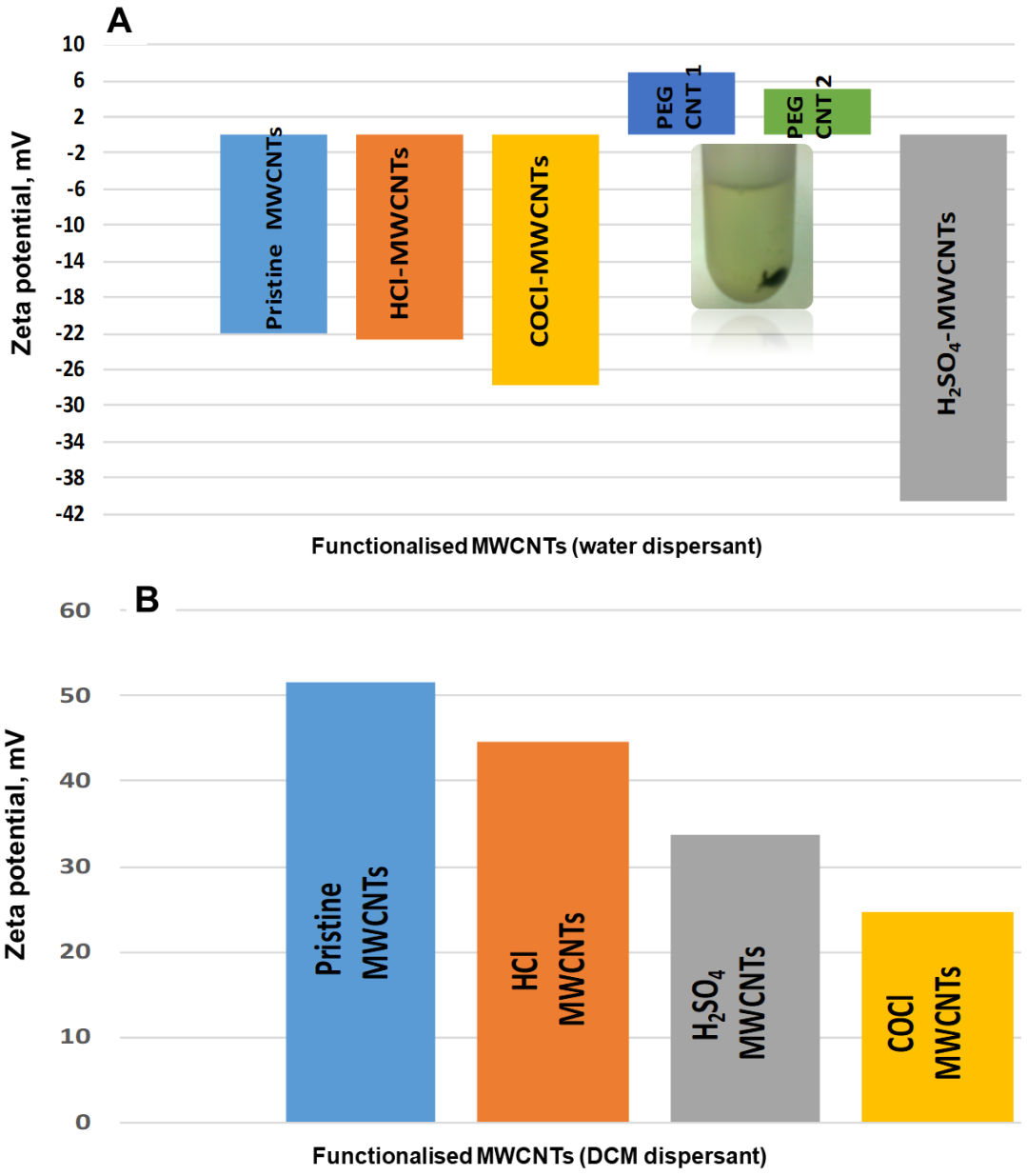


Figure 4.13. Zeta potential of functionalised MWCNTs. CNTs dispersed in water (A). CNTs dispersed in dichloromethane (B).

Polydispersive index (PDI) is used to determine the particle distribution type. It is a measure of heterogeneity of sizes of molecules or particles in a mixture. The

distribution is uniform if the particles have the same size and shape. The uniform distribution has a PDI=0.0, narrow distribution PDI = 0.0 – 0.1, moderate distribution PDI=0.1 - 0.4 and broad distribution >0.4.

In this work, PDI of pristine MWCNTs dispersed in DCM was found to be 0.3 and in water was 0.39. According to these findings, pristine MWCNTs distribution type was moderate in both water (PDI<0.4>0.3) and DCM but far much better in DCM than in water (**Fig.4.12A-B**). The HCl-MWCNTs had PDIs less than 0.4 in both the water and DCM which implied that the distribution was moderate. In water, the PDI was 0.26 and in DCM it was 0.38 as depicted in **Fig. 4.12A-B**.

In H_2SO_4 functionalised MWCNTs in water, the particle size was very small around 253nm as opposed to DCM which was around 1223nm (**Fig. 4.11A-B**). MWCNTs in DCM agglomerated hence a bigger diameter and readily dispersed in water (**Fig. 4.11A-B**). The PDI in water and DCM was 0.344 and 0.400 respectively hence a moderate particle distribution (**Fig.4.12A-B**).

MWCNTs functionalised with $SOCl_2$ dispersed in water had a smaller size as opposed to the MWCNTs dispersed in DCM with diameters of 256 nm and 6220 nm respectively (**Fig. 4.11A-B**). These CNTs dispersed readily in water compared to DCM (**Fig. 4.10A-B**). PDI for CNTs dispersed in water was 0.330 and in DCM was 1.00 (**Fig. 4.12A-B**). CNTs distribution type was moderate for water dispersed and very broad for DCM dispersed.

Particle size in the PEG-MWCNTs in water was very small (97 nm – 99 nm) compared to the pristine, carboxylated and acylated MWCNTs (**Fig. 4.11A-B**). The PEGylated CNT with smaller sizes were dispersed in the solution and those with bigger sizes and unreacted with PEG sedimented at the bottom of the centrifuge tube as observed in **Fig 4.11A** (insert). When CNTs are oxidised with acids, the size of the CNTs is reduced hence an increase in surface area creating more reactive sides for PEG to react with the CNTs. The unreacted and larger particles settle at the bottom of the tubes due to the force of gravity. The PDI was around 0.4 (**Fig. 4.12A-B**) which implied that the PEGylated CNTs had moderate distribution type.

Zeta potential (ZP) gives the magnitude of the charge repulsion/attraction between the particles. ZP plays a major role in the particle stability determination. It is a physical property exhibited by any particle in dispersion. The ZP magnitude can be used in the dispersion system as an indication of potential stability. If all particles in dispersion possess the same charge (negative or positive) ZP of the large magnitude, they repel each other hence no agglomeration. If particles have low ZP then there will be no force to hinder the particles to coagulate (Shieh *et al.*, 2010). Zeta potential distribution types are as follow; rapid coagulation zp =0 – 10 mV, incipient instability zp=10 – 30 mV, moderate stability zp = 30 – 40 mV, good stability zp = 40 – 60 mV and excellent stability.

Pristine, carboxylated and acylated MWCNTs dispersed in water were found to have a negative ZP and those dispersed in DCM positive ZP (**Fig.4.13A-B**). PEGylated MWCNTs dispersed in water were positively charged with small ZP (+5 mV to +7 mV). ZP of pristine MWCNTs in water and DCM was found to be -22 mV and +52 mV respectively (**Fig.4.13A-B**). Zeta potential in the carboxylated and acylated MWCNTs dispersed in DCM was higher than in water which implies that they are more stable in DCM compared to water.

These findings have demonstrated that the carboxylation, acylation and PEGylation of the CNTs dispersed in water reduced the particle size and the particle distribution was found to be moderate. ZP was negative in CNTs dispersed in water and positive in CNTs dispersed in DCM. Functionalisation improved the stability of the CNTs with a higher impact in CNTs dispersed in DCM.

4.3.9. UV-VIS analysis

UV-VIS spectroscopy measures the absorption of a beam of light after it passes through an aqueous sample or after reflection from a sample surface at a single wavelength or over spectral range. UV-VIS spectroscopy was performed to confirm the functionalization of MWCNTs and removal of succinic anhydride following dialysis of DSPE-PEG5000-amine carboxylated with succinic anhydride. It was also performed to confirm the presence of the synthesized DSPE-PEG5000-4-arm- (PEG-amine) in the preparation solution.

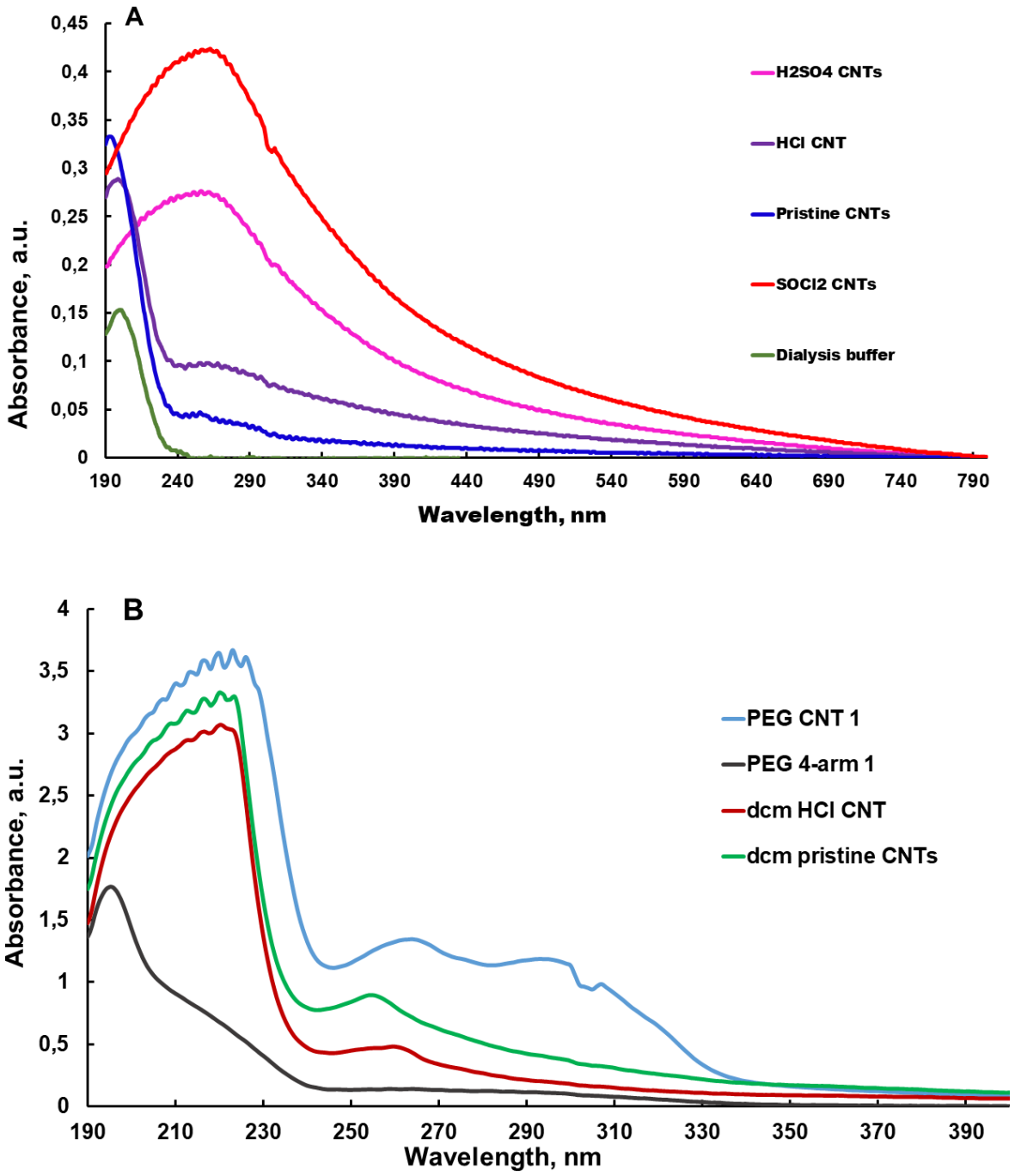


Figure 4.14. Uv-Vis spectra of the functionalized MWCNTs. The functionalised CNTs have different λmax.

The optimal wavelength at which pristine aligned MWCNTs absorbed light was found to be 194 nm. Functionalization changed the optical behaviour of the CNTs. In the HCl, H_2SO_4 and $SOCl_2$ functionalized CNTs, optical wavelengths were 198 nm, 256 nm and 263 nm respectively. The optical wavelength was shifted to the right of the pristine CNTs but within the UV range when CNTs were functionalized with HCl, H_2SO_4 and $SOCl_2$ as depicted in **Fig. 4.14A**.

The readily dispersed CNTs are highly active in the 200 to 1200 nm region. The Uv-Vis technique is used to detect individual CNTs suspended in solution using Beer-Lambert law (Grossiord *et al.*, 2005; Shieh *et al.*, 2010). The highest optical wavelength (262,5 nm) was observed in $SOCl_2$ functionalized CNTs and the least (198 nm) in HCl functionalized CNTs (**Fig. 4.14A**) (Tan *et al.*, 2011). Succinic anhydride is utilised in the synthesis of DSPE-PEG5000-PEG-4-arm amine. The unreacted succinic anhydride is separated from the product of interest via dialysis against neutral de-ionized water. It was detected in the dialysis buffer as depicted by an optimal absorption at 200 nm (**Fig. 4.14A**).

Optimal wavelength of pristine CNTs increased from 194 nm to 220.5 nm and that of HCl functionalized increased from 198 nm to 220 nm respectively when they were dispersed in DCM. PEGylated CNTs optimal wavelength increased slightly from 194 nm to 196 nm (**Fig.4.14B**). The increase in absorbance could be due to the functional groups (carboxylic and acyl groups) that are added to MWCNTs and the size of the particles. These findings have demonstrated the effect of functionalization of the CNTs on their optical properties. The optimal wavelength increased with functionalization.

4.3.10. Development of a nano-electrode

Epoxy resin was used for manufacturing nanoelectrode in our study. Epikote 862 (Diglycidyl Ether of Bisphenol F) is an epoxy resin produced from the chemical reaction of bisphenol F and epichlorohydrin (**Fig.4.15**). It contains no diluent nor modifiers. It possesses the following features;

- Low viscosity
- Low colour
- Reacts with a full range of epoxy curatives
- Good balance of mechanical, adhesive, and electrical properties
- Good chemical resistance
- Superior physical properties vs. diluted resins

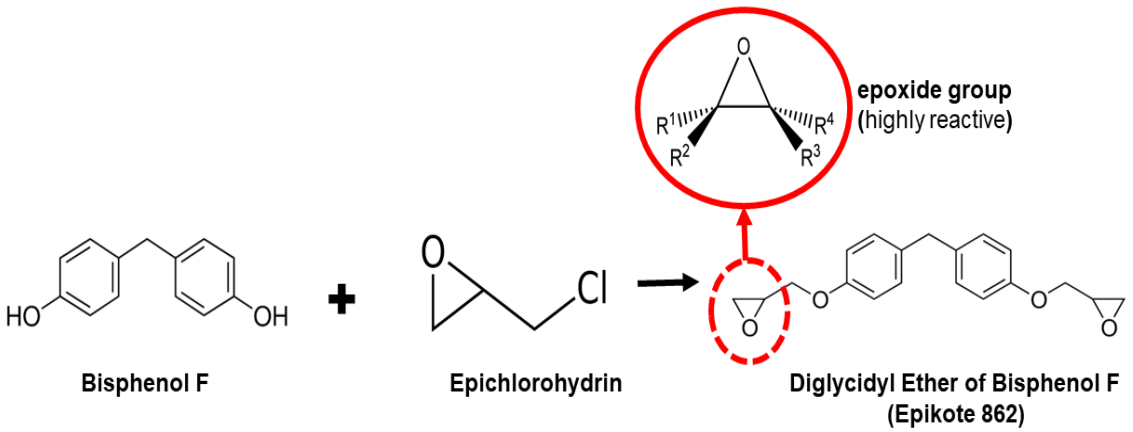


Figure 4.15. Synthesis of Epoxy Resin (Epikote 862). Bisphenol F reacts with epichlohydrin to produce diglycidyl ether of bisphenol F

Epoxy has been a polymer of choice in our work because of its role it plays as the matrix of structural composites. Epoxy forms strong polar bonds when it comes into contact with a surface to enhance the strong adhesiveness. Epoxy is a thermosetting epoxide polymer and it cures when it is mixed with a curing agent such as epicure 3402 (EC3402) (an amine acting as a hardener). Crosslinking of the epoxy resin with a crosslinker helps to attain the desirable mechanical properties (Yasuhiro and Chung, 2008).

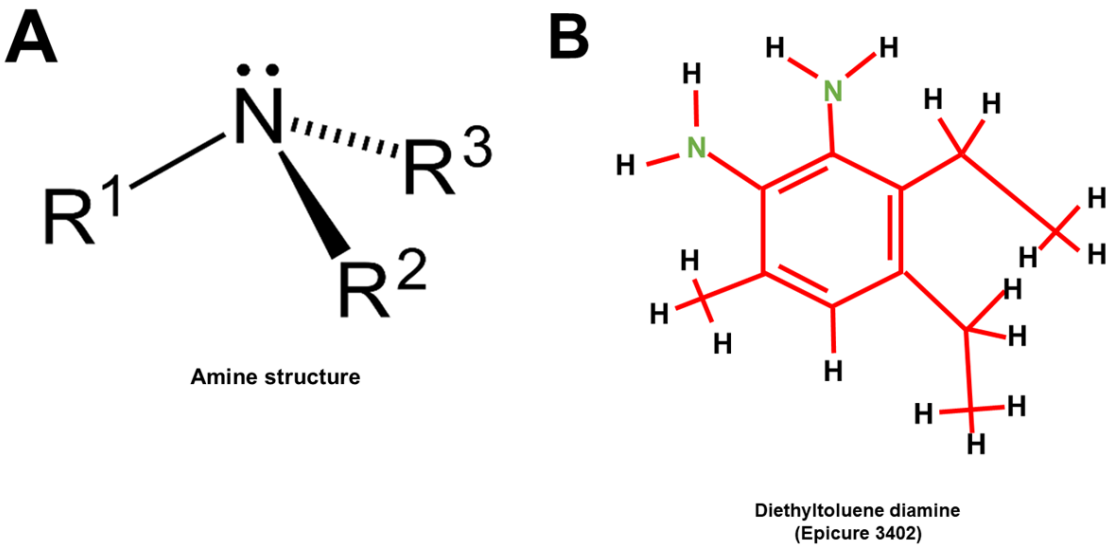


Figure 4.16. Chemical structure of amine (A) and diethyltoluene diamine (B).

A curing agent is composed of active hydrogen atoms coupled to oxygen, nitrogen, or sulfur atoms (**Fig. 4.16A**). The terminal epoxide groups for the reactive groups in the epoxy resin as shown in **Fig.4.15** (*circled red*). Amine-curing agents are the most common for epoxy formulations. Amines are organic compounds that contain nitrogen

as the key atom and are most common in the epoxy formulations as they act as curing agents (**Fig.4.16A-B**).

There are primary, secondary and tertiary amines depending on the replacement of the hydrogen atoms. In primary amines, one of the three hydrogen atoms in ammonia is replaced by an organic substituent whereas in secondary amines, two organic substituents bound to nitrogen atoms, together with one hydrogen atom. In tertiary amines, all three hydrogen atoms are replaced by organic substituents (**Fig.4.16A-B**). An organic compound with multiple amino groups is called a diamine, triamine, and tetraamine depending on the number of amino groups.

An amine-curing agent possesses more than three reactive sites per molecule. These sites enhance a 3D polymer network formation when the curing agent reacts with epoxy resin. A chemical reaction occurs between the active hydrogen atom of the amine and the epoxide group of the resin. The rate of crosslinking and the properties of the resulting polymer are monitored by the structure of the amine-containing organic compound, the number and type of amine groups in the compound (Yasuhiro and Chung, 2008).

In this study, we used Epikote 862 resin (bisphenol F-based epoxy), and Epikure 3402 (diethyltoluenediamine) to develop a carbon-based electrode. The resin and the hardener were selected because of their low viscosity and long potlife allowing sufficient time for processing and characterisation of the samples (Chakraborty *et al.*, 2011). Carbon nanotubes need a mechanical support in order for them to be used as an electrode.

The MWCNTs on Si wafer together with the electrical conducting wire were successfully incorporated in epoxy resin as shown in **Fig.4.17A-B**.

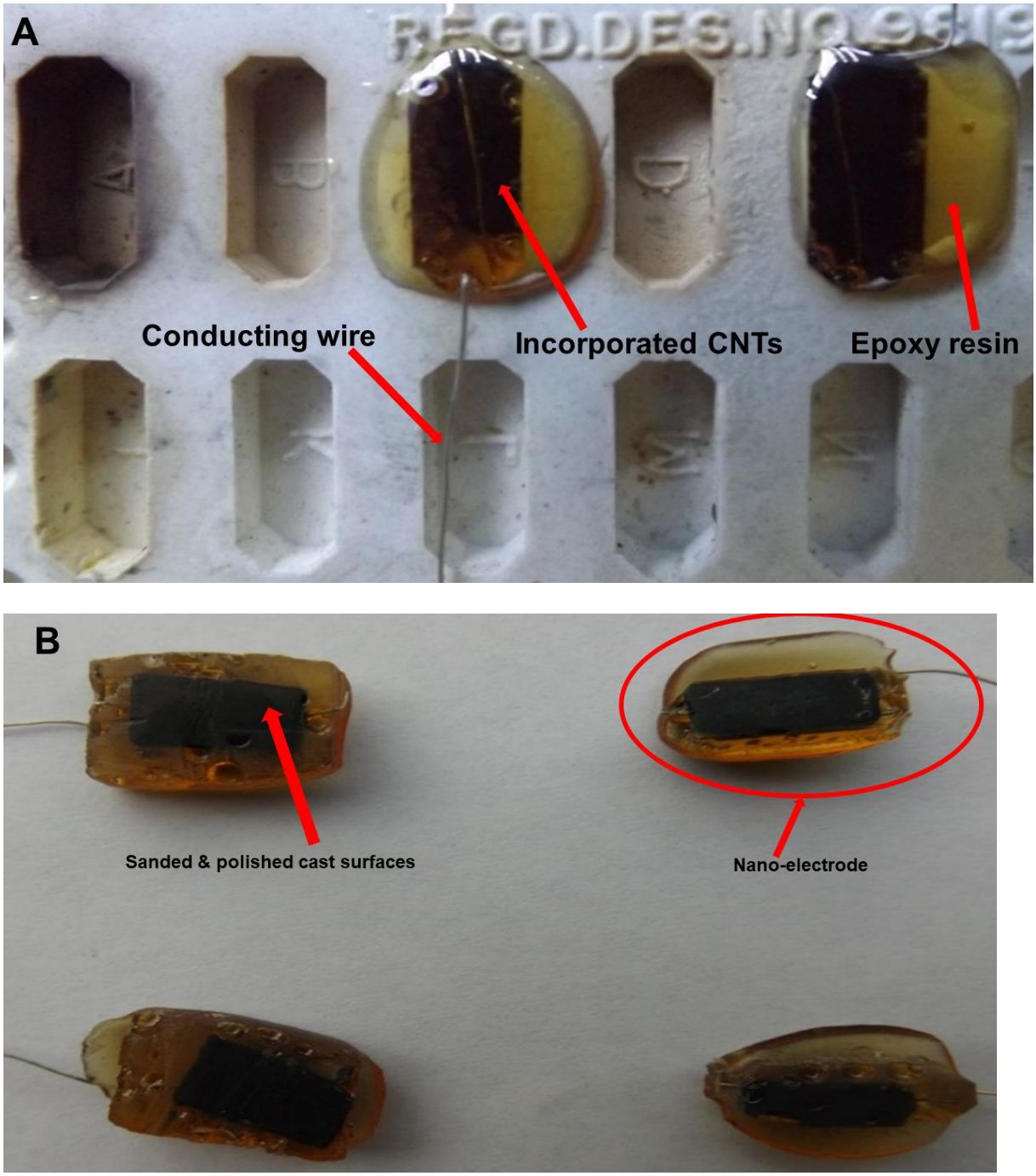


Figure 4.17. Incorporation of VA-MWCNTs in epoxy resin. Silicone rubber moulds for casting epoxy resin (A). Four sanded and polished nano-electrodes (B).

Electrical conducting wire was attached to the surface of the MWCNTs to form a direct contact prior to curing of the epoxy resin. There were very few air bubbles formed if none but at a distance from the MWCNTs. Yun and colleagues embedded free standing CNT array in epoxy resin (Yun *et al.*, 2007). A major challenge is the handling of free standing CNTs as they turn to be disarrayed during the incorporation procedure into the resin. It is also tedious to sand and polish the surface to expose the CNTs.

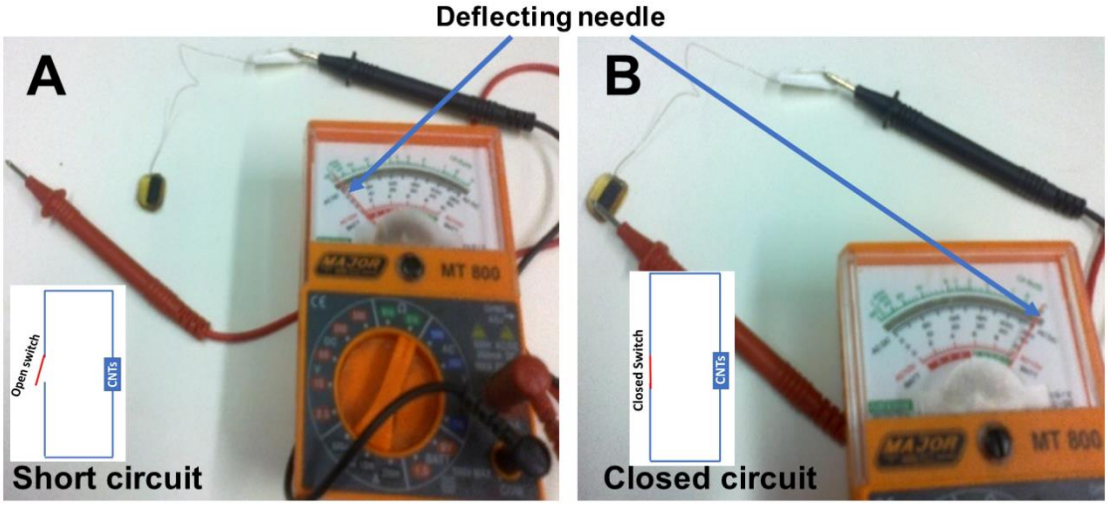


Figure 4.18. Incorporation of VA-MWCNTs in epoxy resin. Silicone rubber moulds for casting epoxy resin (A). Four sanded and polished nano-electrodes (B).

In our study, as-synthesised CNTs on Si wafer were incorporated into epoxy resin with a very thin layer on the CNT surface for easy sanding and polishing (**Fig.4.17A**).

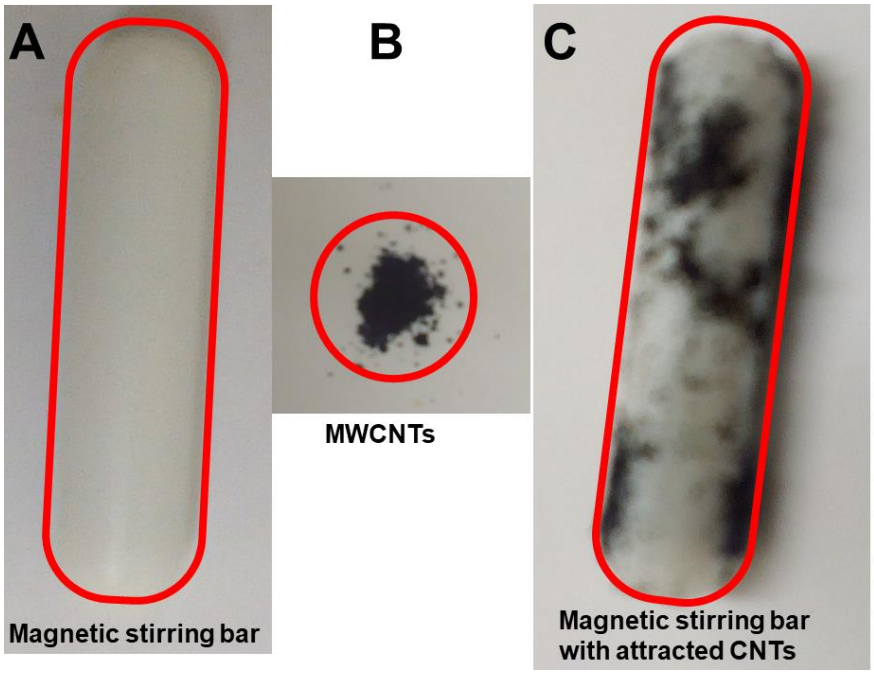


Figure 4.19. Magnetic properties of MWCNTs. Magnetic stirring bar (A). MWCNTs (B). Magnetic stirring bar attracting MWCNTs (C).

The surface of the CNTs covered by epoxy resin was exposed by sanding and polishing. The surface was washed with water and dried (**Fig.4.17B**). When the +ve and -ve terminals of the electrical conductivity meter were attached to the conducting wire and exposed CNTs (**Fig.4.17B**), the needle of the meter deflected from left to extreme right (**Fig.4.18A-B**). This confirmed the electrical properties of the MWCNTs.

Non-conductive and less conductive casts were further polished to expose the MWCNTs to improve the electrical contact.

Furthermore, MWCNTs that were collected from quartz tube wall were placed near the magnetic stirring bar and they were attracted to it (**Fig.4.19A-C**). As-synthesised MWCNTs were attracted by a magnetic bar indicating the presence of iron in the samples (**Fig.4.19A-C**). Magnetic properties are attained as a result of ferrocene used during CNT synthesis. The presence of iron in MWCNTs were confirmed by XRD analysis as seen in **Fig.4.8**.

4.3.11. Microscopical morphological assessment of a nano-electrode

Epoxy resin is one of the thermosetting polymers used in various industries including aerospace, electronic and adhesive industries. Their application is based on their mechanical, chemical and thermal properties (Pillai and Ray, 2011; Jahan *et al.*, 2013).

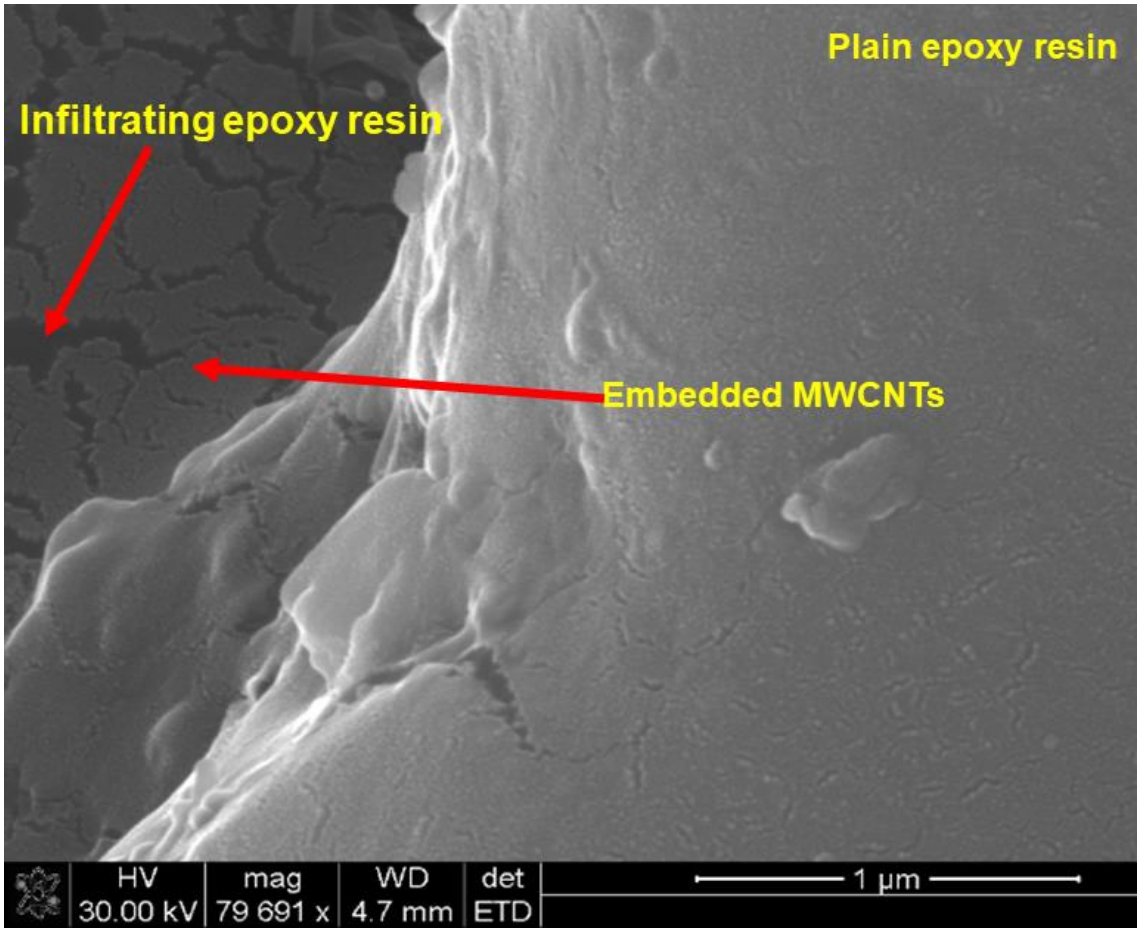


Figure 4.20. Epoxy resin with incorporated MWCNTs. Infiltrating epoxy resin into the carbon nanotubes was observed.

In this study, as-synthesized MWCNTs were incorporated into epoxy resin to give them mechanical support. Epoxy resin incorporated CNTs were exposed by sanding and polishing. They were then coated with Pd/Au and analysed by SEM. The results obtained confirmed successful incorporation of the CNTs into epoxy resin as demonstrated in **Fig.4.20**. Epoxy resin can be seen infiltrating between the CNTs.

4.3.12. Cyclic voltammetry and electrochemical impedance spectroscopy of a nano-electrode

Electroanalytical chemical techniques help to analyze electrode-solution interfacial phenomena such as chemisorption, physisorption, charge transfer, chemical reaction and diffusion mass transport. An interfacial layer called double layer is formed when an electrode is immersed in the electrolyte. This layer is formed between the electrode and the surrounding electrolyte as ions from the electrolyte are attracted to the surface of the electrode but leaving a very small gap between the electrolyte and electrode charges (Scholtz, 2010).

Cyclic voltammetry (CV) is a type of potentiodynamic electrochemical measurement and the working electrode potential is ramped linearly versus time. In CV, a constant and/or varying potential is applied at an electrode's surface and the resulting current is measured with a three electrode system. This method can reveal the reduction potential of an analyte and its electrochemical reactivity. CV is most commonly used because it gives an overwhelming information and in-depth knowledge of the thermodynamic details of different chemical reactions (Uslu and Ozkan, 2011).

CV is a linear potential waveform whereby the potential changes linearly with time. In CV, the potential is measured over time and the rate at which the potential changes as time changes is called the scan rate. The interface dynamics in electrochemical system is measured by EIS which is phase sensitive. A plethora of processes such as, chemical reaction, mass transport and electron transfer have a greater impact on the output from an electrochemical impedance spectrometer. The EIS data is represented as Nyquist plots where imaginary resistance (Z_{im}) is plotted against real resistance (Z_{re}). The size of the semi-circle is dependent of the resistance of the electrode. The bigger the diameter of the semi-circle, the higher the resistance hence the less the current passing through the electrode (Scholtz, 2010).

In our study, cyclic voltammetry and electrochemical impedance spectroscopy (EIS) were used to analyse electrochemical properties of the developed nano-electrodes using Ivium Compactstat Electrochemical workstation. The electrodes were developed to be used in the preparation of immunosensors for detection of biomarkers of ischemic stroke.

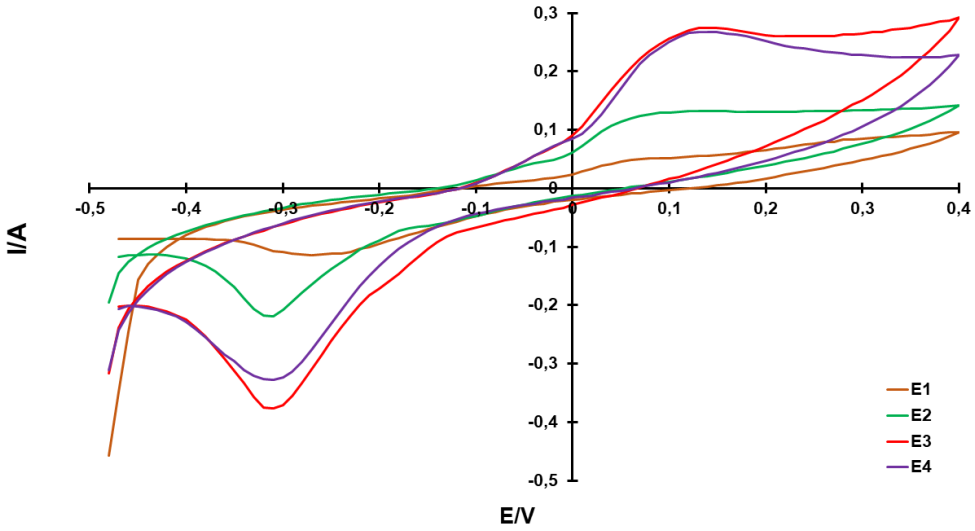


Figure 4.21. Cyclic voltammographs of nano-electrodes. Different shapes of the plots have been observed with different electrodes.

CV data were recorded between -0.4 and 0.4 V with a scan rate of 50 $mV.S^{-1}$ in a solution of 1 mM $K_3Fe(CN)_6$ and 1 mM $K_4Fe(CN)_6$ in 0.1 M KCl. Spectra were taken at frequency of 100 kHz to 100 mHz with an amplitude of 0.01 V and potential of 0.220 V. All nano-electrodes analysed were found to be electrically conductive with E1 being the least conductive and E3 the most conductive as depicted in **Fig. 4.21**.

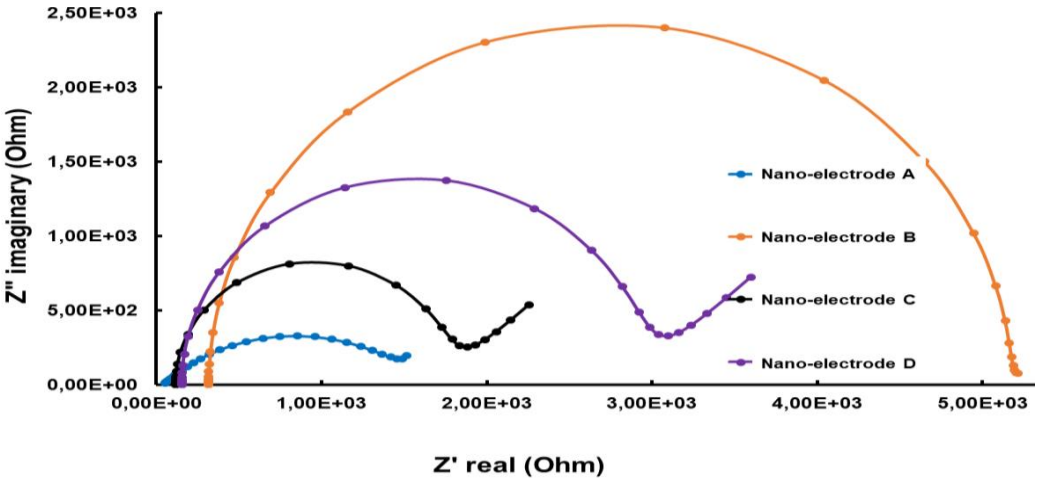


Figure 4.22. Nyquist impedance plots of nano-electrodes. The diameter of each electrode semi - circle increased with an increase in the resistivity

Electrical Impedance Spectroscopy (EIS) data confirmed the electrical resistivity of the nano-electrodes. Nano-electrode A was found to have the least electrical resistivity hence most electrically conductive. Nano-electrode B resistivity was the highest hence least conductive as demonstrated in **Fig. 4.22**. Our findings have demonstrated the potential of the carbon based-electrodes to be applied in the development of immunosensors in the detection of biomarkers of any disease including ischemic stroke.

Pristine carbon nanotubes are inert and hydrophobic. These properties hinder their application in biomedical fields. To employ them in biomedical environment, they need to be functionalised. In this study, pre-formulations were performed on MWCNTs before they could be used in the development of a nano-electrode and functionalisation of MWCNTs for potential application in the detection and treatment of neurological diseases including ischemic stroke. As-synthesised CNTs were purified with HCl, carboxylated with H_2SO4:HNO_3, acylated with $SOCl_2$ and PEGylated with DSPE-PEG5000-4-arm- (PEG-amine) to prepare them for application in targeting atrial natriuretic peptide in ischemic stroke. Well aligned quality MWCNTs were used to develop nano-electrodes for potential application in the detection of biomarkers in neurological diseases including ischemic stroke.

4.4. Concluding remarks

Our findings have demonstrated that the vertically aligned multiwalled carbon nanotubes could be functionalised and PEGYlated for potential application in anti-inflammatory drug targeted delivery to the ischemic site. Our findings also illustrated a potential that these CNTs may have in developing a nano-electrode that could be utilised in the detection of neurological diseases including ischemic stroke.

4.5. References

Avilés, F. *et al.* (2009) 'Evaluation of mild acid oxidation treatments for MWCNT functionalization', *Carbon*, 47(13), pp. 2970–2975.

Barberio, M. *et al.* (2007) 'Electric resistivity of multi-walled carbon nanotubes at high temperatures', *Surface Science*, 601, pp. 2814–2818.

Castell, P. *et al.* (2013) 'Combination of two dispersants as a valuable strategy to prepare improved poly(vinyl alcohol)/carbon nanotube composites', *Composites Science and Technology*, 80, pp. 101–107.

Chakraborty, A. K. *et al.* (2011) 'Carbon nanotube (CNT)-epoxy nanocomposites: A systematic investigation of CNT dispersion', *Journal of Nanoparticle Research*, 13(12), pp. 6493–6506.

Cheng, X. *et al.* (2011) 'Characterization of Multiwalled Carbon Nanotubes Dispersing in Water and Association with Biological Effects', *Journal of Nanomaterials*, 2011, pp. 1–12.

Çınar, N., Yuca, N. and Karatepe, N. (2012) 'Effect of H2 reduction on carbon nanotube synthesis', *The Online Journal of Science and Technology*, 2(2), pp. 20–25.

Farahani, B. V., Behbahani, G. R. and Javadi, N. (2016) 'Functionalized multi walled carbon nanotubes as a carrier for doxorubicin: Drug adsorption study and statistical optimization of drug loading by factorial design methodology', *Journal of the Brazilian Chemical Society*, 27(4), pp. 694–705.

Firme, C. P. and Bandaru, P. R. (2010) 'Toxicity issues in the application of carbon nanotubes to biological systems', *Nanomedicine: Nanotechnology, Biology, and Medicine*, 6(2), pp. 245–256.

Flavin, K. *et al.* (2011) 'Controlled carboxylic acid introduction: a route to highly purified oxidised single-walled carbon nanotubes', *Journal of Materials Chemistry*, 21(44), pp. 17881–17887.

Grossiord, N. *et al.* (2005) 'Time-Dependent Study of the Exfoliation Process of Carbon Nanotubes in Aqueous Dispersions by Using UV−Visible Spectroscopy', *Analytical*

Chemistry, 77(16), pp. 5135–5139.

Jahan, N. *et al.* (2013) ‘Effect of Carboxyl Functionalized MWCNTs on the Cure Behavior of Epoxy Resin’, *Open Journal of Composite Materials*, 3(April), pp. 40–47.

Joshi, M. D. (2016) ‘Advances in Nanomedicine for Treatment of Stroke’, *International Journal of Nanomedicine and Nanosurgery*, 2(3), pp. 2–4.

Lekawa-Raus, A. *et al.* (2014) ‘Electrical properties of carbon nanotube based fibers and their future use in electrical wiring’, *Advanced Functional Materials*, 24(24), pp. 3661–3682.

Li, S. *et al.* (2002) ‘Super-hydrophobicity of large-area honeycomb-like aligned carbon nanotubes’, *Journal of Physical Chemistry B*, 106(36), pp. 9274–9276.

Li, Y., Cheng, B. and Shen, C. (2016) ‘Effect of acid treatment on the morphology of multi-wall carbon nanotubes’, *Journal of Beijing university*, 31(October), pp. 60–64.

Moon, Y. K. *et al.* (2009) ‘Synthesis of length-controlled aerosol carbon nanotubes and their dispersion stability in aqueous solution’, *Langmuir*, 25(3), pp. 1739–1743.

Nunes, A. *et al.* (2012) ‘Application of carbon nanotubes in neurology: Clinical perspectives and toxicological risks’, *Archives of Toxicology*, 86(7), pp. 1009–1020.

Pillai, S. and Ray, S. (2011) ‘Epoxy-based carbon nanotubes reinforced composites’, in Reddy, B. (ed.) *Advances in Nanocomposites - Synthesis, Characterization and Industrial Applications:* In Tech, pp. 727–793.

Scholtz, F. (2010) *Electroanalytical Methods*. Second. Edited by S. Fritz. Germany: Springer.

Sedaghat, S. (2014) ‘Synthesis and Modification of Carboxylated Multi Wall Nanotubes with Atenolol’, *Soft Nanoscience Letters*, 4, pp. 75–81.

Shieh, Y. T. *et al.* (2010) ‘An investigation on dispersion of carbon nanotubes in chitosan aqueous solutions’, *Colloid and Polymer Science*, 288(4), pp. 377–385.

Shulga, E. *et al.* (2011) ‘Functionalisation of aligned carbon nanotubes with nitric acid vapour’, *Micro & Nano Letters*, 6(8), pp. 704–708.

Smith, B. *et al.* (2009) ‘Colloidal properties of aqueous suspensions of acid-treated, multi-walled carbon nanotubes’, *Environmental Science and Technology*, 43(3), pp. 819–825.

Tan, K. H. *et al.* (2011) ‘Optical Studies on Multiwalled Carbon Nanotubes via Modified Wolff-Kishner Reduction Process’, *Advanced Materials Research*, 194–196(2011), pp. 618–624.

Turgunov, M. A., Oh, J. O. and Yoon, S. H. (2014) ‘Surface Modification of Multiwall Carbon Nanotubes by Sulfuric Acid and Nitric Acid’, *Advanced Science and Technology Letters*, 64(Materials), pp. 22–25.

Uslu, B. and Ozkan, S. A. (2011) ‘Electroanalytical Methods for the Determination of Pharmaceuticals: A Review of Recent Trends and Developments’, *Analytical Letters*, 44(16), pp. 2644–2702.

Vardharajula, S. *et al.* (2012) ‘Functionalized carbon nanotubes : biomedical applications’, *International Journal of Nanomedicine*, 7, pp. 5361–5374.

Yasuhiro, Y. L. Æ. and Chung, A. Æ. D. D. L. (2008) ‘Development of epoxy-based electrets’, *Journal of materials Science*, 43, pp. 1650–1663.

Yun, Y. *et al.* (2007) ‘A nanotube array immunosensor for direct electrochemical detection of antigen–antibody binding’, *Sensors and Actuators B: Chemical*, 123(1), pp. 177–182.

CHAPTER 5

DEXAMETHASONE-LOADED, PEGYLATED, VERTICALLY ALIGNED, MULTIWALLED CARBON NANOTUBES FOR POTENTIAL ISCHEMIC STROKE INTERVENTION

Published in Molecules: Komane, Patrick P., Kumar, P., Marimuthu, T., Du Toit, L.C., Kondiah, P.P.D., Choonara, Y.E., P. V. Dexamethasone-Loaded, PEGylated, Vertically Aligned, Multiwalled Carbon Nanotubes for Potential Ischemic Stroke Intervention. *Molecules* 2018, *23* (1406), 1–16.

Abstract

The complete synthesis, optimization, purification, functionalization and evaluation of vertically aligned multiwalled carbon nanotubes (VA-MWCNTs) was reported for potential application in dexamethasone delivery to the ischemic brain tissue. The conditions for high yield were optimized and carbon nanotubes functionalized and PEGylated prior to dexamethasone loading. Morphological changes were confirmed by SEM and TEM. Addition of functional groups to MWCNTs was demonstrated by FTIR. Thermal stability reduced following MWCNTs functionalization as demonstrated in TGA. The presence of carbon at 2Ɵ of 25 ° and iron at 2Ɵ of 45 ° in MWCNTs was illustrated by XRD. Poly-dispersive index and zeta potential were found to be 0.261 and -15.0 mV, respectively. Dexamethasone release increased by 55 %, 65 % and 95 % in pH of 7.4, 6.5 and 5.5 respectively as evaluated by UV-VIS. The functionalized VA-MWCNTs were demonstrated to be less toxic in PC-12 cells in the concentration range from 20 – 20000 µg.mL^{-1}. These findings have demonstrated the potential of VA-MWCNTs in the enhancement of fast and prolonged release of dexamethasone which could lead to the effective treatment of ischemic stroke. More work is under way for targeting ischemic site using atrial natriuretic peptide antibody in stroke rats.

5.1. Introduction

Carbon nanotube synthesis and their application in various fields have become more popular to date. Carbon nanotubes (CNTs) are a fairly new group of nanomaterials that have demonstrated promising results in various areas of nanomedicine due to their unique structures and outstanding physico-chemical properties (Komane *et al.*, 2016). Based on their unique properties, CNTs have attracted much attention since a report by Iijima in 1991 (Iijima, 1991). CNTs are potential candidates for a variety of applications such as chemical sensors, nanoelectronics, catalyst support, targeting of diseased sites and drug delivery systems. The nature and quality of CNTs are highly dependent on the method of synthesis which regulates the graphitization degree, helicity and diameter (Lee *et al.*, 2016).

A spectrum of procedures to produce CNTs have been reported and the most commonly used procedures are arc discharge, laser ablation and chemical vapor deposition. The catalytic chemical vapor deposition (CCVD) is the most popular and preferred technique for the production of MWCNTs in large scale, since it is inexpensive and can produce high quality MWCNTs (Lodhi, Mehra and Jain, 2013). Nebulized spray pyrolysis is an improved version of CVD method with the ultra-high frequency radiation used to nebulize reactants in solution to produce a reactant aerosol. The aerosol is carried into a high temperature furnace by a suitable carrier gas. The reaction is achieved by placing the reaction mixture in a reservoir with a piezo electric transducer at the base and connected to a frequency generator (Roy, David-Pur and Hanein, 2017).

CVD is divided into a floating catalyst method in which a catalyst is in a gas phase and a fixed catalyst method in which a catalyst is supported in a solid phase. In the floating catalyst method, there is no need for catalyst preparation as the catalyst particles are continuously formed (Tewari and Sharma, 2015). A precursor, ferrocene is dissolved in organic solvent which also serve as carbon sources. It is based on the hydrocarbon decomposition on the metallic catalysts such as iron, nickel, cobalt and molybdenum (Rahman *et al.*, 2016).

Dexamethasone is a glucocorticoid with anti-inflammatory properties rendering it potentially effective for the treatment of inflammatory diseases including ischemic

stroke. However, its therapeutic potential is negatively affected by the short circulatory half-life and poor pharmacokinetics requiring administration of higher doses which could lead to serious systemic side-effects (Psarros *et al.*, 2012). In addition, dexamethasone could also cause hemorrhage and edema in stroke patients. If low doses of dexamethasone are conjugated to MWCNTs and targeted to the diseased site by a specific antibody, the current drawbacks may be overcome. Functionalization of these MWCNTs may increase biocompatibility, appendability of the drug to CNTs, and permeability of drug to cells; and decrease of cytotoxicity of the CNTs.

In this study, the effect of various factors such as synthesis temperature, synthesis duration, gas flow rate, catalyst and location of silicon wafer in the furnace influencing the quality and yield of MWCNTs is investigated. For dexamethasone release studies, MWCNTs were first functionalized with acids, acylated, amidated and PEGylated prior to loading dexamethasone. Toxicity of the functionalized carbon nanotubes was evaluated using PC12 cells. Dexamethasone 21 phosphate was successfully loaded onto and released from the PEGylated VA-MWCNTs for the first time. These findings have demonstrated VA-MWCNTs to have a potentially important role in the fast and prolonged release of dexamethasone which could lead to an effective treatment of ischemic stroke. More work is under way for targeting ischemic site using atrial natriuretic peptide antibody in stroke rats.

5.2. Materials and Methods

5.2.1. Synthesis of MWCNTs using Chemical Vapor Deposition

A circular silicon wafer (single side polished, <100>, N-type, contains No dopant, diam. × thickness in. × 0.5 mm) from Sigma-Aldrich Corporation (St Louis, MO, USA) was dissected into 1 cm x 1 cm pieces and sonicated in acetone, methanol and water for 5min. The silicon wafer was loaded into the quartz reactor tube to act as a platform for MWCNTs growth. The quartz tube was then inserted in a horizontal high temperature tube furnace (Elite TSH 12/38/500-2216E, Leicestershire, UK). The reaction vessel was activated with 40 mL catalyst and 95 % baseline argon balanced with 5 % hydrogen was used as a carrier gas. Flow rate was set to 50 $mL.min^{-1}$ to create an inert environment using mass flow controller (D08-4D/ZM, Beijing Sevenstar, Huachuang Electronic Co., Ltd, China). The nebulizer (Dr Hielscher UM20-1.6 MHz Sonic, Germany) was used to generate an aerosol. The temperature was set to 775 $^{\circ}C$ at a ramp of 10 $^{\circ}C.min^{-1}$, gas flow rate to 400 $mL.min^{-1}$ and synthesis time to 45 min.

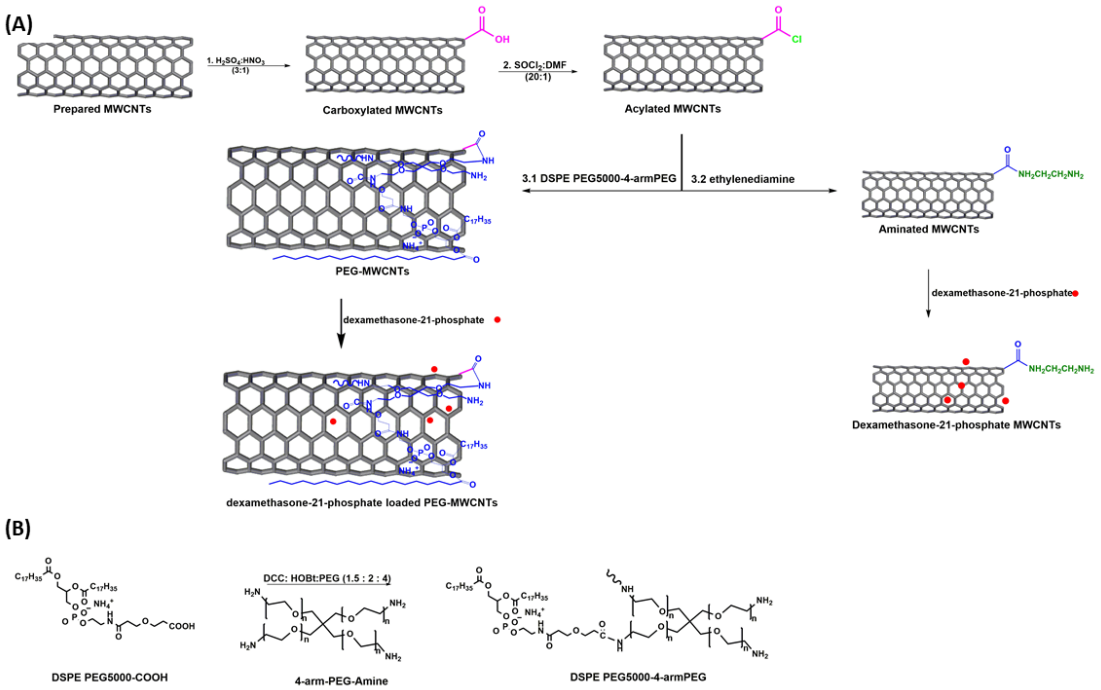
In order to investigate which catalytic system gave optimum yields, reaction vessel was charged with catalytic amounts (25, 50 and 100 mg.mL^{-1}) of respective ferrocene and cobaltocene dissolved in toluene (Sigma-Aldrich Corporation, St Louis, MO, USA), which also served as the carbon source for carbon nanotube growth.

5.2.2. Design and Optimization of formulations using a Design Strategy

A three-factor Box-Behnken experimental design (BBD) was generated using Minitab® V15 statistical software (Minitab® Inc., PA, USA) to determine the optimal pyrolysis conditions for the synthesis of vertically aligned MWCNTs. The variables employed in the experimental design were synthesis time, synthesis temperature and gas flow rate. The lower and upper limits for the synthesis time were 30 min and 60 min, respectively. The synthesis temperature limits were 650 °C and 950 °C and that of gas flow rates were 100 and 600 mL.min^{-1}. The formulation variables were evaluated for their effect on the yield, length, external diameter and internal diameter of MWCNTs on both the quartz reactor tube and silicon wafer.

5.2.3. Functionalization of MWCNTs

The H_2SO_4:HNO_3 functionalized MWCNTs were resuspended in $SOCl_2$: DMF solution (20:1) and refluxed at 70 °C under N_2 for 24hrs (**Scheme 5.1**). The product was centrifuged at 5 000 rpm for 20 min (Eppendorf Centrifuge, 5804, Germany) and the precipitates washed with tetrahydrofuran (THF) at 5 000 rpm for 20 min until the supernatant was crystal clear. The acylated carbon nanotubes (COCl-MWCNTs) were then dried in a vacuum oven at 70 °C for 24 hrs (Trade Raypa Espinar, Barcelona) (Zare-Zardini *et al.*, 2015)**.**



Scheme 5.1. Schematic illustration showing the preparation of PEG-MWCNTs.

DSPE PEG5000-4-arm (PEG-amine) was synthesised by reacting one equivalent DSPE PEG5000-amine (Nanocs Inc, NY, USA) with 5 eq succinic anhydride in dichloromethane (Sigma Aldrich Corporation, St Louis, MO, USA). The reaction was stirred at an ambient temperature for 24 hrs and evaporated to dryness. The product was reconstituted in deionised water and dialysed against water in a SnakeSkin dialysis tubing (Pierce-MWCO 3,5 kDa, Thermo Scientific, USA) for two days at a neutral pH. Dialysis tubing content was lyophilized in a Virtis Freeze Dryer (Gardiner, NY, USA) for 24 hrs. Then 1.5 eq dicyclohexylcarbodiimide (DCC) was mixed with 2 eq hydroxybenzotriazole (HOBt) in dichloromethane (DCM) purchased from Sigma-Aldrich Corporation (St Louis, MO, USA).

The mixture was added to the lyophilised DSPE PEG5000-COOH and reacted at room temperature for an hour. The 4 eq of 4-arm PEG-amine (Nanocs Inc, NY, USA) was reacted with DSPE PEG5000-COOH in DCM for two days. The product was evaporated to dryness and reconstituted in deionised water and stirred for an hour at ambient temperature and filtered through 0.2 µm filter (Liu *et al.*, 2008)**.** Acylated MWCNTs (0.2 mg.mL^{-1}) were sonicated with 0.2 mM DSPE PEG5000-4-arm-(PEG-amine) for 1 hour. The product was centrifuged at 24 0000 x g for 6 hrs (Beckman Coulter, Centrofriger-BL11, P-Selecta, Spain) and supernatant was collected for characterization and drug release studies (**Scheme 5.1**).

5.2.4. Morphological and Molecular Spectroscopic Evaluation of the MWCNTs

MWCNTs were coated with palladium-gold using sputter coater (Emitech K550X, Emitech Ltd, Kent, England) for 4 min at 25 mA and 2 x 10^{-1} mbar and scanned in FEI Nova NanoLab 600 FEG-SEM/FIB (FEI Company, Hillsboro, OR, USA) to determine their morphology and size. SEM-EDX analysis was employed to confirm the elemental composition. TEM samples were dispersed in ethanol, ultrasonicated for 10min (20 kHz sonicator, VibraCell, Sonics and Materials, Inc., Danbury, CT, USA), loaded on a copper grids, dried and loaded into FEI Tecnai T12 TEM operating at 120 kV for scanning and data processed using ImageJ software.

In order to determine the G and D bands and the effect of functionalization, PEGylated and non-PEGylated MWCNTs were analysed using Raman Micro200 (Perkin Elmer, UK). Spectra were collected using laser beam of 785nm wavelength with maximum output of 250 mW from 200 to 2 500 cm^{-1} at 4 cm^{-1} resolution. KBr was mixed with MWCNTs, ground to fine particles, loaded on KBr die and pressed at 4-ton pressure under vacuum for 15 min with KBr press (ICL, International Crystal Labs, Garfield, USA) for molecular and vibrational transitions determination of MWCNTs.

The pellet was scanned with Perkin Elmer Spectrum 2000 FTIR spectrometer (PerkinElmer Spectrum 100, Llantrisant, Wales, UK) at a resolution of 4 cm^{-1} with 10 accumulations with wavenumbers ranging from 4,000 – 400 cm^{-1}. MWCNTs were prepared for ^{1}H NMR by dispersing 10mg of Dex, PEG-MWCNTs and Dex-PEG-MWCNTs in 0,4 mL deuterated water, deuterated methanol and deuterated water respectively. Samples were ultrasonicated for 2 min and analysed with 500 MHz Avance III spectrometer (Bruker Corporation, Billerica, MA).

5.2.5. Thermogravimetric and Porositometric analyses of MWCNTs

Thermal stability of MWCNTs were determined using a thermogravimetric analyzer (PerkinElmer TGA 4000, Llantrisant, Wales, UK). MWCNTs samples were heated from 30 ˚C to 950 ˚C under nitrogen gas purging environment at a constant flow rate of 20 $mL.min^{-1}$ and temperature ramp of 10 ˚C.min^{-1}. Thermograms were generated as percentage weight loss vs. temperature and processed using PyrisTM software (PerkinElmer, Llantrisant, Wales, UK). A porositometric analyzer (Micromeritics, ASAP 2020, Norcross, GA, USA) was employed to determine the porositometric properties

of the pristine and functionalized MWCNTs. Sample was loaded in a sample tube, degassed and analysed by the Brunauer–Emmett–Teller (BET) N_2 gas adsorption method at 77 K.

5.2.6. Particle size, zeta potential, crystallinity and elemental composition MWCNTs

The 5 M HCl functionalized MWCNTs were suspended in deionized water at a concentration of 0.2 $mg.mL^{-1}$ ultrasonicated for 2 hrs and measurements of particle size distributions and zeta potential were obtained using a ZetaSizer NanoZS (Malvern Instruments, Malvern, UK) instrument equipped with non-invasive backscatter technology set at a fixed angle of 173 ° and a light source with wavelength of 532 nm. X-ray diffraction (XRD) patterns of the MWCNTs were examined on X-ray diffractometer (Philips, PANalytical X'pert PRO, X-ray diffraction system.) at 40 kV and 40 mA with Cu Kα radiation (1.54060) equipped with K-beta filter. Each sample was scanned for 2 hrs because of high iron content in MWCNTs and the raw data processed with High Score Plus software.

5.2.7. Dex and Dex-PEG-MWCNTs preparations and drug release Studies

Following 24-hour reaction, Dex-MWCNTs were centrifuged at 5 000rpm for 10min and dried in a vacuum oven for 24 hrs at room temperature. The centrifugation procedure was repeated thrice. Dex was also reacted with PEG-MWCNTs for 24 hrs, centrifuged and the supernatant collected for characterisation and drug release studies. Dex-MWCNTs and Dex-PEG-MWCNTs were dispersed in 10 mL of 0.1 M phosphate buffered saline (PBS) and dialysis performed against 200 mL PBS buffer with pH 7.4, 6.5 and 5.5 respectively in an orbital shaker (YIHDER, Taiwan) at 37°C with 30 rpm speed. Collection of 3 mL of the PBS buffer was done at various time intervals from 0 – 12 hrs. The sink conditions were maintained. The λ_{max} of dexamethasone was determined using UV-VIS (Shimadzu Corporation, Kyoto, Japan) and was found to be 24 nm. Standard curve of Dex was then created using different concentrations and was used to determine concentrations in 3 mL aliquots of PBS buffer collected at various time intervals during a 12-hour dialysis of the Dex-CNT and Dex-PEG-CNT constructs.

5.2.8. Functionalization of MWCNTsCytotoxicity evaluation of VA-MWCNTs

PC-12 cell lines were grown in RPMI1640 medium supplemented with 5 % fetal bovine serum and 10 % horse serum in an incubator at 37 ºC and 5 % CO_2. A mixture of 1 % penicillin and streptomycin solution was added to the culture medium to prevent bacterial contamination. In each well of 96 well plate, $6x10^4$ cells were added and incubated for 24 hours with various concentrations (20, 200, 2000 and 20 00 $\mu g.mL^{-1}$) of each formulation (free Dex, equivalent Dex concentration coupled to PEGylated MWNT and sulfonitric acid treated MWCNTs. Controls (*PC -12 cells not treated with any of the formulations-zero concentration group*) for each formulation were also included in this study for comparison. A volume of 10µL of MTT (3-(4,5-Dimethylthiazol-2-yl)-2,5-Diphenyltetrazolium Bromide) was added to each well and further incubated for 4 hours at 37 ºC and 5 % CO_2.. Solubilisation solution was added to solubilize formazan crystals and the absorbance read at 570 nm using Multilabel Reader (Victor X3, Perkin Elmer, Waltham, MA, USA).

5.3. Results and Discussion

5.3.1. Location of the Substrate, Catalyst Concentration and Acid Purification of MWCNTs

The location of the substrate, synthesis temperature, catalyst concentration, synthesis duration, argon flow rate were varied to determine the optimal pyrolysis conditions for the growth of MWCNTs. Aligned MWCNTs were successfully grown on the silicon wafer when it was placed 14 cm from the furnace inlet **(Figure 5.1A, D, F).** Carbon nanospheres and graphitic flakes were obtained when Si substrates were placed at the furnace centre **(Figure 5.1B-C).** MWCNTs consisted of more than one wall and iron nanoparticles were observed in their cavities **(Figure 5.1E)** and well aligned MWCNTs were obtained when temperatures of 850 °C and 775 °C were used **(Figure 5.1A, F)** whereas higher temperatures around 900 °C led to the formation of carbon flakes and nanospheres **(Figure 5.1B-C).**

Temperatures of 775 °C and 850 °C were found to be the optimal temperatures for iron atoms mobility to form catalytic particles and toluene decomposition to form carbon and nucleate MWCNTs. At temperatures below 750 °C, the iron atoms were not mobile enough to aggregate together into particles to nucleate and grow nanotubes. At temperatures above 850 °C, the catalyst becomes highly mobile and quickly

agglomerates into metal particles that are too large to initiate carbon nanotube nucleation resulting in a process called , '*carbon overcoating'* (Veziri *et al.*, 2008) resulting in the formation of carbon nanospheres and flake-like structures **(Figure 5.1B-C).**

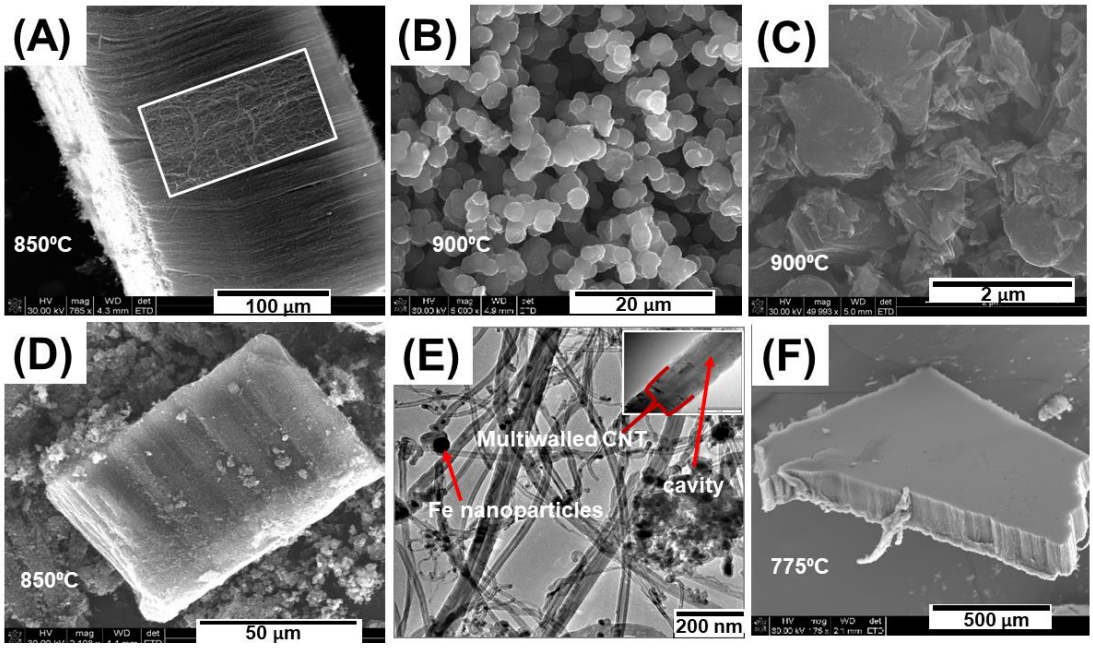


Figure 5.1 Vertically aligned MWCNTs collected from silicon wafer 14 cm from the furnace inlet at 850 °C (A). Carbon nanospheres produced at 900 °C (B). Carbon flakes from the furnace centre at 900°C (C). MWCNTs from quartz tube walls at 850 °C (D). TEM micrograph of aligned MWCNTs (E) with magnified MWCNT insert. MWCNTs grown at 775 °C (F).

Composition and concentration of the catalyst are important in MWCNTs synthesis. Lower concentration leads to SWCNTs formation, while higher concentration leads to MWNTs formation (Allaedini *et al.*, 2016). Different concentrations of ferrocene in toluene (25, 50 and 100 mg.mL^{-1}) was used to evaluate the effect of the content of transition metal on the growth of MWCNTs. The thickness of MWCNTs increased with an increase in the ferrocene content. When 25 mg.mL^{-1} of catalyst was used, MWCNTs with clean surfaces were produced with less or no iron nanoparticle layers on their surfaces **(Figure 5.2A- C).**

Ghaharpour and colleagues have demonstrated in their work that the higher content of catalysts provided better conditions for the growth of carbon nanotubes (Ghaharpour *et al.*, 2016). In this study, a higher concentration of catalyst (100 mg.mL^{-1}) produced a thick layer of iron nanoparticles on the surface of MWCNTs **(Figure 5.2A)** whereas a thin layer was noticed when 50 mg.mL^{-1} ferrocene was used (**Figure 5.1B**). There

was no formation of iron nanoparticle layer when 25 mg.mL^{-1} ferrocene was used as a catalyst **(Figure 5.2C).** Furthermore, acid purification eliminated the contaminants such as amorphous carbon and iron nanoparticles from carbon nanotubes.

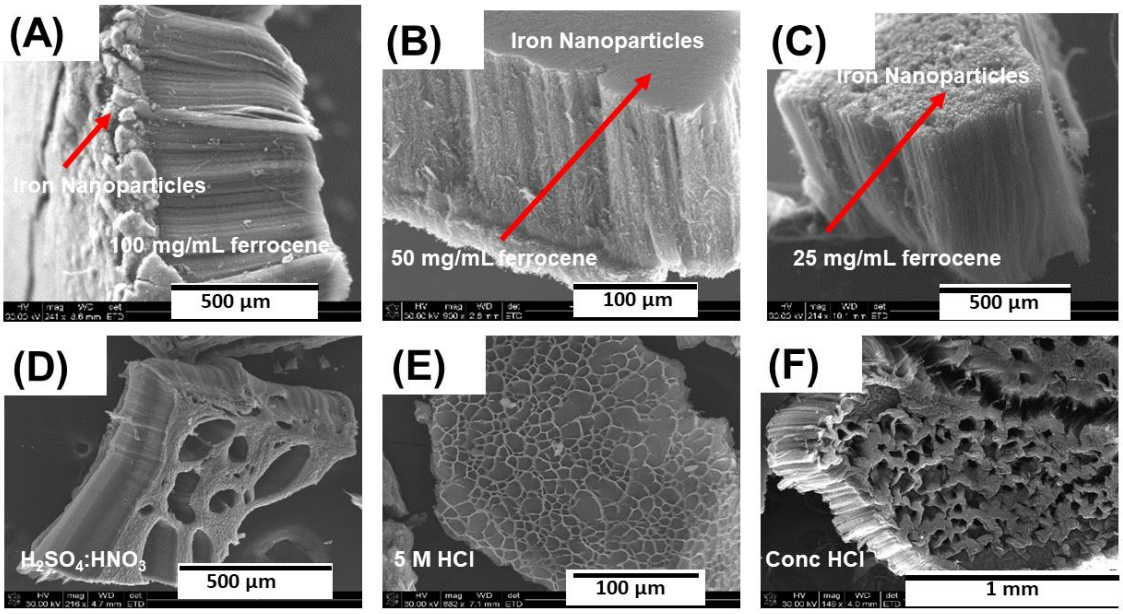


Figure 5.2 MWCNTs at various catalyst concentrations and purified with different acids. MWCNTs synthesised in 100 mg.mL^{-1} ferrocene (A). MWCNTs prepared in 50 mg.mL^{-1} ferrocene (B). MWCNTs when 25 mg.mL^{-1} ferrocene was used (C). MWCNTs treated with different acids namely concentrated H_2SO_4:HNO_3 (3:1) (D), 5 M HCl (E) and concentrated HCl (F).

VA-MWCNTs were treated with different acids for purification to remove amorphous carbon and residual iron. In addition, the treatment was performed to increase dispersibility and hydrophilicity of the MWCNTs. When MWCNTs were subjected to HNO_3:H_2SO_4 (1:3), holes with mean diameter of 104.31 µm were formed on MWCNTs (**Figure 5.2D**). A mixture of HNO_3 and H_2SO_4 oxidized the iron nanoparticle, amorphous carbon and MWCNTs leading to the formation of holes on MWCNTs. When MWCNTs were exposed to 5 M HCl, honeycomb-like structures with a mean diameter of 12.30 µm were generated **(Figure 5.2E).** Concentrated HCl resulted in the oxidation of MWCNTs leading to the formation of holes with mean diameter of 85.82 µm and shrinking on the surface of MWCNTs **(Figure 5.2F).**

5.3.2. Determination of Crystallinity, Thermal properties and Raman Spectroscopy of MWCNTs

Two characteristic peaks were observed at the angle (2Θ) of 25 ° and 45 ° confirming the presence of carbon in MWCNTs and iron in ferrocene, respectively **(Figure 5.3A).**

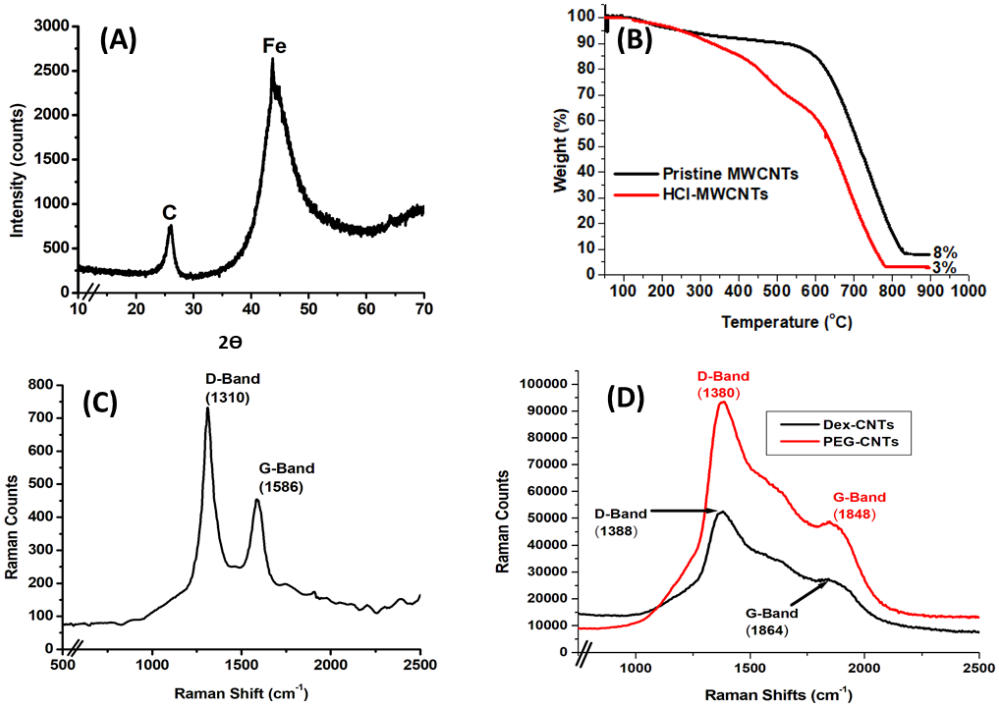


Figure 5.3. XRD diffraction pattern, TGA and Raman spectra of MWCNTs. Diffraction pattern of pristine MWCNTs (A), TGA of both pristine and HCl treated MWCNTs (B). Raman spectrum of pristine MWCNTs (C) and Dex and PEG-CNTs (D).

Thermal stability and purity of MWCNTs were determined using a thermogravimetric analyser. While the TGA curve of the pristine MWNTs showed no significant mass loss up to 600 °C, one sharp mass loss for the functionalized samples was observed in the temperature range from 150 – 775 °C. The sharp mass loss observed in the temperature range of the functionalized samples could be attributed to the HCl on the MWNTs surface, unreacted carboxylic acid groups as well as MWNTs that were oxidized in carboxylation stage (**Figure 5.3B**).

Acid functionalized MWNTs showed the remaining weight to be around 3 % at 775 °C, which is attributed to the metal catalyst or the ash of MWNTs. Pristine MWNTs showed the remaining weight to be ~8 % at 825 °C. Significant weight loss started at 150 °C and 600 °C in acid functionalized and pristine MWCNTs, respectively (**Figure 5.3B**). Complete decomposition occurred at 725 °C and 825 °C in acid functionalized and

pristine MWCNTs respectively. The findings confirm a successful purification of MWCNTs as depicted by less remains in the functionalized MWCNTs as opposed to impure pristine MWCNTs.

MWCNTs were PEGylated and their Raman Spectra determined by Raman Micro200. The D and G bands were observed in the non-PEGylated MWCNTs at 1310 cm^{-1} and 1586 cm^{-1} respectively (**Figure 5.3C**). A shift of both the D and G bands to the right was observed when MWCNTs were functionalized with PEG and dexamethasone as compared to the non-PEGylated CNTs (**Figure 5.3D**). There was a significant rise in the D band intensity and a drop in the G band intensity following functionalization.

Our data agree with the work done by Voge and colleagues as they also observed a shift of D and G bands to the right in the functionalized MWCNTs (Voge *et al.*, 2013). Loading of dexamethasone caused a drastic decrease in the intensities of both bands and this could be due to the linkage that occurred between the PEGylated CNTs and dexamethasone.

5.3.3. Effect of Synthesis Times and Gas Flow Rates on the Length Diameter of MWCNTs

When different reaction times were employed in the synthesis of MWCNTs, a linear relationship was noticed between reaction time, length and external diameter of carbon nanotubes as demonstrated in **Figure 5.4A-B.** An increased catalyst annealing duration led to higher concentration of iron nanodroplets which enabled faster diffusion of carbon leading to more vertically aligned carbon nanotubes and higher growth efficiency. Rahman and colleagues synthesized aligned SWCNTs using annealing times of 10 s, 3 min, 10 min and 15 min. They found that the height of the SWCNT array increased from 229 µm to 246.5 µm as the catalyst annealing time was increased from 3 min to 10 min (Rahman *et al.*, 2016).

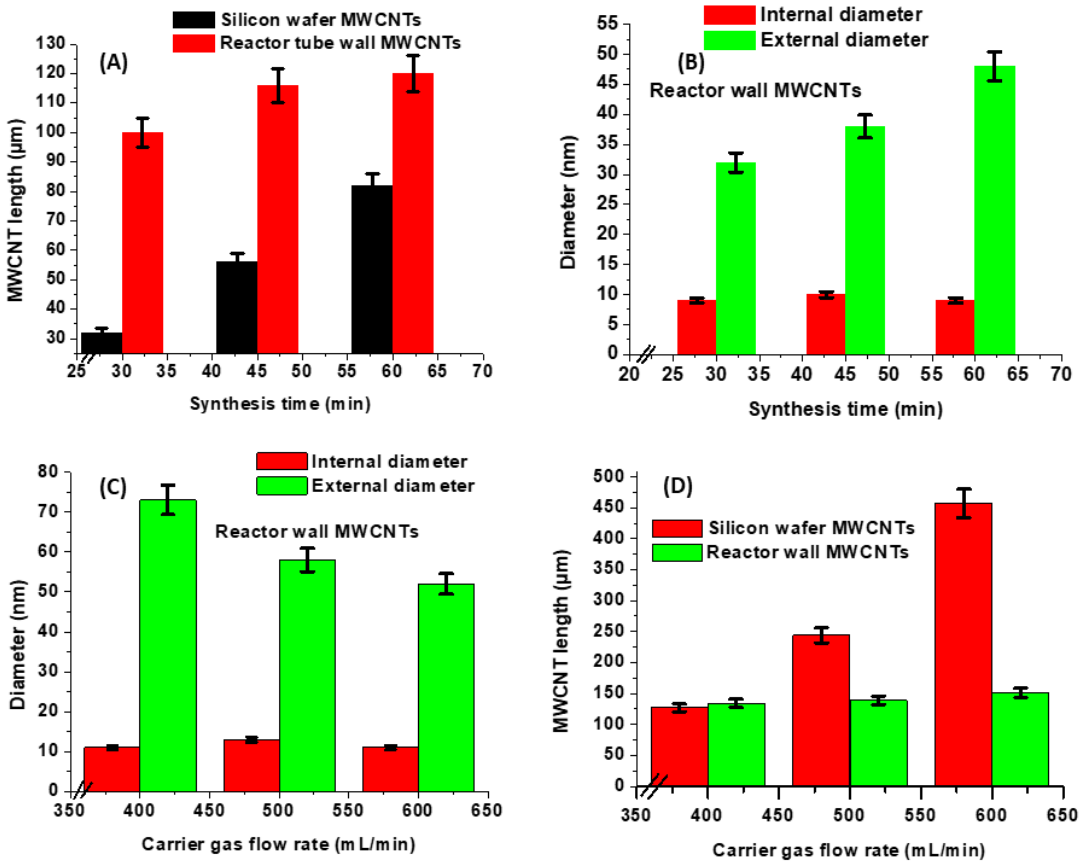


Figure 5.4. Synthesis parameters of MWCNTs. Synthesis time on the length or thickness of MWCNTs on both the silicon wafer (black column) and the reactor tube walls (red column) (A). Synthesis time on both the MWCNTs internal (red column) and external (green column) diameters (B). Carrier gas flow rate on both the MWCNTs internal (red column) and external (green column) diameters (C). Carrier gas flow rate on MWCNTs length on both silicon wafer (red column) and reactor wall (green column) (D).

In this study, various flow rates of argon ranging from 400 to 600 mL.min^{-1} were used and a linear relationship (R^2 = 0.99711) between the gas flow rate and thickness was observed (**Figure 5.4D**). The carrier gas flow rate influenced the distribution of the carbonaceous products on the quartz tube walls and substrate. Tewari and Sharma investigated the effect of carrier gas flow rates of argon, nitrogen and ammonia on the yield of carbon nanotubes and found that there was a direct relationship between the flow rate and the yield of carbon nanotubes (Tewari and Sharma, 2015).

In this study, 95 % argon balanced with 5 % hydrogen was used to produce quality carbon nanotubes. There was no effect on the internal diameter of the MWCNTs as the synthesis time and gas flow rate were increased **(Figure 5.4B-C).** In this work, iron nanoparticles of 10nm in diameter was used and the MWCNTs produced were of the

internal diameter of around 10 nm. The internal diameter of MWCNTs remained constant as it was restricted by the size of iron nanoparticles.

As the synthesis time increased, the walls on MWCNTs increased in number leading to an increase in external diameter **(Figure 5.4B)** as the external diameter is entirely dependent on the growth period of the carbon nanotubes. The external diameter decreased with an increase in the carrier gas flow rate because of carrier gas molecules occupying the catalyst sites to a greater degree than toluene molecules. Khorrami and Lotfi reported that an increase in the carrier gas flow rates decreased the formation of MWCNTs, because carrier gas molecules occupied catalyst sites more than ethanol molecules leading to the reduction of external diameter of the MWCNTs (Khorrami and Lotfi, 2016). In this study, the external diameter dropped with a rise in gas flow rate as demonstrated in **Figure 5.54C**.

5.3.4. Mixture of Ferrocene/Nickelocene/Cobaltocene on MWCNT Growth

Bimetallic nanoparticles are more reliable catalysts than single element catalysts because both metals in the bimetallic nanoparticles can enhance certain functions by playing complementary catalytic roles (De Greef *et al.*, 2015). The yield of CNTs increases many folds in comparison to using monometallic catalysts. It has been found that whilst all the metals are able to produce CNTs, iron catalysts gave a large yield. The superior performance of the iron catalyst was attributed to iron higher carbon solubility, which helps to promote the production of CNTs (Acomb, Wu and Williams, 2016). In this study, a combination of ferrocene and cobaltocene resulted in higher total yield of MWCNTs than ferrocene alone and a mixture of both ferrocene and nickelocene. When a trimetallic catalyst was used, there was a slight reduction in the yield but still higher than ferrocene alone (**Table 5.1**).

Table 5.1. MWNT production using a combination of various catalysts.

Catalyst	Location	Mass (g) before run	Mass (g) after run	Final mass (g)	Total mass (g)	Yield %
Fe 25 mg.mL^{-1}	Wafer	0.1114	0.1222	0.0108	0.1879	--
	QT	-	0.1771	0.1771		
Fe 25 mg.mL^{-1} Ni 1.2 mg.mL^{-1}	Wafer	0.1278	0.1282	0.0004	0.3312	43.27
	QT	-	0.3312	0.3312		
Fe 25 mg.mL^{-1} Co 1.25 g.mL^{-1}	Wafer	0.0933	0.0935	0.0002	0.5994	68.65
	QT	-	0.5992	0.5992		
Fe 25 mg.mL^{-1} Co 1.25 mg.mL^{-1} Ni 1.25 mg.mL^{-1}	Wafer	0.0435	0.0454	0.0019	0.2733	31.25
	QT	-	0.2714	0.2714		
Fe 50 mg.mL^{-1} Co 2.5 mg.mL^{-1} Ni 2.5 mg.mL^{-1}	Wafer	0.1476	0.1481	0.0005	0.5097	63.14
	QT	-	0.5092	0.5092		

5.3.5. Porositometric and Particle Size Distribution Properties of MWCNTs

Following functionalization of CNTs with H_2SO_4, surface characteristics of both the pristine and functionalized MWCNTs were determined by Surface Area and Porosity Analyser. BET measurements of MWCNTs are summarized in **Table 5.2** and isotherms are demonstrated in **Figure 5.5A.** These isotherm plots display the Type IV adsorption as there is formation of monolayers by capillary condensation on mesoporous surfaces of the CNTs. The black and green curves indicate the adsorption of liquid nitrogen and the red and blue curves indicate desorption of liquid nitrogen from the CNTs. The pristine and H_2SO_4 functionalized MWCNTs were found to be mesoporous according to IUPAC based on their pore size range of 13 to 18 nm.

Acid treatment improved MWCNTs surface area as demonstrated by **Figure 5.5A**. Acid treatment increased the surface area, pore size and pore volume of the MWCNTs by 67.27 %, 27.64 % and 76.32 %, respectively as depicted in **Table 5.2**. CNTs are hydrophobic in nature and their dispersibility is achieved by functionalization by attachment of polar groups such as carbonyl (–C(O)–), carboxyl (–COOH), and hydroxyl (–OH) (Yuan and Lee, 2013).

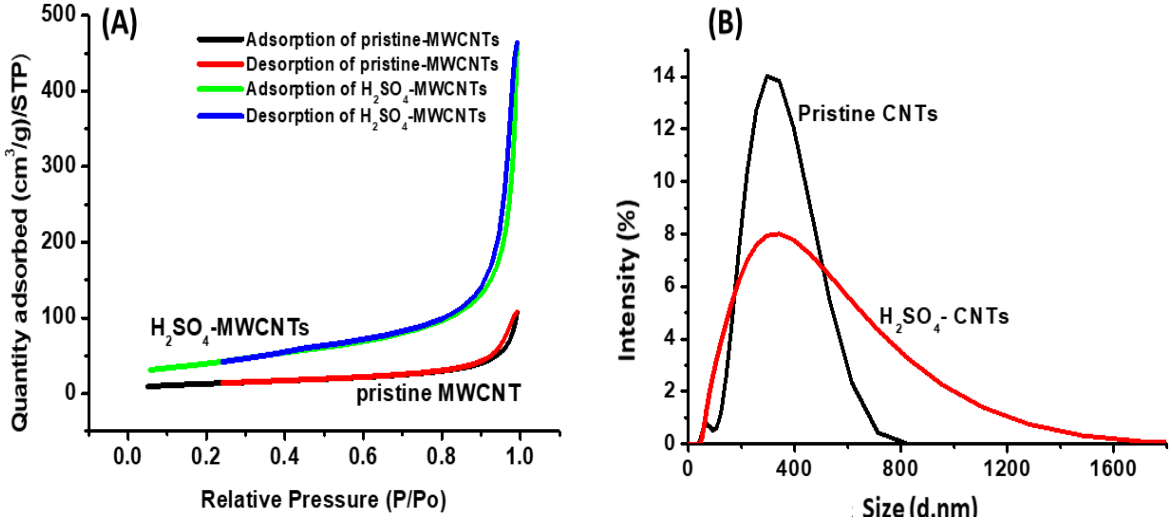


Figure 5.5. Porositometric and particle size properties of MWCNTs. BET isotherms for both the pristine (black curve for N2 adsorption and red curve for desorption) and HCl treated (green curve for N2 adsorption and blue curve for desorption) MWCNTs (A). An increase in particle size distribution was observed in acid treated CNTs as the CNTs are oxidized to produce different sizes (B).

The data obtained confirmed the hydrophobic nature of the pristine MWCNTs and hydrophilic nature of the H_2SO_4 functionalized MWCNTs.

Table 5.2. Surface area of pristine and 5 M HCl functionalized MWCNTs.

Type	BET surface area ($m^2.g^{-1}$)	Pore size (nm)	Pore volume ($m^3.g^{-1}$)
Pristine MWCNTs	47.1563	13.08973	0.154316
5 M HCl-MWCNTs	144.0962	18.08957	0.651660
% Increase	67.27	27.64	76.32

A Zetananosizer ZS (Malvern Instruments, Worcestershire, UK) was used to determine particle size distribution and zeta potential of MWCNTs. Zhao and colleagues demonstrated that defects in MWCNTs were more likely to form and functional groups were successfully grafted onto MWCNTs after oxidation. They also showed that the functionalized MWCNTs with negative groups as observed in Zeta potential measurements had superior suspension stability and could remain as a colloidal solution for 30 days (Zhao *et al.*, 2016).

In this study, the H_2SO_4 functionalized MWCNTs were suspended in deionized water at a concentration of 0,2 $mg.mL^{-1}$ and particle size distributions and zeta potentials were measured. The Z-average diameter and polydispersity index (PDI) were 287.08 nm and 0.261 respectively. This PDI indicates that the MWCNTs have a moderate size distribution. The zeta potential and conductivity were -15.0 mV and 0.0213 $mS.cm^{-1}$ respectively. The MWCNTs possess negative charge on their surface and the zeta potential magnitude of 15 implies that the MWCNTs are slightly agglomerated.

Nanoparticles possess properties that depend entirely on their dimensions. There is currently a plethora of methods for surface characterization of nanoparticles. The PSD values of the MWCNTs are different from SEM and TEM values as the techniques operate differently to measure the dimensions of the particles **(Figure 5.5B).** For particle size distribution (DLS), the particles are suspended in a solution and the measurements are performed while the particles are in solution based on Brownian motion. The individual particles may agglomerate leading to an increase in the hydrodynamic diameter.

In SEM, the particle is in a solid state (dry condition) and the length of the individual particle could be determined easily. For TEM, the particle is also in a solid state and the length of the particle could be determined depending on the size (if too long, it could be determined by SEM). In TEM, the internal and external diameters could be determined as this technique has a better resolution compared to SEM. In general, SEM is suitable for large particles (above 50nm in diameter) while TEM offers accurate results in small particles. DLS is a suitable technique for particles in solutions but inappropriate for polydispersive and heterogenous samples (Eaton *et al.*, 2017).

5.3.6. FTIR Spectroscopy and H^1 NMR Analyses of PEGylated MWCNTs

Relative to the spectrum for pristine MWCNTs (**Figure 5.6A)** the intensity of O-H and C-H streching band increased and broadened in the spectrum of MWCNTs-HCl Figure 6A due to acid treatment Peaks that were observed at 163 cm^{-1} could be ascribed to C=C respectively in both the pristine and functionalized MWCNTs. (Rahman *et al.*, 2016).

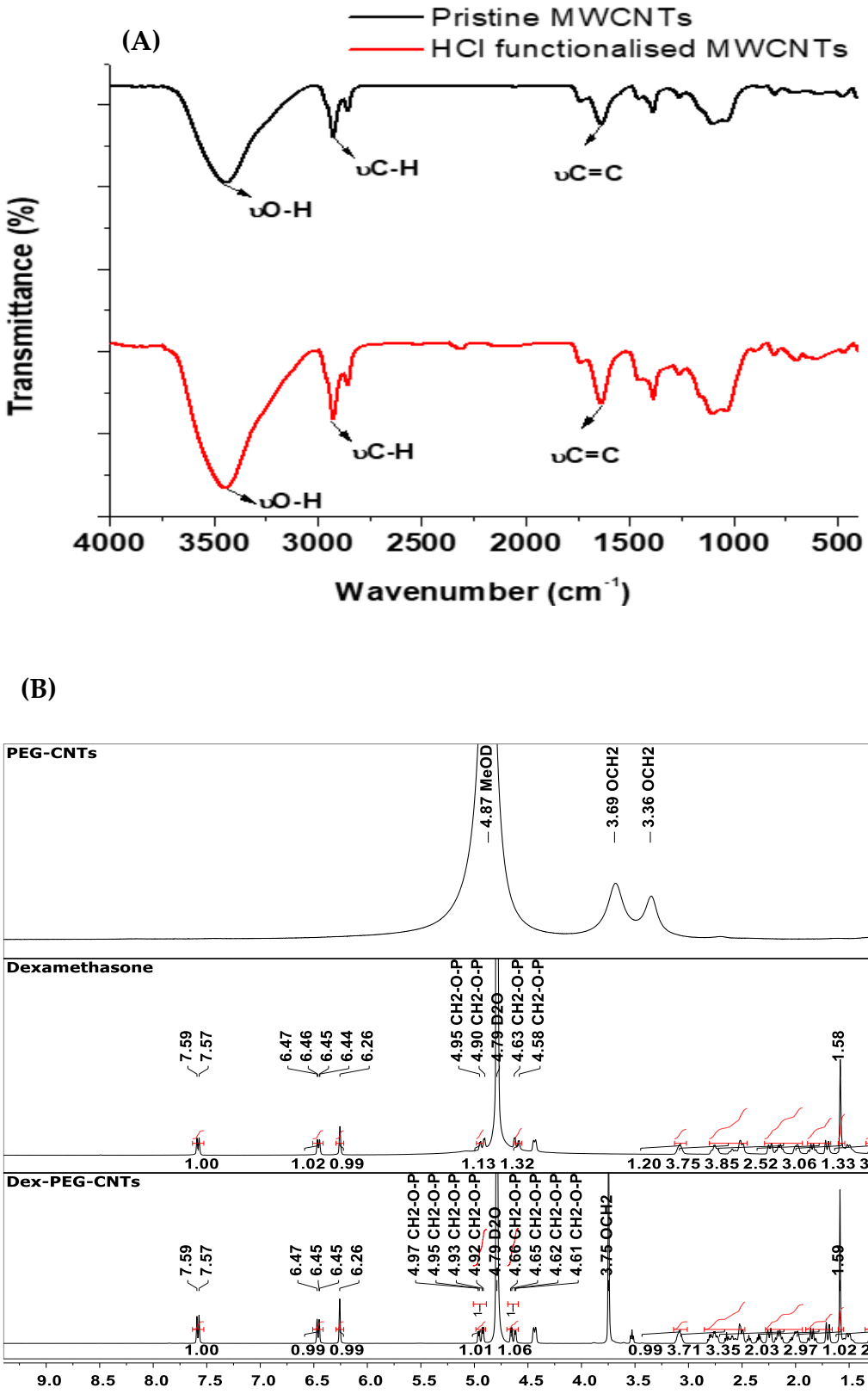


Figure 5.6. Molecular spectral properties of pristine and functionalized MWCNTs. FTIR spectra of pristine (red spectrum) and HCl functionalised (black spectrum) MWCNTs (A). ^{1}H -NMR spectra of PEG-CNTs, Dexamethasone, and Dex-PEG-CNTs (B).

In the ^{1}H-NMR spectrum of PEG- CNTS **(Figure 5.6B)** there are chemical shifts observed only at δ 3.69 and 3.36 ppm which can be ascribed to the methylene protons

on the PEG backbone (Razzazan *et al.*, 2016). The other proton signals were too weak and therefore not observed due to limited solubility of the PEG-CNTS in methanol. Relative to the spectrum of PEG- CNTS **(Figure 5.6B)** there are several new signals in the spectrum of Dexamethsone-21-phosphate loaded-PEG CNTS **(Figure 5.6B)** due to the presence of the loaded drug. For example, the presence of downfield protons 6.26 ppm (C=C-H) and 6.43 ppm are indicative of the steroid ring A system.

Relative to the spectrum of Dexamethsone-21-phosphate **(Figure 5.6B)** there are similar chemicals shifts observed in the spectrum of Dexamethasone-21-phosphate loaded-PEG CNTS **(Figure 5.6B).** Furthermore, these signals show no significant shifts. Chemical shift at 3.75 ppm represents methylene protons on the PEG backbone **(Figure 5.6B)** and confirm the presence of the CNTs. Therefore, based on the ^{1}H-NMR observations it can be proposed that the drug has being loaded into the CNT carrier (**Scheme 5.1**). The proposed loading sites and mechanism of loading that the drug is present in the formulation, where it may reside on the surface, inside the cavity of the tube or possible covalent interactions may occur as there are some (4.94, 4.64 ppm) slight upfield shifts (4.93, 4.61 ppm) (Besley and Noble, 2008).

5.3.7. Dexamethasone Loading to and Release from MWCNTs

Pristine MWCNTs are limited in drug delivery system due to their poor drug entrapment capability (Khorram, Raissi and Morsali, 2017). The successful entrapment of dexamethasone was reported which is enabled due to the novel functionalization carried out. PEG-MWCNTs and non-PEG-MWCNTs were tested using dexamethasone-21-disodium phosphate because of the increased solubility of the phosphate derivative.

For drug entrapment, the drug nanocarriers (carbon nanotubes) are functionalised prior to loading the drug (dexamethasone) onto the nanocarriers. The carbon nanotubes are purified with HCl to eliminate the contaminants and other impurities prior to functionalisation. Carbon nanotubes are refluxed in HCl for 24 hours at 70 °C. The CNTs are then washed with water until pH is 7. They are vacuum dried for 24 hours at 70 °C. The purified CNTs are carboxylated by reflux technique in H_2SO_4:HNO_3 (3:1) for 24 hours at 70 °C. Functionalization of CNTs not only makes it more soluble/dispersible in water but also provides active sites for attachment of drugs. The functionalised CNTs are washed in water until pH is 7 and dried in a vacuum oven for

24 hours at 70 °C. The functionalised CNTs are PEGylated with PEG-amine prior to reaction with dexamethasone. Since the tip caps of CNTs are removed during carboxylation, dexamethasone is entrapped inside the CNT central cavity. The entrapment is determined by dispersing accurately weighed quantity of formulation into phosphate buffers of 5.5, 6.5 and 7.4 in dialysis tubing and incubated at 37 °C to ensure the release of the entrapped drug. Aliquots of 1 mL are withdrawn and dexamethasone concentrations were determined at 242 nm by using UV-Vis spectrophotometer.

The initial release of dexamethasone from non-PEGylated MWCNTs was observed after ½ hr in PBS buffer with pH 5.5 and pH 7.4 (**Fig. 5.7A**). Maximum dexamethasone release occurred after 2hrs and 6hrs following dialysis in a basic and acidic milieu, respectively, and remained constant up to 12 hrs in PEGylated MWCNTs **(Figure 5.7A)**. A change in the release pattern of dexamethasone from MWCNTs was observed in the PEGylated MWCNTs **(Figure 5.7B).** An initial gradual release of dexamethasone occurred after ½ hr following dialysis in all PBS buffers. Maximum dexamethasone release was observed after 2 hrs in pH 7.4 PBS buffer 6 hrs in both pH 6.5 and 5.5 and remained constant thereafter. Only 55 % of dexamethasone loaded on non-PEGylated MWCNTs were released in

PBS buffer with pH 7.4 and 70 % released in a buffer with pH of 5.5 **(Figure 5.7A)**. Venditti and colleagues, in their work, loaded dexamethasone on gold nanoparticles and only 70 % of the loaded drug was released in 5 days (Venditti *et al.*, 2014) (Venditti *et al.*, 2014). Roozbahani and colleagues studied dexamethasone release from laponite nanoplates. In their work, 47 % of dexamethasone was released at pH = 7.4 while 76 % was released at pH = 5.4 after 3 days (Roozbahani, Kharaziha and Emadi, 2017). In our study, a fast release with more than 50 % was observed after 4 hours. Drug remained entrapped due to weak interaction in CNT cavities and cannot achieve 100 % release as a result.

Dexamethasone release was notably improved in PEGylated MWCNTs with 55 %, 65 %, 95 % release in PBS buffers with pH 7.4, ,6.5 and 5.5, respectively **(Figure 5.7B)** as compared to non-PEGylated MWCNT. It is possible that the slow release observed in **Figure 5.7B** is due to the ionic interaction between the opened charged MWCNTs and dexamethasone (Ketabi and Rahmani, 2017).

There are two possible mechanisms that could have taken place, namely drug loading as a result of entrapment into the inner cavities of the carbon nanotubes and ionic interaction as a result of phosphate derivative. The mechanisms of dexamethasone release from PEGylated MWCNTs in acidic and basic milieu have been demonstrated to be different.

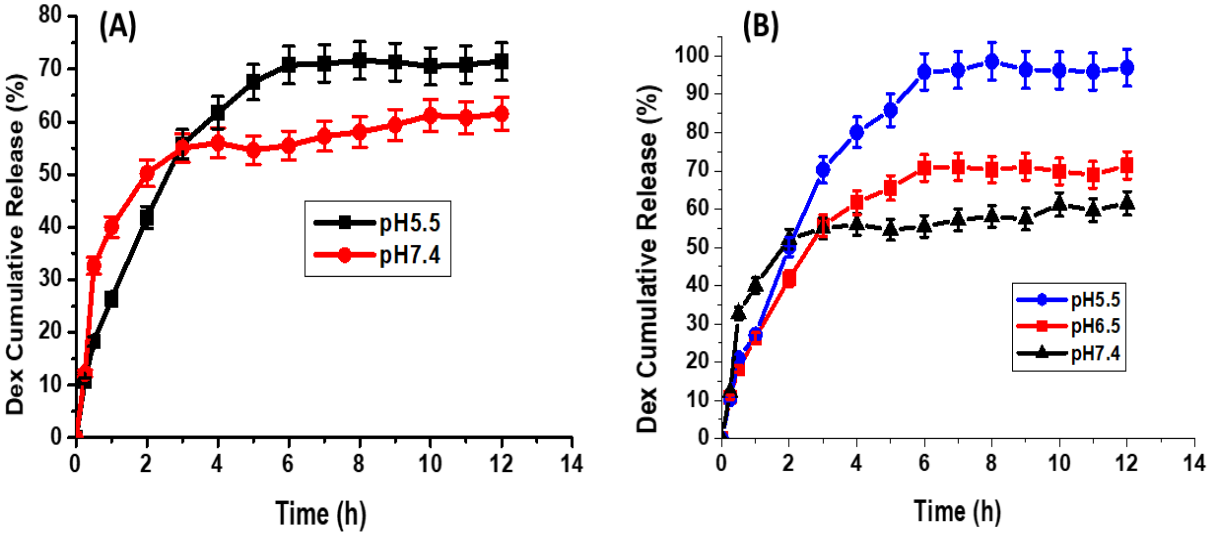


Figure 5.7. Dexamethasone release curves. Dex – MWCNTs in PBS buffer with pH 7.4 and pH 5.5 (A). Dex-PEG-MWCNTs in PBS buffer with pH 7.4, pH 6.5 and pH 5.5 (B).

The burst and subsequent sustained release could play a vital role in the therapeutic treatments, as the initial fast release could rapidly afford a therapeutic dose, and the succeeding sustained release could preserve the therapeutic dose for a prolonged period. The above findings have demonstrated an improved sustained release of dexamethasone when loaded to the PEGylated MWCNTs.

5.3.8. Cytotoxicity Evaluation of the Functionalized Carbon Nanotubes

Pristine carbon nanotubes are toxic, but their toxicities are reduced when they undergo functionalization. PC-12 cell lines were successfully grown in RPMI 1640 medium (**Figure 5.7**) and incubated with various concentrations of dexamethasone and functionalized carbon nanotubes for 24 hours.

Zeinabad and colleagues studied the effects of SWCNTs and MWCNTs in PC-12 cells using concentrations ranging from 0,01 to 100 $\mu g.mL^{-1}$. SWCNTs induced higher *in vitro* cytotoxicity against PC-12 as compared to MWCNTs as demonstrated by MTT

assay. A decline in cell viability was observed as the concentration of the carbon nanotubes was increased (Zeinabad *et al.*, 2016).

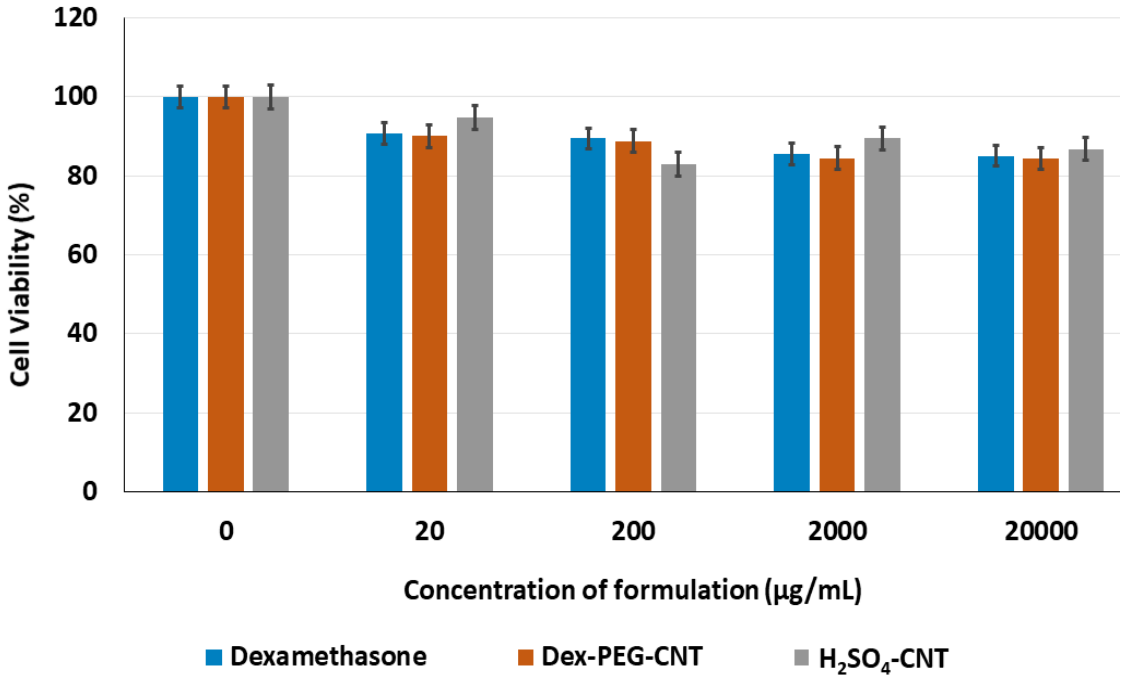


Figure 5.8 Cell viability following incubation with various concentrations of functionalized carbon nanotubes. H_2SO_4-MWCNTs were used as they are highly dispersible and hydrophilic. Blue column = free dexamethasone, brown column = equivalent dexamethasone concentration coupled to PEGylated MWCNTs and grey column for sulfonitric acid functionalized MWCNTs without dexamethasone. Concentrations of each formulation expressed as µg/mL from 0 – 20 000.

Gopinathan and colleagues developed poly(Ɛ-caprolactone)-based nanocomposite (PCL) scaffolds and evaluated their toxicity in PC-12 cells using Cytox 96 cytotoxicity assay kit. Cell viability analyses demonstrated that there was no cell death within 48 hours of incubation of PC-12 cells with the PCL nanocomposites (Gopinathan *et al.*, 2016).

The average diameter of the cells was found to be approximately 50 µm as depicted in **Figure 5.8.** Cell viability was reduced from 100 % to approximately 90 % as demonstrated in **Figure 5.8.** The 10% decrease in viability demonstrated the very low cytotoxic effect of the functionalized carbon nanotubes. Therefore, these functionalized carbon nanotubes could be utilized as nanocarriers of anti-inflammatory drugs such as dexamethasone at a very low dose to the ischemic site in the stroke patient leading to the effective treatment of stroke.

5.4. Conclusion remarks

Vertically aligned MWCNTs were successfully synthesised using chemical vapor deposition technique following optimisation of the synthesis parameters such as time, temperature, location of substrate in the reactor, catalyst and gas flow rates. Carbon nanotubes were successfully purified and functionalized for dexamethasone loading. PEGylation enhanced the release of dexamethasone from the VA-MWCNTs. Functionalized carbon nanotubes had a very low cytotoxic effect in cells. Based on the above findings, functionalized VA-MWCNTs have a potential for sustained delivery of dexamethasone for an extended period to the diseased site.

5.5. References

Acomb, J. C., Wu, C. and Williams, P. T. (2016) 'Applied Catalysis B : Environmental The use of different metal catalysts for the simultaneous production of carbon nanotubes and hydrogen from pyrolysis of plastic feedstocks', *'Applied Catalysis B, Environmental'*, 180, pp. 497–510.

Allaedini, G. *et al.* (2016) 'Carbon nanotubes via different catalysts and the important factors that affect their production : A review on catalyst preferences', *Int j nano dimens*, 7(3), pp. 186–200.

Besley, N. A. and Noble, A. (2008) 'NMR chemical shifts of molecules encapsulated in single walled carbon nanotubes', *Journal of Chemical Physics*, 128(10).

Eaton, P. *et al.* (2017) 'A direct comparison of experimental methods to measure dimensions of synthetic nanoparticles', *Ultramicroscopy*, 182, pp. 179–190.

Ghaharpour, F. *et al.* (2016) 'Parametric investigation of CNT deposition on cement by CVD process', *Construction and Building Materials*. Elsevier Ltd, 113, pp. 523–535.

Gopinathan, J. *et al.* (2016) 'Preparation, characterisation, and in vitro evaluation of electrically conducting poly(ε-caprolactone)-based nanocomposite scaffolds using PC12 cells', *Journal of Biomedical Materials Research - Part A*, 104(4), pp. 853–865.

De Greef, N. *et al.* (2015) 'Direct growth of carbon nanotubes on carbon fibers: Effect of the CVD parameters on the degradation of mechanical properties of carbon fibers', *Diamond and Related Materials*, 51, pp. 39–48.

Iijima, S. (1991) 'Helical microtubules of graphitic carbon', *Nature*, 354(6348), pp. 56–58.

Ketabi, S. and Rahmani, L. (2017) 'Carbon nanotube as a carrier in drug delivery system for carnosine dipeptide: A computer simulation study', *Materials Science and Engineering C*, 73, pp. 173–181.

Khorram, R., Raissi, H. and Morsali, A. (2017) 'Assessment of solvent effects on the interaction of Carmustine drug with the pristine and COOH-functionalized single-walled carbon nanotubes: A DFT perspective', *Journal of Molecular Liquids*, 240, pp. 87–97.

Khorrami, S. A. and Lotfi, R. (2016) 'Influence of carrier gas flow rate on carbon nanotubes growth by TCVD with Cu catalyst', *Journal of Saudi Chemical Society*. King Saud University, 20(4), pp. 432–436.

Komane, P. P. *et al.* (2016) 'Diagnosis and Treatment of Neurological and Ischemic Disorders Employing Carbon Nanotube Technology', *Journal of Nanomaterials*, 2016, p. 19 pages.

Lee, G. *et al.* (2016) ‘Low-temperature grafting of carbon nanotubes on carbon fibers using a bimetallic floating catalyst’, *Diamond and Related Materials*, 68, pp. 118–126.
Liu, Z. *et al.* (2008) ‘Drug Delivery with Carbon Nanotubes for In vivo Cancer Treatment’, *Cancer research*, 68(16), pp. 6652–6660.

Lodhi, N., Mehra, N. K. and Jain, N. K. (2013) ‘Development and characterization of dexamethasone mesylate anchored on multi walled carbon nanotubes’, *Journal of drug targeting*, 21(1), pp. 67–76.

Psarros, C. *et al.* (2012) ‘Nanomedicine for the prevention, treatment and imaging of atherosclerosis.’, *Nanomedicine : nanotechnology, biology, and medicine*, 8 Suppl 1, pp. S59-68.

Rahman, M. *et al.* (2016) ‘Synthesis and optical characterization of carbon nanotube arrays’, *Materials Research Bulletin*, 77, pp. 243–252.

Razzazan, A. *et al.* (2016) ‘In vivo drug delivery of gemcitabine with PEGylated single-walled carbon nanotubes’, *Materials Science & Engineering C*, 62, pp. 614–625.

Roozbahani, M., Kharaziha, M. and Emadi, R. (2017) ‘pH sensitive dexamethasone encapsulated laponite nanoplatelets : Release mechanism and cytotoxicity’, *International Journal of Pharmaceutics*, 518(1–2), pp. 312–319.

Roy, S., David-Pur, M. and Hanein, Y. (2017) ‘Carbon nanotube growth inhibition in floating catalyst’, *Carbon*, 116, pp. 40–49.

Tewari, A. and Sharma, S. C. (2015) ‘Effect of different carrier gases and their flow rates on the growth of carbon nanotubes’, *Physics of Plasmas*, 043501, pp. 1–12.

Venditti, I. *et al.* (2014) ‘Journal of Colloid and Interface Science Direct interaction of hydrophilic gold nanoparticles with dexamethasone drug : Loading and release study’, *Journal of Colloid And Interface Science*, 418, pp. 52–60.

Veziri, C. M. *et al.* (2008) ‘Growth and optimization of carbon nanotubes in activated carbon by catalytic chemical vapor deposition’, *Microporous and Mesoporous Materials*, 110, pp. 41–50.

Voge, C. M. *et al.* (2013) ‘Wrapping and dispersion of multiwalled carbon nanotubes improves electrical conductivity of protein-nanotube composite biomaterials’, *Journal of Biomedical Materials Research - Part A*, 101 A(1), pp. 231–238.

Yuan, Y. and Lee, T. R. (2013) ‘Contact Angle and Wetting Properties’, in Bracco, G. and Holst, B. (eds) *Surface Science Techniques*. Springer, p. 663.

Zare-Zardini, H. *et al.* (2015) ‘In vitro and in vivo study of hazardous effects of Ag nanoparticles and Arginine-treated multi walled carbon nanotubes on blood cells: Application in hemodialysis membranes’, *Journal of Biomedical Materials Research - Part A*, 103(9), pp. 2959–2965.

Zeinabad, H. A. *et al.* (2016) ‘Interaction of single and multi wall carbon nanotubes with the biological systems: Tau protein and PC12 cells as targets’, *Scientific Reports*, 6.

Zhao, Q. *et al.* (2016) ‘A novel method of functionalizing carbon nanotubes via neutralization reaction’, *Materials Letters*, 185(August), pp. 523–525.

CHAPTER 6
ATRIAL NATRIURETIC PEPTIDE CONJUGATION TO FITC LABELLED DEXAMETHASONE LOADED PEGYLATED ALIGNED MULTIWALLED CARBON NANOTUBES FOR TARGETING BRAIN ISCHEMIC SITE

ABSTRACT

In this chapter, we report on the functionalisation of aligned multiwalled carbon nanotubes and coupling of atrial natriuretic peptide (ANP) antibody to dexamethasone loaded PEGylated aligned multiwalled carbon nanotubes. Carbon nanotubes were purified and functionalised using HCl, H_2SO_4, HNO_3 and HNO_3:H_2SO_4. They were further acylated and labelled with fluorescence tag (FITC) prior to conjugation with atrial natriuretic peptide antibody (ANP). Morphological changes were confirmed by SEM and TEM. Successful functionalisation of MWCNTs was demonstrated by Fourier Transform Infrared. The G and D bands were determined by Raman microscopy and their intensities increased with functionalisation and they also shifted to the right. Absorbance was measured by Uv-Vis spectrometer. The fluorescence intensity was recorded using FEEM and Fluorescence spectroscopy. Carbon nanotubes were vertically aligned with more than one layer and Fe nanoparticles were located inside the activities of carbon nanotubes. Maximum absorbance for pristine, HCl, H_2SO_4 and $SOCl_2$ treated carbon nanotubes was found at 199,5 nm, 202 nm, 259 nm and 263,5 nm respectively. Fluorescence labelling reduced the transmission percentage of DEX-PEG-CNT. In addition, a functional group was added to DEX-PEG-CNT at 801nm following coupling of ANP to DEX-PEG-CNT. Fluorescence was detected in fluorescently labelled DEX-PEG-CNT and DEX-PEG-CNT ANP. These findings have demonstrated the coupling capability of ANP to DEX-PEG-CNT which could be used in targeting ischemic site in the brain.

6.1. Introduction

Natriuretic peptides are a family of polypeptide hormones that monitor blood pressure and fluid homeostasis by directly affecting the renal and cardiovascular system (Kim *et al.*, 2014). Natriuretic peptide family consists of atrial natriuretic peptide (ANP), brain natriuretic peptide (BNP), and C-type natriuretic peptide (CNP). Natriuresis is a term used for sodium discharge through urine and has vasodilatory effects. The three peptides are circulatory hormones of the cardiac origin that are secreted by plasma with plasma half-lives of ~4 min for CNP and ~2-3 min for ANP and 21 min for BNP (Syndrome *et al.*, 2014).

CNP is the least secreted hormone with low circulating levels and lacks significant natriuretic activity. ANP and BNP act at their synthesis site and other sites of the body through circulation. Their secretion is triggered by an increase in sodium loads, extracellular volumes and distension of atria and ventricles.

ANP, BNP, and CNP have a unique 17 amino acid residue ring structure. This structure is formed by an intramolecular disulfide bridge between two cysteine residues **(Fig. 6.2**). The amino- and carboxyl terminals vary from peptide to peptide. ANP has 28 amino acids, BNP has 32 amino acids and CNP has 53 amino acids. These peptides exist as pro-hormones with very high molecular weights. They are cleaved by specific enzymes prior to release into the blood circulation. A natriuretic receptor is required in order for ANP and BNP to function. The receptor produces cyclic-GMP to activate vasodilation and natriuresis (Sah and Salahuddin, 2016).

In lab experiments, the ANP gene was introduced into the animal to increase the plasma levels for treatment of hypertension. Cardiac myocytes are responsible for the production, storage, and secretion of ANP. Kim and colleagues have demonstrated in their work that GLP-1R activation promotes the secretion of ANP and a reduction of blood pressure (Kim *et al.*, 2013). It was found that patients with pulmonary hypertension had elevated ANP levels.

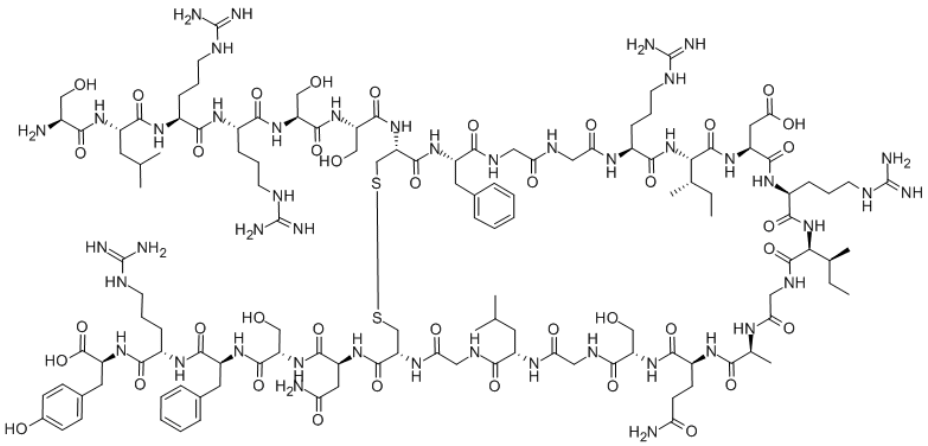


Figure 6.1. Structure of atrial natriuretic peptide (ChemicalBook).

A positive correlation between plasma ANP and PAP (pulmonary artery pressure) was found in patients with different types of congenital heart disease. A clinical study that was conducted in Finland concluded that low mid-regional ANP and N-terminal pro-BNP concentrations predicted type 2 diabetes development. A drop in natriuretic peptide levels are indicative of insulin resistance such as obesity. Low natriuretic peptide concentrations result in much faster blood glucose progression and prediction of diabetes development (Chao, Lv and Wang, 2017).

ANP consists of 28-amino acid and is mainly secreted by cardiac myocytes in the atria. ANP is also secreted in other tissues such as lungs, brain, and adipose tissue for local regulation. Plasma ANP has a half-live of ~2-3 min. This peptide is catalysed by circulating and cell-surface enzymes following binding to the specific natriuretic peptide receptors. ANP release is induced by a rise in atrial pressure and myocardial wall stress. ANP plays a vital role in decreasing the central venous pressure, inhibiting aldosterone secretion, and reducing sympathetic tone. Higher levels of ANP cause renal blood flow and dilation of afferent arterioles. Moreover, ANP in physiological levels inhibits tubular Na+reabsorption and increases water excretion (Nishikimi, Maeda and Matsuoka, 2006) (Ching *et al.*, 2017).

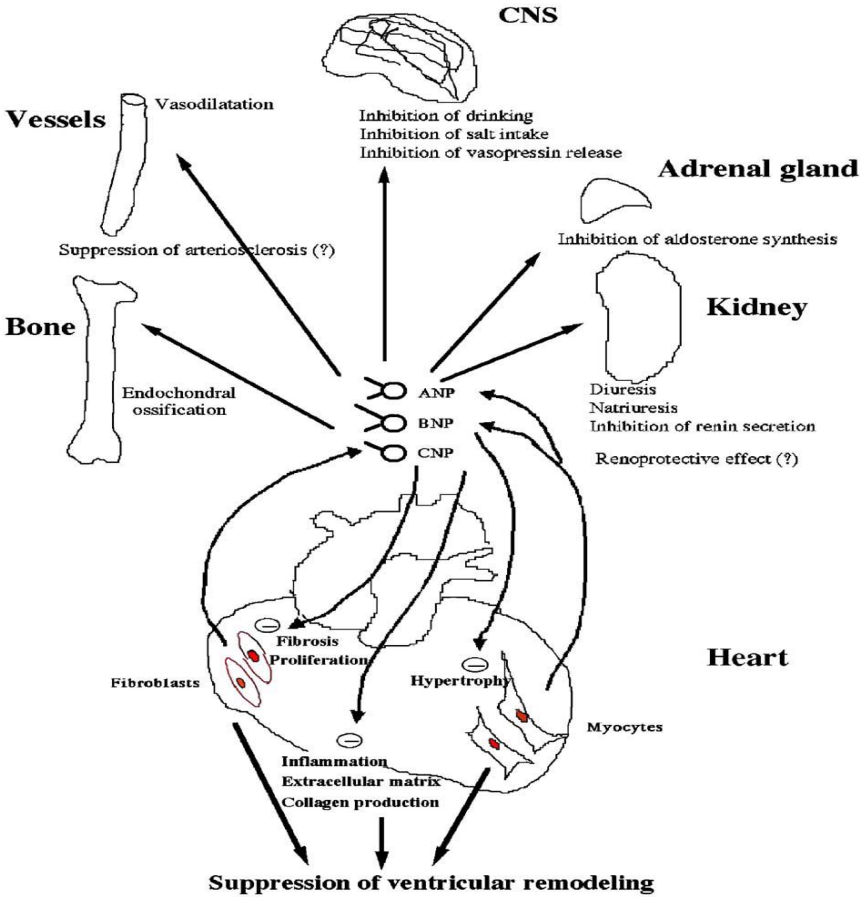


Figure 6.2. Action and mechanism of natriuretic peptides in cardioprotection (Nishikimi, Maeda and Matsuoka, 2006).

ANP and BNP are released as pre-pro-polypeptides. They are inactive proteins that are attached to an N-terminal signal peptide. In order for the ANP/BNP to be active, the N-terminal is cleaved in the endoplasmic reticulum. The proANP (126-amino acid peptide) is stored in cardiac atria granulae following removal of the signal peptide. The secretion of serine protease called corin is activated by elevated angiotensin II, vasoconstriction by endothelin and myocardial stretch. Corin cleaves inactive proANP into the active ANP. BNP activation occurs as in ANP. Pre-pro-polypeptide of BNP has 134-amino acids and the cleavage of the N-terminal signal peptide generates proBNP1-108. This compound is cleaved by the serine proteases furin and corin into inactive N-terminal-proBNP and active BNP1-32 following cellular stimulation (Lee and Daniels, 2016).

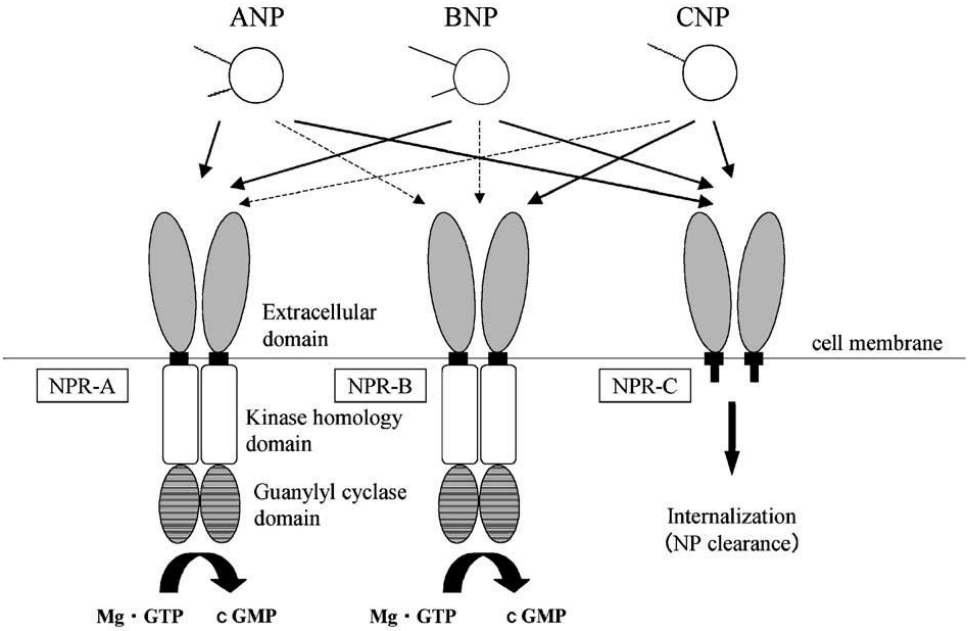


Figure 6.3. Plasma membrane receptors of natriuretic peptide (Nishikimi, Maeda and Matsuoka, 2006).

Natriuretic peptides have different binding affinities to three plasma membrane receptors namely NPR-A (GC-A), NPR-B (GC-B), and NPR-C. NPR-A binds both ANP and BNP, NPR-B binds CNP, and NPR-C binds all three peptides. NPR-A is guanylyl cyclase (GC-A), and binding of ANP and BNP leads to increased levels of cGMP (Nishikimi, Maeda and Matsuoka, 2006). NPR-A functions as a homodimer where two NPR-A bind one substrate molecule. NPR-A is highly expressed in the following tissues; renal arterioles, glomeruli, medulla, adrenal zona glomerulosa, endothelial cells, cerebellum, pituitary and adipose tissue. Low expression of NPR-A was observed in the heart and ileum (Ching *et al.*, 2017). The three natriuretic peptides are regarded as the promising reliable biomarkers for a variety of medical conditions including ischemic stroke (Barbato *et al.*, 2012).

Biomarkers are commonly used in the diagnosis of various diseases including stroke. Diseases can then be treated using a variety of techniques following a proper diagnosis. Carbon nanotubes (CNTs) are promising nanocarriers for the drugs to the point of interest. CNTs possess three important unique features namely large surface area, light weight, and hollow central cavity. These unique features render them ideal for neuro-engineering application. The ultrahigh high surface area is highly desirable for chemical surface modification of CNTs with distinguished therapeutic moiety. Multifunctional CNTs showed high potency in targeting of specific cells, tissues, and

imaging as well. The hollow tube like structure has the added advantages in drug delivery application (Akhter, 2018).

A spectrum of drugs can be encapsulated in their inner cavity, while other important molecules can be attached to the external walls to render them dispersible and biocompatible for targeting purposes. Based on this, we used ANP for targeting ischemic site in the brain in rats with induced stroke. Carbon nanotubes were used as nanocarriers for drug delivery in the brain as they possess unique characteristics including good electrical, penetration capability across cell layer barrier, high payload capacity, good thermal conductivity and large surface area for easy surface modification (Akhter, 2018).

In our study, we used multiwalled carbon nanotubes based on their unique physico-chemical structure to deliver the inflammatory drug dexamethasone to the ischemic site. Aligned multiwalled carbon nanotubes were used in this study as they possess improved physical and electrical properties for better interaction with other molecules. Since pristine carbon nanotubes are inert in the aqueous milieu, they were purified and functionalised with various acids. They were also acylated to ensure higher reactivity and PEGylated to prevent them from being opsonized by macrophages and to avoid cleavage by some enzymes as they travel in circulation to their destiny.

In this study, aligned multwalled carbon nanotubes were successfully synthesised, purified, acylated, PEGylated and coupled to FITC labelled dexamethasone and ANP for targeting of ischemic site in the rat brain.

6.2. Materials and methods

6.2.1. Synthesis of Aligned MWCNTs and morphological evaluation

Vertically aligned multiwalled carbon nanotubes were produced by Chemical Vapour Deposition (CVD) as in **Chapter 3 and 4** for the use in developing FITC-ANP-Dex-PEG-CNT complex for delivery of dexamethasone to ischemic stroke. The reaction vessel was activated with 40mL of 2,5 % ferrocene-toluene catalyst. A 95 % argon mixed with 5 % hydrogen were used as carrier gas and reducing gas respectively. The flow rate of carrier gas was set to 400 $mL.min^{-1}$ and synthesis time to 30 min at atmospheric pressure. Following completion of the reaction, MWCNTs deposited on

the quartz tube walls were collected and weighed. CNTs samples were prepared and analysed as in **Chapter 3 and 4**.

MWCNTs samples were coated with palladium-gold using sputter coater (Emitech K550X, Emitech Ltd, Kent, England) for 4 min at 25 mA and 2 x 10^{-1} mbar and scanned in FEI Nova NanoLab 600 FEG-SEM/FIB to determine their morphology and size. TEM samples were dispersed in ethanol, ultrasonicated for 10 min (20 kHz sonicator, VibraCell, Sonics and Materials, Inc., Danbury, CT, USA), loaded on a copper grids, dried, loaded into FEI Tecnai T12 TEM operating at 120 kV for scanning.

6.2.2. Purification, acid functionalization and acylation of Aligned MWCNTs

A volume of 350 mL of 3,14 g.L^{-1} of MWCNTs in conc HCl was prepared in a round bottom flask and refluxed at 60 °C for 24 hours in a fumehood. The solution was transferred to 1 L flask containing 650 ml ultrapure water. The mixture was filtered through the 0,45 µm filter until the filtrate pH was 7.

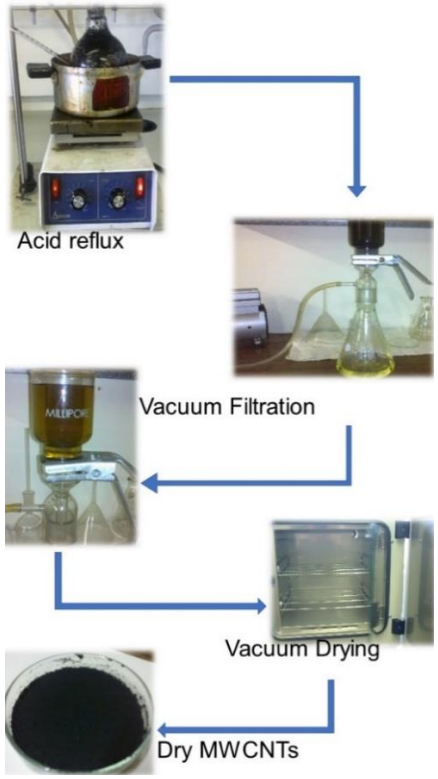


Figure 6.4. Purification steps of MWCNTs by acid reflux.

The filtrant was transferred to petri dish and dried for 24 hours in a dry vacuum oven. Following vacuum drying, the samples were weighed and transferred to a vial. MWCNTs were further refluxed in conc H_2SO_4 at 3,7 g.L^{-1} for 24 hours at 60 °C. The

reflux mixture was diluted with ultrapure water and centrifuged at 5 000 rpm. The pellet was resuspended in ultrapure water and filtered through 0,22 µm until the filtrant pH was 7. Dry functionalised MWCNTs were collected and weight recorded. The MWCNTs were also refluxed with HNO_3 and HNO_3:H_2SO_4.

The H_2SO_4:HNO_3 functionalized MWCNTs were resuspended in $SOCl_2$: DMF solution (20:1) and refluxed at 70 °C under N_2 for 24 hrs. The product was centrifuged at 5 000 rpm for 20min (Eppendorf Centrifuge, 5804, Germany) and the precipitates washed with tetrahydrofuran (THF) at 5 000 rpm for 20 min until the supernatant was crystal clear. The acylated carbon nanotubes (COCl-MWCNTs) were then dried in a vacuum oven at 70 °C for 24 hrs (Trade Raypa Espinar, Barcelona)**.**

6.2.3. Dexamethasone loading to PEG- MWCNTs, FITC labelling and ANP conjugation to FITC labelled PEG-MWCNTs

Following acylation of the CNTs, a solution of 1 $mg.mL^{-1}$ of dexamethasone phosphate-21 was prepared by dissolving 1 mg of dexamethasone in 1mL of deonised water. Dexamethasone (50 $\mu g.mL^{-1}$) was reacted with PEG-MWCNTs in a 5:1 ratio for 24 hours at room temperature. The mixture was centrifuge at 3 500rpm and supernatant was collected, and pellet discarded.

A fresh solution of 1 $mg.mL^{-1}$ of FITC was prepared by dissolving 1mg of FITC in 1 mL of DMSO. This solution was then reacted with Dex-MWCNTs in a ratio of 1:10 at 4 °C for 12 hours in the dark covered with aluminium foil paper as depicted in **Fig. 6.3**. The mixture was dialysed against fresh ultrapure water for 3 days to obtain FITC labelled PEG-MWCNT (**Fig. 6.3**). A volume of 0,3 ml of 10 $mg.mL^{-1}$ SMCC in DMSO was added to 5mL FITC-Dex-PEG-MWCNTs. To this solution, 0,6 mL of 10 x PBS was added and the reaction was incubated for 2 hours at room temperature. Approx. 100 µl ANP (1:200), 500 µl of 10 x PBS and 20 µL of 0,5 M EDTA were added and the mixture was incubated at 4 °C for 24 hours.

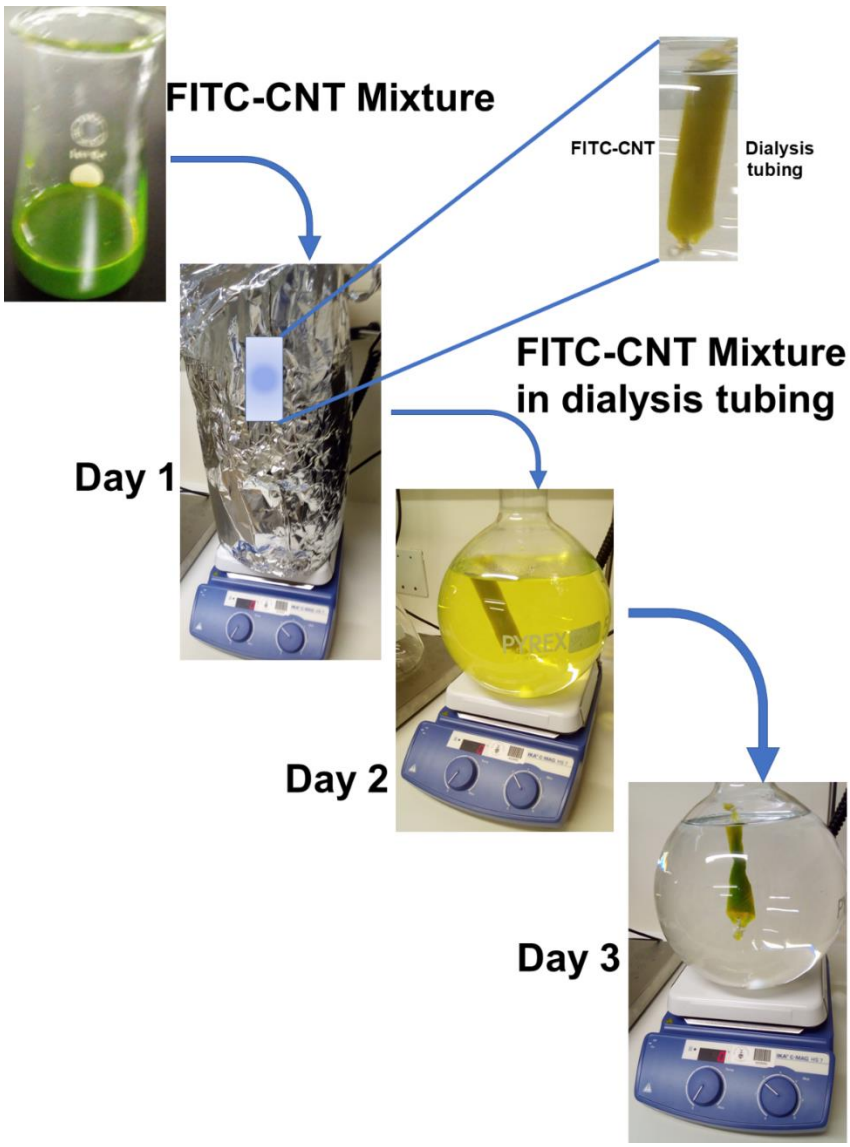


Figure 6.5. FITC labelling of PEG-MWCNTs.

6.2.4. Raman Spectra of the functionalised MWCNTs

Functionalised MWCNTs were analysed using Raman Micro200 (Perkin Elmer, UK). Spectra were collected using laser beam of 785 nm wavelength with maximum output of 250 mW from 200 to 2 500 cm^{-1} at 4 cm^{-1} resolution. Samples were placed on quartz slides on the microscope stage and the focus adjusted to obtain the best image using objective 50 x and 20 x under the bright field. Scanning was performed under the dark field.

6.2.5. Determination of Molecular and Vibrational Transitions of FITC labelled DEX-PEG-MWCNTs

FTIR analysis was performed as in **Chapter 3 and 4**. KBr was mixed with MWCNTs, ground to fine particles, loaded on KBr die and pressed at 4-ton pressure under vacuum for 15 min with KBr press (ICL, International Crystal Labs, Garfield, USA) to produce circular KBr pellet. The pellet was scanned with Perkin Elmer Spectrum 2000 FTIR spectrometer (PerkinElmer Spectrum 100, Llantrisant, Wales, UK) at a resolution of 4 cm^{-1} with 10 accumulations with wavenumbers ranging from 4,000 – 400 cm^{-1}. For aqueous samples, ATR was used for the collection of IR spectra.

6.2.6. Uv-Vis and fluorescence evaluation in the functionalised MWCNTs

Functionalised MWCNTs suspended in water were ultrasonicated prior to scanning. Uv-Vis spectra were measured with a Shimadzu UV2450 spectrometer using a scanning range from 190 to 1 100 nm at room temperature. Excitation and emission scans of the MWCNTs were collected by LS45 Perkin Elmer fluorescence spectrometer with scan range from 200 nm to 800 nm. Fluorescence was also determined by Aqualog FEEM spectrometer (Horiba Scientific, USA).

6.3. Results and discussion

6.3.1. Surface morphological evaluation of MWCNTs

Vertically aligned multiwalled carbon nanotubes were successfully synthesised as demonstrated in **Fig.6.6**. The orientation and type of carbon nanotubes were confirmed by SEM and TEM (**Fig. 6.6B-C**).

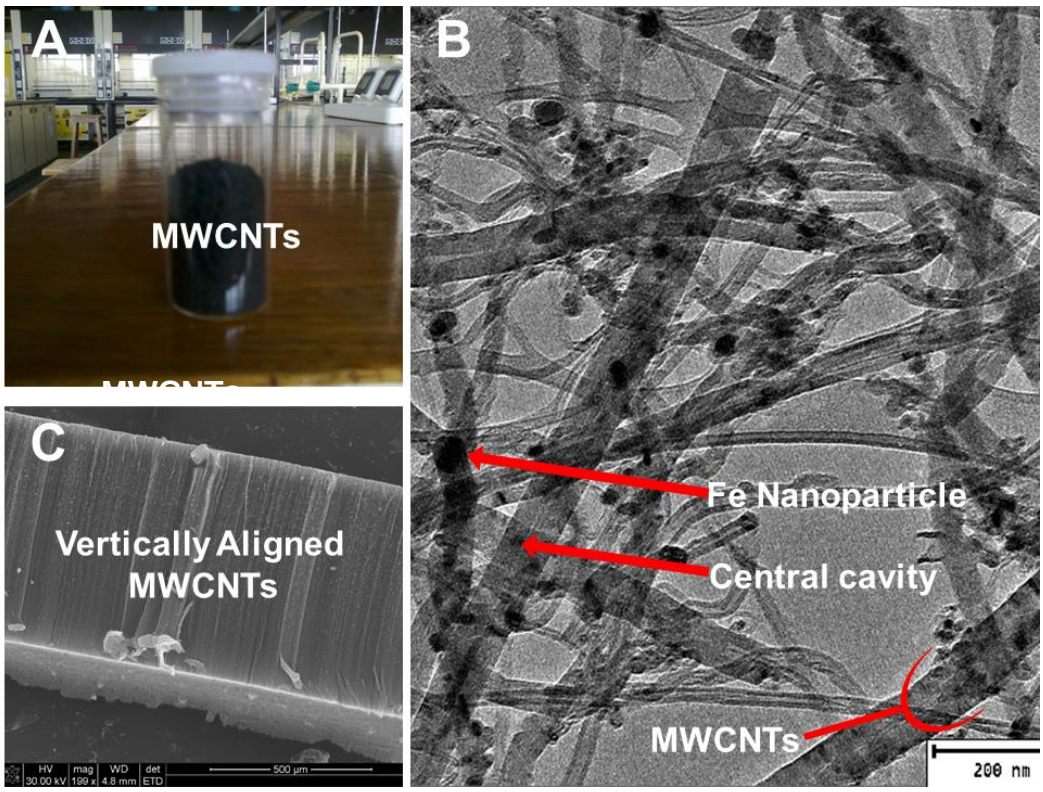


Figure 6.6. Aligned multiwalled carbon nanotubes. MWCNTs harvested from quartz tube wall (A), TEM micrograph of MWCNTs with Fe nanoparticle inside the cavity (B) and SEM micrograph of aligned multiwalled carbon nanotubes (C).

A very thin layer of iron nanoparticles on the top surface of the nanotubes was observed and this could be due to the iron nanoparticles from the catalyst (**Fig.6.6B**). The carbon nanotubes consisted of more than one layer confirming the multiwalled structure and the cavity was observed at the centre with iron nanoparticle inside as confirmed by TEM (**Fig.6.3B**) (Komane *et al.*, 2018).

6.3.2. FTIR assessment of the functionalised MWCNTs

The loading of FITC and ANP had a greater impact on the optical properties of Dex-PEG-CNTs. As demonstrated in **Fig.6.7**, dex peg cnt was found to have four peaks (3410 nm = hydroxyl functional group, 2086 nm = C≡C, 2114 nm = C≡C, 1636 nm = C=C, 790 nm = fingerprint, 799 nm = C-H, 755 nm = C-H). Peak intensity of 1636 and 755 nm in dex peg cnt dropped when FITC was coupled to dex peg cnt which implied that the original functional group was replaced by a new one with less intensity.

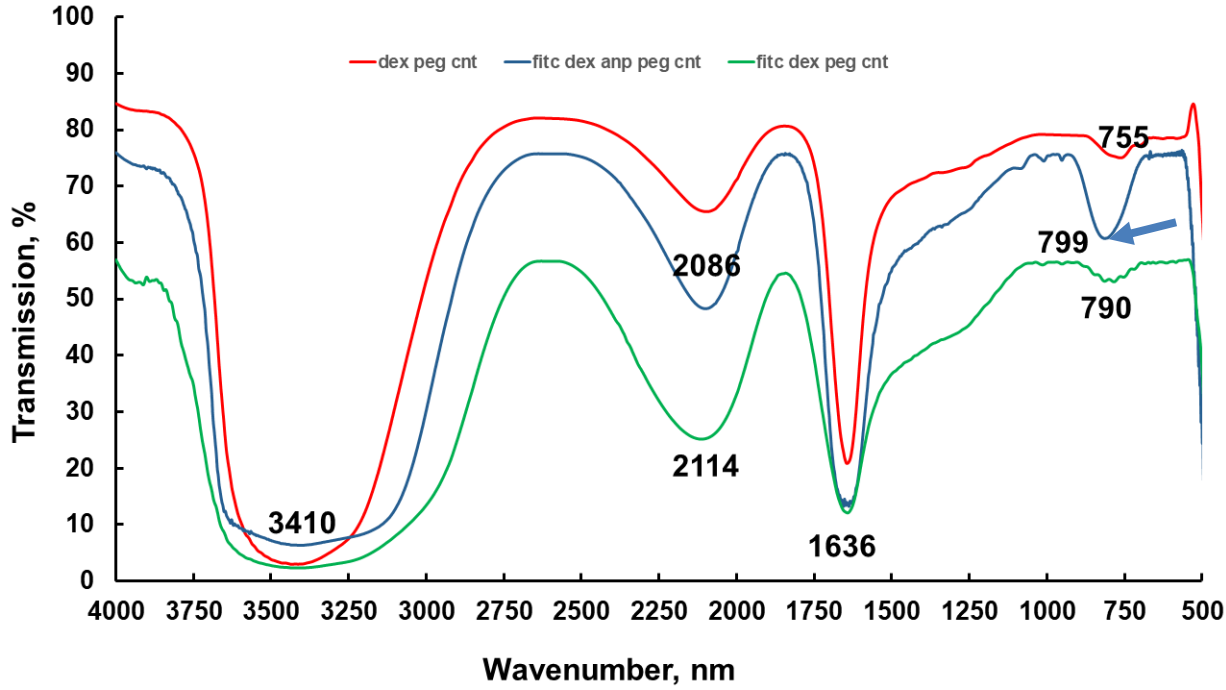


Figure 6.7. FTIR spectra of functionalised PEGylated MWCNT in deionised water.

The intensity of the peak at 1636 nm in dex peg cnt increased when FITC and ANP were coupled to dex peg cnt implying that the functional group increased in size (more of the same group added). The intensity of peak at 755 nm in dex peg cnt increased and became broader and shifted to the left to 799 nm as ANP was coupled to the complex which implied that a new bond was formed due to the addition of ANP (**Fig. 6.7**) (*see blue arrow*).

The peak at 799 nm in FITC-ANP-PEG-CNTs was very prominent compared tp the rest. The peak at 3410 nm had a higher intensity in Dex-PEG-CNTs. In FITC-DEX-PEG-CNT, the peak became weaker and broader as a result of loading of FITC to Dex-PEG-CNT. The intensity and strength of the FITC-Dex-PEG-CNT at 3410 nm was moderate between that of the Dex-PEG-CNT and FITC-Dex-PEG-CNT. In general, this peak was broader and most prominent and was due to the water used as a dispersant for dispersing the functionalised CNTs.

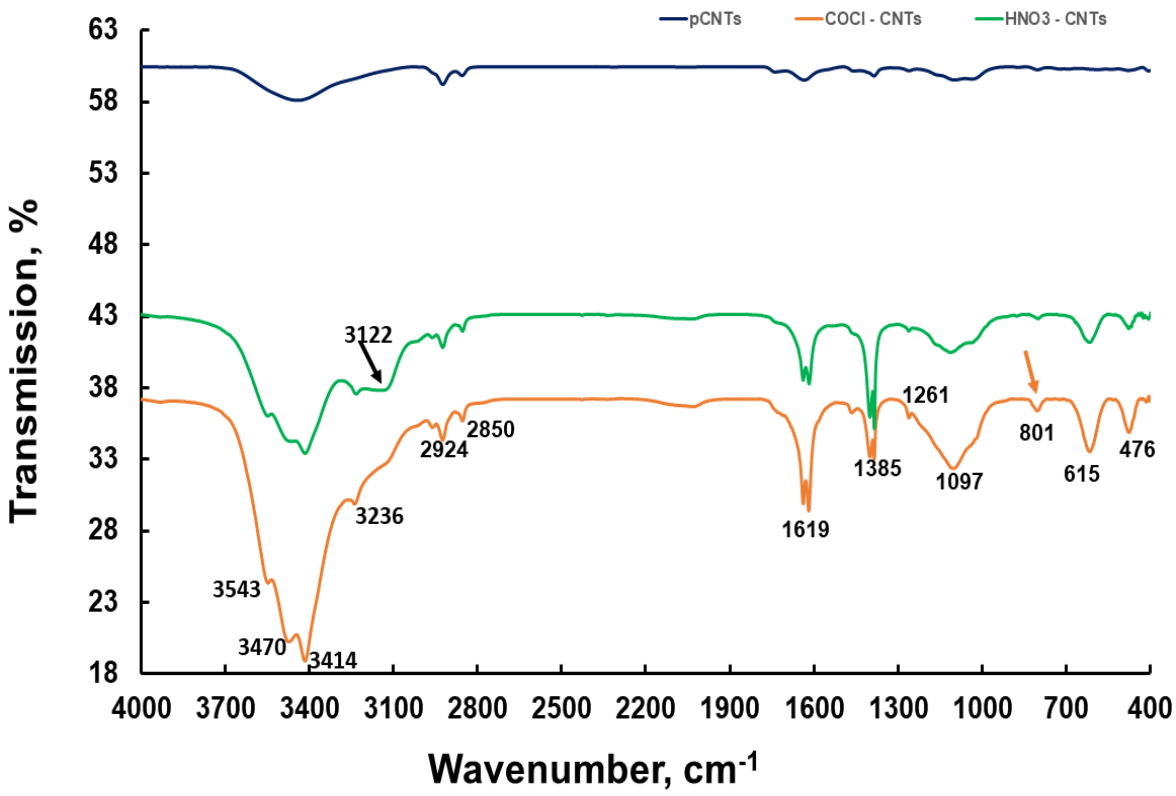


Figure 6.8. FTIR spectra of functionalised MWCNTs (KBr pellets). A circle and arrow indicating an additional peak in $SOCl_2$ functionalised MWCNTs.

In pristine multiwalled carbon nanotubes, the intensity of the major peaks is very low and has 60,5 % transmission as there is no interaction of light with other molecules. The intensity of the major peaks of pristine multiwalled carbon nanotubes increased when carbon nanotubes were functionalised with $SOCl_2$ and HNO_3. There was also a reduction in transmission percentage to 43 % for HNO_3 treated and 37 % for $SOCl_2$ treated MWCNTs.

An additional peak was observed at 801 nm in $SOCl_2$ functionalised MWCNTs. The reduction in transmission percentage and increase in the intensity of the peaks confirmed the interaction of MWCNTs with the functional groups. The peak at 801 nm in $SOCl_2$ confirmed the C-H functional group as demonstrated in **Fig. 6.8** (orange arrow). A peak at 3122 nm was observed in CNTs that were treated with HNO_3 as illustrated in **Fig.6.8** (black arrow). This peak was due to the presence of the aromatic C-H group in CNTs treated with HNO_3.

The following peaks were observed in both $SOCl_2$ and HNO_3 treated CNTs; 3543, 3470, 3414 and 3236 cm^{-1}. These peaks were due to the O-H group from the water during CNT solution preparation. The peaks at 2924 and 2850 nm were due to the C-

H functional groups during a chemical reaction between CNTs and $SOCl_2$ and HNO_3. The peaks that were observed at 1619, 1385, 1261, 1097 cm^{-1} were due to the C=C, C-H, C-C and C-O functional groups respectively. In addition, the peaks that were observed at 615 and 476 cm^{-1} were due to C-Cl groups (**Fig.6.8**). Our findings confirm the successful functionalisation of the MWCNTs with HNO_3 and $SOCl_2$.

6.3.3. Raman evaluation of the functionalised MWCNTs

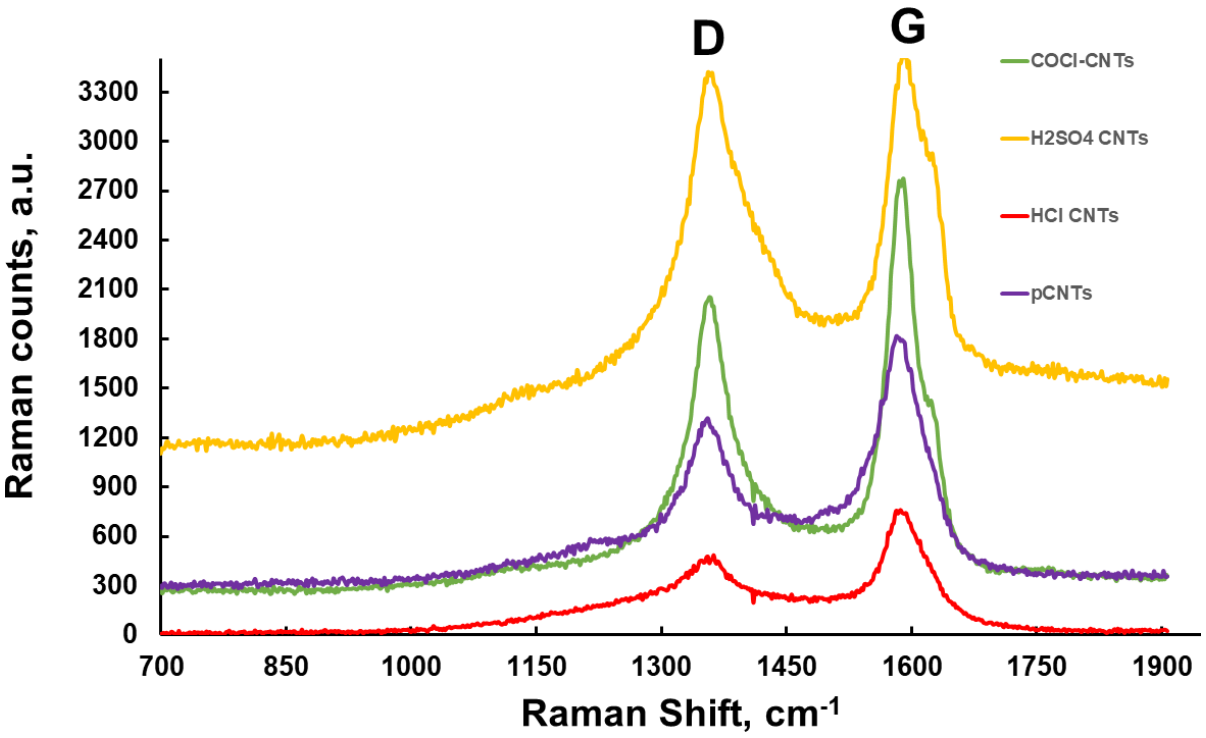


Figure 6.9. Raman spectra of the functionalised multiwalled carbon nanotubes.

Raman analysis was performed in the functionalised MWCNTs using Raman Micro200. The D and G bands were observed at 1362 and 1568 nm respectively. As depicted in **Fig.6.9**, the G (graphene or graphite-like) band intensity is higher than the D (defect or disorder induced) band intensity implying that the multiwalled carbon nanotubes were pure and even purer following purification and functionalization with HCl, $SOCl_2$ and H_2SO_4. MWCNTs functionalised with H_2SO_4 had the highest intensity compared to the rest. In addition, the H_2SO_4 treated MWCNTs had approximately the same G and D band intensities. This is an indicative that the sulphuric acid functionalisation may have caused a defect in the structure of the CNTs as illustrated by an increase in the D band intensity. The intensity of the $SOCl_2$ functionalised MWCNTs was greater than that of the pristine and HCl treated MWCNTs (**Fig.6.9**). Our results agree with the results of Le and colleagues (Bardi *et al.*, 2013).

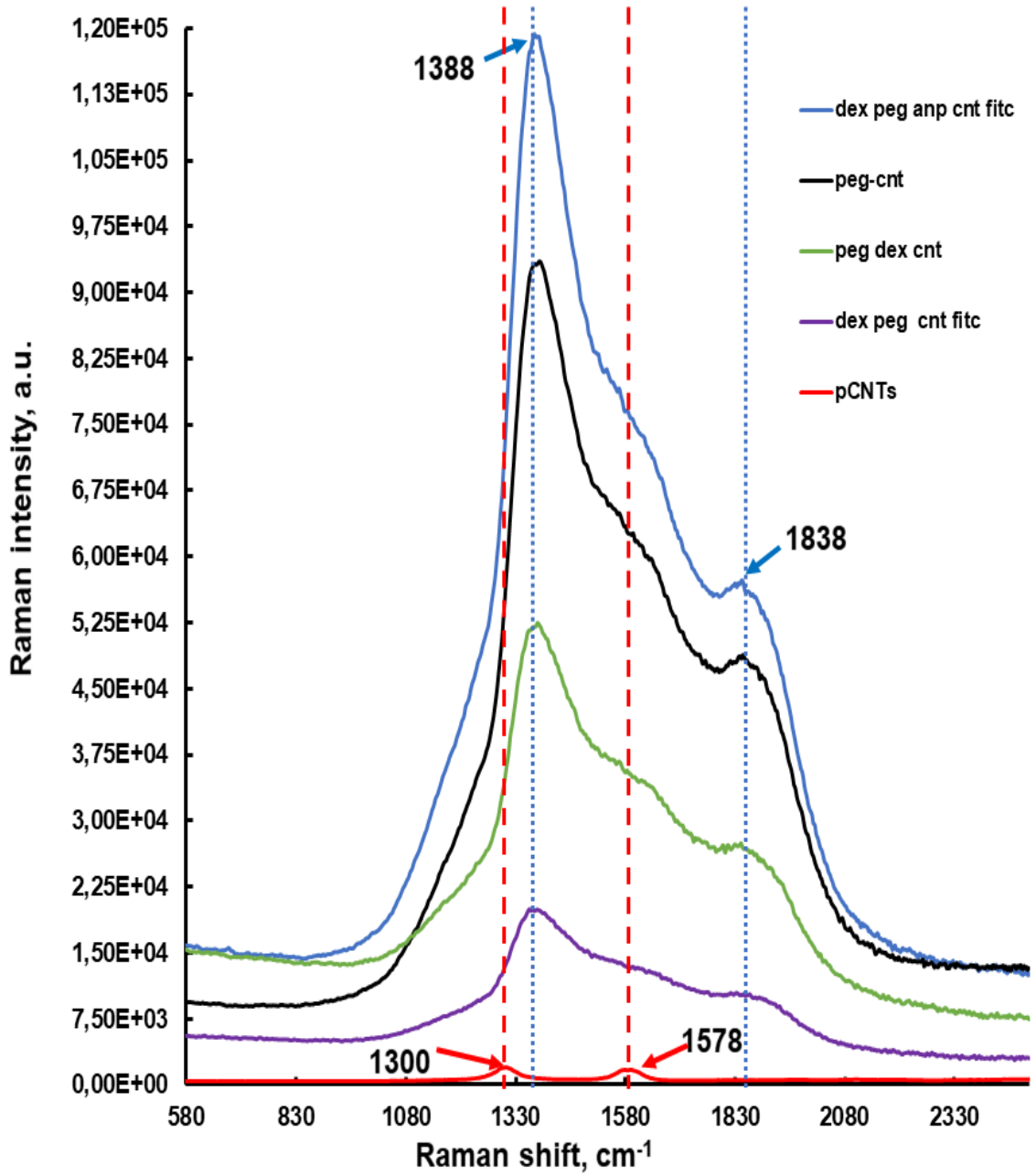


Figure 6.10. Raman spectra of the functionalised PEGylated MWCNTs. Pristine MWCNTs (A). Functionalised MWCNTs (B).

Raman analysis was also done in the MWCNTs that were functionalised with PEG, Dex, FITC and ANP to confirm their attachment to MWCNTs. The pristine MWCNTs has two bands namely D and G. The D (defect or disorder induced) band and G (graphene or graphite like) band at 1342 and 1580 cm^{-1} respectively. The D band is activated by disorders in the carbon systems. The G band with a shoulder around 1604 cm^{-1} is due to the in-plane vibration of the C-C bond in the CNTs (Bokobza and Zhang, 2012).

In our study, the D and G band in the pristine MWCNTs were observed at 1300 and 1578 cm^{-1} respectively. Bokobza and colleagues found that all the Raman bands shifted to the higher wavenumbers when raw bundled carbon nanotubes were dispersed in cyclohexane (Bokobza and Zhang, 2012). The Raman intensity was very low for both the D and G bands compared to the functionalised CNTs as the CNTs were intact and there were no chemical interruptions within the CNT structure. The intensity for both the D and the G band for the pristine MWCNTs was $1,87x10^3$ and $1,63x10^3$ respectively. (**Fig. 6.10**).

Table 6.1. Band shifts and intensities with the degrees of functionalisation.

MWCNT type	**D band intensity** $x10^3$	**G band intensity** $X10^3$	**Level of intensity increase** D band	G band
Pristine CNTs	1,18	1,63	-	-
FITC-Dex-PEG CNTs	19,60	9,81	10x	6x
Dex- PEG -CNTs	51,30	26,60	27x	16x
PEG-CNTs	92,30	47,80	49x	29x
FITC-ANP-Dex-PEG-CNTs	118	55,60	63x	34x

Following functionalisation with various molecules, both bands shifted to the right as depicted in **Fig 6.10**. Furthermore, the bands were widened and the resolution between these two bands was affected significantly. The D band intensity increased astronomically compared to the G band intensity (**Fig.6.10, Table 6.1.)**. Functionalisation increased the D band intensity of the pristine CNTs in FITC-Dex-PEG-CNTs, Dex-PEG-CNTs, PEG-CNTs and FITC-ANP-Dex-PEG-CNTs by 10x, 27x, 49x and 63x respectively. Moreover, the G band intensity of the pristine band in FITC-Dex-PEG-CNTs, Dex-PEG-CNTs, PEG-CNTs and FITC-ANP-Dex-PEG-CNTs were increased by 6 x, 16 x, 29 x and 34 x respectively as illustrated in **Table 6.1**.

These changes could be due to the covalent and non-covalent bonds that were generated during the chemical reactions taking place between the CNTs and the added molecules. The broadening and change in intensity confirmed the interaction between MWCNTs and new functional groups added to the CNTs.

6.3.4. Uv-Vis scanning and FEEM evaluation of the FITC Dex PEG ANP CNTs

Pristine carbon nanotubes are hydrophobic, and they were non-soluble in water as a result (**Fig. 6.11A**). Functionalisation degree and the type of solvent have a greater impact on their dispersibility in aqueous milieu. HCl treated CNTs were slightly soluble in water (**Fig.6.11B**). H_2SO_4.HNO_3 and $SOCl_2$ functionalised carbon nanotubes were readily soluble in water as demonstrated in **Fig.6.11C-D**. Functionalised CNTs were PEGYlated and dexamethasone loaded on them. They were resuspended in deionised water and sonicated for 5min prior to Uv-Vis analysis.

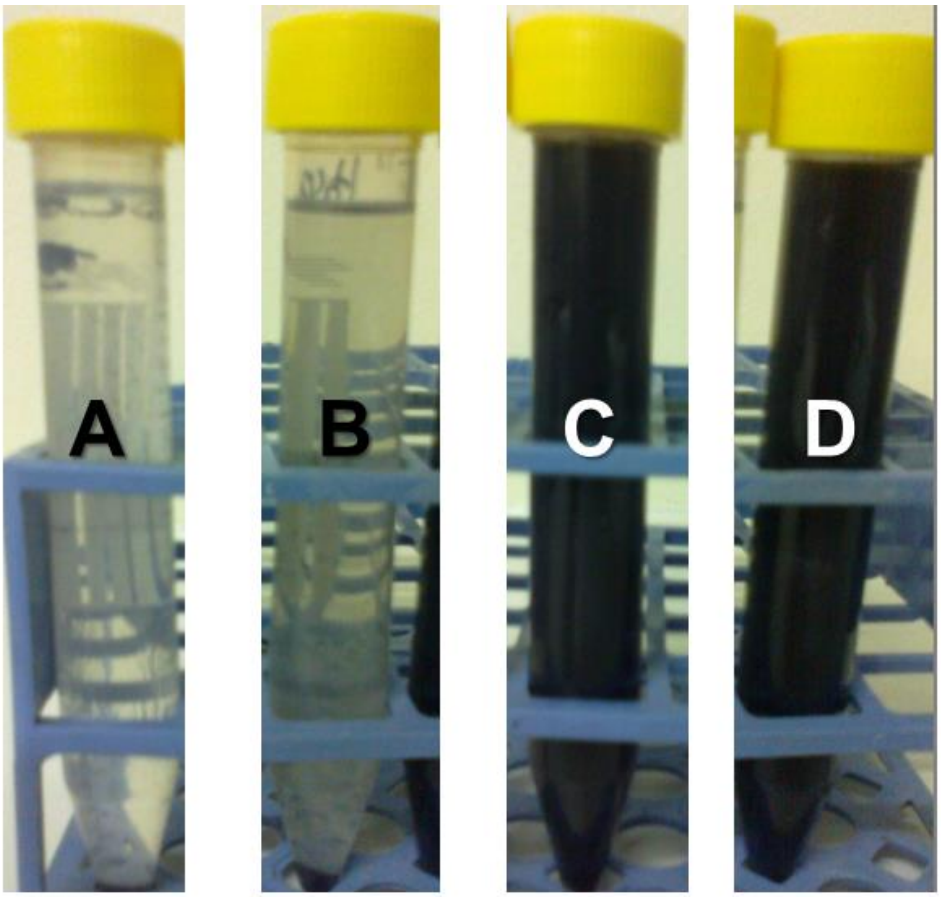


Figure 6.11. Dispersibility of the functionalised CNTs in water. Pristine CNTs (A). HCl treated CNTs (B). H_2SO_4.HNO_3 treated CNTs (C) and $SOCl_2$ treated CNTs (D).

The optimal wavelength at which pristine aligned MWCNTs absorbed light was found to be 194 nm. In the PEG-CNTs and Dex-PEG-CNTs, the optical wavelengths were 225 nm and 245 nm respectively. An additional peak at 265 nm was observed in PEG-CNTs. The optical wavelength was shifted to the right of the pristine CNTs but within the UV range when CNTs were functionalized with PEG and Dex as depicted in **Fig. 6.12**.

PEG-4-arm and Dex optical wavelength were found to be 201 nm and 242 nm respectively. Our results agree with the data of Roozbahani and colleagues. They encapsulated Dex into laponite nanoplatelets and performed Uv-Vis scanning on Dex, Dex encapsulated nanoplatelets and Dex free nanoplatelets. They observed a peak at 242 nm in Dex and Dex encapsulated nanoplatelets. This peak was not observed in Dex free nanoplatelets. This is an indicative that Dex was successfully encapsulated in their nanoplatelets (Roozbahani, Kharaziha and Emadi, 2017).

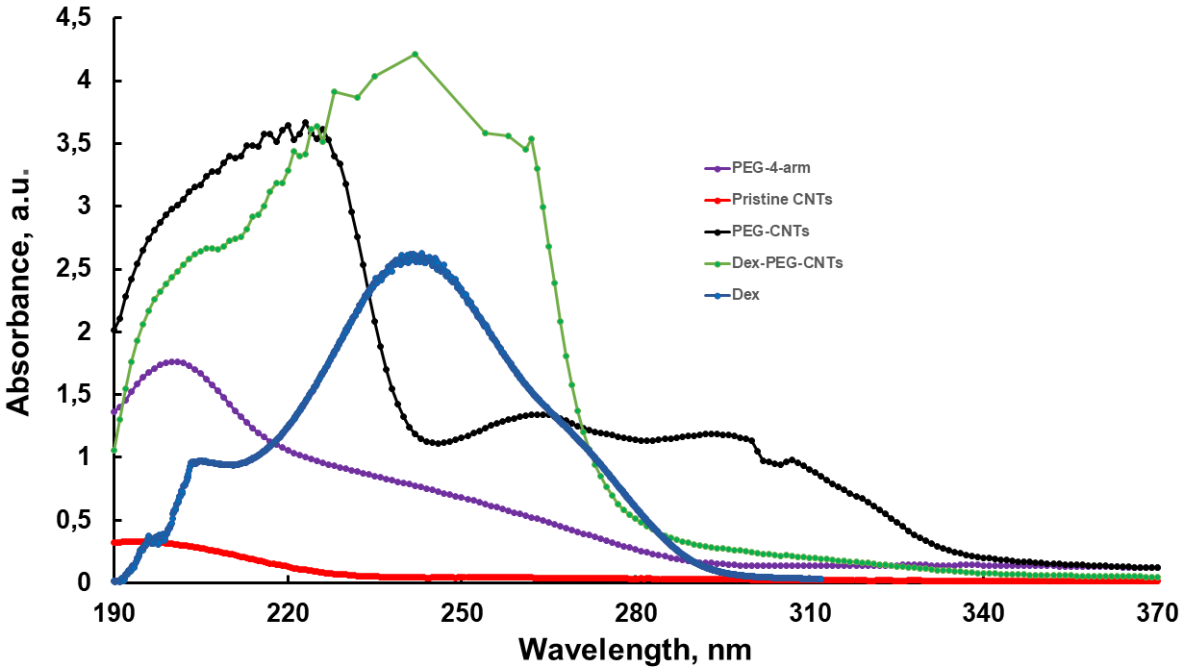


Figure 6.12. Uv-Vis spectra of PEG-CNTs and Dex-PEG-CNTs.

In our study, the peak of Dex around 242 nm was observed in Dex standard and Dex-PEG-CNTs. This peak was not observed in pristine CNTs and Dex free PEG-CNTs. Functionalization changed the optical behaviour of the CNTs. The increase in absorbance could be due to the functional groups (carboxylic and acyl groups) that are added to MWCNTs and the size of the particles. These findings have demonstrated the effect of functionalization of the CNTs on their optical properties. The optimal wavelength increased with functionalization of the CNTs as depicted in **Fig.6.12**.

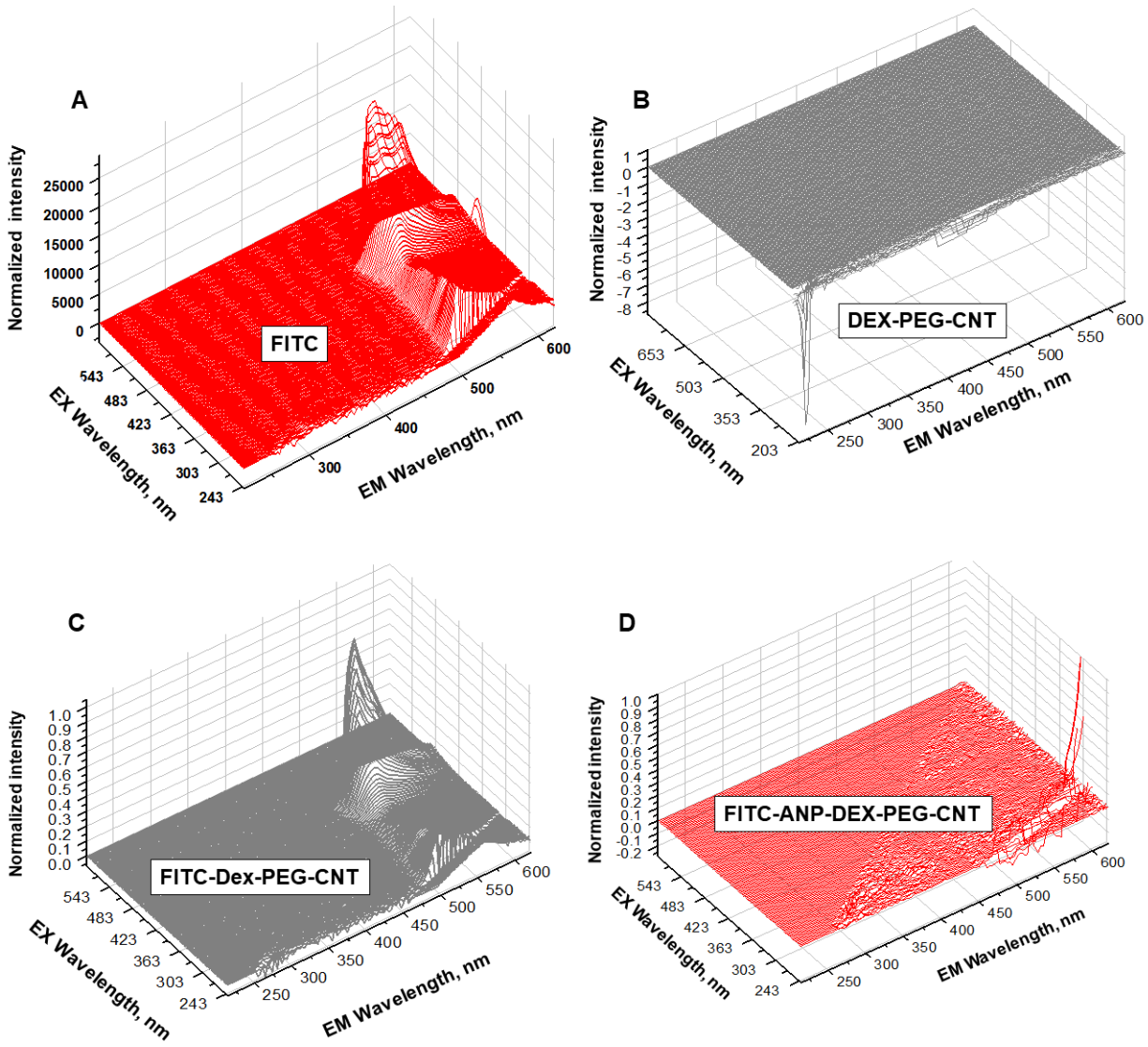


Figure 6.13. FEEM spectra of the functionalised PEGylated MWCNTs. FITC (A), DEX-PEG-CNT (B), FITC-DEX-PEG-CNT (C) and FITC-DEX-PEG-CNT-ANP (D).

The functionalised MWCNTs were scanned using Aqualog Horiba FEEM. Maximum excitation wavelength for FITC was observed at 490 nm and emission at 550 nm as depicted in **Fig. 6.13A.** Fluorescence was not detected in DEX-PEG-CNT as this complex was not labelled with a fluorescent tag (**Fig.6.13B**). Maximum excitation and emission wavelengths in FITC-DEX-PEG-CNT complex were observed at 490 nm and 550 nm respectively **(Fig. 6.13C**). When ANP was coupled to FITC-DEX-PEG-CNT, excitation and emission where observed at 303 nm and 550 nm respectively but with very low intensity (**Fig. 6.13D**). The interaction of ANP with the FITC-PEG-CNTs seemed to have affected the fluorescence of the fluorescent tag. The fluorescence intensity was very low in this complex.

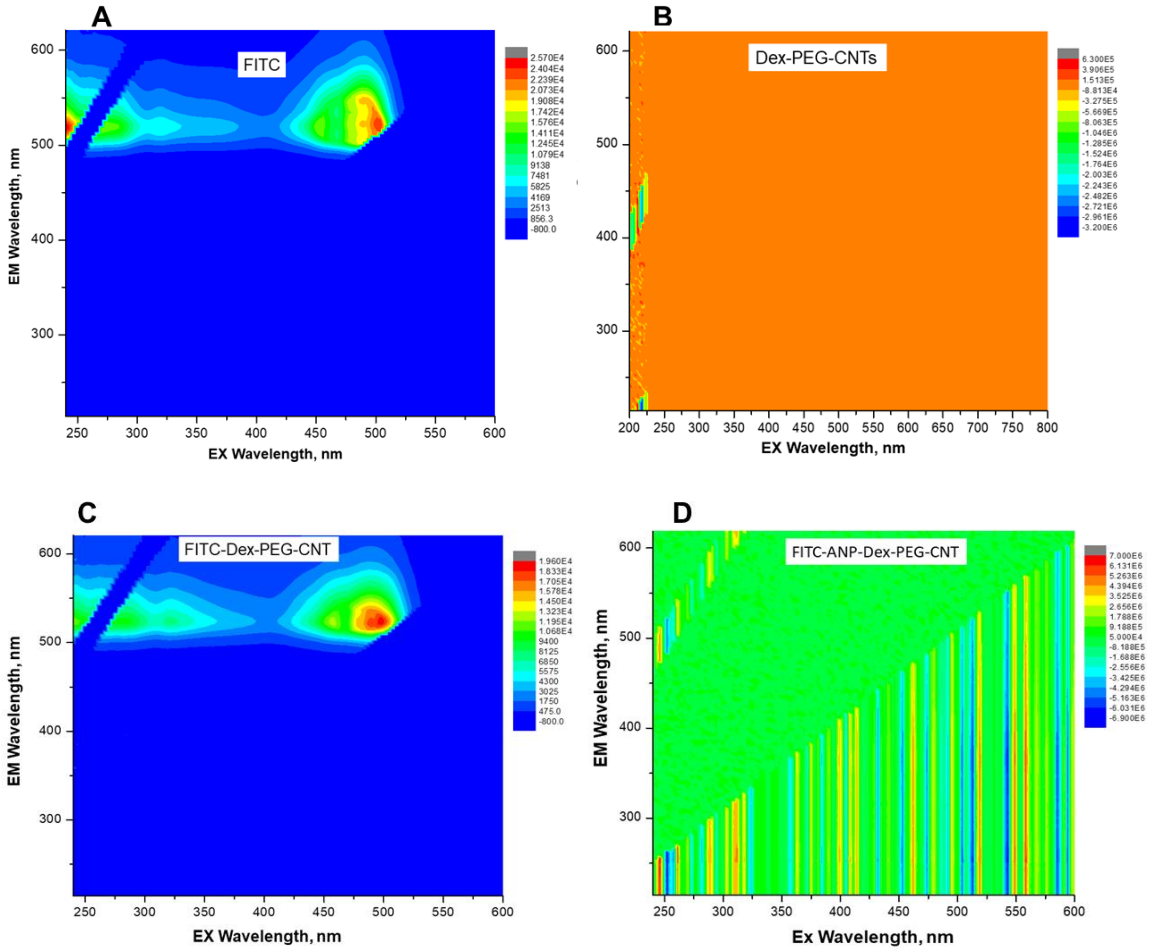
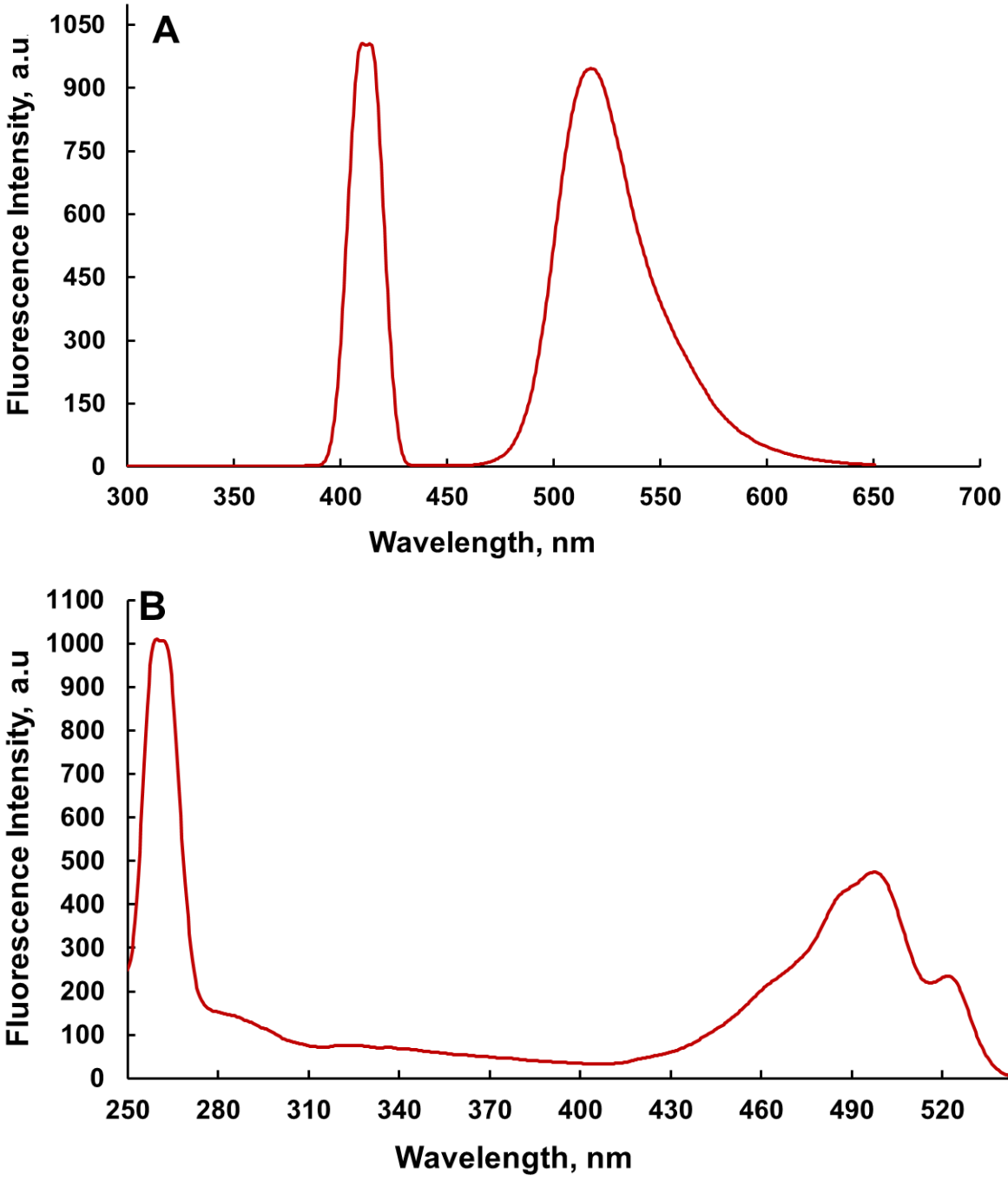


Figure 6.14. Contour maps showing the fluorescence intensities of FITC only and the functionalised MWCNTs. FITC (A). Dex-PEG-CNT (B). FITC-Dex-PEG-CNT (C). FITC-ANP-Dex-PEG-CNT.

Moreover, contour maps were also used to confirm the loading of the fluorescent tag to the carbon nanotubes as illustrated in **Fig. 6.14**. FITC excitation wavelength and emission wavelength were found to be 490 nm and 520 nm respectively (**Fig. 6.14A**). Dex-PEG-CNTs did not express any fluorescence since there was no FITC labelling in this complex (**Fig. 6.14B**). In FITC-Dex-PEG-CNT, the excitation was at 490 nm and emission at 520 nm as a result of FITC that was attached to Dex-PEG-CNTs (**Fig. 6.14C**). The contour map of the FITC-ANP-Dex-PEG-CNTs did not give a clear indication of the fluorescence. The formation of bonds between the ANP and FITC-PEG-CNT might have an impact on the FITC and affected its fluorescence to a certain extent as a result (**Fig.6.14D**). These findings confirmed the successful loading of FITC to Dex-PEG-CNTs-ANP.

6.3.5. Fluorescence evaluation of FITC DEX PEG ANP CNT

The functionalised CNTs were labelled with FITC to prepare them for easy tracking in different organs of the animal following intravenous injection. FITC is attached directly to the amino groups of the carbon nanotubes or amino groups of the DSPE-PEG5000-4-arm-(PEG-Amine) attached to CNTs or both.



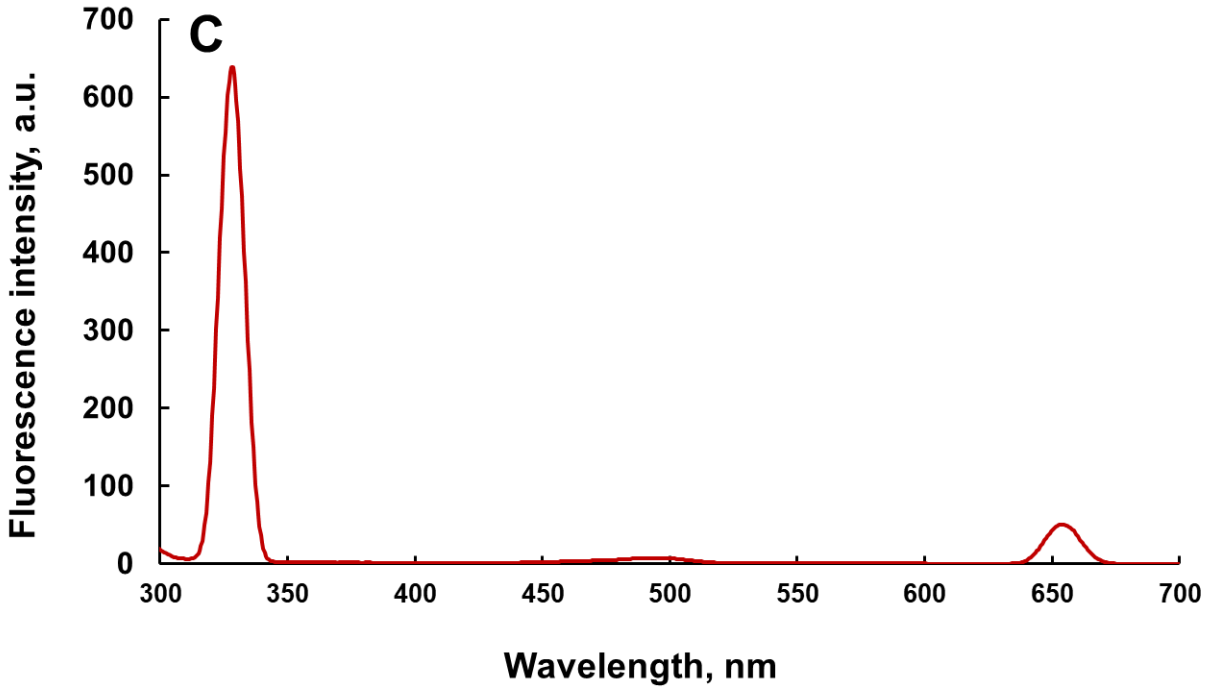


Figure 6.15. Fluorescence spectra of functionalised PEGylated MWCNTs. FITC (A). FITC-DEX PEG-CNT (B). FITC-DEX-PEG-CNT-ANP (C).

In our study, FITC excitation wavelength and emission wavelength were found to be 415 nm and 520 nm respectively using the LS45 Perkin Elmer Fluorescence Spectrometer as depicted in **Fig.6.15A**. DEX-PEG-CNT was fluorescently labelled with FITC and the excitation wavelength and emission wavelength were 263 nm and 500 nm respectively **Fig.6.15B**. When ANP was coupled to FITC-DEX-PEG-CNT, excitation and emission wavelength were shifted to the right to 330 nm and 660 nm respectively as a result of an interaction of ANP with the complex **Fig.6.15C**. These findings have demonstrated a successful loading of FITC to Dex-PEG-CNTs and Dex-ANP-PEG-CNTs.

6.4. Conclusion remarks

Vertically aligned MWCNTs were successfully synthesised and functionalised with $SOCl_2$. The CNTs were further PEGYlated and coupled to dexamethasone. The complex was successfully labelled with FITC and ANP was also attached to the complex. Following characterisation of the synthesised, purified and functionalised complex, our findings have demonstrated a successful development of a nanocarrier equipped with highly relevant molecules with specific functions that have a potential to be applied in delivering dexamethasone to the diseased site in neurological or other diseases.

6.5. References

Akhter, M. H. (2018) ‘Carbon Nanotube : A Drug Delivery Platform in Neurological Disorder’, *Acta Scientific Pharmaceutical Sciences*, 2(7), pp. 60–61.

Barbato, E. *et al.* (2012) ‘NT-proANP circulating level is a prognostic marker in stable ischemic heart disease.’, *International journal of cardiology*, 155(2), pp. 311–2.

Bardi, G. *et al.* (2013) ‘Functionalized carbon nanotubes in the brain: Cellular internalization and neuroinflammatory responses’, *PLoS ONE*, 8(11). doi: 10.1371/journal.pone.0080964.

Bokobza, L. and Zhang, J. (2012) ‘Raman spectroscopic characterization of multiwall carbon nanotubes and of composites’, *Express Polymer Letters*, 6(7), pp. 601–608.

Chao, W. Z., Lv, C. Y. and Wang, Y. (2017) ‘Effect of Salt Intake on Serum Glucagon-Like Peptide-1 Levels in Normotensive Salt- Sensitive Subjects’, *Kidney Blood Pressure*, 710061(277), pp. 728–737.

Ching, P. *et al.* (2017) ‘The renal and cardiovascular effects of natriuretic peptides’, *Advances in Physiology Education*, 41, pp. 179–185.

Kim, M. *et al.* (2013) ‘GLP-1 receptor activation and Epac2 link atrial natriuretic peptide secretion to control of blood pressure’, *Nature Medicine*, 19(5), pp. 567–575.

Kim, S. O. O. M. I. *et al.* (2014) ‘Dendroaspis natriuretic peptide is degraded by a metalloproteinase in the rat kidney’, *Molecular Medicine Reports*, 9, pp. 1037–1043.

Komane, P. P. *et al.* (2018) ‘Dexamethasone-loaded, pegylated, vertically aligned, multiwalled carbon nanotubes for potential ischemic stroke intervention’, *Molecules*, 23(6).

Lee, N. S. and Daniels, L. B. (2016) ‘Pathophysiology Current Understanding of the Compensatory Actions of Cardiac Natriuretic Peptides in Cardiac Failure : A Clinical Perspective A Clinical Perspective on CNPs in Cardiac Failure’, *Cardiac Failure Review*, 2(1), pp. 14–19.

Nishikimi, T., Maeda, N. and Matsuoka, H. (2006) ‘The role of natriuretic peptides in cardioprotection’, *Cardiovascular Research*, 69(2), pp. 318–328.

Roozbahani, M., Kharaziha, M. and Emadi, R. (2017) ‘pH sensitive dexamethasone encapsulated laponite nanoplatelets : Release mechanism and cytotoxicity’, *International Journal of Pharmaceutics*, 518(1–2), pp. 312–319.

Sah, J. P. and Salahuddin, M. (2016) ‘Atrial Natriuretic Peptide : A potential serum marker for diagnosis of type two Diabetes Mellitus’, *RESEARCH JOURNAL OF MEDICINE AND MEDICAL SCIENCES*, 11(1), pp. 22–27.

Syndrome, M. *et al.* (2014) ‘Metabolic Actions of Natriuretic Peptides and Therapeutic Potential in the Pharmacology & Therapeutics Metabolic actions of natriuretic peptides and therapeutic potential in the metabolic syndrome’, *Pharmacology and Therapeutics*.

CHAPTER 7

ANP LEVELS AND BIODISTRIBUTION OF INTRAVENOUSLY ADMINISTERED PEGYLATED ALIGNED MULTIWALLED CARBON NANOTUBES DECORATED WITH DEXAMETHASONE IN ISCHEMIC STROKE SPRAGUE DAWLEY RATS

Abstract

Here, we report successful VA-MWCNT synthesis, purification and functionalisation prior to coupling with a fluorescence tag and targeting ligand. We also report the *in vitro* and *in vivo* non-toxicity of the complex. Cytotoxic effect of the complex was evaluated by MTT assay in PC-12 cells. Atrial Natriuretic Peptide (ANP) levels and biodistribution of dexamethasone decorated PEGylated aligned MWCNTs (dpcaf) in ischemic stroke male Sprague Dawley (SD) rats were reported in this work. Ischemic stroke was induced in SD rats by occluding common carotid artery (CCAO). Blood was collected prior to intravenous (i.v) administration of dpcaf (FITC labeled) to determine the baseline levels of plasma ANP using competitive ELISA technique. The dpcaf was intravenously injected through the tail vein and neurobehavioural assessment performed thrice within 24 hours of reperfusion using behavioural observation and tail suspension method. Rats were euthanized, and blood collected using cardiac puncture for ANP levels determination. Phosphate buffered saline (PBS) perfusion was undertaken and brain, liver, spleen, kidneys, lungs and heart were harvested and preserved in formalin. The organs were homogenised in PBS buffer and supernatants collected for measurement of fluorescence intensities. Blood samples were centrifugated and plasma fractions collected for ANP determination. The dpcaf was detected in all the organs and tissues as demonstrated by the high fluorescence intensity compared to the untreated group. The highest fluorescence intensity was reported in plasma (2179) followed by kidney (1563) and liver (1507). The delivery of dpcaf into the brain was further confirmed my fluorescence microscopy, H & E staining and absorbance spectroscopy. The baseline plasma ANP levels were ranging from 118 to 135,70 $pg.mL^{-1}$ prior to surgery and from 522,09 to 552,37 following CCAO surgery. A decrease in ANP levels to 307,77 $pg.mL^{-1}$ was observed when the rats were treated with dpcaf, pegcnt and dex with a drastic drop in the dpcaf treated group. These findings suggest a beneficial role played by the dpcaf in the reduction of inflammation

in the ischemic stroke induced rats. This could lead to an effective treatment of ischemic stroke.

7.1. Introduction

The application of carbon nanotubes namely, single-walled (SWCNTs) and multiwalled carbon nanotubes (MWCNTs) in biomedical field for drug delivery and treatment of diseases requires a thorough understanding of their fate and toxicological profile following intravenous administration in animals and humans. A plethora of unique physico-chemical properties of carbon nanotubes make it one of the most commercially attractive materials in the world of nanotechnology (Wei *et al.*, 2012; Jacobsen *et al.*, 2017). Carbon nanotubes are classified as an emerging group of nanomaterials that have been shown to have beneficial potential in various fields of nanomedicine due to their characteristic physico-chemical features (Komane *et al.*, 2016). Carbon nanotubes are electrically and thermally conductive and have ultralight weight. They are highly flexible, very strong and inert but can undergo chemical modification with various functional groups depending on their intended use. CNTs structural backbone consists of carbon atoms which exhibit thermal and electronic conductivity including great strength. Based on their unique characteristics, CNTs have attracted much attention since a report by Iijima in 1991 (Iijima, 1991).

Nanomaterials have the ability to minimise invasion and enhance precision and accuracy during therapeutic interventions due to their nano size. These properties have a potential to decrease complication rates of current pharmacological therapies leading to minimization of damage to the healthy surrounding tissues and cells. Furthermore, these properties may make anatomically challenging regions such as the brain accessible for easy treatment (Mattei and Rehman, 2015). Blood brain barrier (BBB) protects the brain from being invaded by unwanted molecules which could damage brain tissue. The BBB forms interface between the blood circulation and the central nervous system (CNS) (Modi *et al.*, 2009).

BBB acts as a barrier to restrict movement of substances between the brain and blood. It plays a crucial role in the maintenance of the central nervous system homeostasis. Furthermore, it acts as a carrier to transport nutrients to the brain and to eradicate metabolites (Wilhelm, Fazakas and Krizbai, 2011).

Furthermore, it acts as a carrier to transport nutrients to the brain and to eradicate metabolites (Wilhelm, Fazakas and Krizbai, 2011). Pristine carbon nanotubes are inert, hydrophobic in aqueous environment and toxic to cells. Functionalization plays a crucial role if CNTs are to be utilized in biomedical field. Functionalization makes CNTs compatible and stable in biological milieu. In addition, it allows coupling of carbon nanotubes with a variety of important molecules. It promotes conjugation of CNTs with different molecules to develop therapeutic and diagnostic systems (Imran *et al.*, 2016).

Various promising data have so far been obtained about the use of CNTs for the treatment of diseases including cancer; however, toxicity of pristine CNTs limits their application in clinical setting. Toxicity also depends on many factors such as size, shape, purity, degree of functionalization, cell or tissue type, route of administration and duration of exposure (Madani, Mandel and Seifalian, 2013). Moreover, toxicity of the CNTs also depends on the internal diameter, external diameter, length, doping, catalyst type, multi- or single-walled arrangement and entangled or aligned orientation.

In our study, MWCNTs were used as nanocarriers of dexamethasone and ANP. In healthy animals and humans, ANP levels are low but their expression increases when the animal is under stress. Furthermore, FITC was also loaded for biodistribution studies to trace the location of the delivered drug. In this study, we have demonstrated the successful synthesis and functionalization of MWCNTs. In addition, we also showed the potential that the complex dpcaf may possess in reducing the symptoms of ischemic stroke.

7.2. Materials and methods

7.2.1. Materials

Ferrocene (98 %, Sigma Aldrich Corporation, St Louis, MO, USA), toluene (ChromaSolv for HPLC, 99,9 %, Sigma Aldrich Corporation, St Louis, MO, USA, HCl (>32 %, Sigma Aldrich Corporation, St Louis, MO, USA), HNO_3 puriss.pa reag >65 %, Sigma Aldrich Corporation, St Louis, MO, USA), $SOCl_2$ reagentPlus (>99 %, Sigma Aldrich Corporation, St Louis, MO, USA), H_2SO_4, puriss, p.a. (95-97 %, Sigma Aldrich Corporation, St Louis, MO, USA), Fentanyl Chloride (2mL/100ug, Kabi Manufacturing PTY(LTD), Eastern Cape, SA., Dormicum (15 mg/3 mL, Roche Products PTY(LTD), Sandton, SA), Lignocaine (Kyron Labs, Benrose, SA), Temgesic (1 mL injection, Indivior, Bristol, UK), Sodium pentobarbitone (200 mg/ml, Bayer, Kempton Park, SA),

PC-12 cells (Separations, Randburg, SA), RPMI1640 (Sigma Aldrich Corporation, St Louis, MO, USA), Sprague Dawley rats (Wits CAS, SA), FITC (Sigma Aldrich Corporation, St Louis, MO, USA), Rat ANP kit (Elabscience Biotechnology Inc, USA), Formaldehyde (CP, 355, Merck, New Jersey, UK), dexamethasone – 21-phosphate (Sigma-Aldrich), ANP antibody (Merck, New Jersey, UK), PBS (Sigma Aldrich Corporation, St Louis, MO, USA), 2-iminothiolane (Sigma Aldrich Corporation, St Louis, MO, USA), FITC isomer I (Sigma Aldrich Corporation, St Louis, MO, USA), NaCl tablets (Sigma Aldrich Corporation, St Louis, MO, USA), DCM (Sigma Aldrich Corporation, St Louis, MO, USA), In vitro Toxicity Assay Kit (MTT based), (Sigma Aldrich Corporation, St Louis, MO, USA).

7.2.2. Aligned Multiwalled Carbon Nanotubes for *in vitro* and *in vivo studies*

Carbon nanotubes were synthesised by CVD as in **Chapter 3**. A CVD system set-up was prepared, and the following parameters were used for the synthesis; synthesis time = 45 min, carrier gas = argon (95 %) balanced with 5 % hydrogen, catalyst = 2,5 % ferrocene in toluene and synthesis temperature = 850 ˚C. Carbon nanotubes were harvested from the walls of the quartz tube and their morphology was determined using SEM and TEM. MWCNTs were purified using HCl and carboxylated using H_2SO_4:NHO_3 (3:1). They were further functionalised by acylation and pegylation. Carbon nanotubes were fluorescently labelled with FITC and dexamethasone and ANP antibody attached to them prior to use in *in vitro* and *in vivo* studies.

7.2.3. Dexamethasone release studies

Dexamethasone was loaded on PEG-MWCNTs as in **Chapter 5**. Dexamethasone was thiolated using 2-iminothiolane in DMSO and reacted with PEG-MWCNTs. Dex-PEG-MWCNTs was centrifuged at 5 000 rpm for 10 min and the supernatant was stored at 4 ˚C for future use. Dex-PEG-MWCNTs were dispersed in 10 mL of 0.1 M phosphate buffered saline (PBS) with pH 7.4, 6.5 and pH 5.5 and transferred into dialysis tubing respectively (**Figure 7.1**).

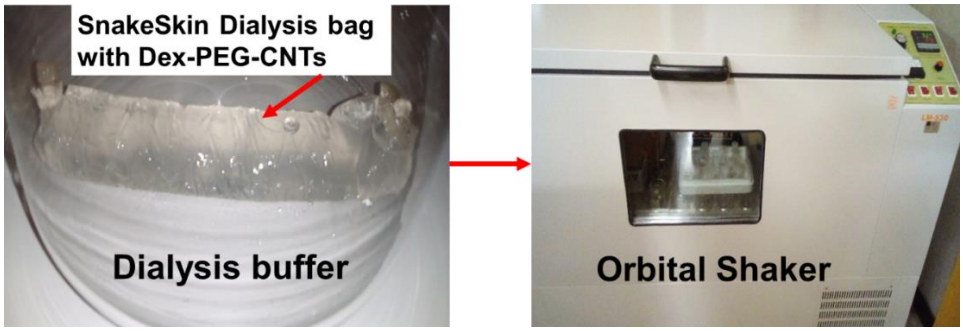


Figure 7.1. Dexamethasone drug release. Dialysis tubing and incubation in orbital shaker incubator.

About 3 mL PBS was collected from both the 200 mL PBS with pH 7.4, 6.5 and 5.5 prior to loading the dialysis tubings containing Dex-MWCNTs and Dex-PEG-MWCNTs. The volumes were replaced with the same amount of the buffer to maintain sink conditions. Dialysis was performed in an orbital shaker (YIHDER, Taiwan) at 37 °C with 30 rpm speed. Collection of 3 mL of the PBS was done at various time intervals (0 hr, 0.5 hr, 1 hr, 2 hr, 4 hr, 6 hr, 8 hr, 10 hr, 12 hr and 24 hr) to determine the time at which Dex is completely released from MWCNTs and PEG-MWCNTs (**Fig. 7.1**). The optimal wavelength of Dex was determined and was found to be 242 nm and the concentrations of Dex in 3 mL aliquots collected at various time intervals during a 24-hour dialysis were determined using UV-VIS (Shimadzu Corporation, Kyoto, Japan).

7.2.4. Evaluation of MWCNT cytotoxicity

CNT toxicity in living cells is currently a controversial issue. Their toxicity needs to be assessed prior to their application in the biological environment. SWCNT is one of the major forms of engineered carbon nanotubes. The cytotoxicity and fibrogenicity the carbon nanotubes depend on a spectrum of factors such as the type of CNT (MWCNT or SWCNT), length, thickness, degree of functionalization, type of synthesis, target organ and many more factors. SWCNTs are more toxic than MWCNTs (Jafar, Alshatti and Ahmad, 2016). The implementation of CNTs in clinical trials is currently limited by this controversial debate.

PC-12 cells (pheochromocytoma) derived from the rat adrenal medulla were used for evaluating the toxicity of the formulations. PC-12 cells have a potential to differentiate into neuronal cells. They are a useful model system for neuronal differentiation and neurosecretion (Veetil and Ye, 2007). For sub-culturing of PC-12 cells (Cellonex), all the worked was executed under sterile conditions. T25 tissue culture flask was pre-

reduced with Cellonex recovery medium in 5 % CO_2 at 37 °C overnight. Cryopreserved PC-12 cells were thawed by warming in hands to avoid contamination by water from the waterbath.

The cell vial was cleaned thoroughly with 70 % ethanol prior to opening. The cells were mixed with 200 µL automatic pipette and 400 µL was transferred into the pre-reduced tissue culture flask. Another T25 tissue culture flask was pre-reduced with Cellonex recovery medium in 5 % CO_2 at 37 ˚C overnight for sub-culturing. Following 24 hour incubation, the cells were split into two groups and topped up with recovery medium and re-incubated for 24 hours. The cells were split again after 24 hours after reaching 80 % confluence.

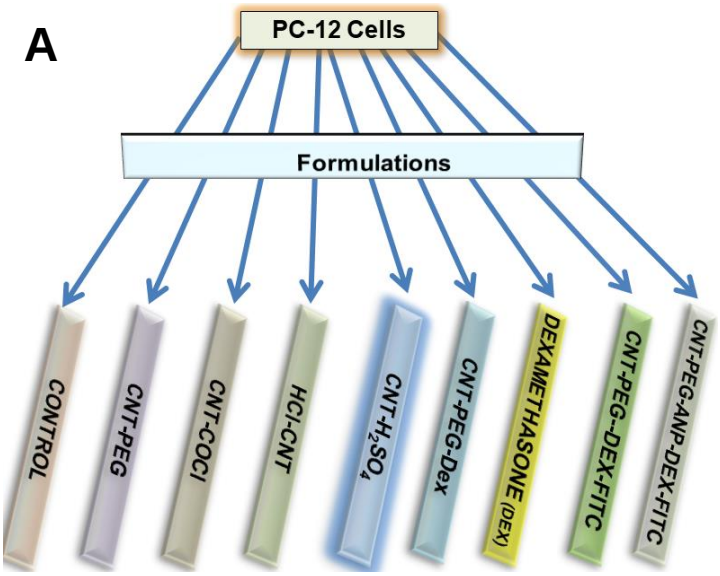
Medium was changed when it changed from red to orange/yellow as an indication that it has been depleted of the necessary nutrients. Cells were centrifugated and culture medium decanted into a sterile glass beaker. The pellet was resuspended in a fresh recovery medium and incubated overnight as previously stated. The medium was replaced for 2-3 days and cell count was performed using Trypan Blue Exclusion technique.

The cells were then grown in an incubator at 37 ˚C and 5 % CO_2 incubator in RPMI1640 culture medium supplemented with glutamine, 5% fetal bovine serum (FBS), 10 % horse serum (HS). FBS and HS were inactivated by heating at 30 min at 56 ˚C in a water-bath prior to introduction into the culture medium to inactivate the complements that may cause cell lysis. A mixture of 1 % penicillin and streptomycin (pen/strep) was added to prevent bacterial contamination. Cells were checked on daily basis for viability and microbial contamination by Trypan Blue Exclusion technique. Cells were checked first for any visible bacterial contamination in their flasks at various magnifications. For cell viability test and counting, cells were homogeneously mixed with Trypan Blue dye at 1:20 ratio, loaded on haemocytometer and viewed under a light microscopy.

The formulations used in this study were as follow; dexamethasone (Dex), H_2SO_4 functionalised MWCNTs (H_2SO_4-CNTs), HCl purified MWCNTs (HCl-CNTs), acylated CNTs ($COCl_2$-CNTs), PEGylated CNTs (PEG-CNTs), dexamethasone loaded PEG-CNTs (DEX-PEG-CNTs), FITC labelled DEX-PEG-CNT (FITC-DEX-PEG-CNT) and ANP coupled FITC-DEX-PEG-CNT (FITC-DEX-PEG-CNT-ANP). Controls were also

included in these experiments to compare them with the treated groups. Cells were divided into 9 groups and treated with various formulations as depicted in **Fig. 7.2A**. The formulations were sterile filtered using 0,22 µm prior to use to avoid contamination.

Following incubation with various formulations, MTT assay was performed to evaluate the cytotoxic effect of the formulations at various doses. The MTT assay measures the activity of living cells using mitochondrial dehydrogenases.



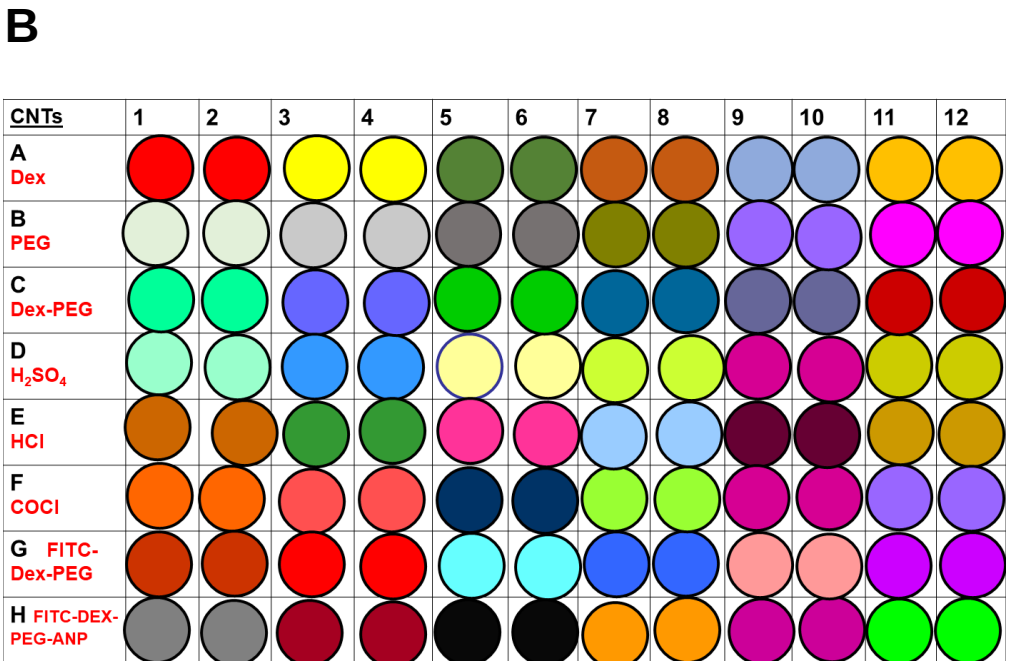


Figure 7.2. Cytotoxicity formulations. Formulation grouping (A). Layout of incubation of cells with the formulations.

PC-12 cells were seeded in a 96 well plate at a concentration of 6 x10^4 cells.mL^{-1} per well with the afore-mentioned formulations and incubated with various concentrations of dexamethasone and functionalized carbon nanotubes ranging from 20 to 20,000 µg.mL^{-1} in PBS (pH 7,4) for 24 hours (**Fig. 7.2B**). Following incubation with various formulations, MTT assay was performed to evaluate the cytotoxic effect of the formulations at various doses. The MTT system is a means of measuring the activity of living cells via mitochondrial dehydrogenases. The MTT is a colorimetric assay for the nonradioactive quantification of cellular proliferation, viability, and cytotoxicity.

The key component is (3-[4,5-dimethylthiazol-2-yl]-2,5-diphenyl tetrazolium bromide) or MTT (**Fig. 7.3**). The MTT assay is based on the cleavage of the tetrazolium salt MTT to formazan by the succinate-tetrazolium reductase system (EC 1.3.99.1) in the presence of an electron-coupling reagent (Riss *et al.*, 2004).

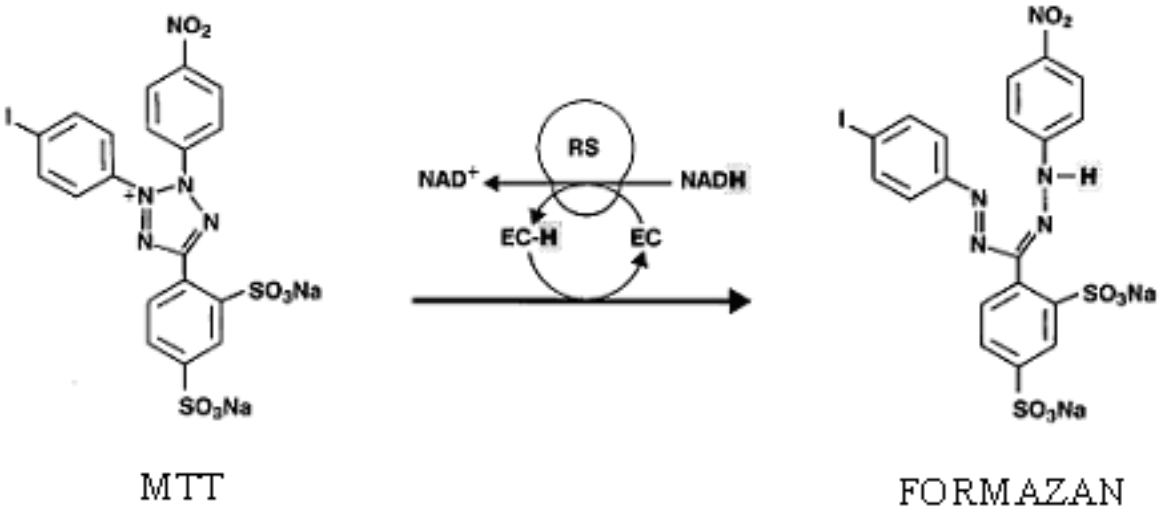


Figure 7.3. Cleavage of the tetrazolium salt MTT to formazan by the succinate-tetrazolium reductase system in the presence of an electron-coupling reagent (Predoi *et al.*, 2007).

This enzyme is one of the mitochondrial dehydrogenases in the endoplasmic reticulum and the bio-reduction occurs only in metabolically intact cells. Solutions of MTT, dissolved in medium or balanced salt solutions without phenol red, are yellowish in colour. Mitochondrial dehydrogenases of viable cells cleave the tetrazolium ring, yielding purple formazan crystals which are insoluble in aqueous solutions (Bahuguna *et al.*, 2017). The crystals are dissolved in acidified isopropanol composed of 10 % Triton X-100 in 0.1 N HCl in anhydrous isopropanol.

The resulting purple solution is spectrophotometrically measured. An increase or decrease in cell number results in a concomitant change in the amount of formazan

formed, indicating the degree of cytotoxicity caused by the test material. Samples (adherent or suspension cells) are cultured in 96-well microplates and incubated with the MTT solution for approximately 4 hours. Following incubation period, a water-insoluble formazan dye is formed and solubilized by solubilization solution. The formazan dye is quantitated using a scanning multi-well spectrophotometer (ELISA reader) at 570 nm. The measured absorbance correlates directly to the number of viable cells.

In our study, MTT was reconstituted by adding 3 mL of PBS to 15 mg MTT vial. About 10 µL of the reconstituted MTT (3-(4,5-Dimethylthiazol-2-yl)-2,5-Diphenyltetrazolium Bromide) was added to each well ($6x10^4$ cells.mL^{-1} /well) following a 24-hour incubation and further incubated for 4h. Following a 24-hour incubation, 100 µL of solubilization solution was added to solubilize the formazan crystals. The plates were shaken using an orbital shaker to dissolve the crystals completely. The absorbance was measured at 570 nm using Multilabel Reader (Victor X3, Perkin Elmer, Waltham, MA, USA).

7.2.5. Animal administration

Male Sprague Dawley rats (360-560 g) were acquired from the Central Animal Service of the University of the Witwatersrand Medical School. All protocols of the study were approved by the Animal Research Ethics Committee (AREC) of the University of Witwatersrand Medical School (Ethics clearance no. **AREC # 2017/03/17/D**). Rats were kept in pairs in Eurostandard Type III cages (425 mm x 266 mm x 155 mm) in an enriched environment air-conditioned with temperature of 26 °C. They were housed in a 12-h light/dark cycle with food and water available *ad libitum* (**Fig.7.4 A-B**).

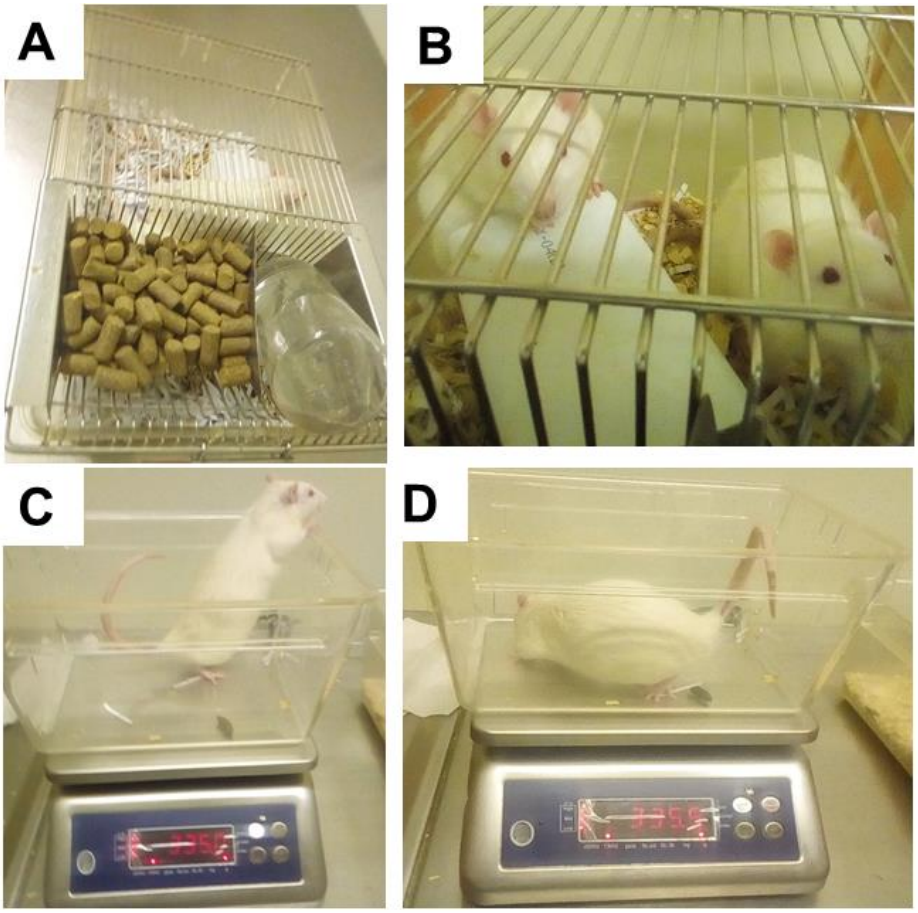


Figure 7.4. Sprague Dawley rats in cages. Environmental enrichment (B). Rats in pairs in enriched environment (B). Weighing of rat (unstable) (C). Weighing of rat (stable) (D).

They were acclimatized in a new environment for at least one week and weighed using stainless steel waterproof scale (Clover Scales (PTY), LTD, Johannesburg) once a week and a day before experiment to monitor their state of health (**Fig.7.4C-D**). Weights were recorded once the rat has settled in the weighing bowl on the balance (**Fig.7.4D**).

A



B

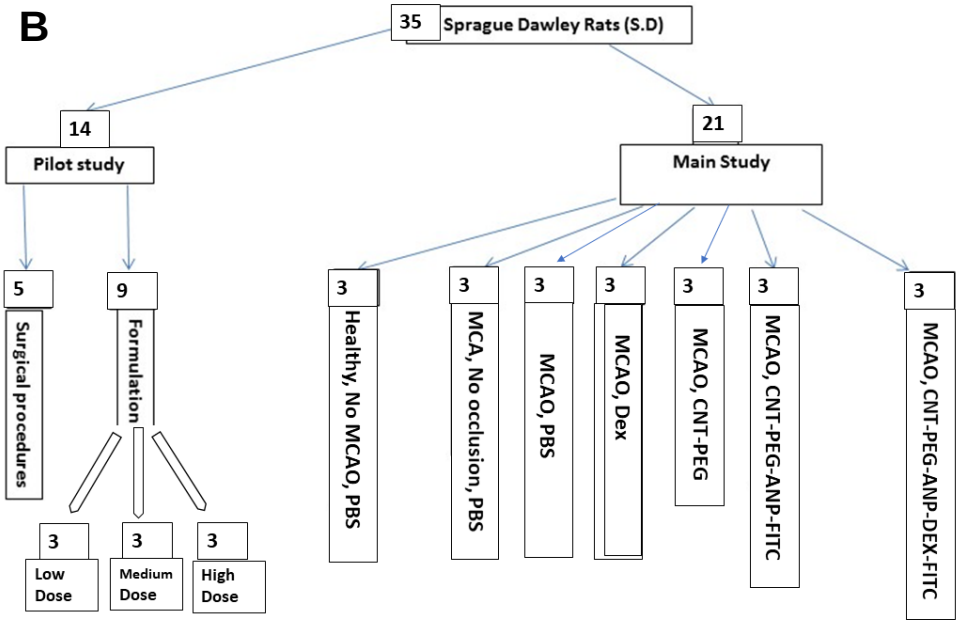


Figure 7.5. Handling of Sprague Dawley rats. Rats transferred to bigger cages and pre-surgery preparation (A). Experimental design for pilot study and main study (B).

Rats were transferred to the bigger Eurostandard Type IV cages (595 mm x 380 mm x 200 mm) and randomly divided into six groups [premedication (premed), control (sham), middle cerebral artery occlusion (MCA) /common carotid artery occlusion (CCAO), FITC-Dex-ANP-PEG-CNT (dpcaf), PEGylated-CNT (PEG-CNT) and Dexamethasone (Dex)] according to the experimental design with each group composed of 3-10 rats and each rat in its own cage (**Fig. 7.5B**). Pain/Health Monitoring Score Sheet based on the Rat Grimace Scale (RGS) technique was used to record the health status and neuronal behaviour of each rat following an experimental intervention.

7.2.6. Preparation of the intraluminal monofilament sutures for MCA occlusion

The 4-0 (1,5 metric ≈ 0,15 mm diameter) and 3-0 (2 metric ≈ 0,2 mm diameter) piece of the nylon suture was cut to the length of 5cm. One tip was heated to form a blunt bulb shape using Bunsen burner. The nylon pieces were immersed in 0,1 % poly-lysine for 30min and dried overnight at 37 ˚C in an incubator (**Fig. 7.6**).

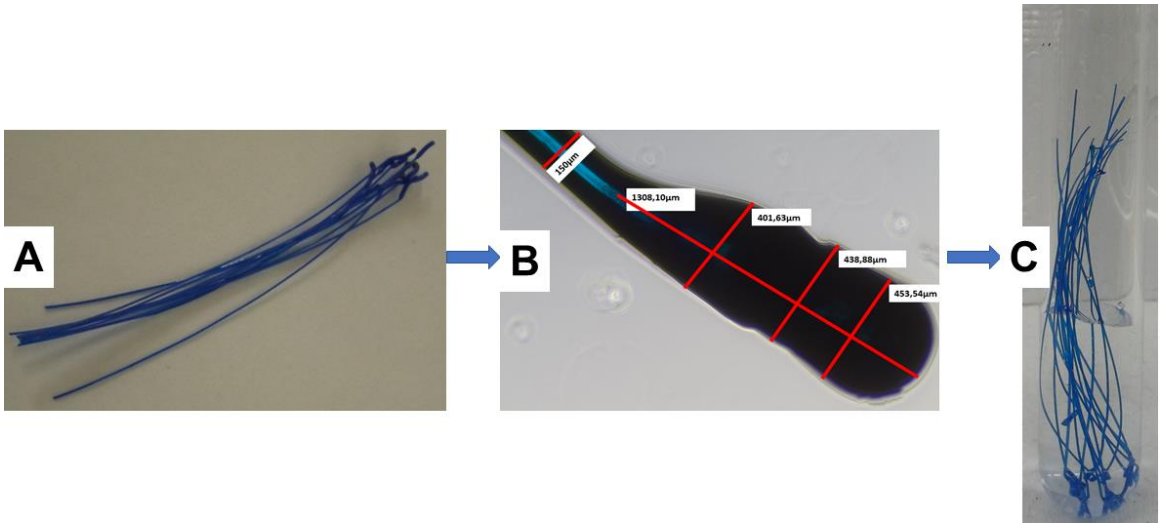


Figure 7.6. Preparation of intraluminal monofilament sutures. Nylon 4-0/3-0 cut to 5cm pieces and blunted at one tip (A). Measurement of the tip dimensions under light microscope (B). Coating of the sutures with 0.1% poly-lysine.

Poly-lysine is an adhesive and its polycationic nature helps to facilitate a strong interaction with the internal wall of the artery to produce a complete occlusion in MCA occlusion. The length and diameter of the tip was measured under microscope to ensure that it fits perfectly well within the ECA to produce a complete occlusion without damaging the artery. The nylon pieces were sterillised under UV overnight prior to use.

Nylon pieces with different diameters and lengths of the bulb tips were used to ensure complete occlusion in middle cerebral artery occlusion procedure.

7.2.7. Middle cerebral artery occlusion (MCAO)

The first two surgeries were conducted to acquire hands-on experience in the surgical procedures of the MCA occlusion. Inhalation anaesthesia was performed using 3 % Isoflurane (**Fig.7.7A**) and was maintained under 1 – 2 % Isoflurane and 200 $mL.min^{-1}$ O_2 using anaesthetic instrument (Ohmeda 7000 Ventilator) (**Fig. 7.7B**). Blood was collected from the tail and transferred into a heparinized tube (**Fig.7.7C**). The neck area was shaved in a supine position under aseptic conditions **(Fig. 7.7D**).

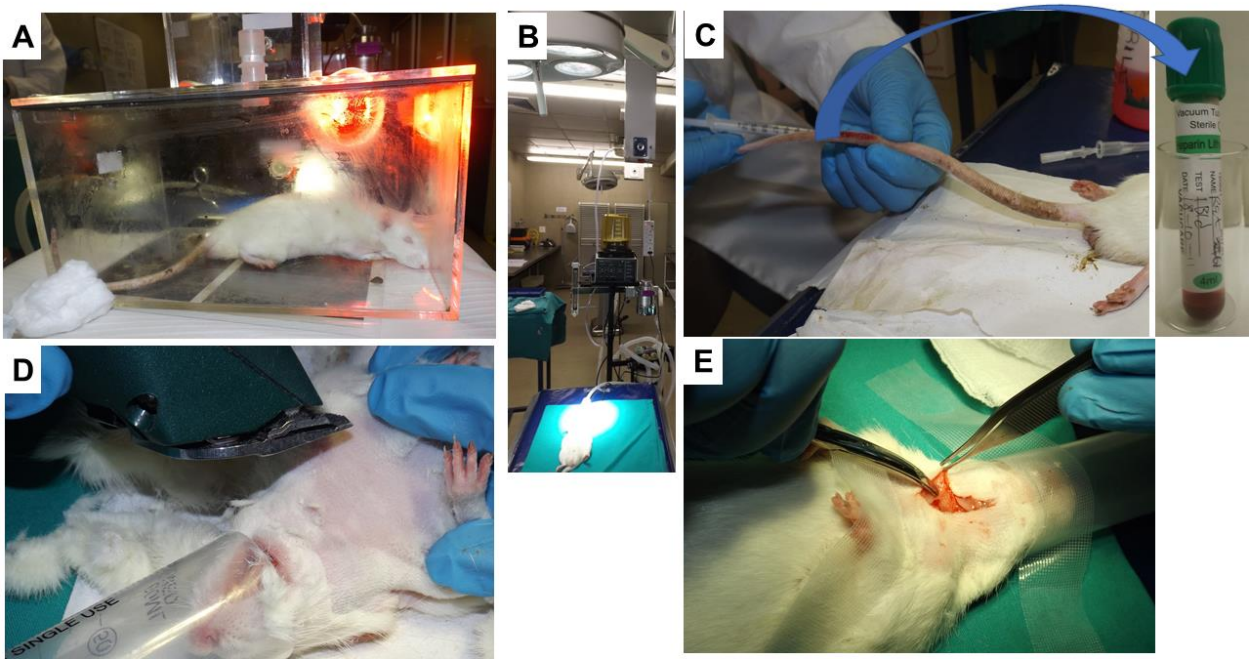


Figure 7.7. Preparation of the rat for surgery. Inhalation anesthesia (A). Anesthetic instrument (B). Venous blood collection from the tail (C). Shaving of the neck area (D). Dissection of the neck area (E).

Once the rat was fully anesthetised, the neck muscles were dissected to expose the common carotid artery (**Fig. 7.7E**). The common carotid artery (CCA) parallel to the vagus nerve was successfully isolated (**Fig.7.8A**).

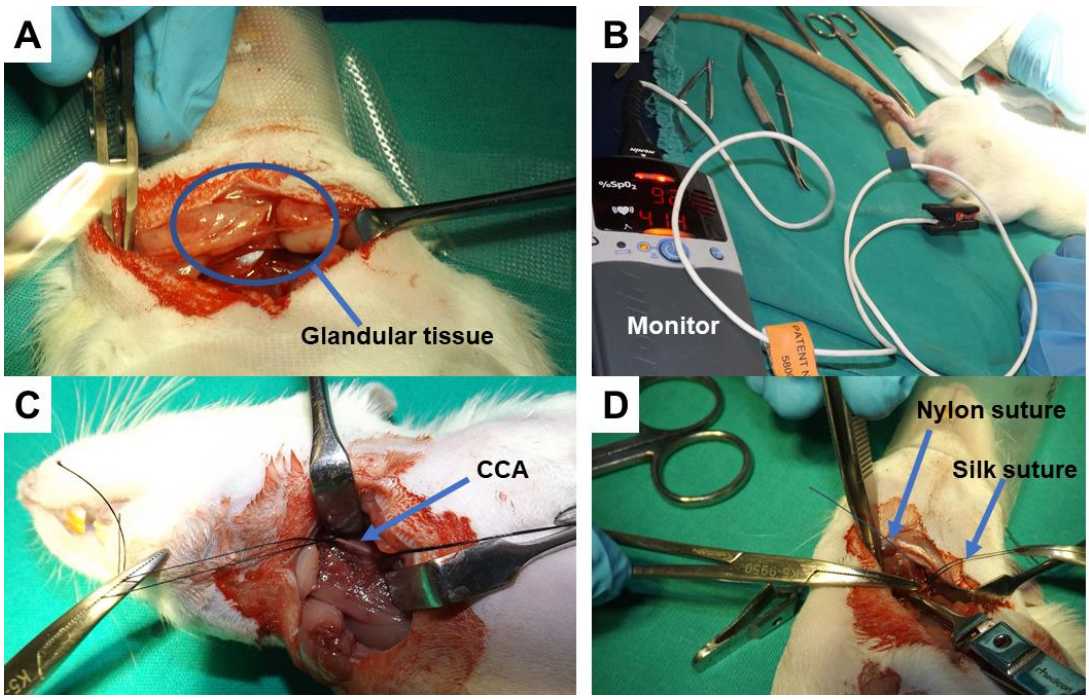


Figure 7.8. Dissection of the neck to isolate CCA and its bifurcation. Dissection of the glandular tissue (A). Measurement of spO2 and heart rate under anaesthesia (B). Isolation of CCA (C). Insertion of nylon suture into the MCA (D).

Surgery was performed further to isolate the bifurcation of the CCA (**Fig. 7.8A**). The status of the rat during the procedure was monitored by measuring spO_2 and heart rate (**Fig. 7.8B**). The internal carotid artery (ICA) and external carotid artery (ECA) were exposed and the intraluminal monofilament suture was inserted into the ICA and pushed further until it reached the middle cerebral artery (MCA) but the rat died during the procedure (**Fig. 7.8D**).

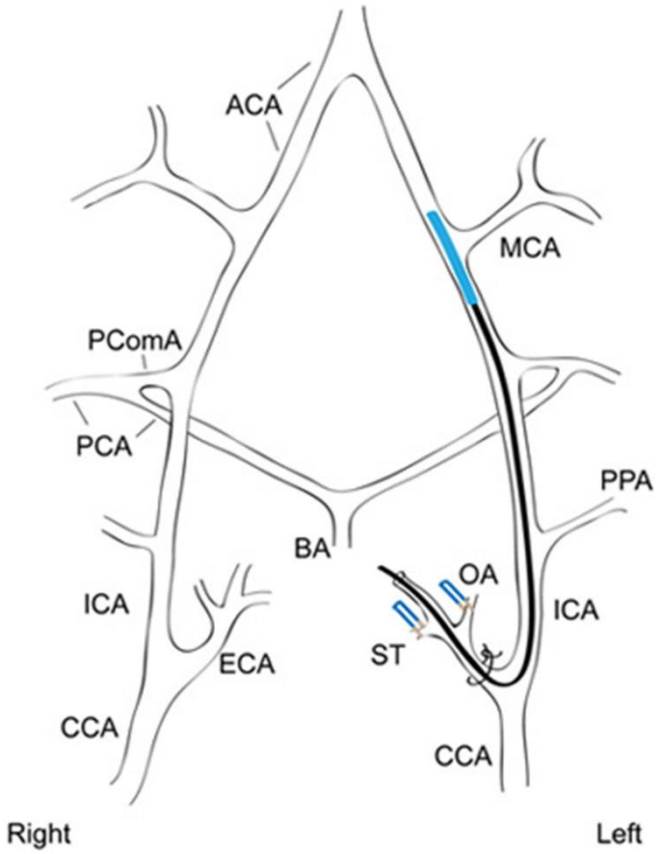


Figure 7.9. Bifurcation of the common carotid artery into ICA and ECA and further bifurcation of ICA and ECA.

In the second four surgeries, rats were anesthetized intraperitoneally with a combination of fentanyl (0,1 mg.Kg^{-1}) and dormicum (5 mg.Kg^{-1}). Anaesthesia was maintained at 1 – 2 % Isoflurane and 200 mL.min^{-1} O_2). CCA was successfully isolated but rat died when inserting the suture. In the third one surgery, inhalation anaesthesia was tried again with 3 % Isoflurane and maintained under 1 – 2 % Isoflurane and 200 mL.min^{-1} O_2. CCA was successfully isolated but rat died before reaching its bifurcation for insertion of the intraluminal monofilament suture.

7.2.8. Unilateral common carotid artery occlusion (CCAO) and neurobehavioural assessment

The MCAO was too invasive and this technique led to a high mortality rate. A less invasive technique namely unilateral common carotid artery occlusion was conducted to induce stroke. Rats were weighed a day before surgery to avoid or minimise stress. Neurobehavioural evaluation was done prior to surgery to establish a baseline. In the fourth one surgery. A long-lasting analgesic (0,1 mL Temgesic) and inhalation

anaesthesia (3% Isoflurane) were used to anesthetise the rat. Local anaesthetic (0,2 mL Lignocaine) was administered subcutaneously on the shaved neck. anaesthesia was maintained under 1 – 2 % Isoflurane and 200 mL.min^{-1} O_2.

A volume of about 0,2 mL blood was collected from the tail vein or saphenous vein prior to surgery, immediately after surgery prior to recovery and after 24-hour reperfusion (**Fig.7.10A)**. The infrared light was used to enhance vasodilatation for easy blood collection (**Fig. 7.10E**). The blood was transferred into the heparinized blood collection tube. Neurobehavioural assessment was performed prior to surgery, immediately after surgery and within 24-hour reperfusion at an interval of 4-6 hours.

The neck was shaved and CCA exposed and ligated with 3-0 silk suture for 30 minutes (**Fig.7.10B-D**). Ligation was removed, wound closed and rat allowed to recover from anaesthesia. Rat fully recovered from anaesthesia and symptoms of stroke were observed and recorded on the pain scoring sheet (**Fig.7.10F**). The same procedure was followed to induce stroke in two rats in the fifth trial, but one rat died while removing the ligation. The same procedure as previously performed was conducted in the sixth surgery with one rat, but the rat did not survive during CCA surgery.

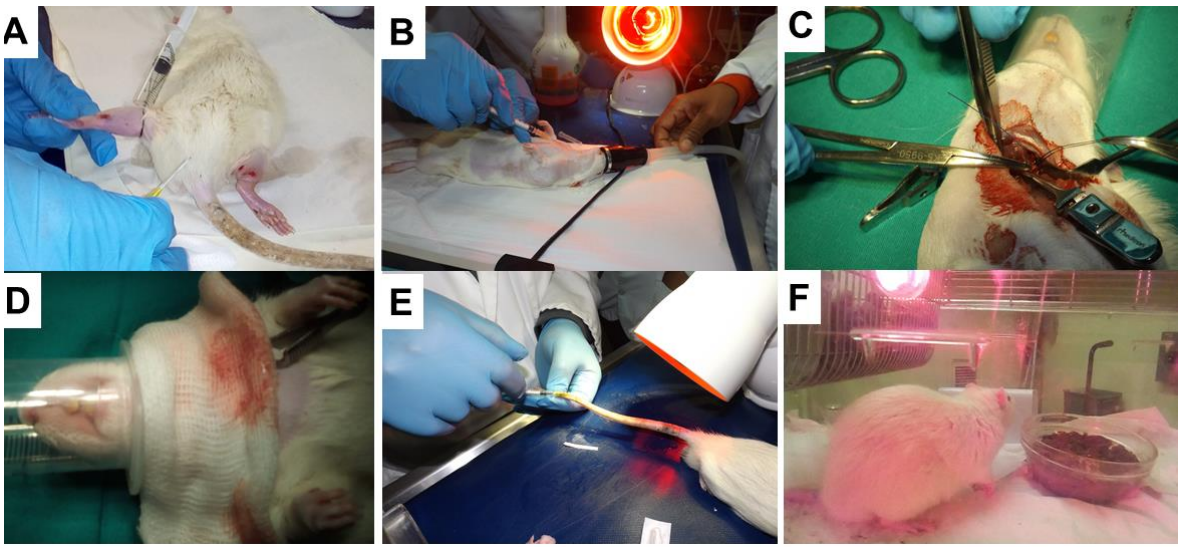


Figure 7.10. Unilateral common carotid artery occlusion. Blood withdrawal from saphenous vein (A). Injection of local anaesthetic (lignocaine) on the neck (B). Occlusion of CCA by clamping (C). 30-minute occlusion (D). Blood withdrawal from the tail vein (E). Recovering from anesthesia (F).

In the seventh one surgery, injectable anaesthesia (Fentanyl + dormicum), analgesic (Temgesic) and local anaesthetic (Lignocaine) were used during anaesthesia prior to

the actual surgery. Anaesthesia was maintained as before and CCA was successfully isolated and clamped for 30 minutes. Occlusion was removed, wound closed and blood collected from the tail vein. For the control group, PBS was injected via tail vein and for the treatment group, the formulations were also injected via tail vein. The rat was allowed to recover from anaesthesia and was transferred to the recovery room for full recovery.

Rats were strictly monitored to ensure that they do not suffer from post-surgery complications. They were checked after every 4 hours and injected with Temgesic every 6 hours. They were then euthanized after 24 hrs and organs (brain, liver, heart, kidneys, spleen and lungs) were collected for biodistribution studies. In the 8^{th} six rat surgery, the same procedure as above was successfully conducted. Neurobehavioural assessment was performed in the 12^{th} - 18^{th} surgery and we observed the symptoms of stroke (one eye dark red and sunken, contralateral circling when rat pulled up by the tail by using the elevated body test). Formulation dose optimization study was also performed by intravenous injection via the tail vein.

7.2.9. Optimization of the formulation dose

This study was undertaken in the 12^{th} – 18^{th} surgeries following the success of the surgical procedures. This study was undertaken to ensure that the doses of the formulations that will be used in the main study were not toxic to the rats. Occlusion was removed, and all the incisions were sutured. Blood (0,2 mL) was collected into heparinized tubes. Dose response studies were performed using 1, 10 and 100 $\mu g.Kg^{-1}$ body weight of dpcaf to determine the dose at which dpcaf was toxic to the rats. Rats were transferred to recovery room and neurobehavioural assessment was undertaken thrice within 24 hours of reperfusion. Pellets were soaked in water to soften them for the rat to feed with ease following surgery. For subsequent experiments, 100 $\mu g.Kg^{-1}$ of dpcaf, pegcnt and dex were injected via tail vein according to the groups prior to recovery.

7.2.10. Humane endpoints and tissue sampling

Final neurobehavioural assessment was performed and rats were weighed prior to the terminal procedure. Rats were terminated by intraperitoneal injection of 1-2 mL.Kg^{-1} sodium pentobarbitone (Eutha-naze). A volume of 4 mL blood was collected into heparinized tubes while the heart was still pumping using a cardiac puncture method. Following the cardiac puncture, perfusion was done using phosphate buffer saline to remove blood from the circulatory network of the rat (**Fig.7.11A-B**). During perfusion, an 18 G needle was attached to the 50 mL syringe and filled up with 50 mL PBS buffer. The PBS buffer was injected into the ventricle of the heart and the appendage of the heart was removed to facilitate the flow of PBS and blood. The PBS injection was done until the organs turned pale or white (**Fig.7.11C-H**).

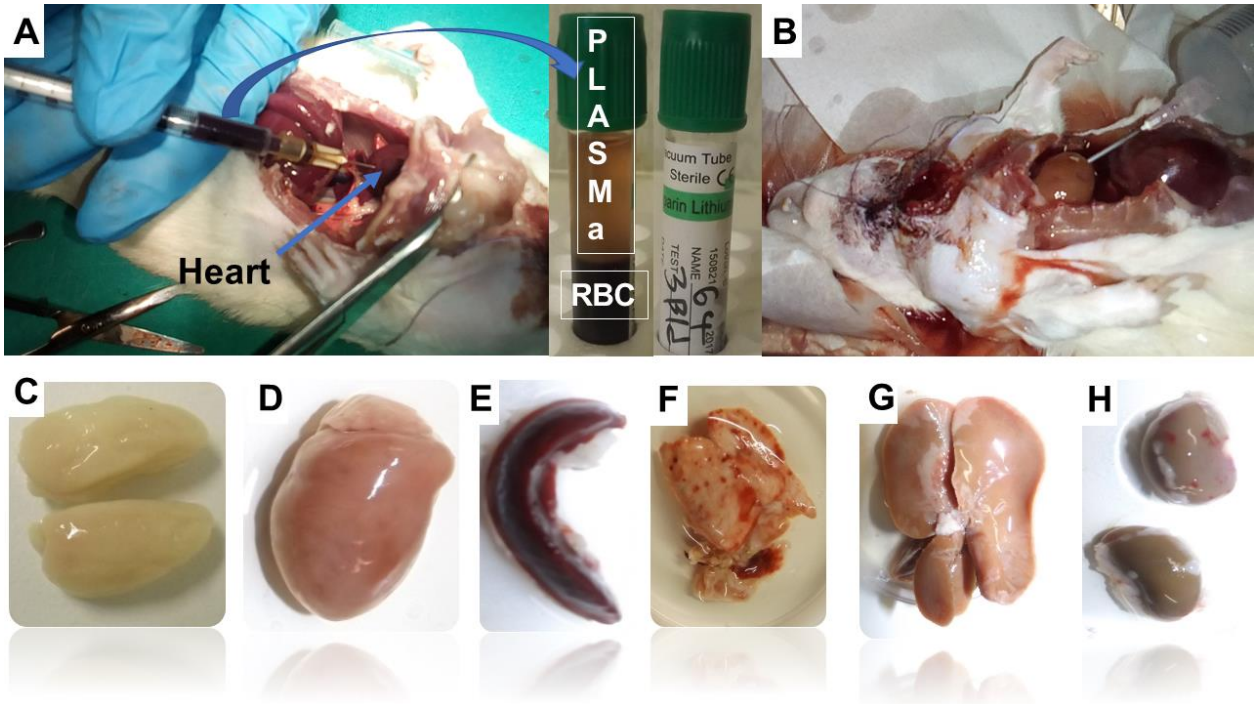


Figure 7.11. Humane endpoints. Cardiac acupuncture (A). PBS perfusion (B). Perfused organs isolated from the rat (C-H).

Heart, lungs, kidneys, spleen, liver and brain were harvested and preserved in 10 % formalin (**Fig. 7.11C-H**). Brain hemispheres were separated, and their weights recorded **(Fig. 7.11C)**. All the organs were stored at 4 ˚C for future use. Blood was centrifugated at 2300 rpm at 8 °C for 15 minutes (Universal 320R, Hettich, Germany) and supernatants (plasma) were collected for ANP assay.

7.2.11. Tissue sample preparation

Tissues were cut into smaller pieces of 0,2 – 0,5 g (Mettler AJ100, Switzerland) and homogenised in 2 – 5 mL phosphate buffered saline (PBS) using a glass homogenizer. They were further homogenised in ice at 10 sec pulse, 60 % amplitude using ultrasonic processor (Sonics Ultracell, Newtown, USA). The homogenates were centrifuged at 12 000 rpm for 10 min in a microcentrifuge (TopScien, Ningbo, China). Supernatants were collected, and fluorescence intensities were determined using microplate spectrophotometer (2030 Multilabel Reader Victor X3, Perkin Elmer, USA).

7.2.12. Determination of Fluorescence intensity in the rat tissues

Standards of dpcaf with the following concentration range (0.2, 0.6, 0.8, 1.4, 2, and 4 $\mu g.mL)^{-1}$ were prepared in PBS buffer with pH 7.4. Black 96 well plate was used to avoid or reduce the autofluorescence from the samples. Each well of the 96 well plate was loaded with 100 µL of each concentration in triplicates. The supernatants from the various tissues of the rat organs were also loaded in triplicates. Fluorescence intensity was measured at excitation wavelength of 490 nm and emission wavelength of 520nm using microplate spectrophotometer (2030 Multilabel Reader Victor X3, Perkin Elmer, USA) equipped with a fluorescence filter with wavelength of 520 nm.

7.2.13. Histological evaluation of the rat brain tissue

Following harvesting of the brains, the right and left hemispheres were separated, weighed and their volumes determined using deionised water in a volumetric flask. They were stored in 10 % formalin for histological evaluation. The histological specimens have to be stained to enhance visualization of the cells because most cells are colourless and transparent. The techniques used in cell visualization are either specific or non-specific. In specific techniques, staining is selective as particular biomolecules within cells are stained. In non-specific techniques, the staining is not specific as most of the cells are stained in much the same way.

Staining works by using a stain and counterstain simultaneously. The dye stains cell components a bright colour and another dye stains the rest of the cell a different colour. Following washing with PBS and dehydration with ethanol, the specimens were

embedded in wax blocks and sectioned into 5µm sections using a microtome, stained with haematoxylin and eosin and mounted on the slides and viewed under a light microscope. Since some specimens were treated with FITC, the slides were also viewed under fluorescence microscope at 10 x objective (Zeiss LSM 780 Confocal Microscope) equipped with 488 nm laser.

7.2.14. Determination of plasma ANP levels in the rat venous blood

Competitive ELISA technique was used in our study to determine the levels of ANP in plasma. Competition/Inhibition/blocking ELISA is predominantly used to measure the concentration of an antigen or antibody in a sample by detecting interference in an expected signal output. In this technique, sample antigen or antibody competes with a reference for binding to a limited amount of labelled antibody or antigen, respectively. The higher the sample antigen concentration, the weaker the output signal, indicating that the signal output inversely correlates with the amount of antigen in the sample.

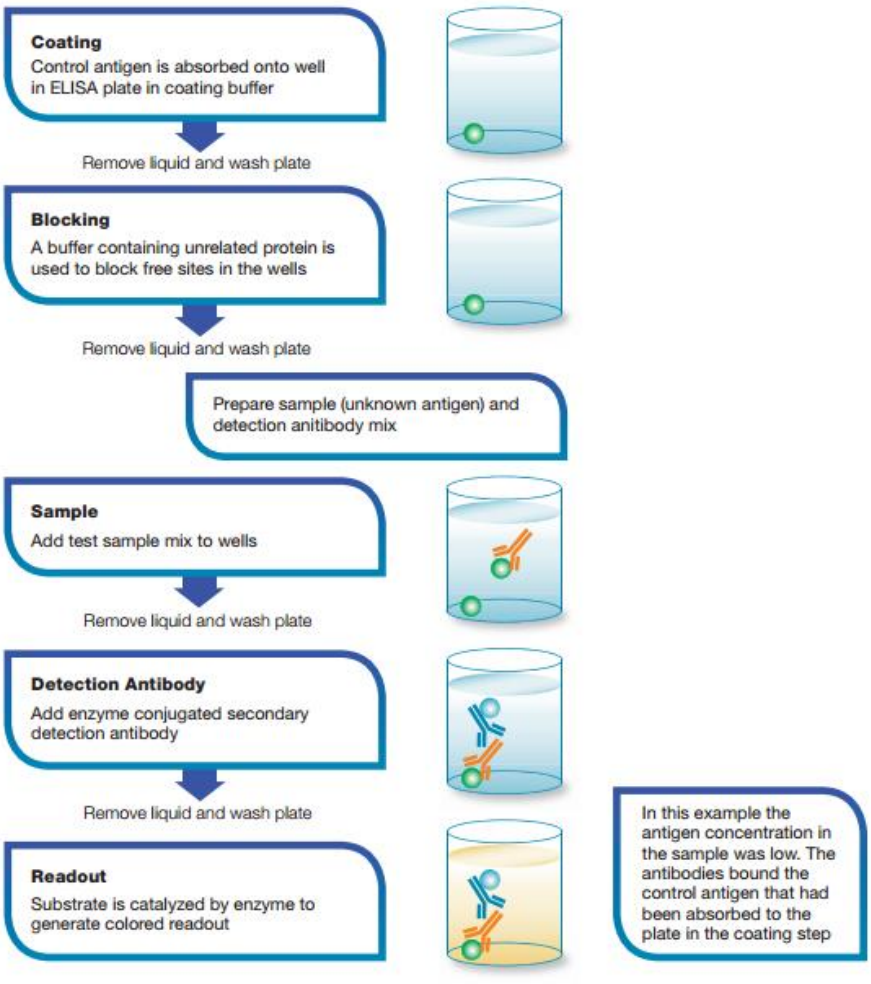


Figure 7.12. Competition ELISA (Bio-Rad, 2017).

In this example in **Fig. 7.12,** a known antigen is used to coat a multiwell plate. Following standard blocking and washing steps, samples containing unknown antigen are added. Labelled detection antibody is then applied to the mixture. If there is a high concentration of antigen in the sample, a significant reduction in signal output will be observed. In contrast, if there is very little antigen in the sample, there will be very little reduction in the expected signal output (Bio-Rad, 2017).

In our study, wash buffer was prepared by adding 30 mL of the concentrated wash buffer to 720 mL of deionized water. The working solution of the ANP standard was prepared by reconstituting 1000pg of the standard in 1 mL of reference standard and sample diluent. Serial dilutions of 2-fold of about 500 µL each from the 1000 pg.mL^{-1} were prepared in reference standard and sample diluent (1000, 500, 250, 125, 62.5, 31.25, 15.63 and 0 pg.mL^{-1}) (**Fig.7.13**). Biotinylated detection antibody working solution was prepared by diluting concentrated biotinylated detection antibody with biotinylated detection antibody diluent in a 1:100 ratio and 5 to 6 mL of the solution was prepared for 96 wells as 50 µL/well was required. Concentrated HRP conjugate working solution was prepared by diluting concentrated HRP conjugate with concentrated HRP conjugate diluent in a 1:100 ratio and 11-12 mL of the solution was prepared for 96 wells as 100 µL/well was required.

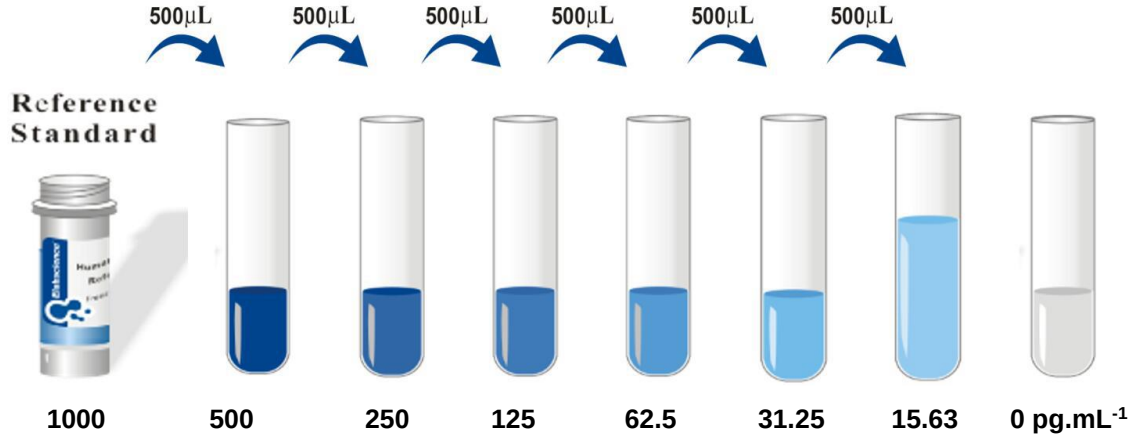


Figure 7.13. Serial dilutions of ANP. Stock solution of ANP at 1000 pg.mL^{-1} was diluted 2-fold up until 15,63 pg.mL^{-1}.

Triplicates of about 50 µL of the standards and samples were pipetted into each well. Biotinylated detection antibody working solution (50 µL) was immediately added into each well. The plate was covered with a sealer and incubated at 37 °C for 45 minutes. The solution was aspirated from all the wells and 350 µL of the wash buffer was added

to the wells and soaked for 1-2 minutes. The plate was washed thrice and patted on dry paper towel to ensure that the solution has been entirely removed. HRP conjugate working solution (100 µL) was added to each well and the plate was incubated for 30 minutes at 37 °C.

The solution was aspirated, and the plate was washed 5 x and patted on a paper towel. Substrate reagent (90 µL) was added to each well and the plate was covered with a sealer and incubated at 37˚C for 15 minutes. Stop solution (50 µL) was added and optical density of each well was measured using a microplate reader (2030 Multilabel Reader Victor X3, Perkin Elmer, USA) set to 450 nm. MyAssay program was used to determine the averages and SEM of the triplicates of the reference standards and samples. A 4-parameter logistic curve was plotted from the standards and the concentrations of ANP determined from the curve.

7.2.15. Biodistribution of dpcaf using Raman Microscopy

Carbon nanotubes can be detected in various tissues as they have very unique structures such as the G and D bands. Different concentrations of dpcaf, PEG-CNTs, PEG-ANP-FITC-CNTs, and Dex (10, 50, 100, 150 and 200 $\mu g.mL^{-1}$) were prepared in PBS (pH 7,4) buffer. The standards were loaded into the capillary tubes, sealed and scanned using Raman spectroscopy technique. The tissues from various organs were also loaded into the capillary tubes and scanned with Raman using laser 785nm and 514nm.

7.3. Results and discussion

7.3.1. Vertically aligned MWCNTs synthesis and purification

Vertically aligned multiwalled carbon nanotubes were successfully synthesised. There was a very thin layer of nanoparticles on the top surface of the carbon nanotubes (**Fig.7.14A**). This top layer was caused by iron from ferrocene used to prepare the catalyst.

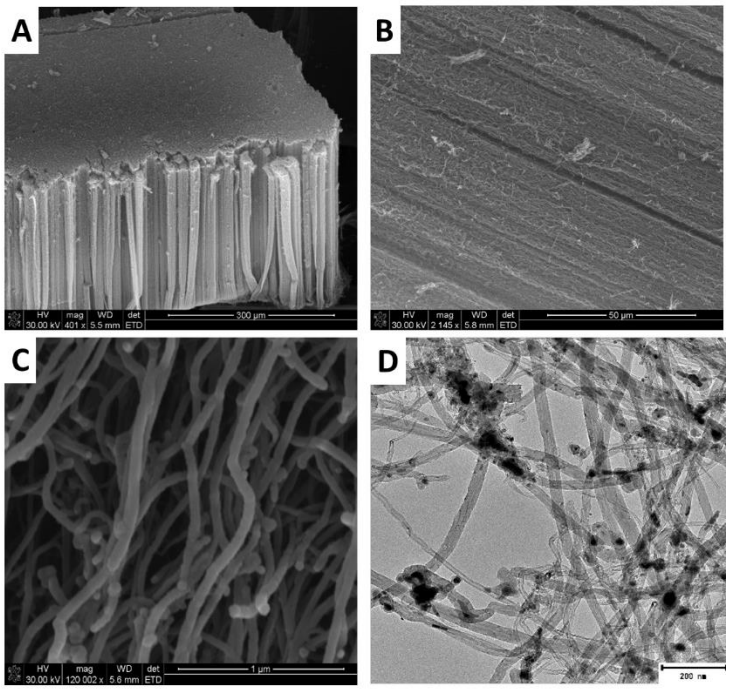


Figure 7.14. Vertically aligned multiwalled carbon nanotubes (VA-MWCNTs) morphology. Carbon nanotubes with nanoparticle layer on top (A). VA-MWCNTs at 2145 x magnification (B). VA-MWCNTs under 120 000 x magnification (C). VA-MWCNT TEM microgram (D).

Vertical orientation of MWCNTs was confirmed by increasing the magnification to 2145 (**Fig.7.14B**). Magnification was increased to 120 000 x and the 3D of the MWCNTs was revealed. The tubular structure of MWCNTs was clearly defined including the cap that seals the end of the tube (**Fig. 7.14D**).

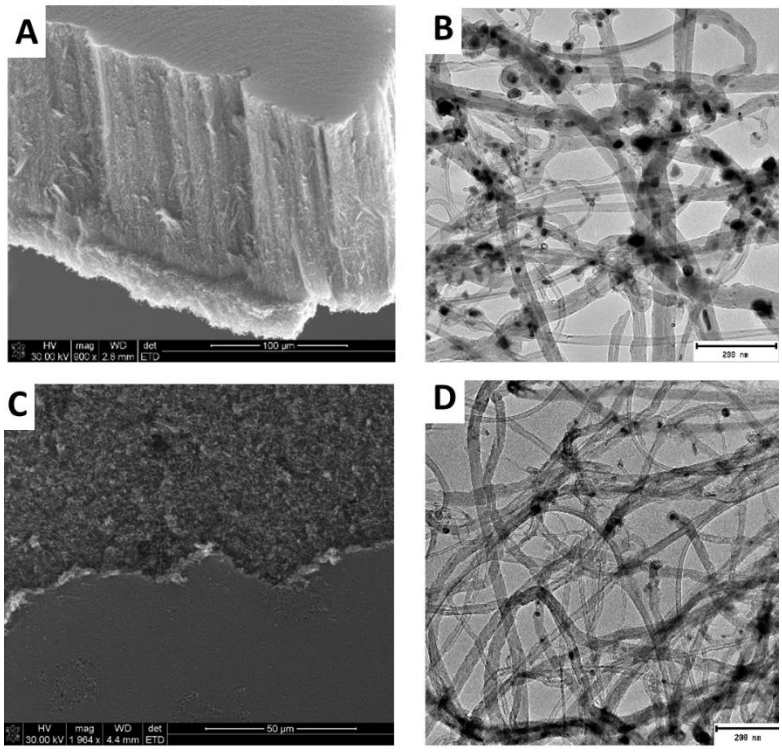


Figure 7.15. Purification of MWCNTs. Pristine VA-MWCNTs prior to purification (A). Pristine MWCNT TEM microgram (B). Top view of MWCNTs following purification with 5 N HCl (C). HCl purified MWCNT TEM microgram.

Pristine MWCNTs were purified using 5 N HCl. Iron from the catalyst reacts with chloride from HCl and the following chemical reaction takes place:

Fe(s) + 2 **HCl**(aq) ⟶ $FeCl_2$(aq) + H_2(g). Amorphous carbon reacts with H_2 to form the C-H bond. It can be seen that there was a successful purification of MWCNTs as depicted in **Fig. 7.15C**. Further confirmation of a successful purification was demonstrated by TEM microgram (**Fig.7.15D**). The MWCNTs are far much cleaner than in **Fig. 7.15D** than in **Fig. 7.15B.**

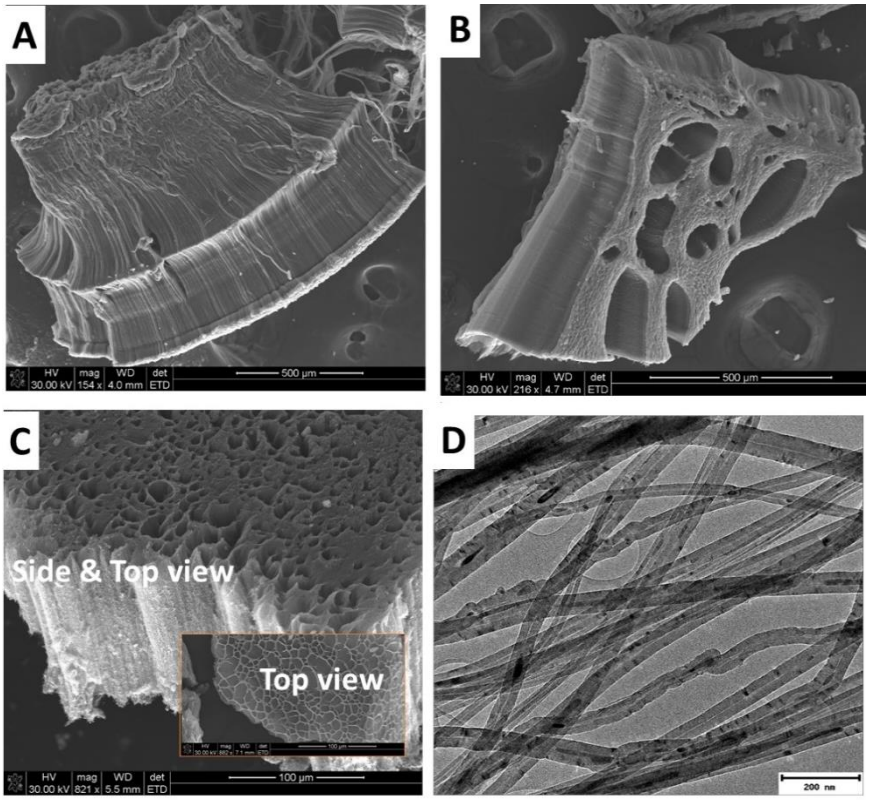


Figure 7.16. Purification of VA-MWCNTs. MWCNTs in conc H_2SO_4 (A). MWCNTs in 2 M H_2SO_4 (B). MWCNTs in 5 N HCl (C). MWCNTs TEM microgram (D).

Conc sulphuric acid was also used to purify the MWCNTs but the morphology of the nanotubes was affected. Addition of conc H_2SO_4 caused the nanotubes to shrink (**Fig.7.16A**). The 2 M H_2SO_4 perforated the top surface and penetrated deeper into the carbon nanotubes and made holes (**Fig. 7.16B**). Honeycomb-like structures were formed following incubation of the MWCNTs with 5 N HCl. The sides were not affected, and it was only the top layer and the CNTs below the top layer that was affected (**Fig.**

7.16C). HCl purified MWCNTs were further analysed with TEM and clean nanotubes with vertical alignment was observed as depicted in **Fig. 7.16D.**

7.3.2. Cytotoxicity of MWCNTs

There is currently a controversial debate on the toxicity of carbon nanotubes in the animals. Clinical application of carbon nanotubes has been hindered by this controversial issue (Li *et al.*, 2017). Functionalised carbon nanotubes are less toxic compared to pristine carbon nanotubes. In our study, pristine CNTs were not used in the *in vitro* studies as they were floating on top of the buffer and was not easy to disperse into the buffer. The functionalised CNTs were dispersed in the buffer and they were used in this study as a result. Various formulations were used at different concentrations to determine the concentration at which the PC-12 cells start dying prior to application in *in vivo* studies.

Cell viability was monitored by Trypan Blue exclusion technique. This staining assay is based on the uptake of trypan blue dye by dead cells due to loss of their membrane integrity. The live cells will exclude the dye and the dead cells will allow the dye to diffuse through the dead cell membrane into the cytoplasm and nucleus of the cell. The dead cells will appear darker than the viable cells due to the absorbed blue (Chung, Kim and Kim, 2015). The live and dead cells are counted on the haemocytometer under the light microscope and the % of the live ones is determined. The PC-12 cells grew successfully with and without treatment with the formulations at various concentrations as demonstrated in **Fig. 7.17A-I**. Only very few cells absorbed Trypan blue dye as a result of death and this could be due to the formulations or other impinging factors as the cells were not in their natural environment. The structure of the PC-12 cells could also be seen clearly under higher magnification (**Fig. 7.17G-I**).

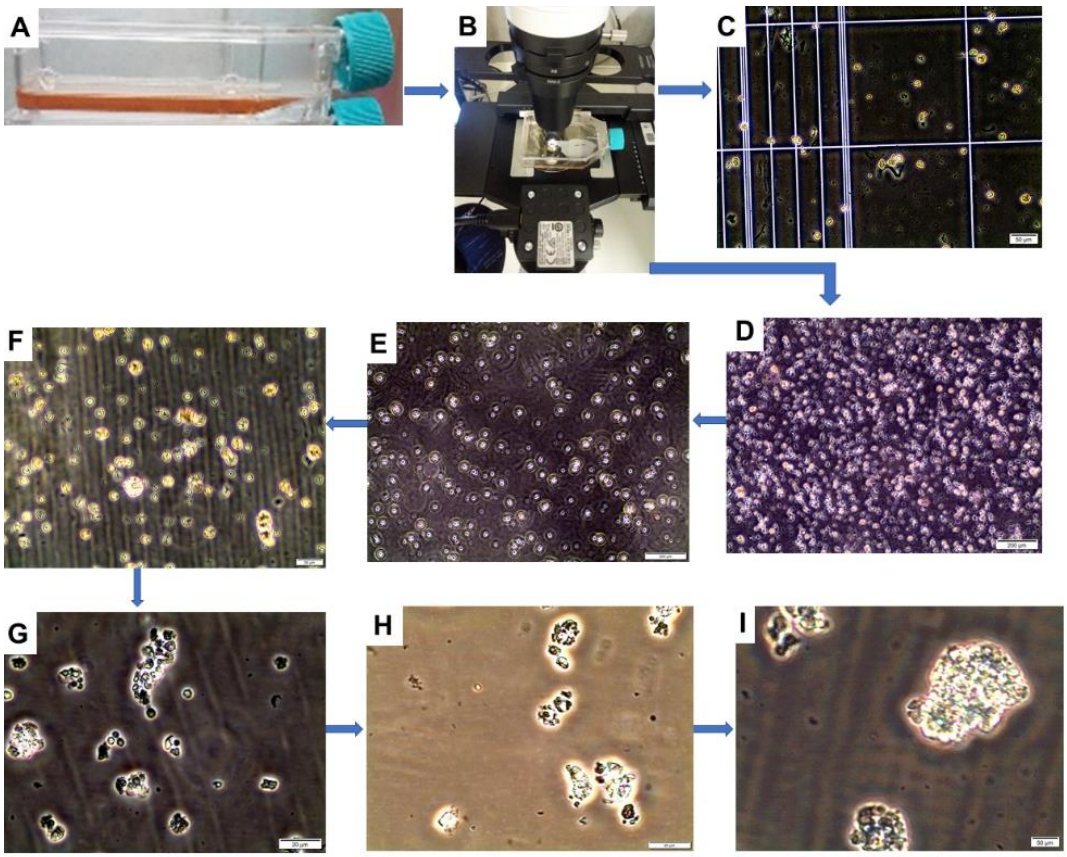


Figure 7.17. PC-12 cells under light microscope and cell viability using Trypan blue exclusion technique. PC-12 cells grown in tissue culture flasks (A). Viewing of cells with inverted light microscope (D-I).

Cytotoxicity was determined by MTT assay. The yellow MTT solutions form blue formazan crystals in the live cells as the mitochondrial dehydrogenases cleave the tetrazolium to insoluble formazan. The crystals are dissolved in acidified isopropanol (10 % Triton X-100 plus 0.1 N HCl in anhydrous isopropanol).

Different concentrations of formulations were used as follow; high (0-200 $\mu g.mL^{-1}$), medium (0-20 $\mu g.mL^{-1}$) and low (0-0,2 $\mu g.mL^{-1}$). The viability was 80-100 % in the cells that were not treated with the formulations in all the concentration categories.

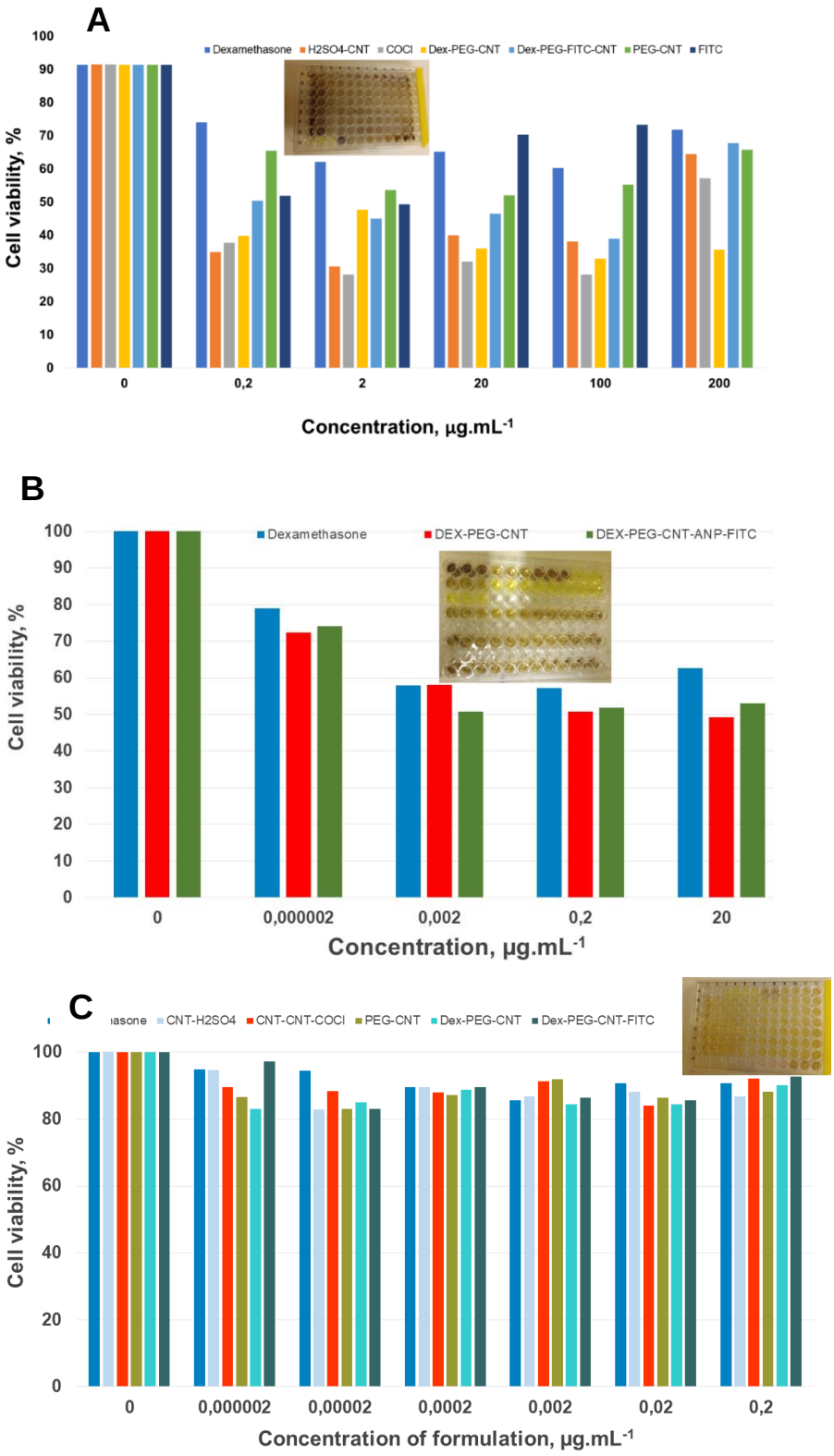


Figure 7.18. Cell viability versus concentration of the formulations. Functionalised MWCNTs at various concentrations were incubated with PC-12 cells at 37 °C for 24 hours. (A-C).

The cell viability in the high concentration range was approximately 68 %, 40 %, 38 %, 38 %, 50 %, 60 % and 61 % in dexamethasone, H_2SO_4, COCl, Dex-PEG, Dex-PEG-FITC, PEG and FITC treated CNTs respectively. in the dexamethasone treated group

in the high concentration range (**Fig 7.18A**). The cell viability in the medium concentration range was approximately 65 %, 60 % and 59 % in dexamethasone, dex-PEG and dex-PEG-ANP-FITC treated CNTs respectively (**Fig. 7.18B**). The cell viability was approximately 95 %, 86 %, 87 %, 86 %, 86 % and 89 % in Dex, H_2SO_4, COCl, PEG, Dex-PEG and Dex-PEG-FITC treated CNTs in low concentration range **(Fig. 7.18C**). The cytotoxicity differed from formulation to formulation and from concentration to concentration.

Our findings have demonstrated the reduction of cell viability with an increase in the concentration of the formulations. The reduced viability also depended on the type of the formulation. Cell viability was much better in the medium and low concentration range as opposed to the high concentration range. Wang and colleagues evaluated the effect of SWCNTs on PC-12 cells and found that long-SWCNTs were more toxic than short-SWCNTs (Wang *et al.*, 2011). As these carbon nanotubes were suspended in culture medium and ultrasonicated prior to use, the toxicity could be due to the fact that CNTs were not functionalised. In our study, the CNTs were functionalised prior to use and PC-12 cells were viable at the stipulated concentration range (more than 80 %).

7.3.3. Animal surgery and neurobehavioural assessment

The intraluminal monofilament nylon sutures were successfully prepared as depicted in **Fig. 7.19**. During the initial stage of the *in vivo* studies, the induction of ischemic stroke by middle cerebral artery occlusion did not go well. The rats were dying every time when the bifurcation of the common carotid artery was reached.



Figure 7. 19. Intraluminal monofilament suture with magnified blunt tip. The tip is clearly blunt to avoid damage to the tissues of the blood vessels.

The MCA occlusion technique was too invasive and some of the blood vessels and nerves might have been damaged during surgery which could have led to the high mortality rates (**Fig. 7.19**). The high mortality rate could also be due to the respiratory complications and severe prolonged pain during surgery. In addition, the baroreceptors at the bifurcation might have been damaged when the rat was dissected in that sensitive area.

An alternative route for inducing stroke was taken and the occlusion of the common carotid artery was successfully done, and the mortality rate dropped to nil. Tail venous blood was collected before and after surgery for determination of the stroke biomarker namely, ANP. Formulations were administered immediately after the blood was collected from the tail following surgery. A far much faster recovery was observed in the group treated with dpcaf compared to the other groups (**Table 7.1).**

Table 7.1 Neurobehavioural assessment of the healthy, stroke induced, non-treated and treated SD rats.

Healthy rats	**Premed (pm)**	**Sham (sm)**	**CCAO (co)**	**DPCAF (df)**	**PEGCNT (pt)**	**DEX (dx)**
• **Healthy** • **Very active and alertful** • **No stroke symptoms** • **Circling both sides when suspended by the tail** • **Pink eyes and of the same size**	• Healthy • Very active and alertful • No stroke symptoms • Circling both sides when suspended by the tail • Pink eyes and of the same size • Small weight loss or unchanged weight	• Healthy • Very active and alertful • No stroke symptoms • Circling both sides when suspended by the tail • Pink eyes and of the same size • Small weight loss or unchanged weight	• Not active • One eye dark and sunken • One forelimb not fully functional • Circling one side when suspended by the tail • Increased weight loss compared to the premeds and shams	• Improved general health • Active and alertful immediately after recovery • Circling both sides when suspended by the tail • Improved eye (slightly reddish to pinkish colour) • Improved gripping in both forelimbs	• Improved general health • Active and alertful immediately after recovery • Circling both sides when suspended by the tail • Improved eye (slightly reddish to pinkish colour) • Improved gripping in both forelimbs	• One eye affected • Slighlty active and alertful • Circling one side and seldomly both sides when suspended by the tail • Slightly reddish and sunken eye • Improved gripping in both forelimbs

We could, therefore deduce that dpcaf played an important role in reducing the symptoms of ischemic stroke and the improvement was far much better than that of pegcnt as depicted in **Table 7.1.** There was no improvement in the health of the rats when dexamethasone alone was used. In addition, there was a quicker recovery from anaesthesia and higher BAR in the dpcaf treated group as opposed to the other groups.

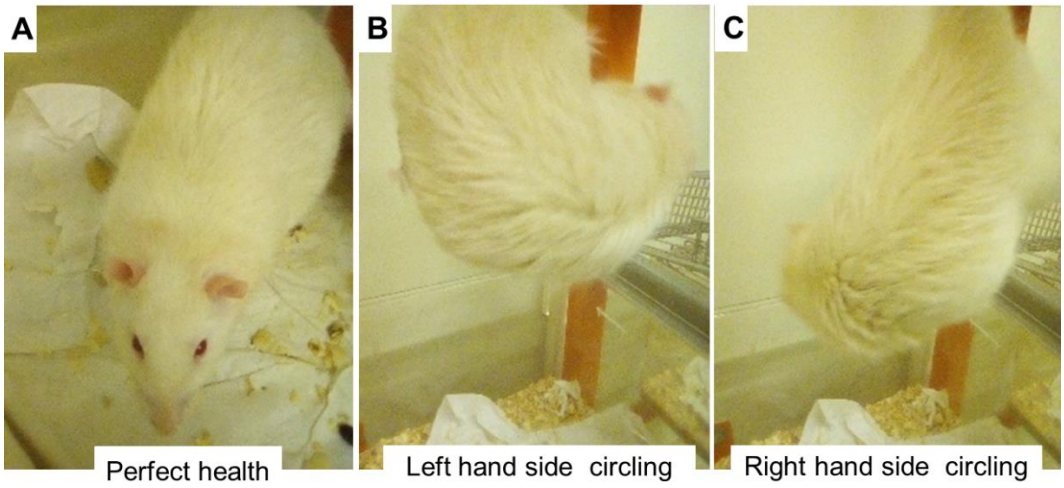


Figure 7.20. Neurobehaviour of Premedication rats. Perfect healthy rat with intact eyes (A). Left hand side circling (B). Right hand side circling (C).

Surgery was not conducted in the premedication group. The rats were injected with fentanyl, dormicum, temgesic and lignocaine and anaesthesia was maintained under isoflurane and oxygen. Both eyes looked intact and healthy. The fur was smooth, and ears raised up. The whiskers looked fine. It was 100 % alertful with a perfect BAR (**Fig.7.20A**) (**Table 7.1**). The rat was circling to both sides and all directions (**Fig. 7.20B-C)**. It could be deduced from the results obtained that premedication did not pose any observable detrimental effect on the rats.

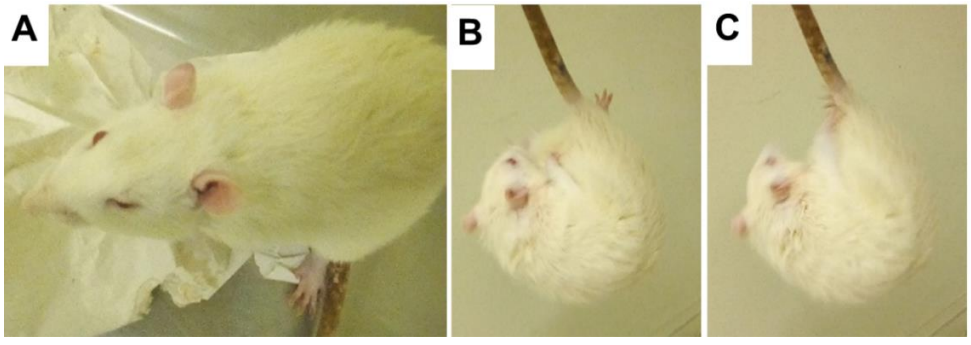


Figure 7.21. Neurobehaviour of CCAO group. Left eye sunken and dark red (A). Right hand side circling (B). Right hand side circling (C).

The left eye was sunken and looked dark red (**Fig. 7.21A**). Contralateral circling to the right when the rat was suspended by the tail was noticed since left common carotid artery was occluded (**Fig.7.21B-C) (Table 1**). The back arch and hunched posture were noticed. These symptoms are indicative of the stroke that was induced by occlusion of common carotid artery.

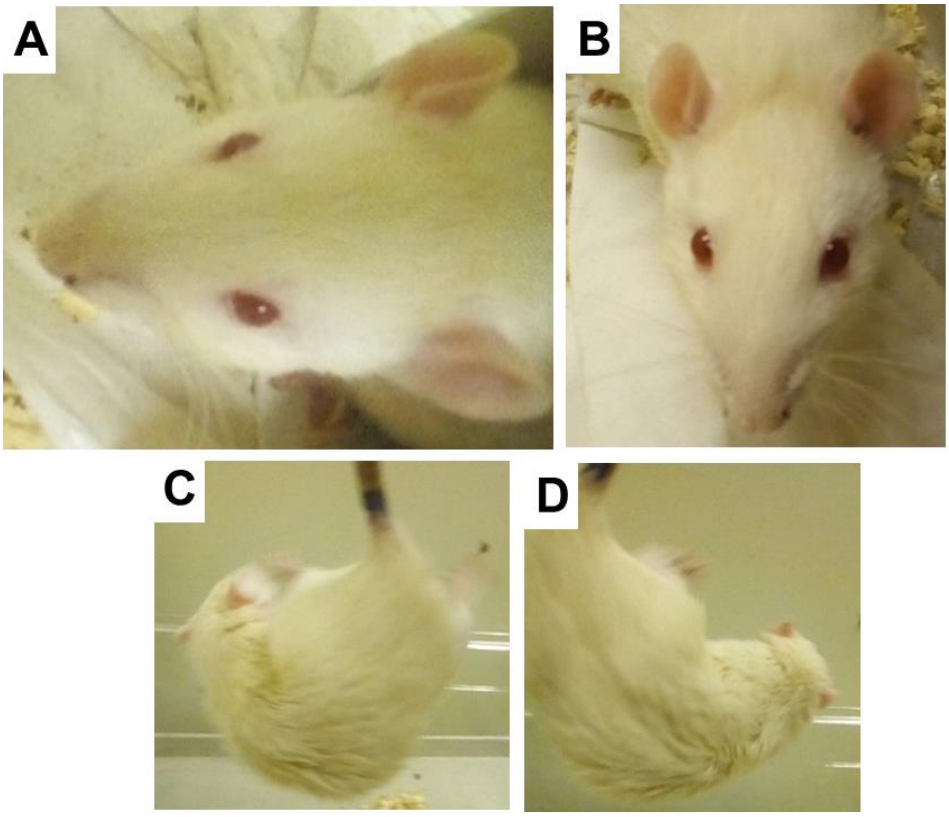


Figure 7.22. Neurobehaviour of dpcaf treated group. Improved eye condition, not sunken and slightly red (A-B). Right hand side circling (C). Left hand side circling (D).

There was an improvement of the eyesight as both eyes looked healthy (**Fig. 7.22A-B**). Left eye was not sunken but was dark red and went back to normal after 5 hours of reperfusion (**Fig.7.22A-B**). Rat circled both sides and, in all directions, when suspended by the tail (**Fig. 7.22C-D**) (**Table 1**). This is an indicative of the effect of dpcaf on the health status of the rat. This implies that dpcaf treated the stroke successfully in this group.

Gholamine and colleagues evaluated neurobehavioural toxicity of single-walled (SWCNTs) and multiwalled carbon nanotubes (MWCNTs) in mice. They found that CNTs could cause behavioural toxicity such as anxiety and depression depending on their structure. Furthermore, they found that MWCNTs were more toxic than SWCNTs

(Gholamine *et al.*, 2017). In their study, carbon nanotubes were not functionalised and were also suspended in PBS and sonicated prior to use. In our study, we did not experience any toxicity as the CNTs were functionalised and PEGylated prior to use.

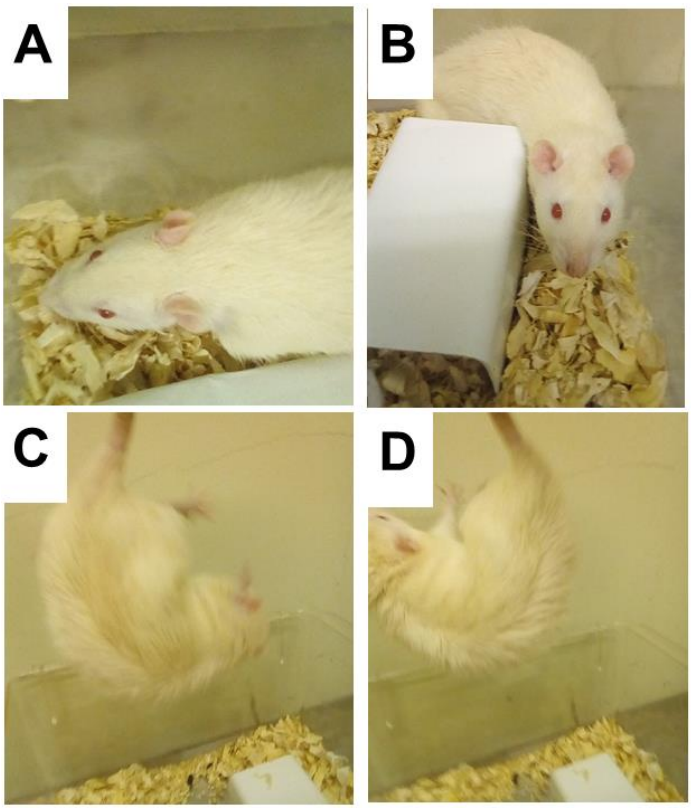


Figure 7.23. Healthy non-ischemic and untreated rats. Perfect healthy rat with intact eyes (A-B). Left hand side circling (C). Right hand side circling (D).

This group was assessed prior to surgery during habituation process. The fur was smooth, and both eyes were bright and reddish pink. The rat was 100 % alertful and spontaneous movement in all directions was observed, and the rat was circling in both directions (**Fig.7.23C-D**) (**Table 7.1**). In general, the rat was 100 % healthy as there were no signs of stress nor symptoms of stroke.

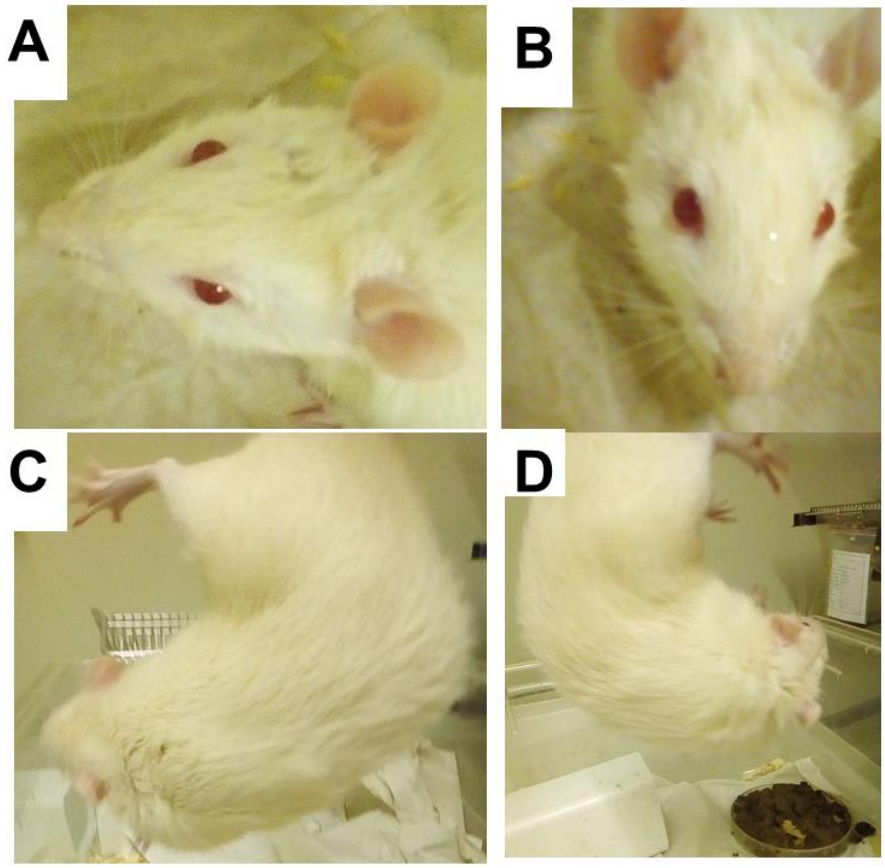


Figure 7.24. PEG-CNT treated rats. Perfect healthy rat with intact eyes (A-B). Right hand side circling (B). Left hand side circling (C).

In this group, there was an improvement in general health of the rat. Both eyes were healthy. The rat was very alertful, and the fur looked very smooth. Spontaneous movement in all the directions and spontaneous circling in both directions was noticed (**Fig. 7.26A-D**) (**Table 7.1**). The improvement in the healthy state of this group is an indicative that the PEGylated CNTs could reduce inflammation in ischemic stroke leading to a healthy state of the rat. This also implies that PEG facilitated the delivery of the CNTs to the diseased site. From the results obtained, it could be deduced that CNTs have a beneficial role in the healing of stroke.

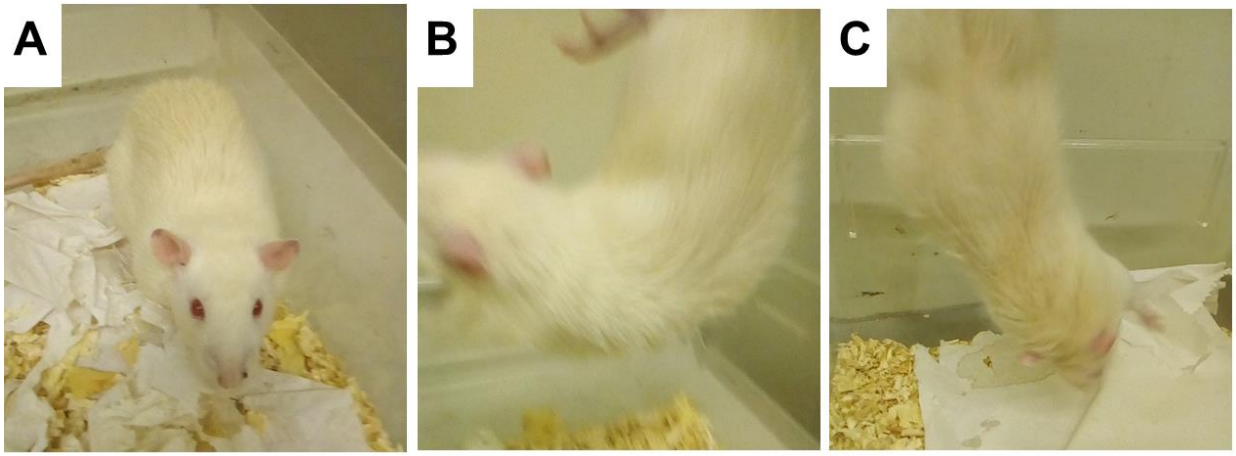


Figure 7.25. Sham group. Perfect healthy rat with intact eyes (A). Right hand side circling (B). leftt hand side circling (C).

In the sham group, the CCA was isolated but not occluded. Following isolation of the CCA, the wound was closed after 30 min. Since the artery was not occluded, the blood supply to the brain was not interrupted. The rat was healthy as if nothing has been done on it. The eyes were bright and reddish pink. The fur was smooth, and no back arch or hunched posture was noticed in this group. Circling was spontaneous on both sides and the spontaneous movement in all directions was noticed (**Table 7.1**).

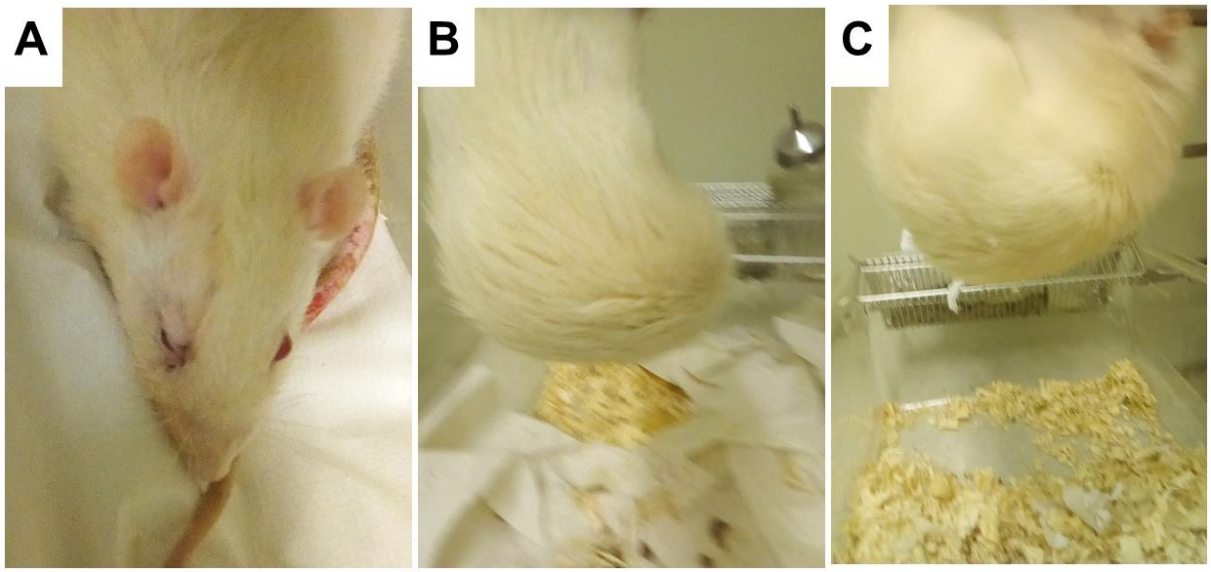


Figure 7.26. CCAO rat (Ischemic) treated with Dex. Right eye sunken and dark red (A). Left hand side circling (B). left hand side circling (C).

In the Dex treated group, the right eye was dark red and sunken. The rat had a back arch and hunch posture and did not look healthy. The spontaneous movement in all directions and spontaneous circling to both directions were not observed. Rat circled to the right-hand side only. From the results observed, it seems that Dex alone did not have any beneficial impact on the health of the rat (**Table 7.1**).

7.3.4. Humane endpoints and sampling

Rats underwent 24-hour reperfusion following surgery and i.v. injection with the formulations. Venous blood withdrawn from the tail (before surgery and after surgery) and blood from the heart (after 24-hour reperfusion) were centrifugated to separate plasma from the RBC (**Fig.7.27A-B)**. Plasma was successfully separated from the red blood cells and stored at -20˚C for ANP measurements.

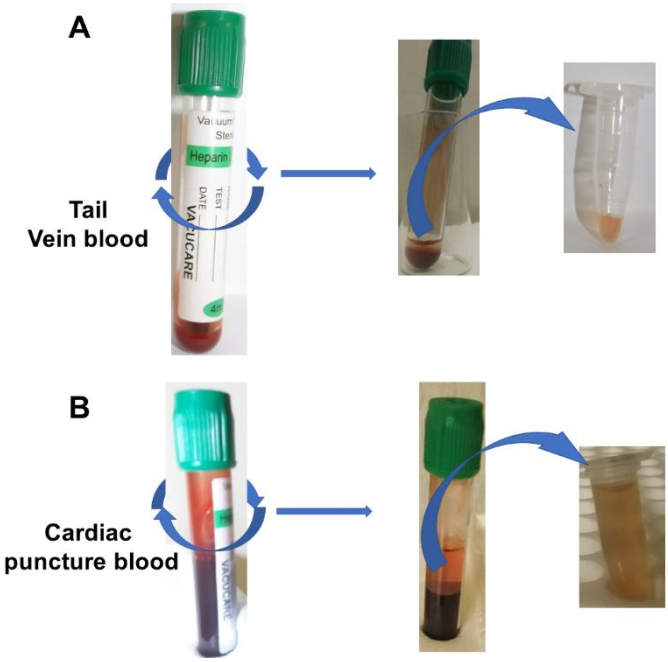


Figure 7.27. Blood collected from the tail vein (A) and heart (B) centrifugated to separate plasma.

Rats were euthanized following 24-hour reperfusion, cardiac puncture was performed, and PBS perfusion was also done. The brain was successfully isolated from the skull. The olfactory bulbs and cerebellum were removed from the brain and the volume of the brain was determined and was found to be approximately 2 mL.

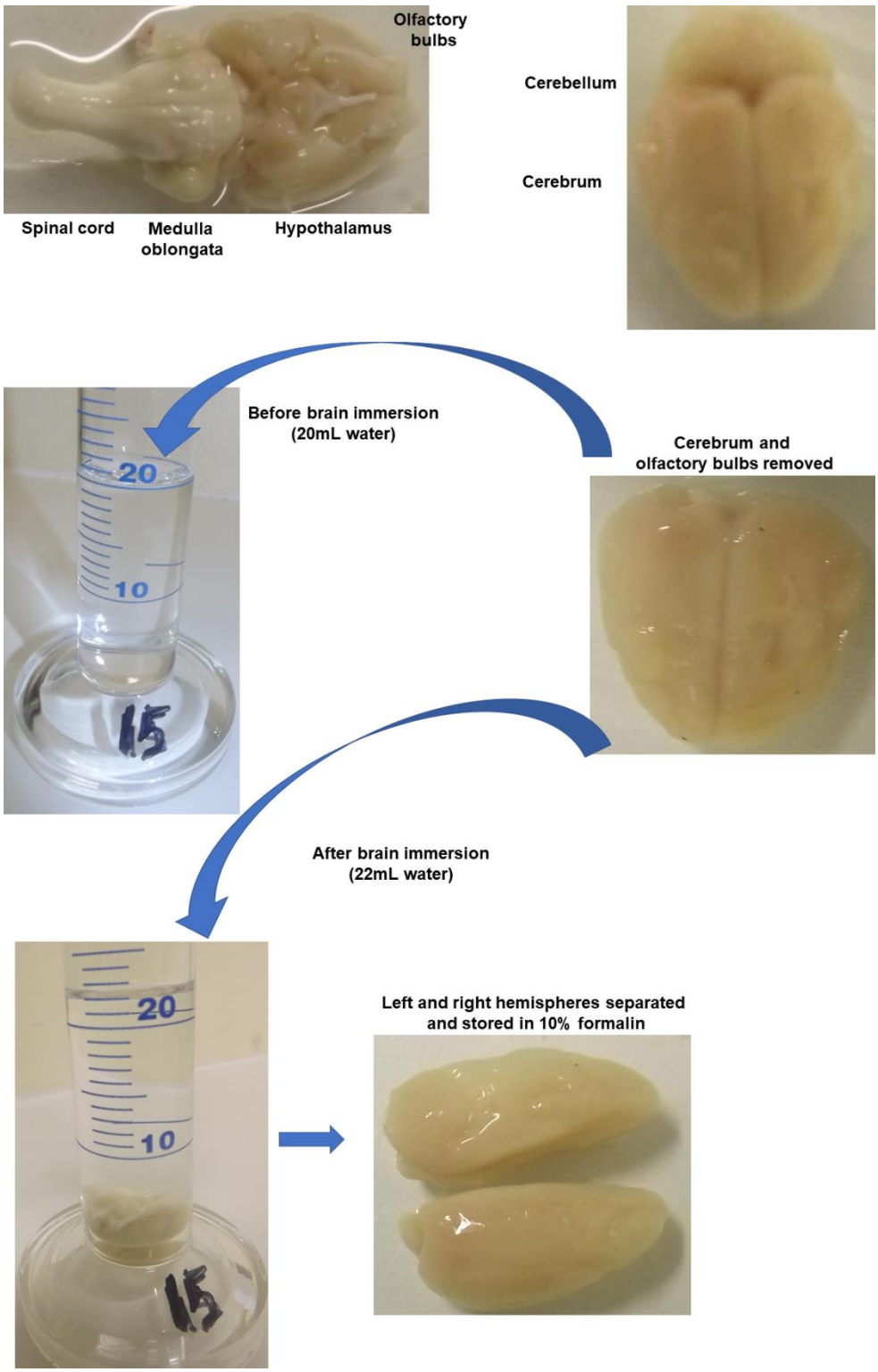


Figure 7.28. Brain preparation for histological evaluation. Left and right hemispheres were separated and stored in formalin.

Brain hemispheres were successfully separated, weighed and stored in 10 % formalin. Perfusion was successful in all organs as depicted by the change in colour from red to pale/white following perfusion with PBS (**Fig. 7.28**).

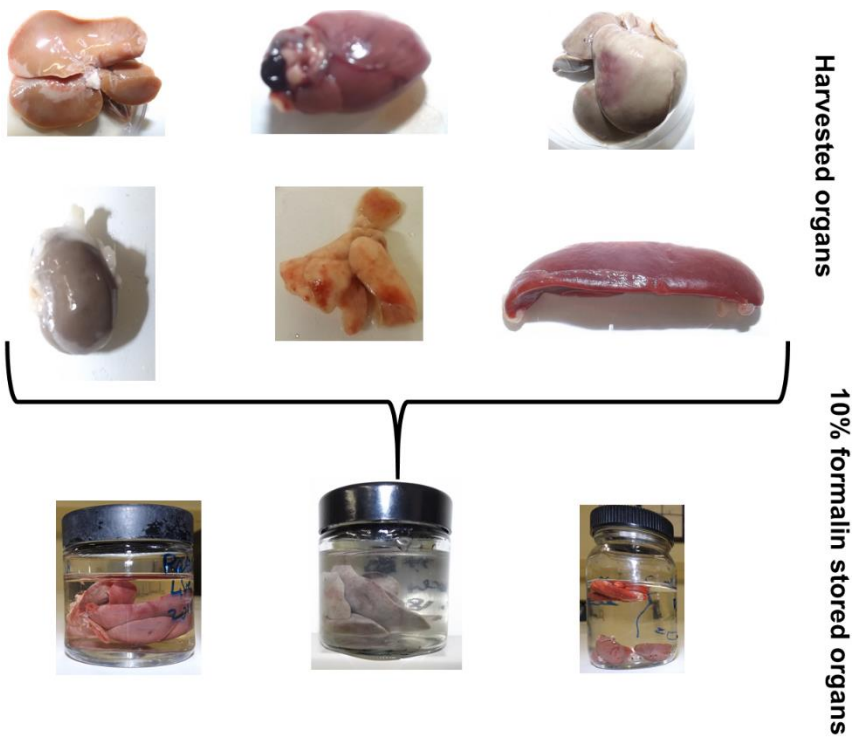


Figure 7.29. Organs harvesting and preservation during perfusion.

The other organs such as liver, heart, lungs, spleen and kidneys were well perfused and successfully isolated as demonstrated in **Fig. 7.29**. The spleen was still red as it is the blood filter and old red blood cells are recycled in this vital organ and it was not easy to perfuse it completely. The harvested organs were stored in 10 % formalin to prevent putrefaction to preserve their anatomical morphology for histological evaluation (**Fig. 7.29**).

7.3.5. Brain and total body weights following CCAO and treatment with the formulations

In the Premed group, there was no change in both the left and the right brain hemisphere weights as the rat did not undergo any surgery. In the Sham group, there was a very slight difference in the hemisphere weight and this could be due to the stress as surgery was performed but there was no occlusion of the vessel. A vast difference in hemisphere weights was observed in the CCAO group. Since the occlusion was performed in the left common carotid artery, the rise in weight of the left hemisphere was highly noticeable. The weight increased as a result of inflammation

that was caused by an induction of stroke. This is an indicative of the brain edema that was generated during stroke induction.

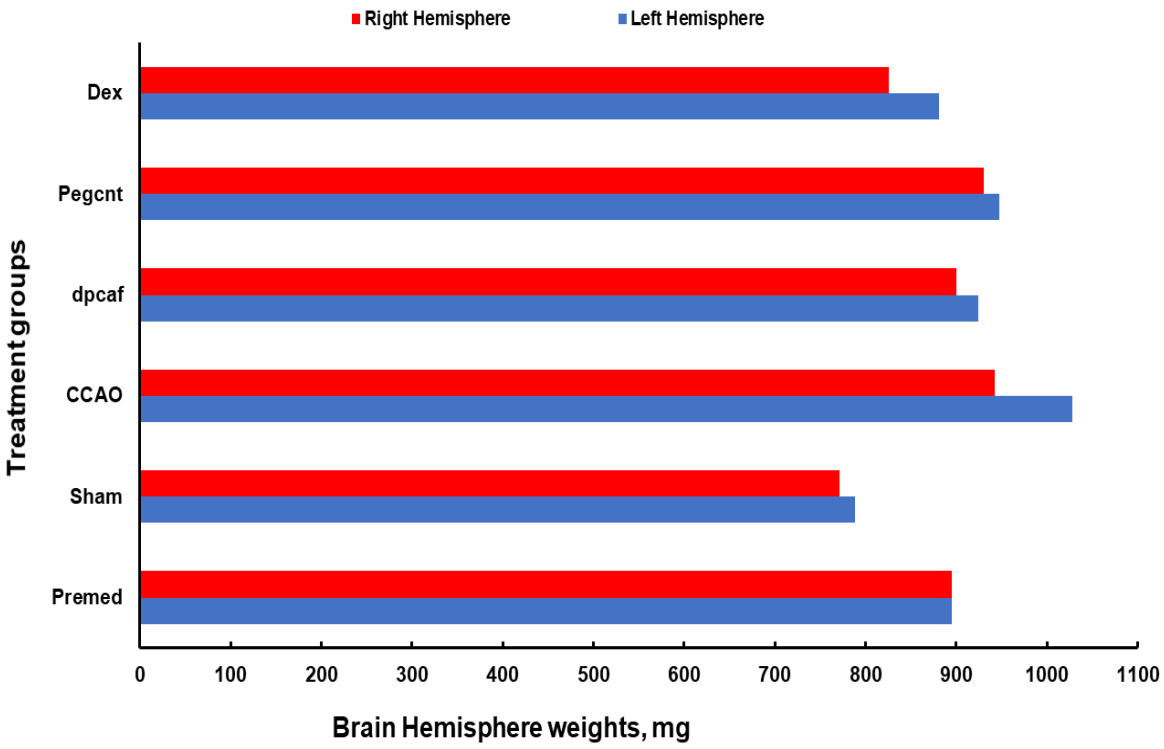


Figure 7.30. Brain hemisphere weights before and after treatment of the rat with the formulations.

From the graph, we could deduce that the brain oedema was triggered by the CCAO as demonstrated by the increase in the weight of the left hemispheres confirming the presence of ischemic stroke in the rats. The left hemisphere weight in the CCAO rat was reduced following treatment of the rats with dpcaf. This implies that the dpcaf formulation reduced the inflammation in the left hemisphere as demonstrated by a drop in the weight of the left hemisphere **(Fig. 7.30**). The left hemisphere weight of the CCAO rat was also reduced in the PEG-CNT group. The data has demonstrated that PEG-CNT reduced the inflammation in the CCAO rat. (**Fig. 7.30**). The reduction in the inflammation could be due to the CNTs that reached the ischemic site. The PEG facilitated the smooth delivery of the CNTs to the site.

In the rats that were treated with Dex only, there was no reduction in the inflammation in the left hemisphere **(Fig. 7.30**). Although Dex is well known for its inflammatory

properties, it could not reduce the inflammation, and this could be due to its low dose affecting its bioavailability to the site of injury.

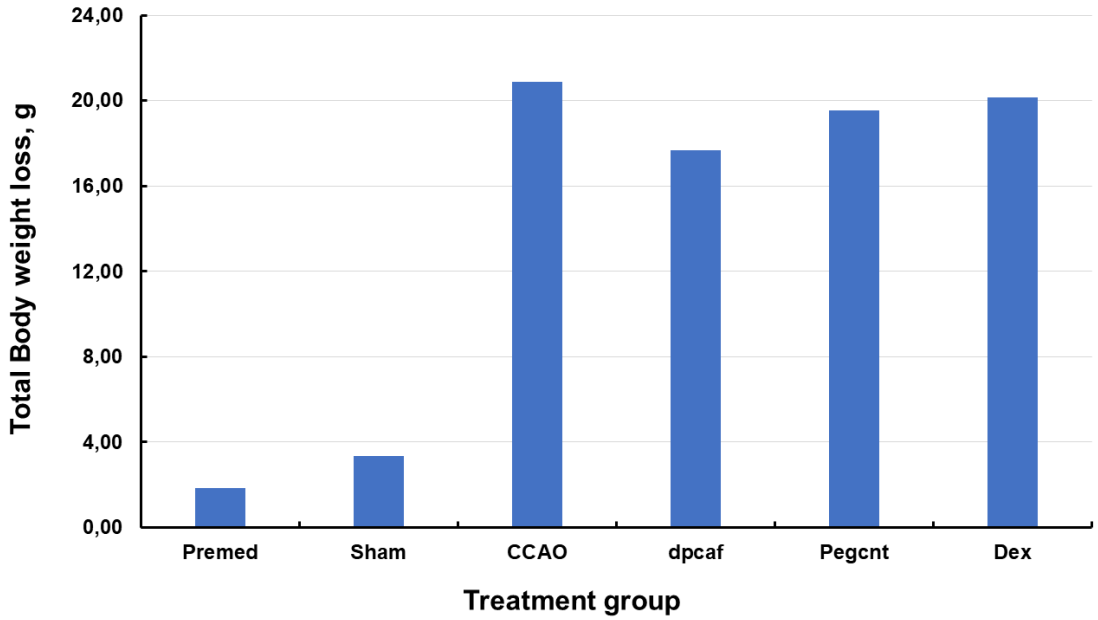


Figure 7.31. Total body weight loss during CCAO and following treatment.

In order to check whether rats were losing weights as a result of intervention, their pre-surgery and post-reperfusion total body weights were recorded. The weight loss for the premed group was very minimal as compared to the other groups. In the sham group, there was a slight increase in the weight loss and this could be due to the stress during surgery to expose the CCA. There was a drastic increase in the weight loss during the CCAO.

The rat experienced a lot of stress and this led to the increase in the weight loss. A drop in the weight loss was observed following the treatment of the rat with dpcaf. A slight decrease in the weight loss was noticed following the treatment of the rat with PEG-CNT and a least drop of weight loss was observed in the Dex treated rats (**Fig. 7.31**). These results have demonstrated the beneficial effect of both the dpcaf and PEG-CNT in the monitoring of weight loss during induction of stroke.

7.3.6. Optimization of the formulation dose and Fluorescence measurements

Since it was not known at which dose the rats would experience any side effects, there was a need to perform dose response experiments. Low, medium and high doses of

dpcaf were i.v. injected in the rats via the tail to determine toxic dose of this formulation prior to use in the subsequent experiments. All the rats survived under all the doses that were evaluated. The rats treated with these doses did not encounter any side effects. This is an indicative that all the doses did not have any toxic effect on the rats. Furthermore, the fluorescence measurements were performed in the rat brains.

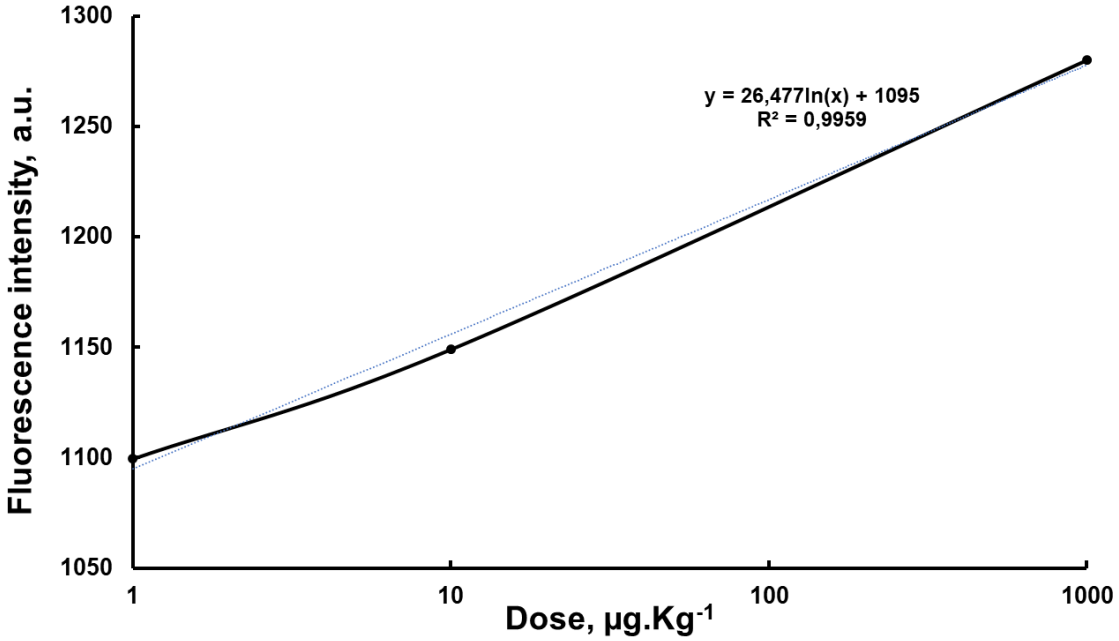


Figure 7.32. Dose response curve of dpcaf in CCAO rats.

Fluorescence intensity was determined by Victor X3 Perkin Elmer microplate reader and plotted against the dose to create a dose response curve. The fluorescence intensity was found to be directly proportional to the dose as illustrated in **Fig.7.32**. In addition, the findings have demonstrated that our complex was successfully labelled with the FITC.

7.3.7. Biodistribution of dpcaf using Raman Microscopy

Since carbon nanotubes have a unique structure, they could be detected in the samples based on the G and D bands. Various concentrations of dpcaf, PEG-CNTs, PEG-ANP-FITC-CNTs, and Dex (10, 50, 100, 150 and 200 $\mu g.mL^{-1}$) were prepared in PBS (pH 7,4) buffer. These formulations were loaded into microcapillary tubes and sealed on both ends by flaming both sides to prevent leakage (**Fig. 7.33**). The tissue samples were also loaded in the same manner.

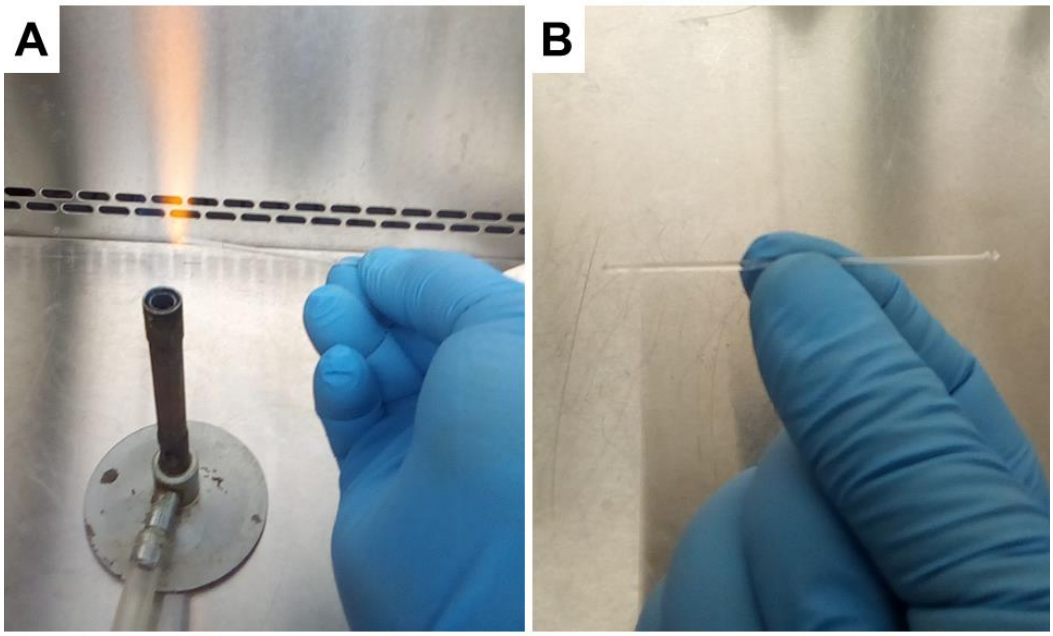


Figure 7.33. Loading of formulations and samples into the microcapillary tubes for Raman analysis. Sealing by flame (A). Sealed microcapillary tube with the formulation/sample inside (B).

The highest concentration dpcaf was scanned using Renishaw microRaman at 514 nm and 785 nm lasers. PEG-CNTs were also scanned. There were no signals in both formulations at both 514 nm and 785 nm. The lack of signals could be due to very low concentration as the signal depends on the concentration in addition to other factors and the instrument has its own LOD.

7.3.8. Biodistribution of dpcaf using Absorption Spectroscopy

Various concentrations of dpcaf ranging from 0-100 $\mu g.mL^{-1}$ were prepared and scanned at 490 nm using Perkin Elmer multilabel reader Victor X3. Calibration curve was contracted and concentrations of dpcaf of the samples from different tissues were determined by extrapolation of the standard curve.

Table 7.2. Concentrations of the standards of dpcaf.

Calibrator	Wells	Concentration, µg/mL^{-1}	Raw	SEM	Backfit	Recovery %
Standard1	A1	0	0,033	0	< Curve	-
	A2		0,033		< Curve	-
	A3		0,033		< Curve	-
Standard2	A4	2	0,044	0	1,997	99,87
	A5		0,044		1,997	99,87
	A6		0,044		1,997	99,87
Standard3	A7	10	0,071	0,000333	8,741	87,41
	A8		0,072		9,003	90,03
	A9		0,072		9,003	90,03
Standard4	A10	20	0,121	0,00186	22,46	112,3
	A11		0,127		24,17	120,9
	A12		0,126		23,89	119,4
Standard5	B1	50	0,202	0,00153	46,27	92,53
	B2		0,207		47,78	95,56
	B3		0,206		47,48	94,95
Standard6	B4	100	0,366	0,00529	97,6	97,6
	B5		0,378		101,5	101,5
	B6		0,384		103,4	103,4

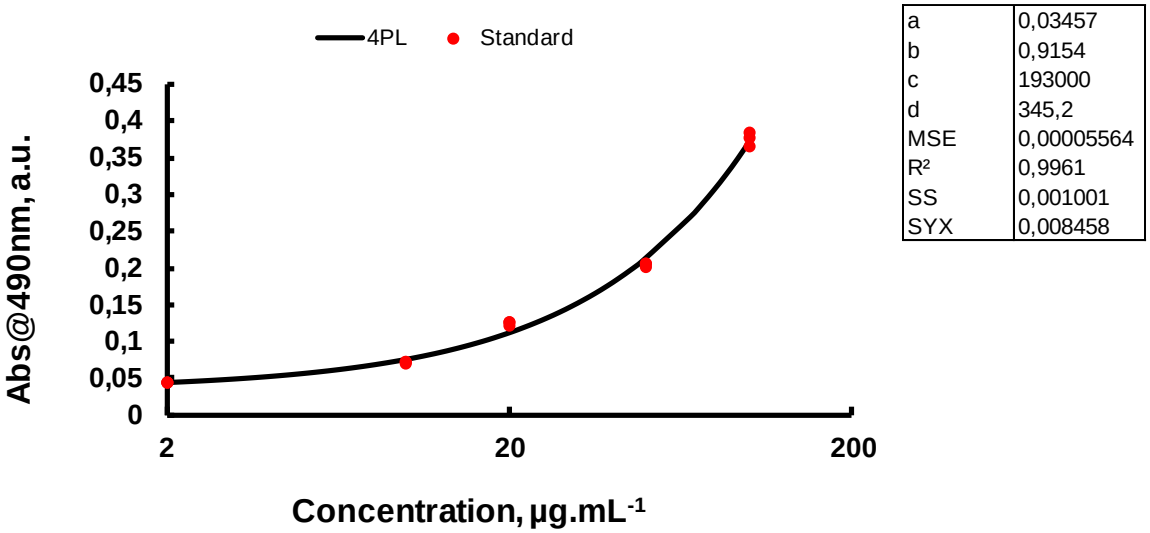


Figure 7.34. Calibration curve of dpcaf.

The absorbance was measured from different tissues such as liver, kidney, lungs, brain, blood and spleen. The highest levels of dpcaf were found in the spleen and liver with 49,66 and 29,42 µg.mL^{-1} respectively.

Table 7.3. Concentrations determined from extrapolation of the standard curve.

	Sample	Wells	Raw	Concentration, µg.mL^{-1}	AverageConcentration, µg.mL-1)	%CV	SD	SEM
	58 Bld	B7	0,098	16,02	15,29	4,16	0,635	0,367
		B8	0,094	14,92				
		B9	0,094	14,92				
	58 heart	B10	0,053	4,114	3,788	14,9	0,566	0,327
		B11	0,049	3,135				
		B12	0,053	4,114				
	58 Spln	C1	0,206	48,01	49,66	5,75	2,85	1,65
		C2	0,222	52,95				
		C3	0,206	48,01				
	58 lungs	C4	0,066	7,427	7,779	10,9	0,844	0,487
		C5	0,071	8,742				
		C6	0,065	7,167				
	58 liv	C7	0,143	29,03	29,42	1,16	0,34	0,196
		C8	0,145	29,62				
		C9	0,145	29,62				
	58 RH	C10	0,108	18,91	18,82	5,28	0,994	0,574
		C11	0,104	17,78				
		C12	0,111	19,77				
	58 LH	D1	0,123	23,2	22,63	2,54	0,575	0,332
		D2	0,119	22,05				
		D3	0,121	22,63				
	58 kid	D4	0,133	26,1	23,69	9,01	2,13	1,23
		D5	0,122	22,91				
		D6	0,119	22,05				

The least concentrations of dpcaf were recorded in the heart and lungs with 3,79 and 7,78 mL^{-1} respectively. The levels of dpcaf in the left hemisphere were higher than in the right hemisphere with 22,63 and 18,82 µg.mL^{-1} respectively (**Table 7.3**). The higher levels of dpcaf in the left hemisphere could be due to the successful targeted delivery of dpcaf to the ischemic side.

7.3.9. Biodistribution of dpcaf using Fluorescence Spectroscopy

The native fluorescence, commonly known as autofluorescence (AF) is a widespread phenomenon and it is caused by the presence of intrinsic biomolecules acting as endogenous fluorophores in the living organisms (Croce, Bottiroli and Unit, 2014). In our findings, the background fluorescence was detected from both the untreated (no FITC) and treated (with FITC) rat organs as a result of autofluorescence. The fluorescence intensity calculations in all the tissues were determined using MyAssays software as follows;

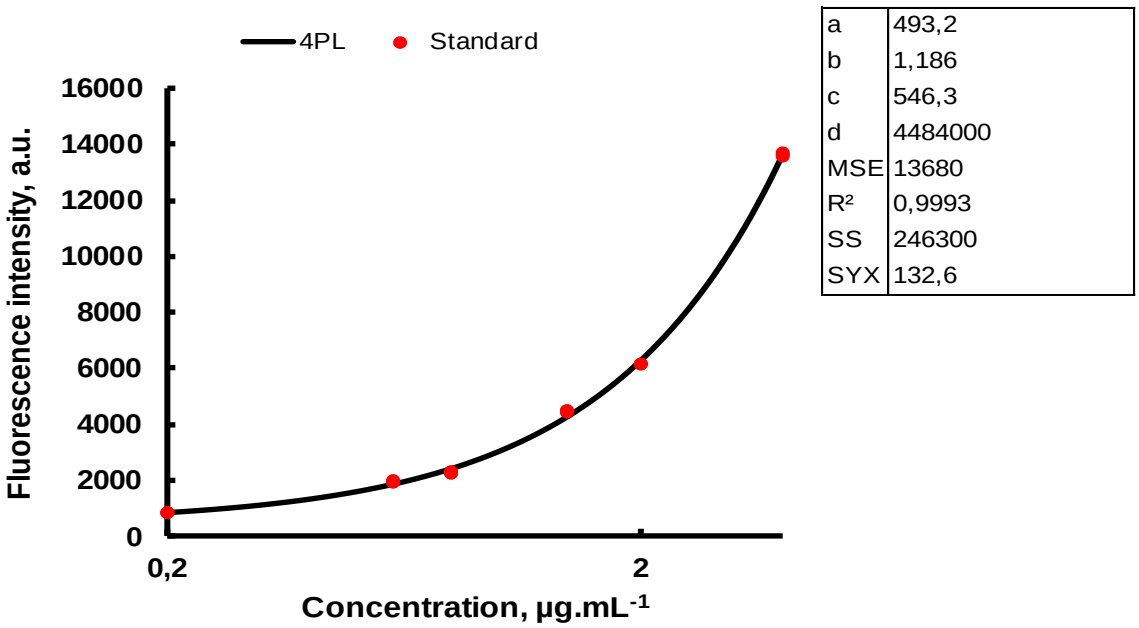


Figure 7.35. 4PL Calibration curve of dpcaf. Various concentrations of dpcaf were prepared and fluorescence intensities were determined to construct this calibration curve.

Table 7.4. Dpcaf calibrators for construction of 4PL standard curve. A set of six standards were prepared and scanned using Victor 3X microplate reader.

Calibrator	Wells	Concentration, ug.mL^{-1}	Fluorescence intensity, a.u.	SEM	Backfit	Recovery %
Standard1	A1	4	13700	25,8	4,015	100,4
	A2		13600		4	100
	A3		13600		3,993	99,82
Standard2	A4	2	6180	7,31	1,972	98,59
	A5		6160		1,966	98,31
	A6		6160		1,965	98,24
Standard3	A7	1,4	4480	8,33	1,462	104,5
	A8		4480		1,46	104,3
	A9		4460		1,454	103,8
Standard4	A10	0,8	2300	8,82	0,75	93,75
	A11		2280		0,743	92,87
	A12		2270		0,7395	92,44
Standard5	B1	0,6	1990	14,1	0,6378	106,3
	B2		1950		0,6263	104,4
	B3		1940		0,6205	103,4
Standard6	B4	0,2	870	3,84	0,1997	99,86
	B5		869		0,1993	99,63
	B6		858		0,1943	97,17

Table 7.5. Sample concentrations of dpcaf treated CCAO rats. The concentrations were extrapolated from the standard curve.

Sample	Wells	Fluorescence intensity, a.u.	Concentration, µg.mL^{-1}	Average Concentration,µg.mL^{-1}	%CV	SD	SEM
df 7 RH	B10	936	0,2288	0,2349	2,58	0,00607	0,00351
	B11	950	0,2349				
	B12	964	0,241				
df 7 LH	C1	822	0,178	0,1832	2,73	0,005	0,00289
	C2	834	0,1835				
	C3	844	0,188				
df 7 kid	C4	1400	0,4181	0,4159	0,517	0,00215	0,00124
	C5	1390	0,4158				
	C6	1390	0,4138				
df 7 liv	C7	1450	0,4383	0,4408	0,535	0,00236	0,00136
	C8	1460	0,4414				
	C9	1460	0,4429				
df 7 spleen	C10	874	0,2015	0,1892	5,64	0,0107	0,00616
	C11	834	0,1835				
	C12	832	0,1826				
df 7 lung	D1	888	0,2077	0,2055	2,26	0,00465	0,00268
	D2	871	0,2002				
	D3	890	0,2086				
df 7 heart	D4	1140	0,3142	0,3169	1,72	0,00546	0,00315
	D5	1160	0,3232				
	D6	1140	0,3134				
df 33 RH	D7	868	0,1988	0,1958	3,06	0,00598	0,00345
	D8	846	0,1889				
	D9	870	0,1997				
df 33 LH	D10	764	0,1512	0,1489	4,93	0,00735	0,00424
	D11	742	0,1407				
	D12	772	0,1549				
df 33 Kid	E1	1510	0,4621	0,4616	0,345	0,00159	0,00092
	E2	1510	0,4629				
	E3	1510	0,4598				
df 33 liv	E4	1140	0,315	0,3125	0,949	0,00297	0,00171
	E5	1140	0,3134				
	E6	1130	0,3092				
df 33 spleen	E7	942	0,2314	0,2361	1,74	0,0041	0,00237
	E8	956	0,2375				
	E9	960	0,2393				
df 33lung	E10	836	0,1844	0,1768	3,73	0,0066	0,00381
	E11	810	0,1725				
	E12	812	0,1735				
df 33 heart	F1	1030	0,2683	0,2697	2,7	0,00728	0,00421
	F2	1050	0,2776				
	F3	1020	0,2632				
df 43 RH	F4	932	0,2271	0,2274	0,586	0,00133	0,00077
	F5	936	0,2288				
	F6	930	0,2262				
df 43 LH	F7	876	0,2024	0,2074	2,36	0,00489	0,00282
	F8	898	0,2122				
	F9	888	0,2077				
df 43 lung	F10	864	0,197	0,203	3,65	0,00741	0,00428
	F11	896	0,2113				
	F12	872	0,2006				

df 43 kid	G1	1630	0,5084	0,5076	0,534	0,00271	0,00157
	G2	1620	0,5046				
	G3	1640	0,5099				
df 43 liv	G4	1740	0,5465	0,5455	0,698	0,00381	0,0022
	G5	1720	0,5413				
	G6	1740	0,5487				
df 43 heart	G7	1310	0,3843	0,3883	1,02	0,00395	0,00228
	G8	1330	0,3922				
	G9	1320	0,3883				
df 43 spleen	G10	850	0,1907	0,1967	2,97	0,00583	0,00337
	G11	864	0,197				
	G12	876	0,2024				
df 52 RH	H1	560	0,04644	0,05243	23,8	0,0125	0,00721
	H2	556	0,04408				
	H3	596	0,06679				
df 52 LH	H4	674	0,1075	0,1065	1,64	0,00174	0,00101
	H5	668	0,1045				
	H6	674	0,1075				
df 52 Spleen	H7	644	0,09226	0,09959	17,4	0,0174	0,01
	H8	698	0,1194				
	H9	634	0,08707				
df 52 liv	H10	1180	0,3314	0,3295	0,515	0,0017	0,000979
	H11	1170	0,3289				
	H12	1170	0,3281				

Some of the tissue fluorescence intensities were out of the calibration curve as highlighted in yellow but the MyAssays software could calculate the exact concentration despite the fact that they were outside the range.

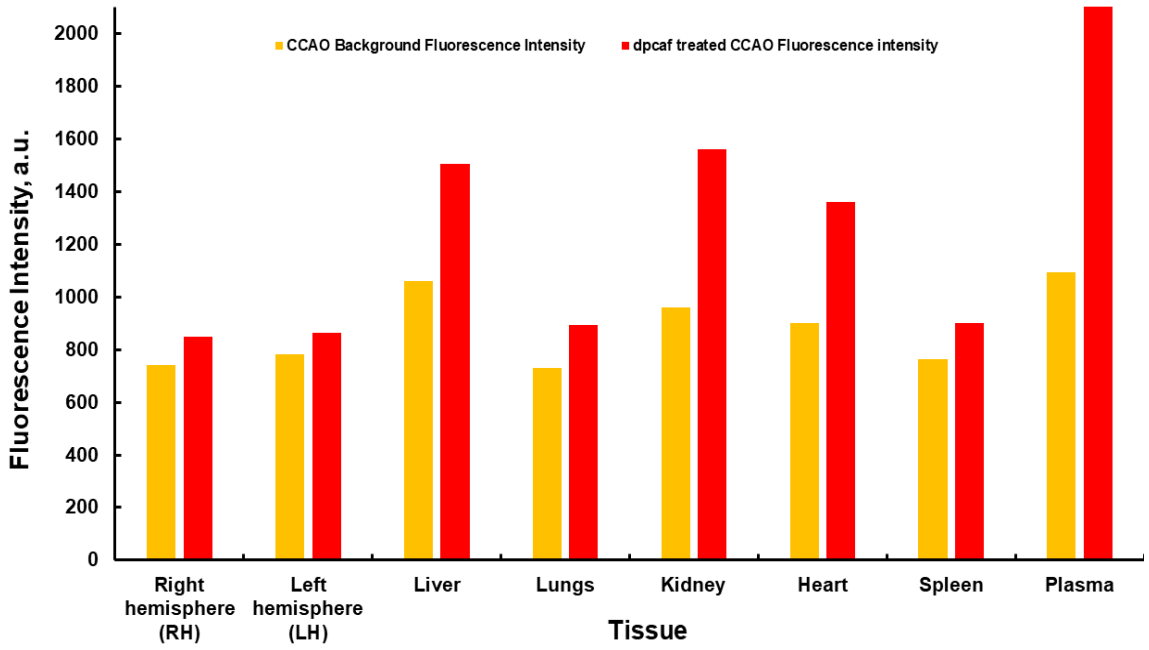


Figure 7.36. Average fluorescence intensities in various organs in CCAO (no treatment) and CCAO-dpcaf treated rats.

The fluorescence was higher in the organs of the dpcaf treated group since the FITC was incorporated in the formulation for tracking the location of the complex in various

organs. The highest fluorescence was observed in plasma followed by kidney, liver and heart (i.e. plasma > kidney > liver > heart). There was not much difference in the fluorescence intensity in the lungs, spleen and brain as illustrated in **Fig. 7.36**.

The high level of fluorescence intensity in plasma compared to other organs is an indicative that the drug was still in the blood and not completely cleared out of the blood circulation. This implies that 24-hour reperfusion period was not enough to clear the drug out of circulation. More time was needed for the complete delivery of the drug to the brain and clearance out of the circulation. It could be that it is slowly released, and this could extend its time in the circulation to improve bioavailability. The formulation has been delivered in all the organs as demonstrated by the presence of fluorescence intensity in all the organs (**Fig. 7.36**).

7.3.10. Determination of plasma ANP levels in the rat venous blood

ANP levels are very low in the non-ischemic healthy rat. The levels are elevated when the rat is under stress such as ischemic stroke. When the cardiac muscle is distended, ANP and BNP are released. Natriuretic peptides (NPs) are involved in the long-term regulation of sodium and water balance, blood volume and arterial pressure. These natriuretic peptides stimulate vasodilation and thereby decrease blood pressure. The NPs increases glomerular filtration rate (GFR) leading to stimulation of natriuresis and diuresis (Ching *et al.*, 2017). Furthermore, NPs inhibit renin release thereby decreasing angiotensin II and aldosterone which lead to further natriuresis and diuresis (**Fig. 7.37**).

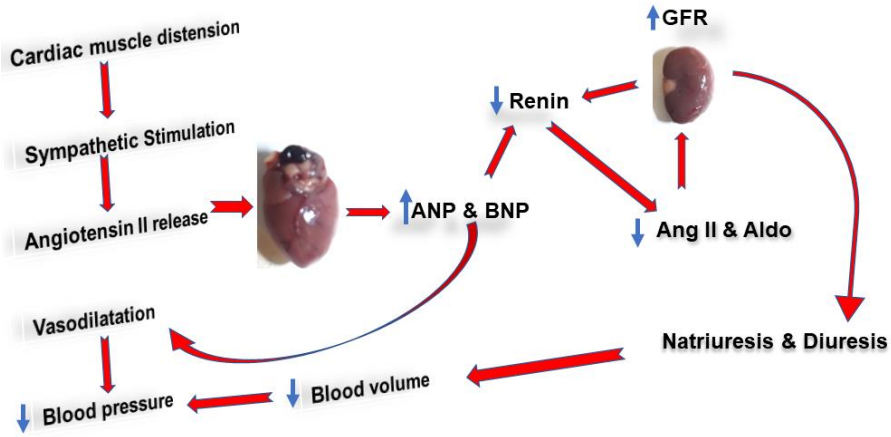


Figure 7.37. ANP and BNP involvement in natriuresis and diuresis**.**

Rat ANP ELISA kit (Elabscience, USA) was used for the determination of plasma ANP levels in the non-ischemic untreated and ischemic treated rats. This ELISA kit uses the Competitive-ELISA principle. The micro ELISA plate was pre-coated with Rat ANP. During the reaction, Rat ANP in the sample or standard competes with a fixed amount of Rat ANP on the solid phase supporter for sites on the Biotinylated Detection Ab specific to Rat ANP. Excess conjugate and unbound sample or standard are washed from the plate, and Avidin conjugated to Horseradish Peroxidase (HRP) are added to each microplate well and incubated. Then a TMB substrate solution is added to each well and the blue colour develops (**Fig. 7.38**).

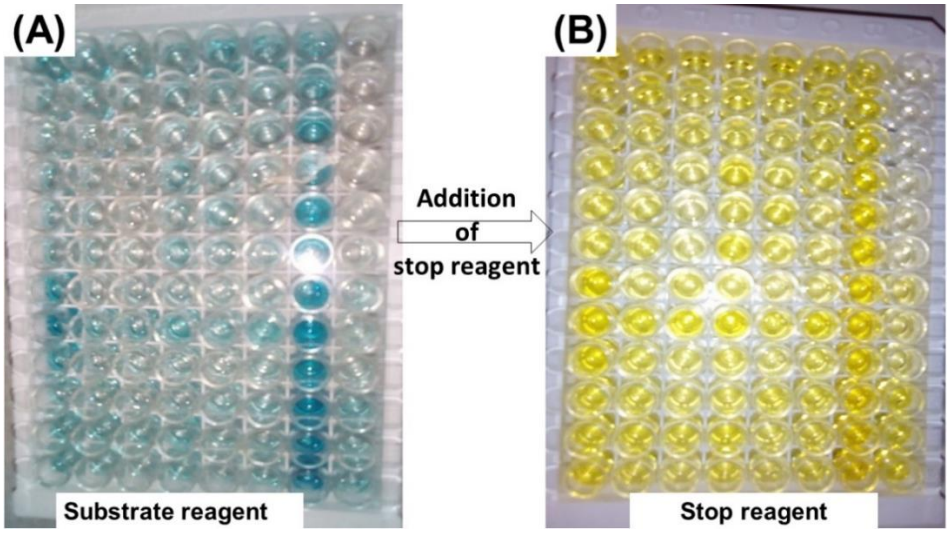
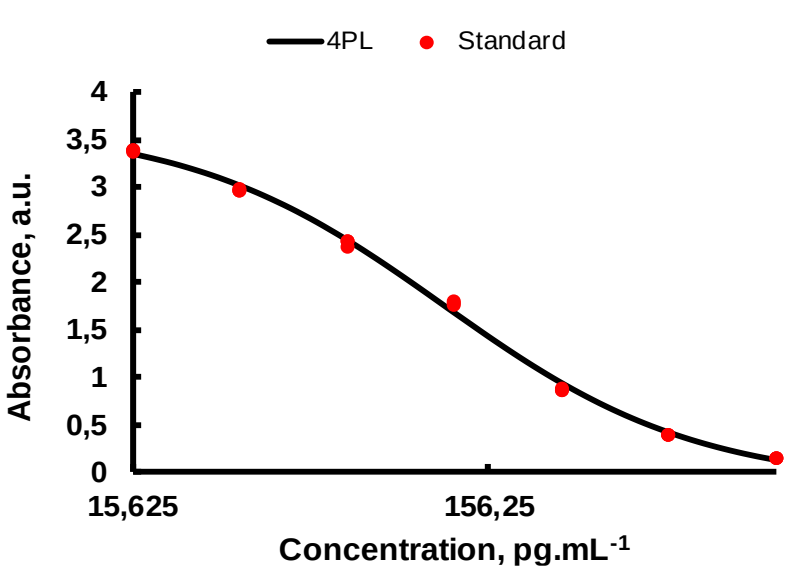


Figure 7.38. Competitive ELISA of ANP. Substrate addition to the plate wells (A). Stop reagent addition to the plate wells (B).

The enzyme-substrate reaction is terminated by the addition of stop solution and the colour change changes to yellow **(Fig. 7.38)** and measured spectrophotometrically at a wavelength of 450 nm ± 2 nm. The concentration of Rat ANP in the samples is then determined by comparing the OD of the samples to the standard curve (**Fig. 7.39)**.



a	-0,1357
b	-1,217
c	115,9
d	3,657
MSE	0,003327
R^2	0,9976
SS	0,06986
SYX	0,0641

Figure 7.39. A four-parameter logistic curve was plotted and ANP concentrations of the unknowns were determined by extrapolation from this curve.

Table 7.6. ANP calibrators for construction of 4PL standard curve. A set of six standards were prepared and scanned using Victor 3X microplate reader.

Calibrator	Wells	Concentration, pg.mL^{-1}	Raw	SEM	Backfit	Recovery, %
Standard1	A1	1000	0,152	0,000864	903,3	90,33
	A2		0,149		911,3	91,13
	A3		0,15		909,4	90,94
Standard2	A4	500	0,389	0,00312	521,2	104,2
	A5		0,389		520,6	104,1
	A6		0,398		512,2	102,4
Standard3	A7	250	0,852	0,0068	273,3	109,3
	A8		0,874		266,6	106,6
	A9		0,869		268	107,2
Standard4	A10	125	1,8	0,00986	112,2	89,78
	A11		1,76		115,5	92,4
	A12		1,77		114,5	91,63
Standard5	B1	62,5	2,36	0,0211	67,54	108,1
	B2		2,43		63,28	101,3
	B3		2,42		63,74	102
Standard6	B4	31,25	2,97	0,00615	33,53	107,3
	B5		2,98		33,01	105,6
	B6		2,96		34,05	109
Standard7	B7	15,63	3,38	0,00544	14,35	91,85
	B8		3,4		13,48	86,29
	B9		3,39		13,94	89,25

Table 7.7. Sample concentrations of plasma ANP. The concentrations were extrapolated from the standard curve.

Sample	Wells	Raw	Concentration, pg.mL^{-1}	Average concentration, pg.mL^{-1}	%CV	SD	SEM
pd 2	C1	0,251	692,1	704,1	1,91	13,4	7,74
	C2	0,245	701,6				
	C3	0,236	718,6				
pd 4	C4	0,258	681,4	703,5	3,28	23,1	13,3
	C5	0,245	701,8				
	C6	0,231	727,5				
co mca 6	C7	0,242	707,8	703,6	1,93	13,6	7,84
	C8	0,238	714,5				
	C9	0,253	688,4				
df 7	C10	0,171	854,2	843,4	1,14	9,61	5,55
	C11	0,176	840,5				
	C12	0,178	835,6				
sm 9	D1	0,195	797,8	795,3	1,01	8,04	4,64
	D2	0,193	801,8				
	D3	0,2	786,4				
co 8	D4	0,324	590,5	673,2	10,8	72,9	42,1
	D5	0,246	701,2				
	D6	0,23	728				
co 10	D7	0,288	636,6	637,4	1,36	8,65	5
	D8	0,281	646,5				
	D9	0,293	629,3				
pm 11	D10	0,237	716,3	718,7	1,04	7,48	4,32
	D11	0,239	712,7				
	D12	0,231	727,1				
df 14	E1	0,325	589,1	572,9	2,57	14,7	8,51
	E2	0,342	569,2				
	E3	0,35	560,3				
co 15	E4	0,286	639,7	646,9	1,05	6,82	3,94
	E5	0,276	653,2				
	E6	0,28	647,7				
df 16	E7	0,224	739,4	724,6	1,84	13,3	7,7
	E8	0,234	721,2				
	E9	0,239	713,4				
dx 17	E10	0,21	767,1	757,6	2,09	15,8	9,14
	E11	0,21	766,4				
	E12	0,224	739,3				
pt 20	F1	0,326	587,5	578,1	2,06	11,9	6,89
	F2	0,346	564,7				
	F3	0,331	582,2				
dx 21	F4	0,216	754,9	764,2	2,71	20,7	12
	F5	0,219	749,8				
	F6	0,2	788				
pt 24	F7	0,199	788,5	808,7	2,21	17,8	10,3
	F8	0,184	822,2				
	F9	0,187	815,6				

df 25	F10	0,347	563,8	570,8	1,22	6,95	4,01
	F11	0,34	571				
	F12	0,335	577,7				
co 26	G1	0,329	583,6	590,2	1,17	6,92	3,99
	G2	0,318	597,4				
	G3	0,325	589,4				
df 33	G4	0,344	567,4	563,3	0,963	5,43	3,13
	G5	0,353	557,2				
	G6	0,345	565,5				
dx 34	G7	0,216	754,6	775,4	2,33	18,1	10,4
	G8	0,2	786,3				
	G9	0,201	785,3				
pm 37	G10	0,266	668,1	668,1	2,83	18,9	10,9
	G11	0,254	687				
	G12	0,279	649,2				
pm 38	H1	0,284	641,8	646,5	0,679	4,39	2,53
	H2	0,28	647,2				
	H3	0,278	650,5				
pm 39	H4	0,262	675,6	660,9	1,96	13	7,48
	H5	0,278	651				
	H6	0,274	656,2				
pm 40	H7	0,269	663,4	655,1	1,12	7,34	4,24
	H8	0,277	652,3				
	H9	0,279	649,4				
co liv 25	H10	1,59	134,1	134,8	0,808	1,09	0,628
	H11	1,58	136				
	H12	1,59	134,1				

Atrial natriuretic peptide (ANP) was determined by using the Rat ANP ELISA kit. The absorbance of ANP concentrations ranging from 0 – 1 000 $pg.mL^{-1}$ were recorded by Victor x3 Perkin Elmer microplate reader at 450 nm. Absorbance was plotted against concentration and the concentrations of the unknowns were determined from this standard curve by extrapolation (**Fig. 7.40**). The slope is negative as this is a competitive ELISA procedure.

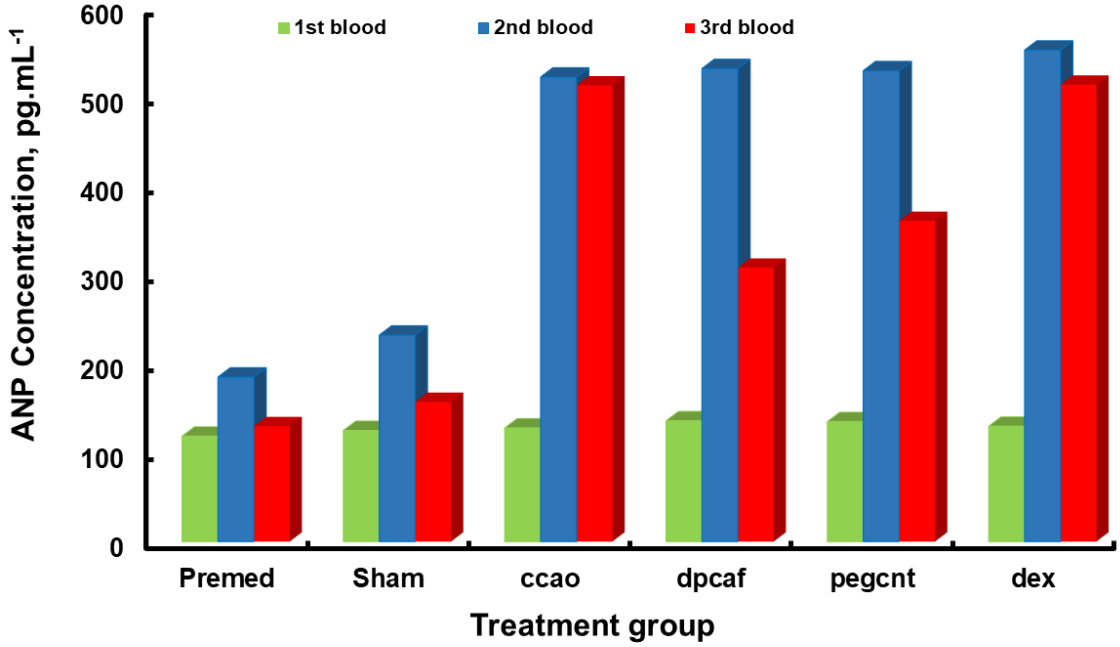


Figure 7.40. Rat Plasma ANP levels from first, second and third blood withdrawal before and after surgery including 24-reperfusion.

Plasma ANP levels were measured before CCAO, immediately after CCAO and after 24 hours of reperfusion **(Fig. 7.40**). Baseline levels of plasma ANP was found to be around 100 $pg.mL^{-1}$. Levels went up following CCAO and dropped when rats were treated with dpcaf and pegcnt (**Fig. 7.40**). An increase in ANP levels in CCAO group is due to the stroke that was induced in this group. Levels of ANP are very low in healthy rats but increase when the rat is under stress such as stroke to suppress inflammation. These data have demonstrated the effectiveness of pegcnt and dpcaf in reducing inflammation in stroke induced rats as demonstrated by the drop in the levels of ANP in dpcaf and pegcnt treated rats.

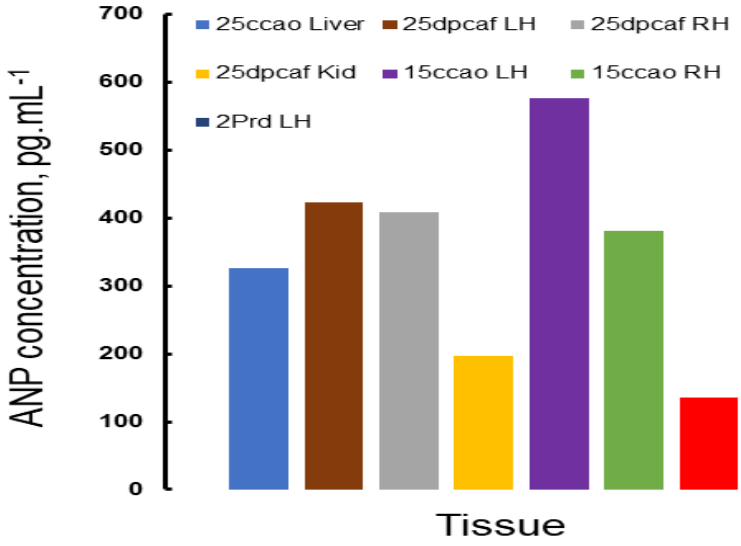


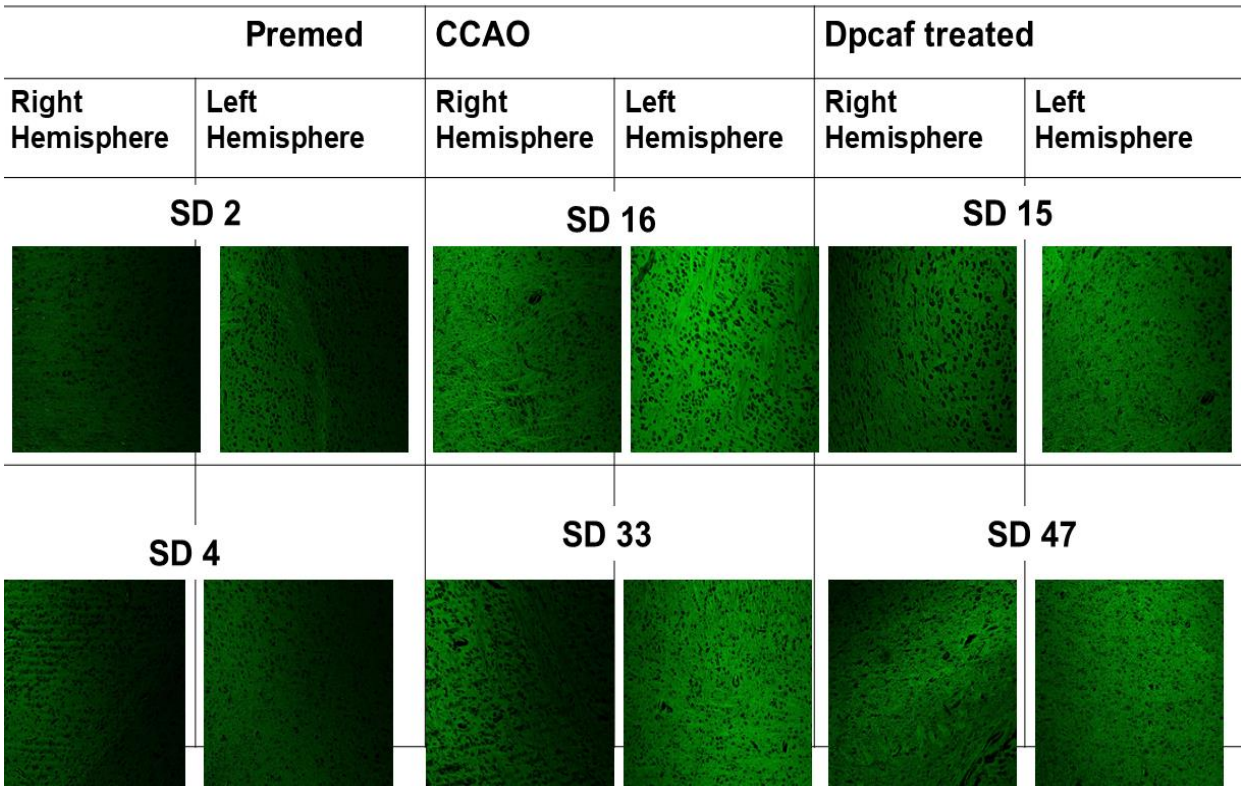
Figure 7.41. ANP levels in different tissues of the treated and untreated rats.

The levels of ANP depend on many factors such as tissue type, age, heath status and gender. In our study, ANP levels were also determined in various organs of the rat. The levels were lower in the premed group as stroke was not induced in this group (**Fig.7.41**) (*red bar*). ANP was also detected in the kidneys from the CCAO dpcaf treated group but slightly higher than in the premed group (**Fig.7.41**) (*yellow bar*). The highest levels of ANP were found in the CCAO group without treatment as a result of the stroke that was induced in the left hemisphere (**Fig.7.41**) (*purple bar*). ANP in the right hemisphere was lower than in the left hemisphere with stroke as stroke was not induced in the right hemisphere (*green bar*). A reduction in the ANP levels was observed in the dpcaf treated groups (**Fig.7.41**) (*blue, brown and grey bars*).

7.3.11. Histological evaluation of dpcaf delivery into the brain by Fluorescence microscopy

Delivery of dpcaf in the brain was further confirmed by fluorescence microscopy (Zeiss LSM 780 Confocal Microscope) as depicted in **Table 7.8**. The fluorescence detected in the premedication group is due to the tissue background. The intensity of fluorescence was very low as demonstrated by the darker background in the premed group compared to the treated groups. The tissues produce autofluorescence when exposed to 488 nm laser but the autofluorescence is suppressed by the presence of the fluorescently labelled complex as depicted in **Table 7.8**. The fluorescence intensity increased in the CCAO and dpcaf treated groups.

Table 7.8. Histological evaluation of the rat brain tissue following treatment with dpcaf.



The fluorescence intensity in the left hemisphere was higher than that of the right hemisphere as illustrated in **Table 7.8**. The difference in the intensity could be due to the fact that stroke was induced in the left hemisphere hence higher intensity of fluorescence. The complex has the anti-ANP attached to it and will be transported to the diseased site and will bind to the ANP molecule as its level is increased in the site of ischemia. This is indicative of the successful delivery of the drug to the site of interest in the brain.

7.3.12. Histological evaluation of dpcaf delivery into the brain by H & E staining technique

Ischemic stroke is a cerebrovascular disease which include risks such as necrosis, apoptosis and cerebral infarction following cerebral ischemia and reperfusion (I/R) (Pathways, 2018). Unstained tissue does not have a contrast and it requires staining for microscopic evaluation to evaluate the extent of damage of a tissue. The staining process utilises different dyes that selectively stain particular cell components as to be able to distinguish different cell components from each other. Ionic bonding is very

important in histological staining. It involves the electrostatic attraction between the ions of positive and negative charge.

Haematoxylin alone is not a dye and will not stain tissues directly as a result. In order for it to function, it requires a mordant which is a metal cation like aluminium. Haematoxylin, acts as a cationic basic dye when complexed with aluminium. It possesses a positive charge and reacts with negatively charged basophilic cell components. Haematoxylin stains the nuclei blue. Eosin acts as an anionic acidic dye. It has a negative charge and reacts with positively charged acidophilic components in the tissue. It stains cytoplasm pink.

In our study, H & E staining technique was used to evaluate the anatomical structural changes of the neuronal tissue following induction of ischemic stroke and reperfusion injury. There was no difference in the morphology of the neuronal tissue in the right and left hemispheres of the sham group. The staining was very intense because nuclei absorb H & E stains and become blue/dark purple.

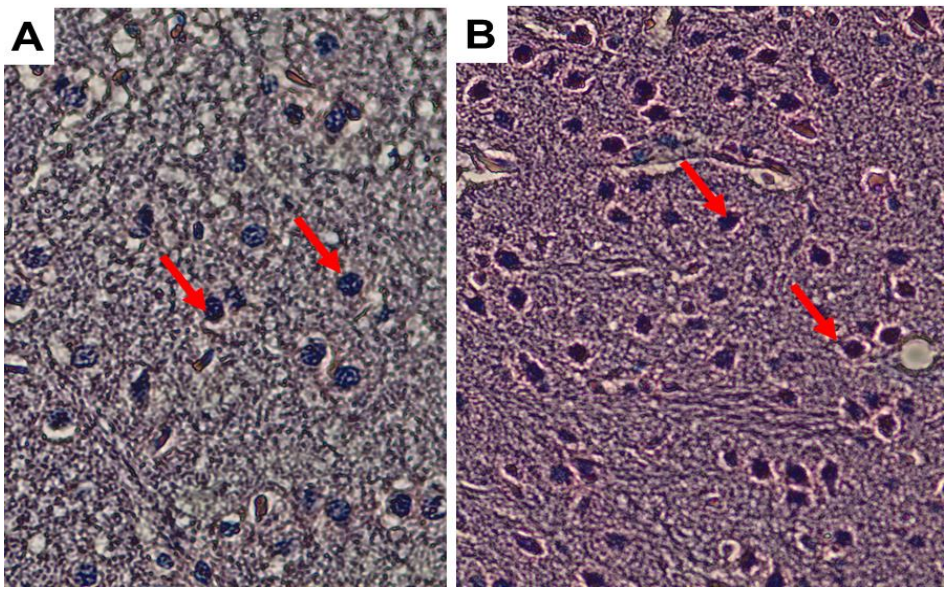


Figure 7.42. H & E micrograph of the sham rat. Right hemisphere (A). Left hemisphere (B).

Nuclei were big, round, compact and clearly visible with well- defined nuclear membranes as demonstrated in **Fig. 7.42A-B (***red arrows***).** The right hemisphere tissue was as normal as in the sham group since it was not tempered with (**Fig. 7.42A-B**). The nuclei in the right hemisphere of the CCAO group were normal compared to

the left hemisphere nuclei **(Fig.7.42A**) (*red arrows*). The nucleolus vanished, and nuclear membrane dissolved. Cavitation or vacuolation was observed in the neuronal cells (**Fig. 7.42B**) (*blue and yellow arrows*).

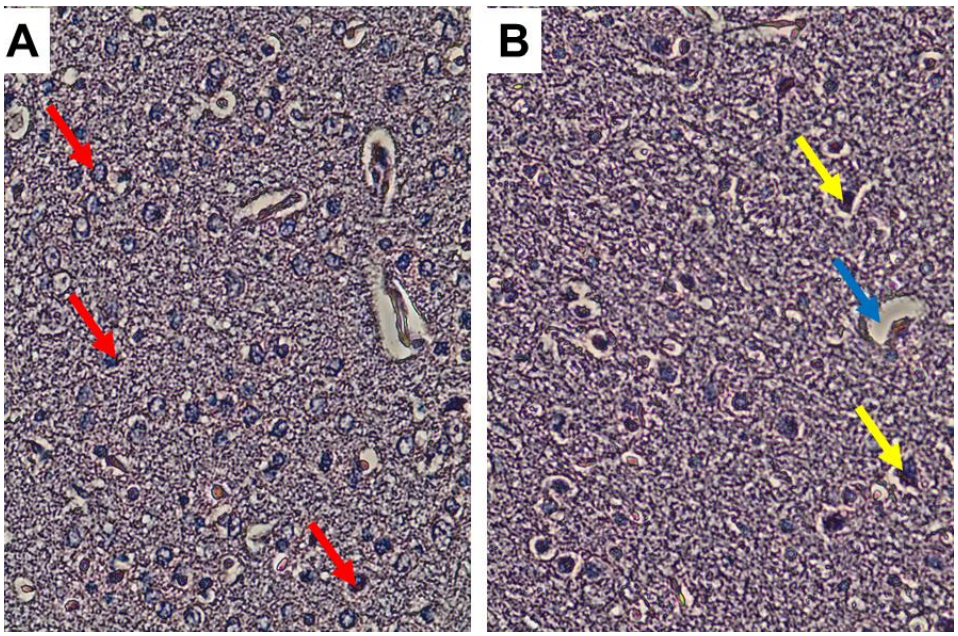


Figure 7.43. H & E micrograph of the CCAO rat. Right hemisphere (A). Left hemisphere (B).

Following treatment with dpcaf, nuclei of the right hemisphere looked intact and the morphology of the left hemisphere was immensely improved (**Fig.7.43A-B**) (*red and blue arrows*).

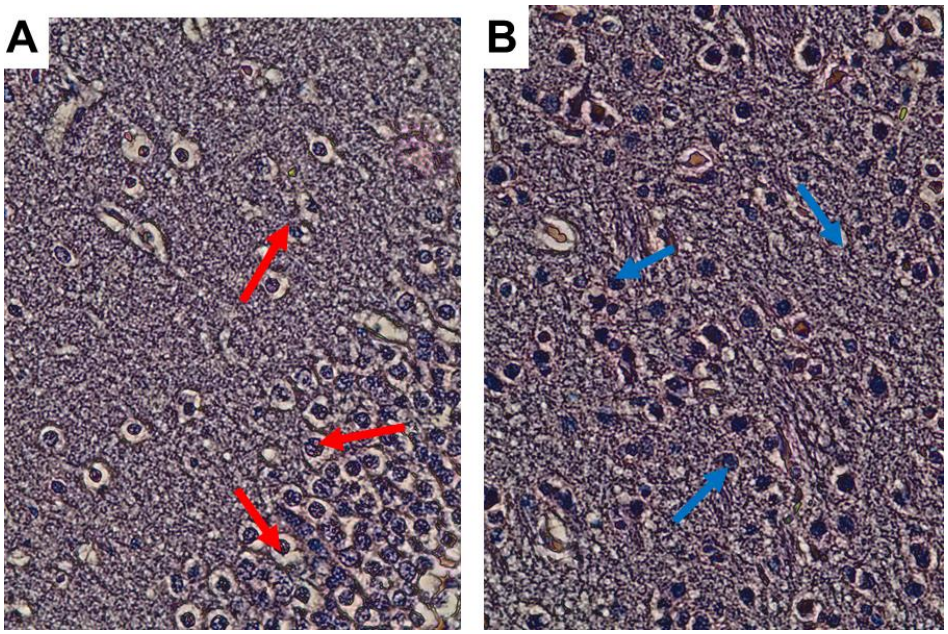


Figure 7.44. H & E micrograph of the dpcaf rat. Right hemisphere (A). Left hemisphere (B).

The staining became intense as the nuclei absorbed the H & E stain and became blue/dark purple. The normal structural form of the nucleus was regained as illustrated in **Fig. 7.44B**. Our findings have demonstrated the potential of dpcaf in the reduction of inflammation and improvement of the healthy state of the neuronal tissues that underwent neurological damage and morphological changes during I/R.

7.4. Concluding remarks

Vertically aligned MWCNTs were successfully synthesised, purified and functionalised. FITC, the fluorescent tag and ANP, the targeting ligand were also successfully coupled to the DEX-PEG-CNT. Toxicity of this formulation was evaluated in PC-12 cells using MTT assay. From our findings, this complex was found to be non-toxic as more than 80% of the cells incubated with this formulation were viable. Furthermore, this formulation was also found not to be toxic when dose response studies were performed in the rats intravenously injected with this complex at various doses.

Stroke was successfully induced using common carotid artery occlusion as demonstrated by the stroke symptoms in the rats following the occlusion procedure. ANP levels were increased following the common carotid artery occlusion and decreased after treatment with dpcaf and pegcnt. Fluorescence spectroscopy and microscopy confirm a successful delivery of the drug and its nanocarrier to the ischemic site of the brain. These results have demonstrated the targeting ability and anti-inflammatory properties of the complex which could lead to effective and efficient treatment of ischemic stroke.

This carbon nanotube system for targeting of inflammatory biomarkers in ischemic stroke patients needs to be refined and further evaluated for clinical application in future. Once it has been thoroughly evaluated, it will then be further assessed in non-human primates prior to application in humans. The immunosensor also requires further development and be assessed for application in the diagnosis of ischemic stroke.

This theranostic tool will revolutionize the diagnosis and therapy of ischemic stroke in the health industry and this may lead to the reduction of mortality rate and disability as a result of stroke hence an improvement in the global economy.

7.5. References

Bahuguna, A. *et al.* (2017) ‘MTT assay to evaluate the cytotoxic potential of a drug’, *Bangladesh Journal of Pharmacology*, 12(2), pp. 115–118.

Bio-Rad (2017) ‘ELISA Basics Guide’, in *ELISA Basics Guide*. UK: Bio-Rad Laboratories.

Ching, P. *et al.* (2017) ‘The renal and cardiovascular effects of natriuretic peptides’, *Advances in Physiology Education*, 41, pp. 179–185.

Chung, D. M., Kim, J. H. and Kim, J. K. (2015) ‘Evaluation of MTT and Trypan Blue assays for radiation-induced cell viability test in HepG2 cells’, *International Journal of Radiation Research*, 13(4), pp. 331–335.

Croce, A. C., Bottiroli, G. and Unit, C. (2014) ‘Autofluorescence spectroscopy and imaging : a tool for biomedical research and diagnosis Autofluorescence ’:, *European Journal of Histochemistry*, 58(2461), pp. 320–337.

Gholamine, B. *et al.* (2017) ‘Neurobehavioral toxicity of carbon nanotubes in mice : Focus on brain-derived neurotrophic factor mRNA and protein’, *Toxicity and industrial Health*, 33(4), pp. 340–350.

Iijima, S. (1991) ‘Helical microtubules of graphitic carbon’, *Nature*, 354(6348), pp. 56–58.

Imran, M. *et al.* (2016) ‘Carbon nanotubes from synthesis to in vivo biomedical applications’, *International Journal of Pharmaceutics*, 501(1–2), pp. 278–299.

Jacobsen, N. R. *et al.* (2017) ‘MiniReview Biodistribution of Carbon Nanotubes in Animal Models’, *Basic & Clinical Pharmacology & Toxicology*, 121, pp. 30–43.

Jafar, A., Alshatti, Y. and Ahmad, A. (2016) ‘Carbon nanotube toxicity: The smallest biggest debate in medical care’, *Cogent Medicine*, 3(1).

Komane, P. P. *et al.* (2016) ‘Diagnosis and Treatment of Neurological and Ischemic Disorders Employing Carbon Nanotube Technology’, *Journal of Nanomaterials*, 2016, p. 19 pages.

Li, Z. *et al.* (2017) ‘Functionalized single-walled carbon nanotubes : cellular uptake , biodistribution and applications in drug delivery’, *International Journal of Pharmaceutics*, 524(1–2), pp. 41–54.

Madani, S. Y., Mandel, A. and Seifalian, A. M. (2013) ‘A concise review of carbon nanotube’s toxicology.’, *Nano reviews*, 4, pp. 1–14.

Mattei, T. A. and Rehman, A. A. (2015) ‘“Extremely minimally invasive”: recent advances in nanotechnology research and future applications in neurosurgery’, *Neurosurgical Review*, 38(1), pp. 27–37. doi: 10.1007/s10143-014-0566-2.

Modi, G. *et al.* (2009) ‘Nanotechnological applications for the treatment of neurodegenerative disorders’, *Progress in Neurobiology*, 88(4), pp. 272–285.

Pathways, M. (2018) ‘Neuroprotective Effects of Radix Scrophulariae on Cerebral Ischemia and Reperfusion Injury via’, *molecules*, 23(2401), pp. 1–19.

Predoi, D. *et al.* (2007) ‘Characteristics of hydroxyapatite thin films’, *Journal of Optoelectronics and Advanced Materials*, 9(12), pp. 3827–3831.

Riss, T. L. *et al.* (2004) *Cell Viability Assays*, *Assay Guidance Manual*.

Veetil, J. V and Ye, K. (2007) ‘Development of immunosensors using carbon nanotubes.’, *Biotechnology progress*, 23(3), pp. 517–31.

Wang, J. *et al.* (2011) ‘Cytotoxicity of single-walled carbon nanotubes on PC12 cells’, *Toxicology in Vitro*. Elsevier Ltd, 25(1), pp. 242–250.

Wei, Q. *et al.* (2012) ‘Biodistribution of co-exposure to multi-walled carbon nanotubes and nanodiamonds in mice’, *Nanoscale Research Letters*. Nanoscale Research Letters, 7(1), p. 1. Available at: Nanoscale Research Letters.

Wilhelm, I., Fazakas, C. and Krizbai, I. A. (2011) ‘In vitro models of the blood-brain barrier’, *Acta Neurobiol Exp*, 71, pp. 113–128.

CHAPTER 8

CONCLUDING REMARKS, RECOMMENDATIONS AND FUTURE PERSPECTIVES

8.1. Concluding remarks

Stroke was ranked as the second most common single cause of death in the developed world succeeding cardiac disease (Chen *et al.*, 2010). It became the third leading cause of death after heart and oncologic diseases (Shahpouri *et al.*, 2012; Tjoumakaris, Pascal M. Jabbour and Rosenwasser, 2012; Jivan, Ranchod and Modi, 2013; Modi, 2013; Hlavica *et al.*, 2015) and the second most common cause of dementia (Glickman *et al.*, 2011). It is currently the fourth leading cause of death after cardiac, oncologic and pulmonary diseases (Towfighi and Saver, 2011; Maldonado, Kazmi and Suarez, 2014; Lin and Sanossian, 2015) and the primary leading cause of long-term disability globally (Deb, Sharma and Hassan, 2010). Prevalence of stroke is expected to rise globally in the years to come as the world population older than 65 years of age increases by 9×10^6 people annually. The impact of stroke on the world economy may be atrocious if effective preventive strategies are not put in place to help decrease curb the burden of this disease. The use of the current diagnostic tools such as Computed Tomography (CT) and Magnetic Resonance Imaging (MRI) is limited by availability, cost and radiation exposure. The current treatment of stroke with thrombolytic agents such as recombinant Tissue Plasminogen Activator (rTPA) and anti-inflammatory agents such as glucocorticoids namely methylprednisolone and dexamethasone have some drawbacks which need to be dealt with in order to use these glucocorticoids for the intended purpose. The therapeutic potential of these corticosteroids is hindered by their short circulatory half-lives and poor pharmacokinetics. Higher doses need to be administered for these drugs to be effective and this could lead to adverse systemic side-effects. Nanotechnology has demonstrated promising results in resolving the shortcomings of the present diagnosis and therapy of ischemic stroke. Nanomedicine is an emerging field of medicine where engineered nanomaterials are utilized for the detection, treatment and prevention of certain diseases including neurological disorders. Carbon nanotubes (CNTs) are emerging group of nanomaterials that has shown promising outcomes for the advancement in technology in the field of medicine. They have a variety of unique

properties making them useful tools in neurobiological applications. Carbon nanotubes have the potential to be implemented in biomedical fields as theranostic tools for diagnosis and therapy of ischemic stroke based on their unique physico-chemical characteristics.

The research in this thesis involved the synthesis, purification, functionalisation and characterisation of vertically aligned multiwalled carbon nanotubes for potential application in the diagnosis and treatment of ischemic stroke. In addition, the advanced drug delivery and nanotechnology were also involved in the design and formulation of the carbon nanotube system for targeting of inflammatory biomarkers in ischemic stroke. The findings from this research confirmed the successful synthesis of vertically aligned multiwalled carbon nanotubes and their functionalised state. Furthermore, the *in vitro* studies in PC-12 cells and *in vivo* studies in SD rats validated the efficacy of the carbon nanotubes system. The core aim of this study was to devise a carbon nanotube system for targeting of inflammatory biomarkers in ischemic stroke and was achieved by incorporation of the dexamethasone into carbon nanotube and the complex was successfully delivered to the ischemic site of the stroke induced SD rats as confirmed by fluorescence spectroscopy, fluorescence microscopy and H & E histological evaluation.

The *in vitro* studies utilising PC-12 cells illustrated the non-cytotoxic effect of the functionalised carbon nanotube system at low doses as confirmed by high cell viability at low doses. The *in vivo* studies of the functionalised nanotube system served to evaluate the performance of the system in the treatment of ischemic stroke. The spectroscopic, neurobehavioural evaluation and histological analyses established the level of recovery pre- and post-stroke induction in response to treatment with the functionalised nanotube system. The developed functionalised carbon nanotube system was demonstrated to be capable of reducing the inflammation in stroke leading to improvement of the status of health in the stroke induced rats following treatment.

8.2. Recommendations

This thesis presented extensive discussions on the design, development, characterisation and *in vitro* analysis of the proposed system for treatment of ischemic stroke. Characterisation of the system was performed up to the preclinical stage of *in vivo* evaluation in rat stroke model (Sprague Dawley rat). Although our findings illustrated improved recovery from stroke following treatment with the functionalised carbon nanotube system, it may be suggested that the performance verification be conducted over an extended period of 48-72 hours or even more instead of 24 hours. An extended period could assist in the collection of more results for the maximal recovery from stroke. It may also provide a better understanding of the anti-inflammatory action rendered by this system. The extension of timeframe could also be linked to the increased number of rats to cater for the variations in the healing capabilities of individual rats. The system presented in this thesis had only one anti-inflammatory drug coupled to it. The efficacy of this system could also be improved by an addition of one or more anti-inflammatory drugs. Combinatory drugs may be more effective as compared to a single drug since the combinatory drugs work synergistically with each drug having its own potency. The functionalised carbon nanotube system presented in this thesis could further be evaluated for cytotoxicity prior to clinical application to ensure that it is safe to use. The factors hindering the commercialisation and clinical use of this system are as follow; large scale production, specialised equipment for production, effective sterilisation, packaging and stability of the product. A lot of work needs to be done in order for this system to be implemented in clinical use. A specialised instrumentation for a rapid production and excellent reproducibility would be required for this system.

8.3. Future Perspectives

A carbon nanotube system was successfully developed and evaluated with spectroscopic, microscopic and histological techniques. Its toxicity was assessed in *in vitro* and *in vivo* studies. The functional recovery results obtained from *in vivo* studies had demonstrated the superior performance of the nanotube system and thus holds potential for patenting, clinical trials and commercialization for use in stroke patients. The modification of the system by adjusting the concentration of the individual

components, e.g. dexamethasone, PEG and multiwalled carbon nanotubes could improve the performance of this system. The length and thickness of the CNTs could also play a major role in the efficacy of this system. The system modification could also extend its healing capability of ischemic stroke to other diseases. Moreover, the utilisation of carbon nanotubes and polymers such as PEG in the development of this system may have a significant contribution towards the support of green chemistry.

In conclusion, vertically aligned MWCNTs were successfully synthesised, purified and functionalised. FITC, the fluorescent tag and ANP, the targeting ligand were also successfully coupled to the DEX-PEG-CNT. Toxicity of this formulation was evaluated in PC-12 cells using MTT assay. From our findings, this complex was found to be non-toxic as more than 80 % of the cells incubated with this formulation were viable. Furthermore, this formulation was also found not to be toxic when dose response studies were performed in the rats intravenously injected with this complex at various doses. Stroke was successfully induced using common carotid artery occlusion as demonstrated by the stroke symptoms in the rats following the occlusion procedure. ANP levels were increased following the common carotid artery occlusion and decreased after treatment with dpcaf and pegcnt. Fluorescence spectroscopy and microscopy confirm a successful delivery of the drug and its nanocarrier to the ischemic site of the brain. These results have demonstrated the targeting ability and anti-inflammatory properties of the complex which could lead to effective and efficient treatment of ischemic stroke. This carbon nanotube system for targeting of inflammatory biomarkers in ischemic stroke patients needs to be refined and further evaluated for clinical application in future. Once it has been thoroughly evaluated, it will then be further assessed in non-human primates prior to application in humans. The immunosensor also requires further development and be assessed for application in the diagnosis of ischemic stroke. This theranostic tool will revolutionize the diagnosis and therapy of ischemic stroke in the health industry and this may lead to the reduction of mortality rate and disability as a result of stroke hence an improvement in the global economy.

8.4. References

Chen, R.-L. *et al.* (2010) ‘Ischemic stroke in the elderly: an overview of evidence.’, *Nature reviews. Neurology*, 6(5), pp. 256–265.

Deb, P., Sharma, S. and Hassan, K. M. (2010) ‘Pathophysiologic mechanisms of acute ischemic stroke: An overview with emphasis on therapeutic significance beyond thrombolysis.’, *Pathophysiology*. Elsevier Ireland Ltd, 17, pp. 197–218.

Glickman, S. W. *et al.* (2011) ‘Discriminative capacity of biomarkers for acute stroke in the emergency department.’, *The Journal of emergency medicine*, 41(3), pp. 333–9.

Hlavica, M. *et al.* (2015) ‘Pharmacological recanalization therapy in acute ischemic stroke – Evolution, current state and perspectives of intravenous and intra-arterial thrombolysis’, *Journal of Neuroradiology*, 42(1), pp. 30–46.

Jivan, K., Ranchod, K. and Modi, G. (2013) ‘Management of ischaemic stroke in the acute setting: review of the current status.’, *Cardiovascular journal of Africa*, 24(3), pp. 86–92.

Lin, M. P. and Sanossian, N. (2015) ‘Reperfusion Therapy in the Acute Management of Ischemic Stroke’, *Cardiology Clinics*, 33(1), pp. 99–109.

Maldonado, N. J., Kazmi, S. O. and Suarez, J. I. (2014) ‘Update in the Management of Acute Ischemic Stroke’, *Critical Care Clinics*, 30(4), pp. 673–697.

Modi, G. (2013) ‘Editorial Acute ischaemic stroke : highlighting the need for early intervention’, *Cardiovascular journal of Africa*, 24(3), p. 51.

Shahpouri, M. M. *et al.* (2012) ‘Anticoagulant therapy for ischemic stroke: A review of literature.’, *Journal of research in medical sciences*, 17(4), pp. 396–401.

Tjoumakaris, S. I., Pascal M. Jabbour, A. S. D. and Rosenwasser, L. F. G. and R. H. (2012) ‘Endovascular Management of Acute Ischemic Stroke’, in Rodriguez, P. J. C. G. (ed.) *Acute Ischemic Stroke*, pp. 121–144.

Towfighi, A. and Saver, J. L. (2011) ‘Stroke declines from third to fourth leading cause of death in the United States: Historical perspective and challenges ahead’, *Stroke*, 42(8), pp. 2351–2355.

APPENDICES

APPENDIX A1

Hindawi Publishing Corporation
Journal of Nanomaterials
Volume 2016, Article ID 9417874, 19 pages
http://dx.doi.org/10.1155/2016/9417874

Review Article

Diagnosis and Treatment of Neurological and Ischemic Disorders Employing Carbon Nanotube Technology

Patrick P. Komane,[1,2] Yahya E. Choonara,[1] Lisa C. du Toit,[1] Pradeep Kumar,[1] Pierre P. D. Kondiah,[1] Girish Modi,[3] and Viness Pillay[1]

[1]*Wits Advanced Drug Delivery Platform Research Unit, Department of Pharmacy and Pharmacology, School of Therapeutic Sciences, Faculty of Health Sciences, University of the Witwatersrand, Johannesburg, 7 York Road, Parktown 2193, South Africa*
[2]*Department of Applied Chemistry, University of Johannesburg, P.O. Box 17011, Doornfontein, Johannesburg 2028, South Africa*
[3]*Department of Neurology, Division of Neurosciences, Faculty of Health Sciences, University of the Witwatersrand, Johannesburg, 7 York Road, Parktown 2193, South Africa*

Correspondence should be addressed to Viness Pillay; viness.pillay@wits.ac.za

Received 7 June 2016; Revised 19 September 2016; Accepted 28 September 2016

Academic Editor: Taslim A. Al-Hilal

Copyright © 2016 Patrick P. Komane et al. This is an open access article distributed under the Creative Commons Attribution License, which permits unrestricted use, distribution, and reproduction in any medium, provided the original work is properly cited.

Extensive research on carbon nanotubes has been conducted due to their excellent physicochemical properties. Based on their outstanding physicochemical properties, carbon nanotubes have the potential to be employed as theranostic tools for neurological pathologies such as Alzheimer's disease and Parkinson's disease including ischemic stroke diagnosis and treatment. Stroke is currently regarded as the third root cause of death and the leading source of immobility around the globe. The development and improvement of efficient and effective procedures for central nervous system disease diagnosis and treatment is necessitated. The main aim of this review is to discuss the application of nanotechnology, specifically carbon nanotubes, to the diagnosis and treatment of neurological disorders with an emphasis on ischemic stroke. Areas covered include the conventional current diagnosis and treatment of neurological disorders, as well as a critical review of the application of carbon nanotubes in the diagnosis and treatment of ischemic stroke, covering areas such as functionalization of carbon nanotubes and carbon nanotube-based biosensors. A broad perspective on carbon nanotube stimuli-responsiveness, carbon nanotube toxicity, and commercially available carbon nanotubes is provided. Potential future studies employing carbon nanotubes have been discussed, evaluating their extent of advancement in the diagnosis and treatment of neurological and ischemic disorders.

1. Introduction

Neurological and ischemic disorders incorporate a variety of sporadic and hereditary conditions. They are characterized by the progressive loss of structure and function of neurons often associated with neuronal death. The causes of neurological and ischemic diseases are very complex and are linked to a variety of factors such as aging, lifestyle, environmental factors, and heredity [1–3].

Alzheimer's disease (AD) and Parkinson's disease (PD) are the most common neurodegenerative diseases. An estimated 24 million people around the globe suffer from dementia and AD comprises 60% of this number. AD is characterized pathologically by cerebral atrophy and clinically by memory and learning impairment [2]. According to the Alzheimer's Association, 13% of people over 65 suffer from AD in developed countries. It is the fifth leading cause of death in patients at this age [4]. The cause of AD is unknown and current treatments are symptomatic. Current treatments for cognitive impairment in AD are based on neurotransmitter or enzyme replacement. These provide a wide spectrum of symptomatic benefits and include acetylcholinesterase inhibitors, antioxidants, amyloid-targeted drugs, and nerve growth factors. It seems that none of the available therapies are able to cure AD or to attenuate its progression. Nanotechnology may provide a possible solution to overcome many obstacles for the treatment of AD by affording targeted drug

APPENDIX A2

molecules

MDPI

Article

Dexamethasone-Loaded, PEGylated, Vertically Aligned, Multiwalled Carbon Nanotubes for Potential Ischemic Stroke Intervention

Patrick P. Komane [1,2], Pradeep Kumar [1], Thashree Marimuthu [1], Lisa C. du Toit [1], Pierre P. D. Kondiah [1], Yahya E. Choonara [1] and Viness Pillay [1,*]

[1] Wits Advanced Drug Delivery Platform Research Unit, Department of Pharmacy and Pharmacology, School of Therapeutic Sciences, Faculty of Health Sciences, University of the Witwatersrand, Johannesburg, 7 York Road, Parktown 2193, South Africa; patrickk@uj.ac.za (P.P.K.); pradeep.kumar@wits.ac.za (P.K.); thashree.marimuthu@wits.ac.za (T.M.); lisa.dutoit@wits.ac.za (L.C.d.T.); pierre.kondiah@wits.ac.za (P.P.D.K.); yahya.choonara@wits.ac.za (Y.E.C.)

[2] Department of Applied Chemistry, University of Johannesburg, 27 Nind Street, Doornfontein, Johannesburg 2028, South Africa

* Correspondence: viness.pillay@wits.ac.za; Tel.: +27-11-717-2274

Received: 30 April 2018; Accepted: 7 June 2018; Published: 10 June 2018

check for updates

Abstract: The complete synthesis, optimization, purification, functionalization and evaluation of vertically aligned multiwalled carbon nanotubes (VA-MWCNTs) was reported for potential application in dexamethasone delivery to the ischemic brain tissue. The conditions for high yield were optimized and carbon nanotubes functionalized and PEGylated prior to dexamethasone loading. Morphological changes were confirmed by SEM and TEM. Addition of functional groups to MWCNTs was demonstrated by FTIR. Thermal stability reduced following MWCNTs functionalization as demonstrated in TGA. The presence of carbon at 2θ of 25° and iron at 2θ of 45° in MWCNTs was illustrated by XRD. Polydispersive index and zeta potential were found to be 0.261 and −15.0 mV, respectively. Dexamethasone release increased by 55%, 65% and 95% in pH of 7.4, 6.5 and 5.5 respectively as evaluated by UV-VIS. The functionalized VA-MWCNTs were demonstrated to be less toxic in PC-12 cells in the concentration range from 20 to 20,000 µg/mL. These findings have demonstrated the potential of VA-MWCNTs in the enhancement of fast and prolonged release of dexamethasone which could lead to the effective treatment of ischemic stroke. More work is under way for targeting ischemic sites using atrial natriuretic peptide antibody in stroke rats.

Keywords: multiwalled carbon nanotubes; chemical functionalization; chemical vapor deposition; PEGylation; ischemic stroke article; yet reasonably common within the subject discipline

1. Introduction

Carbon nanotube synthesis and their application in various fields have become more popular to date. Carbon nanotubes (CNTs) are a fairly new group of nanomaterials that have demonstrated promising results in various areas of nanomedicine due to their unique structures and outstanding physicochemical properties [1]. Based on their unique properties, CNTs have attracted much attention since a report by Iijima in 1991 [2]. CNTs are potential candidates for a variety of applications such as chemical sensors, nanoelectronics, catalyst support, targeting of diseased sites and drug delivery systems. The nature and quality of CNTs are highly dependent on the method of synthesis which regulates the graphitization degree, helicity and diameter [3].

A spectrum of procedures to produce CNTs have been reported, and the most commonly used procedures are arc discharge, laser ablation and chemical vapor deposition. The catalytic chemical

APPENDIX B1

DEXAMETHASONE RELEASE FROM ALIGNED MULTIWALLED CARBON NANOTUBES FOR THE TREATMENT OF ISCHEMIC STROKE

Patrick P. Komane[1,2], Yahya E. Choonara[1], Pradeep Kumar[1] and Viness Pillay[1]

[1]Wits Advanced Drug Delivery Platform Research Unit, Department of Pharmacy and Pharmacology, School of Therapeutic Sciences, Faculty of Health Sciences, University of the Witwatersrand, Johannesburg, 7 York Road, Parktown, 2193, South Africa

[2]Department of Applied Chemistry, University of Johannesburg, PO Box 17011, Doornfontein, 2028 Johannesburg,South Africa

Introduction: There is a lack of ultrasensitive diagnostic tool and an effective treatment of ischemic stroke. Carbon nanotubes have a potential to be employed in the diagnostic and treatment of ischemic stroke. Multiwalled carbon nanotubes have the ability to deliver and release dexamethasone to the ischemic site for the treatment of ischemic stroke.

Methods: In this study, vertically aligned multi-walled carbon nanotubes (VA-MWCNTs) were purified with HCl, carboxylated with H_2SO_4:HNO_3 (3:1) and acylated with $SOCl_2$. MWCNTs were refluxed at 80˚C for 24 hours during purification, carboxylation and acylation. MWCNTs were centrifuged at 5000rpm for 20min. The supernatants were filtered and precipitates washed with water until neutral pH. MWCNTs were extracted from the filters and dried in a vacuum oven. Dexamethasone was coupled to acylated MWCNTs by amidation procedure. Thermal stability, thickness, diameter, particle size, zeta potential (ZP), polydispersive index (PDI), functional groups and hydrophilicity of the MWCNTs were measured using TGA, SEM, TEM, DLS, FTIR and contact angle meter. Dexamethasone release from the MWCNTs was determined using UV-VIS spectrophotometry.

Results: Functionalization of the MWCNTs with HCl and H_2SO_4:HNO_3 reduced the thickness of the MWCNTs. The external diameters of the MWCNTs were drastically reduced but the internal diameters remained relatively constant. A drastic decrease in the contact angle was observed when MWCNTs were functionalised with H_2SO_4:HNO_3. HCl functionalization of the MWCNTs had an insignificant change on the MWCNTs hydrophobicity. Functionalization with $SOCl_2$ caused a significant reduction in the hydrophobicity of the MWCNTs. There was a drastic reduction in size and PDI when the CNTs were functionalised with H_2SO_4:HNO_3. MWCNTs were found to have moderate stability with PDI of 0.4 and ZP of – 40mV. FTIR revealed the additional functional groups on the functionalized MWCNTs. There was a drastic drop of weight when the temperature reached 500˚C to 600˚C for both the pristine and HCl-CNTs. Pristine and HCl functionalized MWCNTs went to a complete decomposition whereas the H_2SO4:HNO_3 and $SOCl_2$ functionalised MWCNTs did not decompose completely as a result of additional functional groups. Dexamethasone (Dex) was released after 30 minutes in both PBS buffers of pH 5.5 and 7.4. Dex release was constant over a period of 24 hours in PBS of pH 5.5. The release remained constant over a period of 12 hours and increased to 24 hours in PBS buffer of pH 7.4.

Conclusions: Our findings have demonstrated that dexamethasone could be coupled to functionalised VA-MWCNTs and be released after 30 minutes from the VA-MWCNTs.

Learning Objectives

1. Functionalize and characterize VA-MWCNTs.
2. Differentiate between the pristine MWCNTs and functionalized MWCNTs.
3. Evaluate the release of dexamethasone from VA-MWCNTs.

APPENDIX B2

A Carbon Nanotube-Based Immunosensor for Detection of Atrial Natriuretic Peptide in Ischemic Stroke

Authors P. P. Komane, Y.E. Choonara, V. Pillay
Affiliation/Company Wits Advanced Drug Delivery Platform, University of the Witwatersrand, Faculty of Health Sciences
Department of Pharmacy and Pharmacology, 7 York Rd, Parktown, 2193 Johannesburg, South Africa

Purpose: The current diagnosis and treatment of ischemic stroke are not sensitive enough to detect stroke at an early stage and to treat it effectively. Carbon nanotubes have the potential for early diagnosis and effective treatment of stroke. Atrial Natriuretic Peptide (ANP) is a biomarker for stroke. In this study, aligned multi-walled carbon nanotubes were synthesized for immunosensor development to detect ANP levels in stroke.

Methods: Vertically aligned multi-walled carbon nanotubes (MWCNTs) were produced on a silicon wafer with quartz tube walls by chemical vapour deposition. The reaction duration, concentration of ferrocene, synthesis temperature, gas flow rate and substrate location in the reactor tube were varied to determine optimal conditions for the production of aligned MWCNTs. The effect of bimetallic and trimetallic catalysts on the yield of MWCNTs was evaluated using ferrocene-cobaltocene, ferrocene-nickelocene and ferrocene-cobaltocene-nickelocene. MWCNTs were analyzed using EDS and X-ray mapping to assess the coating effect of iron on nickel and cobalt. The crystallinity and elemental composition of the MWCNTs was measured by XRD. For purification, MWCNTs were subjected to thermal oxidation at a temperature of 450˚C for 1h at 200mL/min oxygen. CNTs were then transferred into a vial and 5M HCl was added and incubated for 2h at 80˚C. The morphology, length and diameter of the MWCNTs were determined by SEM and TEM. Resistivity was measured using electrical resistivity meter. The surface area, pore size and volume of the MWCNTs were determined using a surface area and pore size analyzer. Thermogravimetric analysis was performed to obtain the thermal stability and degradation temperature of the MWCNTs. Wettability of MWCNTs was measured using a goniometer. MWCNTs were incorporated into epoxy resin for mechanical support. SEM was performed to confirm the incorporation of the carbon nanotubes into the epoxy resin. Cyclic voltammetry and electrochemical impedance spectroscopy were used to measure current flow and dielectric properties of the immunosensors. The cyclic voltammetry data was recorded between -0.4 and 0.4 V with a scan rate of 50mV/s. The electrochemical impedance spectroscopy spectra were recorded at frequency of 100kHz to 100mHz at an amplitude 0.01V and potential 0.220V.

Results: Well-aligned quality MWCNTs were obtained when the silicon wafer was placed 125mm from the entrance of the horizontal tube furnace. The ideal synthesis temperature for the vertically aligned MWCNTs was at 775°C. A thick layer of iron nanoparticles and amorphous carbon were observed when concentrations of a catalyst higher than 2.5% were used. Superior synthesis of aligned MWCNTs was also observed when an argon flow rate of 400mL/min and a synthesis time of 45 min were used. MWCNTs with an average internal diameter of 11nm and average external diameter of 48nm were obtained as confirmed by TEM. An average length of the aligned MWCNTs was 150µm as measured by SEM. MWCNTs had strong electrical conductivity at temperatures ranging from 26.85-76.85°C. The pore size, surface area and pore volume increased from 13.090nm, 47.156m^2/g and 0.154m^3/g to 18.090nm, 144.096m^2/g and 0.658m^3/g respectively when MWCNTs were purified by thermal and acid oxidation. A combination of ferrocene with either cobaltocene or nickelocene resulted in higher yield of MWCNTs. The total yields of MWCNTs for ferrocene-cobaltocene, ferrocene-nickelocene and ferrocene-cobaltocene-nickelocene were 69%, 43% and 31% respectively. Crystallinity and elemental composition of the MWCNTs were determined by XRD and two characteristic peaks were observed at the angle (2Θ) of 25˚and 45˚. These peaks were due to the carbon in MWCNTs and iron in ferrocene respectively. EDS and X- ray mapping data revealed the elemental composition and the arrangement of iron around cobalt and nickel. The contact angle of the CNTs decreased from 146.4±7.9˚ to 44.8±77˚ after purification as confirmed by the goniometer. Honeycomb like structures were formed on the surface of the MWCNTs when treated with 5M HCl during the purification process. Acid treatment reduced the thermal stability and decomposition temperature of MWCNTs from 554.33˚C to 538.86˚C and from 877.5˚C to 824.7˚C. MWCNTs were successfully incorporated into the epoxy resin as observed by SEM. Electrical impedance spectra and cyclic voltammetry data confirmed the low resistivity hence high electrical conductivity of the carbon based immunosensor.

Conclusions: These findings suggest that well aligned MWCNTs can be synthesized and functionalized with HCl to increase the surface area, pore size, pore volume and hydrophilicity. These properties are crucial for enhancing the loading capacity of ANP for diagnosis and targeting of the ischemic site as well as for the delivery of an anti-inflammatory drug to the site for effective and efficient treatment of ischemic stroke.

APPENDIX B3

VERTICALLY ALIGNED MULTIWALLED CARBON NANOTUBES FOR USE IN DETECTION AND TREATMENT OF ISCHEMIC STROKE

Patrick P. Komane[1,2] Sabelo D Mhlanga[3] and Girish Modi[4]

[1]Wits Advanced Drug Delivery Platform Research Unit, Department of Pharmacy and Pharmacology, School of Therapeutic Sciences, Faculty of Health Sciences, University of the Witwatersrand, Johannesburg, 7 York Road, Parktown, 2193, South Africa [2]Department of Applied Chemistry, University of Johannesburg, PO Box 17011, Doornfontein, 2028 Johannesburg, South Africa, [3]Nanotechnology and Water Sustainability (NanoWS) Research Unit, College of Science, Engineering and Technology, University of South Africa, Florida, 1709, Johannesburg, South Africa, [4]Department of Neurology, Division of Neurosciences, Faculty of Health Sciences, University of the Witwatersrand, 7 York Road, Parktown, 2193, Johannesburg, South Africa

patrickk@uj.ac.za, mhlansd@unisa.ac.za and girish.modi@wits.ac.za

Abstract

Carbon nanotubes have been extensively studied due to their excellent physico-chemical properties. They have a potential to be employed as theranostic tools in the diagnosis and treatment of ischemic stroke. In this study, vertically aligned multiwalled carbon nanotubes (VA-MWCNTs) were synthesized on a substrate using chemical vapour deposition. Parameters such as location of the substrate in the furnace, synthesis temperature, synthesis duration and gas flow rate were varied to obtain optimal conditions for MWCNT production. MWCNTs were obtained when the silicon wafer was placed half way between the centre and entrance of the furnace at 775°C with 2.5 % ferrocene with a gas flow rate of 400 ml.m^{-1} and synthesis duration of 45 min. The CNTs with average length of 127 um, average internal diameter of 11 nm and average external diameter of 73 nm were obtained. They were found to be strongly electrically conductive at temperatures from 36.85°C-76.85°C when temperatures from -73.15°C to 76.85°C were used. The CNT yield was also found to be improved by a mixture of Fe/Co and 599.40 mg of CNTs were produced compared to 331.2 mg produced when Fe/Ni was used. Honeycomb like structures were formed on the surface of the CNTs when treated with 5M HCl. These findings suggest that well aligned MWCNTs can be produced and be treated with 5M HCl to increase their surface area, pore size and pore volume in order to cater for high payload for targeting and delivery of drugs for diagnosis and treatment of ischemic stroke simultaneously.

Keywords: Carbon nanotubes, CVD, Pyrolysis, Ferrocene, Multiwalled CNTs, Stroke.

Session:



Graphical abstract: Nanoscience image

References:

1. A. Fabbro, S. Bosi, L. Ballerini, M. Prato. Carbon Nanotubes: Artificial Nanomaterials to Engineer Single Neurons and Neuronal Networks. ACS Chem Neurosci., 2012, 3:611–618.
2. S. Marchesan, K. Kostarelos, A. Bianco, M. Prato. The winding road for carbon nanotubes in nanomedicine. Mater Today, 2015, 18:12–19.

APPENDIX C1

STRICTLY CONFIDENTIAL

ANIMAL ETHICS SCREENING COMMITTEE (AESC)

CLEARANCE CERTIFICATE NO. 2017/03/17/D

APPLICANT: Mr P Komane

SCHOOL: Pharmacy and Pharmacology
DEPARTMENT:
LOCATION:

PROJECT TITLE: A functionalised carbon nanotube system for targeting of inflammatory biomarkers in ischemic stroke using Sprague Dawley rats

Number and Species

70 X 300-350g male Sprague Dawley rats

Approval was given for the use of animals for the project described above at an AESC meeting held on 2017/03/28. This approval remains valid until 2019/04/19.
Unreported changes to the application may invalidate the clearance given by the AESC
An annual progress report must be provided

The use of these animals is subject to AESC guidelines for the use and care of animals, is limited to the procedures described in the application form and is subject to any additional conditions listed below:

None

Signed: _____ Date: 20 April 2017
(Chairperson, AESC)

I am satisfied that the persons listed in this application are competent to perform the procedures therein, in terms of Section 23 (1) (c) of the Veterinary and Para-Veterinary Professions Act (19 of 1982)

Signed: _____ Date: 20 April 2017
(Registered Veterinarian)

cc: Supervisor: Professor V Pillay
Director: CAS

Works 2000/lain3015/AESCCert.aps

APPENDIX D1

TURNITIN REPORT

PP_KomaneThesis_2019.docx

ORIGINALITY REPORT

8%	5%	6%	2%
SIMILARITY INDEX	INTERNET SOURCES	PUBLICATIONS	STUDENT PAPERS

PRIMARY SOURCES

1	www.mdpi.com Internet Source	2%
2	Patrick Komane, Pradeep Kumar, Thashree Marimuthu, Lisa Toit, Pierre Kondiah, Yahya Choonara, Viness Pillay. "Dexamethasone-Loaded, PEGylated, Vertically Aligned, Multiwalled Carbon Nanotubes for Potential Ischemic Stroke Intervention", Molecules, 2018 Publication	<1%
3	Gomez-Ballesteros, Jose L., Juan C. Burgos, Pin Ann Lin, Renu Sharma, and Perla B. Balbuena. "Nanocatalyst shape and composition during nucleation of single-walled carbon nanotubes", RSC Advances, 2015. Publication	<1%
4	wings.buffalo.edu Internet Source	<1%
5	gen.liebertpub.com Internet Source	<1%
	www.turkupetcentre.net	

6	Internet Source	<1%
7	www.dataphysics-instruments.com Internet Source	<1%
8	Nanotechnology for Sustainable Development, 2014. Publication	<1%
9	Lekawa-Raus, Agnieszka, Jeff Patmore, Lukasz Kurzepa, John Bulmer, and Krzysztof Koziol. "Electrical Properties of Carbon Nanotube Based Fibers and Their Future Use in Electrical Wiring", Advanced Functional Materials, 2014. Publication	<1%
10	www.coursehero.com Internet Source	<1%
11	www.cfrjournal.com Internet Source	<1%
12	Falah H. Hussein, Firas H. Abdulrazzak. "Synthesis of Carbon Nanotubes by Chemical Vapor Deposition", Wiley, 2018 Publication	<1%
13	Azam, Mohd Asyadi, Nor Syafira Abdul Manaf, Elyas Talib, and Mohd Shahril Amin Bistamam. "Aligned carbon nanotube from catalytic chemical vapor deposition technique for energy	<1%

	storage device: a review", Ionics, 2013. Publication	
14	"Pan Vascular Medicine", Springer Nature, 2002 Publication	<1%
15	en.wikipedia.org Internet Source	<1%
16	www.cvphysiology.com Internet Source	<1%
17	www.intechopen.com Internet Source	<1%
18	Stavropoula I., Pascal M., Aaron S., L. Fernando, Robert H.. "Chapter 6 Endovascular Management of Acute Ischemic Stroke", InTech, 2012 Publication	<1%
19	Submitted to University of Malaya Student Paper	<1%
20	pubs.acs.org Internet Source	<1%
21	www.resins.com Internet Source	<1%
22	Submitted to Hindustan University Student Paper	<1%
	Khurshed A. Shah, Bilal A. Tali. "Synthesis of	

23	carbon nanotubes by catalytic chemical vapour deposition: A review on carbon sources, catalysts and substrates", Materials Science in Semiconductor Processing, 2016 Publication	<1%
24	www.nature.com Internet Source	<1%
25	Submitted to Institute of Graduate Studies, UiTM Student Paper	<1%
26	www.micromeritics.com Internet Source	<1%
27	Submitted to Universiti Sains Malaysia Student Paper	<1%
28	Submitted to University of Johannsburg Student Paper	<1%
29	Shanyong Zhang. "Titanium carbonitride-based cermets: processes and properties", Materials Science and Engineering: A, 1993 Publication	<1%
30	M. Barberio, M. Camarca, P. Barone, A. Bonanno, A. Oliva, F. Xu. "Electric resistivity of multi-walled carbon nanotubes at high temperatures", Surface Science, 2007 Publication	<1%
	Mukul Kumar. "Chapter 8 Carbon Nanotube	

31	Synthesis and Growth Mechanism", InTech, 2011 Publication	<1%
32	Tang, C.F.. "Zinc oxide/redox mediator composite films-based sensor for electrochemical detection of important biomolecules", Analytical Biochemistry, 20080915 Publication	<1%
33	Submitted to University Tun Hussein Onn Malaysia Student Paper	<1%
34	Amit K. Chakraborty. "Carbon nanotube (CNT)–epoxy nanocomposites: a systematic investigation of CNT dispersion", Journal of Nanoparticle Research, 08/28/2011 Publication	<1%
35	library.iyte.edu.tr Internet Source	<1%
36	S. Itaba. "Presence of C-type natriuretic peptide (CNP) in guinea pig caecum: role and mechanisms of CNP in circular smooth muscle relaxation", Neurogastroenterology and Motility, 6/2004 Publication	<1%
37	Alireza Valizadeh, Nasrin Sohrabi, Fariba Badrzadeh. "Electrochemical detection of HIV-1	<1%

by nanomaterials", Artificial Cells, Nanomedicine, and Biotechnology, 2017
Publication

38	Submitted to Imperial College of Science, Technology and Medicine Student Paper	<1%
39	Yu-Cheng Liu. "Development of epoxy-based electrets", Journal of Materials Science, 03/2008 Publication	<1%
40	Curtis W. Hoganson. "Mn2+ reduces Yz + in manganese-depleted Photosystem II preparations", Photosynthesis Research, 12/1989 Publication	<1%
41	Pierre P.D. Kondiah, Lomas K. Tomar, Charu Tyagi, Yahya E. Choonara, Girish Modi, Lisa C. du Toit, Pradeep Kumar, Viness Pillay. "A novel pH-sensitive interferon-β (INF-β) oral delivery system for application in multiple sclerosis", International Journal of Pharmaceutics, 2013 Publication	<1%
42	Submitted to University of Sheffield Student Paper	<1%
43	www.bjbms.org Internet Source	<1%

44	Claude André Degueldre. "The Analysis of Nuclear Materials and Their Environments", Springer Nature, 2017 Publication	<1%
45	calhoun.nps.edu Internet Source	<1%
46	www.slideshare.net Internet Source	<1%
47	Submitted to Higher Education Commission Pakistan Student Paper	<1%
48	Submitted to Bradford College, West Yorkshire Student Paper	<1%
49	Submitted to National postgraduate Medical College of Nigeria Student Paper	<1%
50	www.chemical-supermarket.com Internet Source	<1%
51	Submitted to Yeditepe University Student Paper	<1%
52	Fengxiang Zhang, Hong Yee Low. "Anisotropic Wettability on Imprinted Hierarchical Structures", Langmuir, 2007 Publication	<1%
	Submitted to National University of Singapore	

53	Student Paper	<1%
54	Submitted to Monash University Student Paper	<1%
55	Slovin, Mitchell Ross, and Michael R. Shirts. "Identifying Differences and Similarities in Static and Dynamic Contact Angles between Nanoscale and Microscale Textured Surfaces Using Molecular Dynamics Simulations", Langmuir Publication	<1%
56	Submitted to University of Edinburgh Student Paper	<1%
57	Internet Source	<1%
58	archive.org Internet Source	<1%
59	S. M. Wagh, K. V. Koranne, R. B. Mankar, R. L. Sonolikar. "Gas holdup in a two-phase reversed flow jet loop reactor", The Canadian Journal of Chemical Engineering, 2010 Publication	<1%
60	Submitted to Lehigh University Student Paper	<1%
61	Submitted to Newham Sixth Form College,	

	London Student Paper	<1%
62	Submitted to Stourbridge College Student Paper	<1%
63	etd.lsu.edu Internet Source	<1%
64	www.spandidos-publications.com Internet Source	<1%
65	link.springer.com Internet Source	<1%
66	Xuelian Cheng. "Characterization of Multiwalled Carbon Nanotubes Dispersing in Water and Association with Biological Effects", Journal of Nanomaterials, 2011 Publication	<1%
67	www.horsejunction.co.za Internet Source	<1%
68	Kitchen, S., H. Beckmann, Y. Katterle, S. Bruns, D. Tseneklidou-Stoeter, and M. Maas Enriquez. "BAY 81-8973, a full-length recombinant factor VIII: results from an International comparative laboratory field study", Haemophilia, 2016. Publication	<1%
69	www.science.gov Internet Source	<1%

70	www.scilit.net Internet Source	<1%
71	Advances in Experimental Medicine and Biology, 2006. Publication	<1%
72	www.mysciencework.com Internet Source	<1%
73	Aguilar, Zoraida P.. "Targeted Drug Delivery", Nanomaterials for Medical Applications, 2013. Publication	<1%
74	www.google.com.mx Internet Source	<1%
75	"Day 4 - Tuesday 31 August 2004", European Heart Journal, 09/02/2004 Publication	<1%
76	www.jbc.org Internet Source	<1%
77	Submitted to University College London Student Paper	<1%
78	www.jiskha.com Internet Source	<1%
79	pericles.pericles-prod.literatumonline.com Internet Source	<1%
80	dspace.vutbr.cz Internet Source	<1%

81	www.faqs.org Internet Source	<1%
82	Mahtab Gharibi, Farnaz Tahriri Zangeneh, Fereydoon Yaripour, Saeed Sahebdelfar. "Nanocatalysts for conversion of natural gas to liquid fuels and petrochemical feedstocks", Applied Catalysis A: General, 2012 Publication	<1%
83	jmolecularpsychiatry.biomedcentral.com Internet Source	<1%
84	J. I. Read, M. I. Wilkinson, N. W. Evans, G. Gilmore, J. T. Kleyna. "The importance of tides for the Local Group dwarf spheroidals", Monthly Notices of the Royal Astronomical Society, 2006 Publication	<1%
85	Fiorito, Filomena, Carlo Irace, Antonio Di Pascale, Alfredo Colonna, Giuseppe Iovane, Ugo Pagnini, Rita Santamaria, and Luisa De Martino. "2,3,7,8-Tetrachlorodibenzo-p-Dioxin Promotes BHV-1 Infection in Mammalian Cells by Interfering with Iron Homeostasis Regulation", PLoS ONE, 2013. Publication	<1%
86	epdf.tips Internet Source	<1%

87	McGuire, K.. "Synthesis and Raman characterization of boron-doped single-walled carbon nanotubes", Carbon, 2005 Publication	<1%
88	baadalsg.inflibnet.ac.in Internet Source	<1%
89	Jui-Yeh Rau, Jyh-Cherng Chen, Ming-Yen Wey, Min-Der Lin. " Effects of H O and Particles on the Simultaneous Removal of SO and Fly Ash Using a Fluidized-Bed Sorbent/Catalyst Reactor ", Industrial & Engineering Chemistry Research, 2009 Publication	<1%
90	J Capelo. "Ozone treatment for mercury determination in white wines", Talanta, 2003 Publication	<1%
91	Karimian, Najmeh, Anthony P.F. Turner, and Ashutosh Tiwari. "Electrochemical evaluation of troponin T imprinted polymer receptor", Biosensors and Bioelectronics, 2014. Publication	<1%
92	www.freepatentsonline.com Internet Source	<1%
93	Hernadi, K.. "On the role of catalyst, catalyst support and their interaction in synthesis of carbon nanotubes by CCVD", Materials	<1%

	Chemistry & Physics, 20030115 Publication	
94	tel.archives-ouvertes.fr Internet Source	<1%
95	refubium.fu-berlin.de Internet Source	<1%
96	Matias Bargheer. "Coherence and control of molecular dynamics in rare gas matrices", Chemical physics, 2007 Publication	<1%
97	Tjong, S.C.. "Structural and mechanical properties of polymer nanocomposites", Materials Science & Engineering R, 20060830 Publication	<1%
98	xa.yimg.com Internet Source	<1%
99	Filipe Vargas Ferreira, Luciana De Simone Cividanes, Felipe Sales Brito, Beatriz Rossi Canuto de Menezes et al. "Functionalizing Graphene and Carbon Nanotubes", Springer Nature, 2016 Publication	<1%
100	Cardiovascular Biomarkers, 2006. Publication	<1%
101	Putz, Ana-Maria, Marius Lazea, and Adrian Chiriac. "About the SPECTRAL-SAR Overcome	<1%

to Statistical Approach of QSAR : An Ecotoxicity Case of Aliphatic Amines", QSAR and SPECTRAL-SAR in Computational Ecotoxicology, 2012.
Publication

102	Michael Rychlik. "Rapid degradation of the mycotoxin patulin in man quantified by stable isotope dilution assays", Food Additives and Contaminants, 2003 Publication	<1%
103	Chi-Yu Lu, Yung-Ming Chang, Wei-Lung Tseng, Chia-Hsien Feng, Chin-Yuan Lu. "Analysis of angiotensin II receptor antagonist and protein markers at microliter level plasma by LC–MS/MS", Journal of Pharmaceutical and Biomedical Analysis, 2009 Publication	<1%

Exclude quotes	On	Exclude matches	Off
Exclude bibliography	On		